This is to certify that the
dissertation entitled

ON THE USE OF A REGIONAL-SCALE NUMERICAL
CLIMATE MODEL IN WIND ENERGY APPLICATIONS

presented by

KARSTEN ALEXANDER SHEIN

has been accepted towards fulfillment
of the requirements for the

Doctoral degree in Geography

Major Professor's Signature

8/17/05

Date

ON THE USE OF A REGIONAL-SCALE NUMERICAL CLIMATE MODEL IN WIND ENERGY APPLICATIONS

By

Karsten Alexander Shein

A DISSERTATION

Submitted to
Michigan State University
in partial fulfillment of the requirements
for the degree of

DOCTOR OF PHILOSOPHY

Department of Geography

2005

ABSTRACT

ON THE USE OF A REGIONAL-SCALE NUMERICAL CLIMATE MODEL IN WIND ENERGY APPLICATIONS

By

Karsten Alexander Shein

This research explores the performance of a regional scale numerical climate model (MM5) with respect to the estimation of the wind resource over the Great Lakes region of North America. Three model domain resolutions (36 km, 12 km and 4 km) are evaluated for accuracy. Additionally, the ability of the model to accurately estimate the wind resource distribution at specific locations is investigated by employing various spatial aggregation schemes over the model domain.

The results of this evaluation of the MM5 model indicated that a coarser resolution domain provides the most reliable estimates of the wind resource over the region. Furthermore, only the nearest grid point appears to be a necessary estimator of the wind regime at a particular location. Using this information, the MM5 model estimates were compared with estimates produced by three statistical models, a joint probabilistic model, a measure-correlate-predict model, and a Krige model, all of which have been used with prior success in wind resource estimation. Of the three statistical models, the joint probabilistic and measure-correlate-predict models provided the best estimates over the region and were thus compared with the MM5 estimates.

It was determined that none of the three models significantly outperformed the others, even at relatively remote locations within the study area. However, it also was noted that the MM5 model contained a much higher systematic proportion of total estimative bias, and that it might be possible to improve the estimates. A multiple linear regression based upon Latitude was fit to the estimated Weibull parameters from the MM5 model and a significant improvement was noted. However, the improvement failed to cause the MM5 to significantly outperform the other models. Thus, this research concludes that in its present state and relative complexity of implementation relative to established statistical models, MM5 would not be a logical choice for estimating the wind resources of the Great Lakes region.

Keywords: wind resource analysis, numerical climate model, Great Lakes

For my wife, soul mate and media naranja, Walli Ann.

ACKNOWLEDGEMENTS

I am indebted to my principal advisor, Dr. Jeffrey A. Andresen for his guidance and council throughout my graduate work at Michigan State University. I also am grateful to the members of my doctoral committee, Drs. Julie Winkler, Jay Harman, Jean Palutikof, Bill Northcott, and Fred Nurnberger. Their instruction, comments and council throughout this endeavor has proven invaluable.

Additionally, I am deeply thankful to the United States Forest Service North Central Research Station for providing the MM5 data needed to complete this research. In particular, I wish to thank Drs. Warren E. Heilman, Joseph J. (Jay) Charney, Brian E. Potter, and especially Xindi Bian for their implementation of the MM5 regional climate model, for helping me to understand the way in which the model was set up, and for assisting me greatly in assembling the model output. Without the efforts of these fine people, this project would not have been possible. Furthermore, the material presented herein is based upon work supported by the National Science Foundation under Grant No. 0302469.

Finally, I wish to acknowledge my lovely wife, Dr. Walli Ann Wisniewski. It was she who ultimately gave me the drive and desire to keep pushing ahead when there seemed to be no light at the end of the tunnel. Her encouragement and love were without measure.

TABLE OF CONTENTS

LIST OF TABLES

LIST OF FIGURES

KEY TO SYMBOLS OR ABBREVIATIONS

°	degrees (unit of compass direction)
ρ	Air density (kilograms per cubic meter)
A^2	Anderson-Darling test statistic
A^{2*}	Anderson-Darling test statistic for small samples
ASOS	Automated Surface Observing System
AWOS	Automated Weather Observing System
c	Weibull distribution scale parameter (in m s^{-1})
d	Index of Agreement (based on MSE)
d^2	Index of Agreement (based on RMSE)
e	Residual of estimated values or inverse of natural logarithm
E	East
FAA	U.S. Federal Aviation Administration
FSMM5	U.S. Forest Service operational MM5 model
GMT	Greenwich Mean Time (see also UTC or Z)
k	Weibull distribution shape parameter
kt	knot (nautical mile per hour)
kW	Kilowatts (1000 watts)
kWh	Kilowatt hours
m	meters
m s^{-1}	meters per second
METAR	Routine meteorological report
MM5	Mesoscale Model Version 5 (Pennsylvania State University)
MSE	mean squared error
MW	Megawatts (1000 kW)
n	frequency count
N	North
NOAA	U.S. National Oceanic and Atmospheric Administration
NWS	U.S. National Weather Service
p	probability level
P	Wind Power (usually in W m^2)
QC	Quality Control
RMSE	root mean squared error
s	standard deviation
S	South
t	Student's T-test statistic
u or U	horizontal wind speed
UTC	Universal Time Coordinated (see also GMT or Z)
v or V	horizontal wind speed (used for wind vectors to differentiate from u)
W	West
WECS	Wind Energy Conversion System (e.g., wind turbine or wind farm)
z	height (in m) above the ground
Z	Zulu time (see also GMT or UTC)

Chapter 1. Introduction

The power contained in moving air has been harnessed for work by human beings for thousands of years. The use of wind power has included sailing ships, grinding grain, pumping water, and most recently the generation of electricity. A key component of the efficient use of wind power is some prior knowledge of the magnitude and consistency of the resource. Optimal locations for exploiting the wind resource have long been identified as those having relatively consistent, moderately high wind speeds. Prior to the introduction of meteorological instruments or observations, the identification of such locations, both on land and over water was generally made through personal experience and knowledge handed down between generations. Such thought and planning is clearly evident in the presence of antique wind mills in many of these locations, the continued use of older sailing routes by modern vessels, as well as in the place names of many of locations to reflect the windy conditions (*e.g.*, Vindeby, Denmark; Punta Viento, Puerto Rico; Venta de Olivos, Spain; Windy Point, Canada; Buenos Aires, Argentina). However, prior to the development and installation of modern wind energy conversion systems (WECS), or wind turbines for the generation of electricity, there was little need to quantify the wind resource. The wind was simply utilized when it blew, and locations without sufficient wind resources were usually abandoned in favor of winder locations. Although primitive anemometers have been in existence since at least 1000 AD (Põtz, 1988), and wind vanes from several millennia earlier (Neumann and Parpola, 1983) the relatively low power required by wind mills and sailing vessels was generally satisfied by siting in consistently windy locations (*e.g.*, hillocks, ridges, coastal bluffs) and supported by the use of alternative energy sources when the wind was unavailable (*e.g.*, animal or water driven mills, oars on sailing vessels). Put simply, either it was suitably windy, or it was not. Any resulting assessment was therefore qualitative rather than quantitative.

The concept of generating electricity by connecting a windmill rotor to a turbine is a relatively recent one in the history of wind power. Arguably the first successful wind turbine was the Brush post mill turbine in Cleveland, Ohio in 1888 (Dodge, 2002, DWIA, 2003). However, the Brush turbine and subsequent attempts at electricity generation from the wind met with limited success, until the 1920s when the more aerodynamic design of aircraft propellers and more efficient turbines became available. In the 1920s, many hundreds of small Jacobs Wind-machines were used at rural farms throughout the US and Canada (Dodge, 2002). Although these turbines were abandoned after the US government's rural electrical cooperative program brought grid electricity to rural areas in the early 1930s, the intermittent operation of these turbines as a result of variable winds clearly highlighted the need for a better understanding and quantification of the wind resource if wind energy was to become a viable source of grid-based electricity.

The Danes were the first to experiment with the commercial production of wind electricity, taking advantage of the naturally moderate and steady winds over the Danish peninsula (DWIA, 2003). However, low fossil fuel prices rendered the numerous Danish wind turbines economically obsolete soon after World War I. The United States took advantage of a suitably windy location, Grandpa's Knob in Rutland, Vermont to establish a grid-connected 1.25 Megawatt (MW) turbine during fuel shortages of WW II in 1941.

Experience with this turbine further highlighted the need for a scientific approach to wind turbine siting when in 1945, after only a few hundred generation hours, high winds broke off a blade, ending its operational life (Dodge, 2002). Unfortunately, interest in wind as an energy source waned with the ample and inexpensive generation of fossil and nuclear energy in the 1950s and 1960s. Thus there was also little interest at the time from the scientific community in better understanding the wind as a resource.

Unlike a conventional windmill that simply transforms wind power directly into an end use (grinding or pumping), the quantity of electricity generated by a wind turbine is not only dependent on the design of the turbine, but is also highly dependent on the magnitude of the wind speed. Following Rohatgi and Nelson (1994), the power density (P) of the wind is a function of the air density (ρ), the cube of the wind speed (V) and the swept area (A) which can be written functionally as:

$$P = 1/2\, \rho\, V^3\, A \qquad 1.1$$

Although a wind turbine may sweep a large area, a further consideration is that a turbine can physically extract only a fraction of the overall wind power flowing through the turbine's swept area before the loss of kinetic energy to the turbine becomes too great to maintain inflow speeds. This limitation is roughly 59% of the power potential calculated by Equation 1.1 and is known as Betz law (Betz, 1926, Rohatgi and Nelson, 1994, Hansen, 2000). Additionally, due to the loss of energy to the internal mechanisms of the turbine itself (*e.g.*, gears), modern turbines are capable of extracting around 30% of the overall power contained in the wind. This proportion is the turbine's efficiency.

Due to the turbine efficiency and engineering factors such as blade aerodynamics, wind turbines have an operating envelope such that peak power production is only possible in a range of relatively strong wind speeds (*e.g.*, 15-25 m s^{-1}), called the rated speeds. Below about 3 m s^{-1}, there is insufficient wind power to turn the turbines. Above that speed, often called the startup speed, the turbine will generate exponentially more power as wind speeds increase, until peak production is obtained at the rated wind speeds. Beyond the envelope of rated wind speeds, the turbine blades are feathered and the turbine is shut down to prevent potential damage from over speeding. Figure 1.1 represents a turbine power curve from the Bonus 2 Megawatt (MW) wind turbine (data source: http://www.bonus.dk) and illustrates the relationship between wind speeds and turbine power production. The Bonus turbine produces no power below 4 m s^{-1} or above 25 m s^{-1}, and rated (2 MW) power only when winds are between 16 and 25 m s^{-1}. While the power curve of Figure 1.1 describes the Bonus 2 MW turbine in terms of aforementioned critical wind speeds, most wind turbines exhibit a similar profile. Thus, while a wind turbine is similar to a conventional windmill in that it will produce power under almost any wind, its optimal efficiency is limited to a rather small range of moderately high wind speeds. To properly site a turbine, a location is sought where wind speeds fall within the operational range with relatively high frequency.

Furthermore, it is undesirable to have a turbine in a location where winds experience rapid and/or frequent changes in speed or direction. Such wind variability results in excessive stress being placed on the turbine orientation gears and on the blade angle gears. As a wind turbine may cost well over one million US dollars to install and have a lifespan of 20-30 years (AWEA, 2002), it is advantageous for a turbine operator to not only identify a location where winds are frequently within the peak operating range of the turbine in order to maximize the potential power output from the turbine, but also where fluctuations in wind speed and direction are relatively low to minimize overall wear and tear on the turbine.

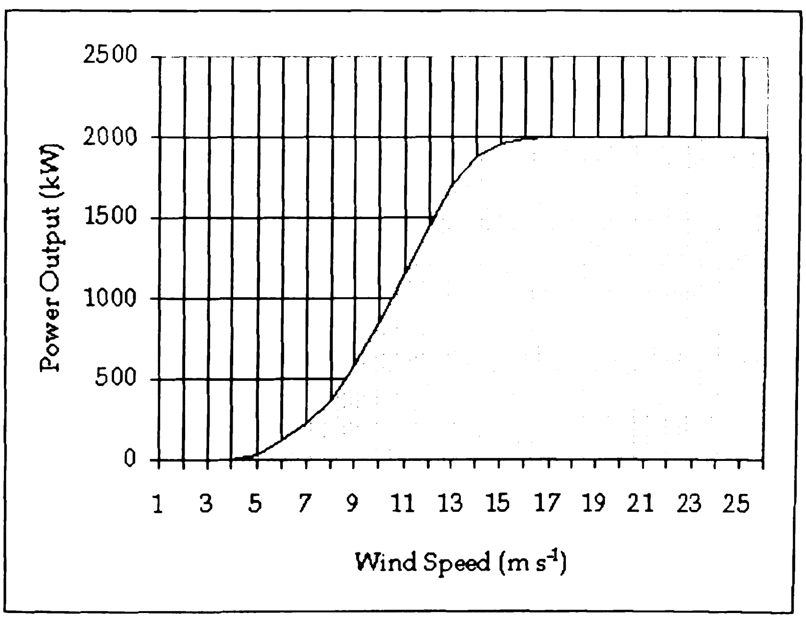

Figure 1.1 An idealized wind turbine power curve, derived from the Bonus 2 MW wind turbine (data sources: http://www.middlegrunden.dk and http://www.bonus.dk).

Although the energy crisis of the 1970s renewed interest in wind energy, a shortcoming to early WECS development was the relative inefficiency and low power output of early wind turbines. In general, turbines were limited to under 1 MW of rated power output (*i.e.*, output at rated wind speeds) so a great number of turbines were required to generate commercially viable quantities of energy (*e.g.*, the massive array at Tehachapi Pass, CA). Additionally, turbines of the 1970s-1990s had relatively high startup and rated speeds. These limitations necessitated the identification of locations that met the stringent resource criteria of contemporary turbines. As a result there was a great deal of scientific interest in accurately estimating the wind resource and a number of notable works, such as the United States Wind Atlas (Elliott *et al.*, 1987) were published (see Figure 1.2). Unfortunately much of the wind resource research at the time was based on a sparse, irregular and often inhomogeneous network of anemometers (*e.g.*, Elliott *et al.*, 1987, Goodin *et al.*, 1979). As a result, many regions deemed as having insufficient winds to generate consistent power from WECS were dismissed from consideration. Similarly, subsequent research on estimating wind resources in such locations was largely overlooked with but a few exceptions (*e.g.*, Wendland, 1982).

Recent advances and improvements in wind energy conversion systems (WECS) technology have led to wind power becoming a viable commercial form of electricity production in many parts of the world. Turbine efficiency, blade aerodynamics and tall tower engineering have all advanced to where it is now possible to produce electricity from a wind turbine at a cost of less than 5 cents per kilowatt hour (kWh) in optimal geographic locations. Such a cost is similar, if not less than the costs associated with producing that power from fossil fuels or radioactive materials, and without many of the environmental issues associated with the latter generation methods (IEA, 2001, Thor and Weis-Taylor, 2002). These technological advances have, in many places, been matched by a favorable administrative climate that has enacted tax credits, removed zoning restrictions and offered grants or low-interest development loans in an effort to actively develop the wind energy potential in those regions (*e.g.*, Germany, Denmark, United States, Spain, India; AWEA, 2004a).

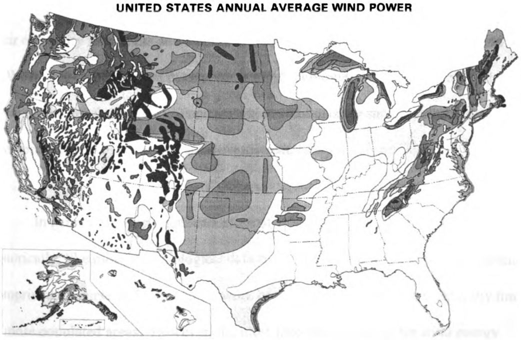

Figure 1.2 Wind power potential for the United States, from the Wind Energy Atlas of the United States (Elliott *et al.*, 1987). Darker shaded regions have greater potential than lighter regions. See Elliott *et al.* (1987) for a quantitative description of each wind power category.

As a result of new technologies, governmental support, and a recognized need for localized energy production (as evidenced by the California energy crisis of 2000), over 8,000 MW of wind power generation capacity was installed worldwide in 2003 (with 1,687 MW installed in the United States and 5,467 MW in Europe). This brings the total worldwide wind power conversion capacity to over 40,300 MW as of early 2004, up from 24,000 MW in 2001 (AWEA, 2002, 2004b). This developmental trend shows no signs of slowing and includes newly industrialized and developing countries which seek to meet increasing electricity demands and build energy independence. It is estimated that an installed wind energy capacity of over 200,000 MW will be in operation by the end of the decade (EWEA and Greenpeace, 2002). Several German States obtain more than 10% of their electricity from wind and Denmark produces over 20% of its electricity from wind (AWEA, 2004a). If current development trends continue, many wind farms will, by necessity be developed in locations for which wind data are sparse and where past studies had deemed the wind resource to be insufficient.

In general, the historical collection of wind speed and direction data has historically, like most meteorological data collection, been limited to discrete locations comprising a sparse and irregular network of observation stations, and generally limited to more populated areas. However, the most favorable locations for wind energy conversion systems are those regions with strong (*e.g.*, mean wind speeds (u) exceeding around 7 m s^{-1}) but steady winds. Due to either relatively harsh environmental conditions or physical limitations on human habitation, these areas generally tend to have low populations or may be devoid of people altogether (*e.g.*, offshore) and thus usually contain few meteorological observation stations (*e.g.*, Willmott *et al.*, 1991, Robeson, 1993, Klink, 1999). It is therefore necessary to somehow estimate the wind resource over regions where little or no observational data exist.

Although a great deal of early research on wind resources has been devoted to the estimation of speeds at locations lacking adequate observations, such estimates have invariably been hindered by the underlying characteristics of the wind field (*e.g.*, serial correlation, non-stationarity, anisotropy). The successes and limitations of earlier works will be discussed in more detail in the following chapter. Despite limitations to the success of estimating the wind resource at poorly instrumented locations, certain regions have been identified that clearly have wind resources amenable to WECS development.

Offshore (*i.e.*, over open water) and coastal winds in particular have long been acknowledged as being generally stronger and exhibiting greater persistence than nearby inland winds due to large fetches of low surface roughness over the water bodies (*e.g.*, Eichenlaub, 1979, Pryor and Barthelmie, 2001, Palutikof *et al.*, 2002). Additionally, offshore locations may not be as limited by many of the societal objections and zoning issues often associated with land-based WECS development (Still, 2001). Thus it is not surprising that within the wind energy sector an increasing number of WECS development initiatives are focused offshore and along coastal bluffs. Indeed, several along-shore and offshore (hereafter referred to as the shore zone) wind farms are already operating in the UK, Denmark and Germany. Additional shore zone projects are under consideration for the United States, Brazil, and Ireland (AWEA, 2004a). Because of the importance of the shore zone wind resource to developing wind energy capacity, there is a critical need for its accurate estimation of potential wind resource (Troen and Petersen, 1989).

Unfortunately, unless a sufficient series of wind data exists for a considered location, the identification of an optimal WECS development site can be difficult. Most wind farm locations are initially selected *a priori*, from regionalized isotach (wind speed) and isogon (wind direction) maps in wind atlases (*e.g.*, Elliott *et al.*, 1987, Troen and Petersen, 1989). Once selected, a developer is advised to erect an anemometer and collect wind data for a year or more, subsequently employing empirical interpolation techniques to decide whether the site is optimal or not.

The empirical techniques that are used in estimating the wind resource of a location have been shown by numerous researchers to work reasonably well for estimating wind at a candidate location if that location is within a relatively short distance of the nearest meteorological station and the intervening terrain is relatively homogeneous (*e.g.*, Justus *et al.*, 1976, Goodin *et al.*, 1979, Haslett and Raftery, 1989). Because such techniques are empirical, their potential accuracy is limited both spatially and temporally. Temporally, the accuracy of wind resource estimation tends to be limited to the data which are available. No information is available for trends, cycles or anomalies beyond the period of record. Additionally, such methods are limited by the degree of spatial coherence present in the wind field and the distance from the location of interest and the surrounding meteorological stations. In this context, such methods cannot address any of the smaller scale influences on wind that may occur between the candidate location and the meteorological series, instead aggregating the influences of such local-scale contributions into a set of static coefficients and shunting any departures from those terms into the error of the model. Although such issues can be investigated through an assessment of spatial coherence, only a few works have addressed these issues outside of complex terrain (Robeson and Shein, 1997, Klink, 1999).

As the lack of an adequate observational network has been repeatedly recognized as a limitation to reliable and accurate wind resource estimation over large regions, the use of dynamical atmospheric relationships to produce plausible wind estimates at uninstrumented locations has been investigated. Over the past few decades, there has been a growing interest in the use of numerical weather models for forecasting the wind resource over a region, with a number of such models subjected to testing and validation over different areas (*e.g.*, Sherman, 1978, McQueen *et al.*, 1995, Frank *et al.* 2001). However, again, the performance of these models with respect to wind over non-complex terrain has been largely overlooked and little work has investigated the ability of such models to adequately reproduce the statistics of the long-term wind resource.

1.1 Statement of Purpose

A review of the literature, which follows in the next chapter, reveals that short-term forecasting is the primary reason for interest in using RCMs in the context of wind energy. In such context, RCMs have been extensively investigated for producing a wind forecast out to about 48 hours at specific locations, and individual wind speed estimates are validated for accuracy. Although a cursory examination of observed versus model estimated hourly wind speeds is conducted herein, it is not the purpose of this research to perform such an evaluation. Rather, an RCM can also be used to generate a longer-term distribution of wind speeds for a location or over a region of hundreds of square kilometers. While individual estimates may differ substantially from their respective observations, the overall distribution, if accurate, would permit high confidence *a posteriori* selections of optimal WECS locations within the region at locations where few, if any, observations exist.

Unfortunately, this use of the RCM in wind energy has been largely overlooked on this point. In fact, the literature appears to be uncharacteristically silent on the use of an RCM as a method for generating spatially coherent and accurate estimates of the long-term wind resource over a region. This research seeks to remedy that deficiency in the science by taking the first step and validating the performance of an RCM for estimating the climatology of wind speeds over a region. Therefore, it is the goal of this research to investigate the utility of a regional-scale numerical climate model (or RCM) as a means to accurately estimate the wind resource over the Great Lakes region of North America (Figure 1.3), an area that is currently of interest for WECS development.

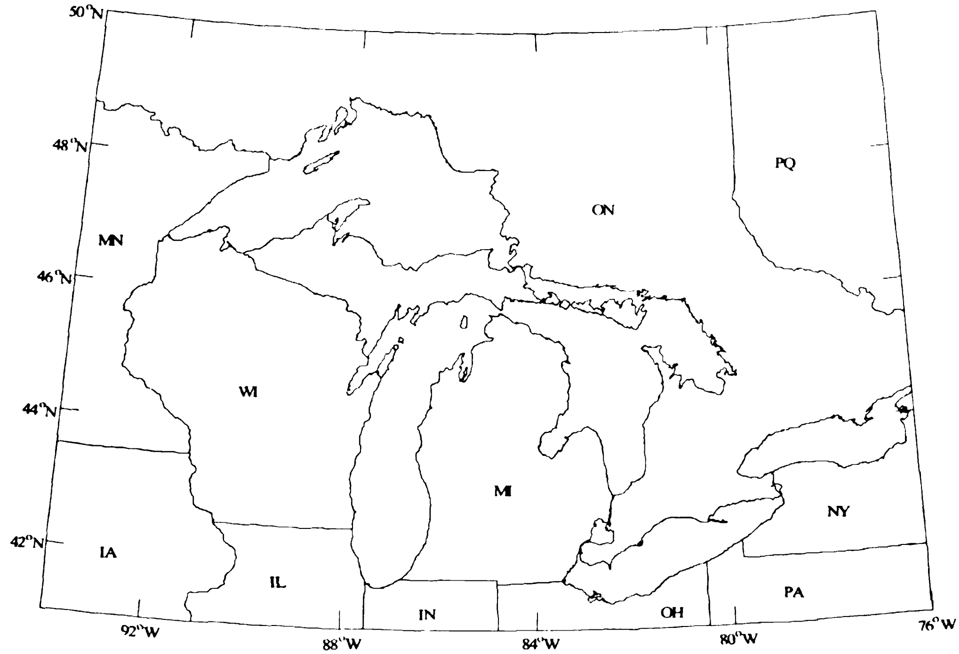

Figure 1.3 The study area; the Great Lakes region of North America.

Within the scope of this research, the foci are fourfold. The primary goal of this research is to determine whether a regional numerical climate model can adequately estimate the wind climatology over a region. Before a numerical climate model can be expected to be capable of plausibly estimating the long-term climatology of the wind field over a region, it must be shown that the model can adequately reproduce the statistics of the regional wind field as derived from observational data. To that end, the first focus of this research is to validate the estimative ability of the near-surface wind output from a widely used RCM, the Pennsylvania State University / National Center for Atmospheric Research (PSU/NCAR) Mesoscale Model, more commonly known as MM5

(Haagenson *et al.*, 1994). This validation will serve as the framework under which the subsequent analysis of this research will be conducted.

Second, execution of regional-scale numerical climate models tends to be computationally intensive. One of the most critical factors governing computational intensity, as well as estimation accuracy is the resolution, both spatial and temporal of the model simulation. To optimize the performance of an RCM, a balance must be achieved between computational intensity and estimation bias. The use of finer spatial or temporal resolution must be justified by appropriate levels of error reduction. If error cannot be significantly reduced by increasing resolution, the increase in computational intensity may not be justified. However, decreasing resolution to reduce computational intensity may mask many local-scale effects (*e.g.*, boundary layer, land cover) and increase error to unacceptable levels. To address this issue, this research will seek to establish the optimal spatial and temporal resolution for wind resource estimates over the Great Lakes. Such optimization will allow the RCM to be run most efficiently in terms of CPU utilization and bias minimization.

Third, because dynamically-driven RCMs such as MM5 tend to be computationally intensive at any meaningful resolution, and require both meteorological and computer expertise to install, run and properly interpret output, there must be a compelling advantage to their use over established stochastic and probabilistic methods of wind resource estimation. To that end, this research will assess the performance of wind resource estimates of the MM5 RCM against the performance of traditional estimation methods commonly employed in the wind energy industry.

Finally, the output of the MM5 RCM will be analyzed to determine whether stochastic corrections can be applied to reduce any systematic bias in the estimates produced. Several researchers have raised the question of spatio-temporal accuracy in RCM forecasts of meteorological variables (Colle *et al.*, 1999, Tustison *et al.*, 2001, Mass *et al.* 2002). While a model may produce accurate estimates of a variable, those estimates may be systematically shifted in space-time such that it appears the model has low skill. This research will seek to identify what, if any systematic bias is occurring in the RCM output and attempt to explain the cause of that bias.

Given that the overall goal of this research is to reduce the uncertainty surrounding RCM estimates of a regional wind climatology, it is expected that this research will facilitate the integration of regional-scale dynamical models of the atmosphere into wind farm siting approaches and allow developers to select sites with greater confidence in the wind climatology than had previously been available from *a priori* approaches. Such research is especially relevant to regions where wind observation networks may be too sparse to achieve a meaningful wind energy climatology.

Chapter 2. Literature Review

As was discussed in the previous chapter, the accurate estimation of the wind resource of a location is of critical importance to the success of any WECS installed there. The capital costs of installing a wind turbine or wind farm are currently estimated to be about $1000 US per kilowatt of energy capacity (IEA, 2001). Thus, simple economics dictate that if the wind resource at a location is deemed insufficient for the profitable production of electricity, the site ought not be considered for WECS development. In addition to the consideration of the overall wind resource at a location, it has become increasingly necessary to more precisely specify the resource in terms of its distribution. This is largely due to the fact that turbine manufacturers such as Vestas or GE now offer a series of wind turbines, each specifically designed for different wind climatologies such as lighter or more variable wind speeds (Filtenborg, 2004). Also, as the number of WECS installations increase worldwide, there is growing interest in exploiting wind resources in more remote locations; locations that may not have adequate wind measurements.

To those ends, most research directed toward wind energy climatology has focused on accurately estimating the statistical properties of the wind at a location or over a region, providing robust estimations of the distribution of those winds, and the estimation of wind regimes in locations for which there exist few or no data. Within the context of this research, a discussion follows of the advances and limitations offered by prior work in this area.

2.1 Wind Resource Identification and Analysis

The goal of wind resource estimation in the context of wind energy conversion is to reproduce the statistical properties of the long-term wind field at a "candidate" location, or over a geographical area such that errors between the observed wind climatology and that which is estimated are minimized. Thus, nearly all wind energy climatological analysis is concerned with either statistical evaluation or modeling the resource, or most frequently, both. Unfortunately, while the use of wind as a source of power is not a recent idea, it was not really until the energy crisis of the 1970s that it became the focus of substantial scientific investigation. As such, little research on wind climatology is known prior to that time period.

A number of early works (*e.g.*, Putnam, 1948, Dinkelacker, 1949, Golding, 1955; Hewson, 1975, Justus *et al.*, 1976, Hennessey, 1977, Widger, 1977) sought to examine the statistical properties of winds at locations where there existed relatively long (10-30 years) records of wind observations. Much of this work assumed that the locations at which one might wish to consider a wind turbine installation were rural or remote locations at which the wind record was sparse at best. Thus, from the beginning most research has sought to evaluate and summarize the wind regime at locations where the wind data must be estimated prior to undertaking a summary analysis. Whether a researcher is concerned with evaluating the wind at a specific location or over a wide area, both methodologies involve interpolative modeling.

Even the earliest approaches (*e.g.*, as discussed in Putnam, 1948), recognized that the properties of wind within the boundary-layer were such that the wind at a location could not simply be assumed equivalent to the wind measured at a nearby anemometer. The primary reason is the effect of localized variations in surface conditions and atmospheric modifications operating on spatial scales less than the distance between the two points, such as thermal and mechanical turbulence. A thorough discussion of the influence of many of these small-scale effects can be found in such boundary-layer references (*e.g.*, Oke, 1988; Geiger *et al.*, 1995; Stull, 1999; Arya, 2001).

However, it is also well known that the winds at all levels are driven by the overlying pressure gradient that exists at much larger (synoptic and even global) scales (Panofsky, 1958; Wallace and Hobbs, 1977). Thus, while not equivalent, the winds at one location will tend to be somewhat related in space and time to winds at a nearby location. It is this assumption that has driven most empirical estimation techniques developed for wind resource estimation.

2.1.1 Properties of the wind field

In order to instigate a model of winds at a location or over a region, it first is necessary to understand the properties and behavior of the wind resource as it pertains to wind energy conversion. On this point there exist a number of useful references.

2.1.1.1 Statistical measures

The properties of the wind field over a location or region have been known for some time. Putnam (1948), Dinkelacker (1949), and Golding (1955) each address many of the aspects of the wind field that are important to wind energy conversion. Among the most important in their estimation were the mean and standard deviation of the wind speed. Although the direction of the wind is important from a climatological standpoint, it is generally less critical for wind turbine operation in that even the earliest turbines were mounted on a pivoting gear that allowed for their continual orientation into the wind (Putnam, 1948). Thus, initially the variability of the wind direction was solely important as a measure of stress on the pivot gear. Greater directional variability meant the turbine would be shifting direction more frequently to capture the wind. More recently, with the implementation of complex models for wind speed estimation, knowledge of the wind direction has become critical (*e.g.*, Walmsley *et al.*, 2001).

Although a number of notable works, primarily wind energy atlases (*e.g.*, Elliott *et al.*, 1987 and Troen and Petersen, 1989) have focused on estimating and presenting the mean and standard deviations of wind speed and power over large regions, they have not been limited to those variables. The mean and standard deviation of wind velocity are now recognized as rather basic reference statistics of somewhat low utility to wind energy conversion (Justus *et al.*, 1976). Instead, the extractable wind power is largely a function of not only the wind speed, but also the distributions of those speeds. Rohatgi and Neslon (1994) present an excellent overview on the characteristic relationships between the wind resource and wind power.

In order to derive total potential power of the wind, it is only necessary to have information on the wind speed and the air density. From Equation 1.1, if area A is set to 1 square meter, the power contained in a square meter of wind will be equivalent to half the quantity of the air density times the cube of the wind speed, with resulting units in Watts. Because of its exponential relationship with wind speed, this formulation more heavily weights strong winds. This relationship is well described in Shein (1995). Unfortunately, this power also is of limited utility, for wind turbines are incapable of utilizing the entire spectrum of wind speeds with maximum efficiency. Appropriate estimation of wind power requires the calculation of extractable power, not only as a function of wind speed, but also as a function of the extraction performance of the turbine itself. This latter factor relies heavily on the capacity of the turbine and its performance through the various portions of the wind speed distribution.

2.1.1.2 Wind speed distributions

Justus *et al.* (1976) properly addressed this issue by examining the distribution of wind speeds relative to an idealized turbine operation curve (such as is presented in Figure 1.1). In such a curve, a turbine does not operate when wind speeds are below its so-called cut-in threshold (normally about 3 or 4 m s^{-1}). Above that threshold, the turbine will produce only an exponentially incremental proportion of its maximum power until wind speeds reach the turbine's rated speed (normally around 12 m s^{-1}). Between this speed and an upper threshold, the turbine will produce its rated power. But when wind speeds exceed the upper rated threshold (often called the cut-out speed; about 25 m s^{-1}), the turbine will cease operation to prevent wind related mechanical damage. Thus, any wind speeds below the cut-in or above the cut-out speeds are lost to power production, and thus the actual convertible wind power at those speeds can be set to zero. As an example, a calculation of potential power over the rated speed range (12-25 m s^{-1}) yields 1,037 W m^{-2} to 9,375 W m^{-2}. Assuming a turbine with 1 megawatt (MW) of rated power sweeping an area of 5,027 m^2 (40 m rotor radius), the potential power of the wind through the turbine blades ranges from 5.22 MW to 47.13 MW. Even after factoring in the Betz limit (as discussed in the previous chapter) of 59% extractability, the potential wind power is 3.08 to 27.8 MW. The turbine, limited to 1 MW output at all rated speeds converts only from 4% to 32% of the available wind power. The rest of the power is simply not extractable by the turbine. The same relationship holds true for the range of speeds between the cut-in and rated speed. Thus is it perhaps more appropriate to describe the power contained in the wind as a function of the actual power produced by a turbine, or, in the absence of that, to examine the distribution of the wind speeds relative to an idealized power curve, as described by Justus *et al.* (1976).

As a result of the importance of variable power output relative to wind speed, the investigation of wind speed distributions has rightly occupied a substantial portion of wind power climatology research. Even prior to the surge of interest in wind energy applications in the 1970s, a number of early works addressed wind speed frequency distributions. Dinkelacker (1949), for example determined a Plank distribution to be appropriate for wind speeds in Germany. Crutcher and Baer (1962) enjoyed some success fitting a bivariate normal distribution instead. However, Smith (1971) and later Hennessey (1977) correctly noted that the bivariate normal distribution involves mathematical complexities that limit its utility for wind energy applications. It should also be noted that under certain circumstances, the bivariate normal distribution can be simplified to a Rayleigh distribution (Hennessey, 1977). In 1948, Putnam had suggested that wind speed distributions could be approximated with a Pearson Type III distribution, more commonly known as a Gamma distribution. Sherlock (1951) corroborated the utility of this distribution. Although it took approximately two decades, in the mid-1970s a number of researchers converged upon a special two-parameter case of the Gamma distribution known as the Weibull distribution (Weibull, 1951) that had been used extensively in engineering failure analyses.

Because of its two (and occasionally three) parameters, the Weibull distribution quite often provided more accurate fits to empirical data. The aforementioned Rayleigh distribution is actually a special case of the Weibull distribution. It appears that the earliest known application of the Weibull distribution to near surface wind speed was Davenport (1963), who used the distribution to discuss wind loadings on buildings. Among the first studies to investigate the use of the Weibull distribution for wind speeds in the context of wind energy research was Justus *et al.* (1976) who compared the Weibull distribution to a lognormal distribution (as had been employed with success by Luna and Church, 1974) and found it to be superior.

Since 1976, the Weibull distribution has gained wide acceptance among wind energy researchers (*e.g.*, Justus *et al.*, 1976, Hennessey, 1977, Corotis *et al.*, 1978, Brown *et al.*, 1981, Conradsen *et al.*, 1984, Poje and Cividini, 1988; Wieringa, 1989; Beyer and Nottebaum, 1995). Even though a particular wind speed distribution cannot automatically be assumed to follow a Weibull distribution, the Weibull probability density function (elaborated upon in Chapter 3) is versatile enough to accommodate a great many of the unimodal, zero-bounded distributions of wind speed that could conceivably be found in nature. To that end, even a distribution that approaches normality (save for the zero bound) can be adequately approximated by a Weibull distribution by setting the shape parameter equal to 3.7.

2.1.1.3 Data collection

In addition to providing a description of the wind resource in terms of summary statistics and probability distribution functions, there are the added issues of the collection and behavior of the resource itself. If the data are of low quality or not representative of the true winds at a location, any resulting analysis will be suspect. Because this issue is quite involved, and has been addressed in other notable works (*e.g.*, Peterson *et al.*, 1998a) it will only be cursorily summarized here.

In terms of wind data, there are three areas in which measurement error can be introduced. The first is from the instrument itself. Although a number of instruments are available to a wind researcher, including pressure plates, pitot tubes, and more recently, propeller vanes and thermal and ultrasonic anemometers, the three-cup anemometer has emerged as the most widely used anemometer for wind speed information (Fritschen and Gay, 1979, Wyngaard, 1981, Beljaars, 1987, Kristensen, 1999). The three-cup anemometer has been widely utilized since its invention in 1846 and is prized for its robustness and reliability (Kristensen, 1999). While two notable shortcomings of the cup anemometer are its threshold speed (the speed below which the momentum of the wind is insufficient to initiate rotation) and a tendency for the anemometer to over-speed in higher wind speeds (Kaganov and Yaglom, 1976, Wyngaard, 1981, Kristensen, 1999, 2002), it is the nature of the observation (wind power production) that largely negates these shortcomings in the data collection (Palutikof *et al.*, 1984). Thus, if the anemometer being utilized is properly maintained and calibrated, instrumental error in wind resource research using data collected by such instruments can generally be considered inconsequential.

A second issue related to wind data collection is the representativeness and homogeneity of the data. Although a great deal of research has been done in the area of wind resource analysis, very little has examined how representative a wind observation is of the true wind regime over the immediate vicinity. With specific mention to wind, Wieringa (1980) examined the regional representativeness of winds measured by anemometers at airports and found that, with the exception of locations where the wind field was modified by local terrain or other obstacles, measurements were indeed representative of the immediate vicinity. However, Shein (1995) noted that at several airport locations in the Midwest United States, anemometers were placed in locations where the wind field would be at least partially biased by obstacles. It is assumed, based on the criteria set forth for the new generation of automated surface observing systems by the US Federal government (OFCM, 1994) and later refined by the Federal Aviation Administration (FAA, 1999) and the National Oceanic and Atmospheric Administration (NOAA, 2000) that such unrepresentative siting has been since rectified.

Furthermore, if one examines the station histories of many of the anemometers used in wind resource studies to date, one will often find a history filled with discontinuities associated with station relocations and anemometer height adjustments (Shein, 1995, NCDC, 1994a and b). Thus it is often necessary to adjust the observed data from one height to another in order to standardize it (Peterson *et al.*, 1998a, Robeson and Shein, 1997, Klink, 1999). If information on roughness length is available, the log-wind profile can be used to adjust the wind speeds from one height to another (Tennekes, 1973). Where this information is unavailable, the wind speed power law is utilized (Touma, 1977, Petersen and Hennessey, 1978). Invariably, either adjustment will introduce some bias into the observations as both provide estimates of wind speed at the adjusted height. Again, OFCM (1994) prescribes a set of anemometer siting standards that set the height at the World Meteorological Organization standard of 10 m (although procedures for station relocation are not discussed).

Much of the bias in empirical methods of low-level wind vector estimation can be attributed to a failure to appropriately account for the boundary-layer dynamics (*e.g.*, stability, turbulence, thermal structure, roughness) that modify the wind vector from one location to the next and from time t to $t+1$. Furthermore, each of these boundary-layer conditions acts on the wind at different temporal and spatial scales, resulting in a wind vector response at certain scales more so than others. Thus, the scale at which the data is collected, both spatially and temporally is important.

In general, the collection of data on wind speed and direction has, like most meteorological data collection, been limited to heavily populated areas. However, the most favorable locations for wind energy conversion systems are those regions with strong but steady winds. These areas generally tend to have low populations or may be devoid of people altogether (*i.e.*, offshore) and thus contain sparse and irregular networks of meteorological observation stations (*e.g.*, Willmott *et al.*, 1991; Robeson, 1993; Klink, 1999). As such, the spatial scale of observations of wind may be on the order of 100 km. Any variations in surface roughness, albedo, obstacle height or density, or terrain at scales below that of the network density will generate smaller scale influences on the regional wind field that would be invisible to the observation network (Tetzlaff, 1984).

The same consideration is important for the temporal resolution of the network. Van der Hoven (1957) describes a number of significant signals within the wind speed spectrum. If the sampling interval is too small, the signal will be dominated by the noise of localized influences such as thermal and mechanical turbulence and be useless to wind power estimation. If the sampling interval is too large, a number of regional or synoptic signals of critical interest to a wind resource modeler (*e.g.*, the diurnal cycle or a sea breeze circulation) would not be resolved by the data. Most wind energy research has settled on the use of hourly wind observations as a good tradeoff between the reduction of localized "noise" and the capture of the majority of regional signals. However, it is unclear whether this hourly temporal resolution is selected by choice or simply because a majority of wind observing stations collect observations at this resolution.

2.1.1.4 Serial correlation and stationarity

As interest in modeling wind speeds and wind speed distributions has grown, other statistical properties of the wind have gained importance. These properties, such as serial correlation and stationarity, are most important in stochastic model construction, but also are critical in the statistical evaluation of model performance.

As a result of wind being a continuous field, serial correlation in wind speeds exists in both space and time. To that end, a wind speed observation at a specific place or time cannot be truly considered independent of the wind speed that was observed at a preceding time or an adjacent place. Serial correlation in space is the measure of covariance between simultaneous observations from adjacent locations, often as a function of the distance between them (Davis, 1986). Temporally, serial correlation, also called autocorrelation, is the measure of covariance between sequential observations at the same location, and is a function of the time between observations (Wilks, 1995). Terrain complexity plays a large deterministic role in the degree of serial correlation, both spatial and temporal. Spatially, as local terrain and obstacle influences tend to modify near-surface flow rather rapidly (depending on surface complexity), the modified flow will appear to be less related to the flow measured at an adjacent station as the distance between the stations increases (Steinitz *et al.*, 1971, Wylie *et al.*, 1985). At distances more than a few kilometers, most of the synoptic and diurnal thermal signal that is manifested as serial correlation appears to be lost in localized noise (Wylie *et al.*, 1985, Robeson and Shein, 1997, Toriumi *et al.*, 2000). Thus, for most wind resource studies, where stations typically are tens if not hundreds of kilometers apart, spatial serial correlation is generally minor and usually ignored. In addition, Robeson and Shein (1997) also have demonstrated that temporal sampling intervals also play a critical role in determining spatial coherence (*i.e.*, distance decay of serial correlation).

Temporal autocorrelation of winds also has been explored in the literature (*e.g.*, Wylie *et al.*, 1985, Brett and Tuller, 1991) and found to be rather substantial at short lags. Like with space, serial correlation in time is largely a function of the distance (in this case the temporal distance between observations) and the relative influence of the local terrain. A number of works have examined the behavior of wind speed at various sampling intervals and have found that shorter sampling intervals tend to capture a greater amount of the temporal autocorrelation, up to a point (Beljaars, 1987). Beljaars (1987) confirmed Fiedler and Panofsky's (1970) assertion that a sampling interval of 10 minutes represents the boundary of the spectral gap dividing the synoptic signal and local turbulence. At higher frequency sampling intervals, temporal autocorrelation drops as local turbulent influences dominate. Furthermore, Shein (1995) noted that both spatial and temporal autocorrelation became incoherent at aggregation intervals greater than daily. Thus, it appears that the greatest temporal autocorrelation appears in wind observations where the sampling or averaging interval is between 10 minutes and 1 day. Additionally, Brett and Tuller (1991) and Shein (1995) have demonstrated that temporal autocorrelation at the hourly level is often quite high (*e.g.*, around 0.9) at a lag of one hour, but decreases rapidly with subsequent time intervals. Brett and Tuller (1991) also indicated that lag 1 temporal autocorrelation also decreases noticeably as the surrounding terrain becomes less homogeneous, indicating a decrease of synoptic influence. Unfortunately, most wind studies utilize either hourly or three-hourly observations and lag 1 temporal autocorrelation values remain high, even in relatively complex terrain. However, work in autocorrelation modeling and statistical testing (*e.g.*, Bayley and Hammersley, 1946, Box and Jenkins, 1976, Wilks, 1995) has provided methods for computing "effective" sample sizes that compensate for the dependence induced by serial correlation in a data series. Wilks (1995) also describes a variance inflation factor that can be used to estimate the time interval between "effectively independent samples." Often the autocorrelation in the wind speed itself is used as a modeling tool as with Markov chains (*e.g.*, Dukes and Palutikof, 1995) or with autoregressive models (*e.g.*, Brown *et al.*, 1984).

Non-stationarity is another issue in wind speed modeling. It refers to a mean value that is changing as part of a trend, linear or otherwise, over a given period of time or a given area of space (Cressie, 1993). Non-stationarity often is referred to as drift or anisotropy. The difficulty with non-stationarity is that most statistical procedures for evaluating a series of data in either space or time are invalidated by non-stationary data.

Put simply, most statistical procedures rely on an unchanging mean (Box and Jenkins, 1976, Davis, 1986). A trend in the mean of the data over space or time represents a systematic behavior and a level of dependence to an external factor. Thus, any change in the mean over space or time must either be accounted for, as in a model, or removed prior to statistical evaluation to ensure stationarity. For example, in the kriging work of Haslett and Raftery (1989) or the time-series modeling of Brown *et al.* (1984), the spatial and temporal drift in wind speeds was determined to be significant and had to be accounted for as part of the resulting models to ensure that the residuals would be independent and randomly distributed.

2.1.1.5 Resource variability

Lastly, while the standard deviation of the winds about a mean value, and the wind speed frequency distribution hint at the degree of variability inherent to the data, these measures do not reveal longer-term behavior in the resource. In fact, the idea of a single statistic such as standard deviation, or a single distribution encompassing all available data implies an assumption that the data are indeed stationary and unchanging in time. A number of works have clearly demonstrated that this is not the case (*e.g.*, Haslett and Raftery, 1989, Palutikof *et al.*, 1986, 1987, 1993, Shein, 1995, Klink, 1999).

Palutikof *et al.* (1987) for example, showed that mean wind speeds at a single station in the UK varied between 5.2 and 7.3 m s^{-1} over a period of 56 years. Klink (1999) corroborated work by Shein (1995) that the variability of wind speeds about the annual mean also could not be considered constant. All of the aforementioned works also demonstrated that the interannual variability in winds at a location are not necessarily consistent over the surrounding region. Klink (1999) noticed that interannual variations in mean and variability had a strong seasonal component, implying that seasonal changes in surface roughness, and thus local changes may exert a large influence. Palutikof *et al.* (1986, 1993) alternatively suggested that a portion of the non-stationarity in wind records is likely due to external forcings such as larger-scale climatic change. Spatially, Carlin and Haslett (1982) looking at wind speed distributions concluded that the variability from station to station was such that a Weibull distribution fit to one station was not necessarily transferable to other locations.

However, despite the aforementioned evidence of long-term variations in wind speed, other researchers claim the degree of variability is statistically insignificant for resource analysis. Golding (1955) for example, referencing the same observation station as Palutikof *et al.*, (1987) – Southport (UK) – indicated that annual means of 37 of the years of record were within 10% of the long-term mean. Justus *et al.* (1979) and Corotis *et al.* (1977) further corroborate (to a 0.1 confidence level) that annual mean wind speeds at a location fall within 10% to 18% of the long-term mean. However, neither of these researchers investigated the presence of trends or long-term cycles in their data, thus ignoring the possibility that the reported deviations might not be constant in time. For example, both Shein (1995) and Lun and Lam (2000) demonstrate that certain trends in Weibull parameters exist over long periods of data.

Clearly, no model or statistical evaluation of the wind resource at a location or over a region can ignore any systematic behavior such as longer-term or spatial variability in the data and be capable of achieving robust or unbiased results. Additionally, the presence of longer-term or spatial variability raises the question of how much data and how dense a network is necessary to accurately address the wind resource. Concerning temporal series lengths, Justus *et al.* (1979), based on their aforementioned results concluded that longer periods of record do not significantly increase estimation accuracy, and thus are unwarranted. However, despite this assessment, there remains some debate in the literature surrounding how much data is needed to assess the long-term wind resource at a location. Estimates range from as low as less than 1 year (Barros and Estevan, 1983) up to 20 years (Petersen *et al.*, 1998a). General consensus in the literature is that 1 year is a minimum amount, with 3 to 10 years being the standard, and if examining longer-term variability (*e.g.*, Palutikof *et al.*, 1987) several decades are mandated.

Commonly, models have been used to stochastically generate longer, synthetic series of data at locations where the researcher feels the observational record is too short (*e.g.*, Justus *et al.*, 1979, Haslett and Raftery, 1989, Derrick, 1992, Hannah *et al.*, 1992, Dukes and Palutikof, 1995, Garcia-Rojo, 2004). In general, it is these models that form the basis of most wind energy resource estimation and thus are discussed in the next section on wind resource modeling. However, one of the primary shortcomings of these models is that they attempt to correlate data between stations that may be some distance from one another.

Spatially, sparse anemometer networks have always presented a problem. Although there may well exist a systematic relationship between two stations, it is likely to be of low signal strength and obscured by irresolvable local noise generated at the sub-network scale (*i.e.*, at distances less than the distance between stations). The spatial decay of this spatial serial correlation, which ultimately forms the basis for most stochastic resource models, decays rapidly with distance, even over relatively homogeneous terrain (Robeson and Shein, 1997). While the local influence on a wind speed record at two adjacent locations might be empirically deduced, it becomes a much more complex issue when the model attempts to interpolate at too many locations or continuously over a larger region (*e.g.*, Nielsen, 1999). To that end, some researchers have sought out more spatially continuous alternative wind data such as those derived from satellite sampling (Pryor *et al.*, 2004) or gridded geostrophic wind fields (Palutikof *et al.*, 2002), relegating anemometer-based observations to model validation. Dynamically-driven, numerical climate models represent an alternate approach (*e.g.*, Pielke, 1985, Draxler, 1990, Ayotte *et al.*, 2001, de Rooy and Kok, 2004). Currently however, the majority of research using numerical models is focused on forecasting wind velocities rather than estimating wind characteristics over extended periods of time (*e.g.*, Perez *et al.*, 2003). This research seeks to rectify that deficiency.

2.2 Statistical Wind Field Modeling

The preceding section discussed the basis for evaluating the wind regime over a location or an area. These aforementioned considerations subsequently lay the groundwork for most modeling efforts that have been developed to describe wind resources. Methods for estimating the wind resource can be divided into three categories or types, which are not mutually exclusive: stochastic models, probabilistic models, and dynamical models. Strictly speaking, probabilistic models are also stochastic in that they are based on empirically-estimated parameters, and many models that are described as 'stochastic' function only with the proper specification of an underlying frequency distribution. Thus, although they are separated for clarity in the subsequent sections, most models share some underlying theoretical background and are not exclusive to those categories.

2.2.1 Stochastic models

Much early work on wind resource estimation involved the development and use of stochastic models. Early attempts to estimate the wind at a candidate location were largely parametric and usually limited to the identification of a long-term mean wind speed (*e.g.*, Hewson, 1975, Baker *et al.*, 1979, Justus *et al.*, 1979). Because the variability of the wind was largely ignored, it is not surprising that these early models met with only limited success and utility.

Among the earliest stochastic methods were so-called method-of-ratios, or climatological reduction approaches (Putnam, 1948, Conrad and Pollack, 1962). This approach estimates the long-term mean wind speed at the candidate site from the linear relationship between short-term records at the candidate site paired to observations at nearby anemometers having longer observational records. Climatological reduction is the forerunner of the more recent Measure-Correlate-Predict model that will be discussed later. The reduction approach was further advanced by Feller (1966), who incorporated the idea that spatial cross-correlation could be used to identify and give preference to those neighboring stations that shared the greatest similarity with the short record at the candidate site. A major shortcoming of the reduction method is that it relies heavily on the quasi-stationarity of observational anomalies at both the candidate location and the anemometer location (Justus *et al.*, 1979). As was previously mentioned, in most cases the behavior of wind speed is heavily influenced by autocorrelation, non-stationarity and cyclical influences (*e.g.*, diurnal and seasonal signals), the behavior of which may be non-linear and vary substantially from one location to another, even over small distances (Justus *et al.*, 1979).

Stochastic models of wind resource estimation have more frequently trended toward regressive type models that take advantage of the known dependence of either the observations to previous observations in time (autoregressive models), the relationship between observations at one location and another (correlation models), or a combination of the two. Autoregressive models were originally developed to forecast the behavior of economic indicators (Box and Jenkins, 1976), but their versatility toward any variable that demonstrated a temporal dependence tendency, such as wind, was quickly discovered (Katz and Skaggs, 1981).

Among the first researchers to examine the use of autoregressive (AR) models for wind speed estimation were Goh and Nathan (1979), but they met with limited success due in part to their assumption of a stationary Gaussian wind speed distribution. Chou and Corotis (1981) rectified this issue by employing a non-stationary Weibull function as the underlying distribution. However, a difficulty with early AR models, such as that developed by Eidsvik (1981) was the lack of explicit inclusion of a diurnal cycle. As such, early AR models were clearly not parsimonious at orders of 24 hours and greater (Eidsvik, 1981). Following early attempts, McWilliams and Sprevak (1982) and Brown *et al.* (1984) presented AR model approaches that took both a non-Gaussian distribution and diurnal cycle into account and constructed second order autoregressive models that used the autocorrelation function and diurnal signal to transform the data into a stationary Gaussian distribution that could be more accurately estimated. Haslett and Raftery (1989) developed an autoregressive-moving average model to estimate long-term wind power potential at several locations in Ireland, with good success. Similar regression model approaches have been undertaken by Goh and Eu (1986), Hannah *et al.* (1992), Sfetsos (2000), Walmsley *et al.* (2001), and Milligan *et al.* (2003). Finzi *et al.* (1984) elaborated upon the AR model by including the 500 mb geopotential height (as a measure of geostrophic flow) and found success in forecasting winds over the Po Valley. Additionally, Haslett and Raftery (1989) extended their autoregressive modeling into the spatial domain, developing a Krige model to estimate long-term resources over the entire country of Ireland.

Unlike autoregressive models, correlation-based models do not model nor imply dependence of a wind speed record upon itself. Rather, these models attempt to statistically assess the systematic covariance between two separate wind speed series. In doing so, such models seek to develop a relationship that describes and exploits the similarities of the two series in order to synthetically extend the length of one to the limits of the other (Sansom and Tait, 2004). As such, correlation models have found a great deal of favor and use in wind resource estimation, primarily due to the sparse networks of anemometer stations normally available to researchers (*e.g.*, Barros and Estevan, 1983).

Correlation models take several forms and can be both stochastic as well as probabilistic. Although spatial correlation is discussed in Putnam (1948) and Golding (1955), it is not until Walmsley and Bagg (1978) that a spatial correlation model for wind appears in the literature. Walmsley and Bagg used a correlation matrix from a short record of data and multiplied it by longer series data to develop synthetic data series at the locations in their study. Gunst (1995) described several methods for spatially correlating multiple meteorological variables, including optimal spatial-averaging. Gunst pointed out that the discounting of non-stationarity and autocorrelation limited the utility of most spatial correlation methods.

In 1992, Derrick developed what he called a Measure-Correlate-Predict (MCP) model. Since then, this type of model has become a standard tool in wind resource analysis. Derrick (1992) separated by direction, paired observations of wind at two stations. For each direction, a linear regression equation was fit to the data, using the data from the long-record station as the predictor, and the data from the shorter-record station as the predictand. From these equations, a long-term synthetic series could then be generated at the short-record location given the speed and direction at the long-record station. There are a number of limitations to the implementation of such a scheme, including the distance between the stations involved, the potential non-linearity of the relationship, and the potential for the relationship to vary in time. Additionally, Van Lieshout *et al.* (2004) note that the MCP did not perform well in complex terrain. However, since its formal introduction, most spatial correlation techniques have utilized some variation of an MCP approach (*e.g.*, Gerdes and Strack, 1999, Salmon and Walmsley, 1999, Toriumi *et al.*, 2000). Related alternatives to MCP are a similar joint-probabilistic approach or a categorical probabilistic adjustment which are discussed in a later section.

An area of recent increased interest is in the use of artificial neural networks (ANN) for the spatial correlation of wind speeds. A number of researchers have experienced moderate success in their development and application of ANNs to near-surface wind speeds (*e.g.*, Kariniotakis *et al.*, 1996, Alexiadis *et al.*, 1998, 1999, Pinson *et al.*, 2003, Kretzschmar *et al.*, 2004). However, while this approach may provide accurate results, it is used primarily in wind energy forecasting rather than the estimation of a wind resource climatology and thus is of limited relevance to this research. Additionally, subsequent replication of this method can often be confounded when the physical underpinning of the so-called hidden layers of the ANN model are not clearly described.

Often a researcher requires an estimation of the properties of the long-term wind resource over a region rather than at a specific location. As such, a logical extension of spatial correlation methods is to apply the methods to either a series of regular (grid) locations over a region in order to develop a continuous surface (*e.g.*, Haslett and Raftery, 1989), or to utilize the information at existing locations to specify a regional value that abuts other regional values to form a continuous surface (*e.g.*, Goodin *et al.*, 1979 or Nielsen, 1999).

However, rather than estimating synthetic series at hundreds or thousands of grid points over a region, most all spatial fitting techniques used in wind resource estimation focus on the more economical fitting of the statistical parameters of the wind record, such as the mean or variance. There exist a number of methods for providing this spatial interpolation. Techniques include inverse-distance weighting (Sherman, 1978, Goodin *et al.*, 1979, Palomino and Martín, 1995), kriging (Haslett and Raftery, 1989), and optimal spatial interpolation (Julian and Thiebaux, 1975; Thiebaux, 1975). However, many of these models are hampered by relatively sparse anemometer networks (Goodin *et al.*, 1979). If interpolation must take place over large areas and long distances, local interstation effects on wind speed (and associated errors), although important, will be not be resolved.

Interest in including terrain effects in spatial interpolation models of wind speed has led to a number of advances in improving spatial estimations. Developments in this area include an elevation difference variable incorporated into an inverse-distance weighting scheme (Palomino and Martín, 1995). Taylor and Lee (1984) present a comprehensive work regarding the theory and applications of flow over low hills. Flow over more complex terrain, however, is not as well understood, although significant advances have been made (*e.g.*, Gunn and Furmage, 1976; Sherman, 1978; Weber, 1990, Ayotte *et al.* 2001).

2.2.2 Probabilistic models

Because of the importance of the distribution of wind speeds to wind power production, it is not surprising that a majority of wind speed models have been of the probabilistic type. The appeal of probabilistic models is largely a result of their ability to reduce a broad spectrum of wind speeds to just a few parameters that, in turn can be utilized to estimate wind power at a location. In their simplest form, these are models that seek to fit a theoretical probability distribution to observed data at a location. The transformation from an empirical to a theoretical distribution more readily facilitates a statistical analysis of the distribution. More complex approaches attempt to develop correlations in distributions between stations in order to produce a regional wind distribution estimation (e.g., Justus *et al.*, 1976, Haslett and Raftery, 1989).

Among the simplest probabilistic techniques used in wind resource analysis are so-called Monte Carlo simulations such as Markov chains (*e.g.*, Sahin and Sen, 2001). These methods utilize either the empirical probability density function of the observed data or the transitional probability of one observation to the next to generate a synthetic series with the same underlying distribution as the original data and the same transitional probabilities between events. Such methods have been used with success by many researchers. Kaminsky *et al.* (1991) for example, used a "one-step" Markov chain to simulate high frequency wind speeds. Unfortunately, such models appear to underestimate the probability of low frequency events (Dukes and Palutikof, 1995). Dukes and Palutikof (1995) used a similar approach to generate an hourly-averaged wind speed series as well as 3-second gust information. Others who have utilized Markov chain approaches include Sahin and Sen (2001) and Nfaoui *et al.* (2004), but it appears from the literature that such approaches are less preferable than modeling empirically-fit theoretical probability distribution functions to observed series.

As has been mentioned earlier in the chapter, there has been a wealth of research devoted to accurately specifying the generalized distribution of wind speeds. A number of potential distributions have been investigated, including the Gaussian (or so-called normal) distribution (Justus *et al.*, 1979, McWilliams and Sprevak, 1982), the inverse

Gaussian distribution (Bardsley, 1980), a truncated normal distribution (Al-Alawy and Mohammed, 1985), and a log-normal distribution (Luna and Church, 1974). However, as has been discussed, the simplicity and versatility of the Weibull variant of the Gamma distribution eventually was identified as the most versatile option for continued model development (Corotis *et al.*, 1978) and has been repeatedly proven to provide an acceptable fit to a wide variety of wind speed distributions (*e.g.*, Justus *et al.*, 1976, 1978, Corotis *et al.*, 1978, Hennessey, 1977, Brown *et al.*, 1981, Carlin and Haslett, 1982, Conradsen *et al.*, 1984, Rainbird *et al.*, 1996, Torres *et al.*, 1999, Quine, 2000, Celik, 2003). As a result, it has received widespread use in estimating the wind resources of a variety of locations.

If long records of wind speed data are available at a location (or locations), the fitting of a theoretical probability distribution, like a spatial correlation method, becomes unnecessary for describing the wind resource. An empirical distribution of the data record will suffice and summary statistics may be produced. The utility of fitting a Weibull probability density function to the data occurs when the data at a location are not of sufficient length, or perhaps non-existent. In these cases, a Weibull probability model may be estimated from available data at a location or interpolated from the data of a nearby location. These techniques generally follow the spatial correlation and interpolation methods described previously.

Using Weibull probability models, researchers have estimated the wind resource at locations worldwide. For example, Merzouk (2000) used the Weibull distribution to estimate the wind power potential at 64 locations in Algeria and surrounding countries. Poje and Cividini (1988) performed a similar Weibull analysis of locations in Croatia. Perhaps the greatest use of the Weibull function in wind resource analysis work is with respect to the numerous wind resource atlases that have been produced over the past three decades (*e.g.*, Elliott *et al.*, 1987, Troen and Petersen, 1989). Weibull modeling has been used extensively in the case of the European Wind Atlas (Troen and Petersen, 1989).

In the European Wind Atlas, a noteworthy Weibull model was utilized. The model is known as the Wind Atlas Analysis and Application Program, or WAsP (Petersen *et al.*, 1984, Mortensen *et al.*, 1993). WAsP is primarily a probabilistic model because its basis is a Weibull distribution. However, the versatility of WAsP lies in the numerical way in which it migrates a distribution calculated at one location to estimate the wind resource at another location from which no data are available. WAsP accomplishes this by first separating wind speed data from established anemometer locations into 12 directional bins. These distributions are then upscaled to be regionally representative (in an area of approximately 100 km radius surrounding the station) by applying numerical transfer functions that are designed to remove the station observation bias introduced by local surface roughness, sheltering obstacles and local orography (Troen and Petersen, 1989). The adjusted observational series is then used to estimate a regionally representative Weibull distribution. Transference to another location within that 100 km radius is then accomplished by reversing the model and adding in local characteristics for the new location. Troen and Petersen (1989) note that the greatest con

hon

2.3

ap

fo

fo

pr

re

w

f

p

confidence in WAsP results is obtained in regions of relatively low complexity and high homogeneity.

2.3 Dynamical Models

The alternative to the aforementioned stochastic, probabilistic and empirical approaches to wind resource estimation is the use of a numerical model to estimate and forecast wind vectors. Due primarily to computing limitations, early work in this area focused on the use of primitive equation general circulation models of the atmosphere to provide low-resolution (*e.g.*, greater than 2° Latitude by Longitude) estimates of the wind resource at relatively coarse time intervals such as 12- or 24-hours. When the objective was to simulate higher resolution (both spatially and temporally) wind fields, generally for forecasting, more compact mesoscale atmospheric models were employed, and their potential usefulness in wind research has been explored (*e.g.*, Pielke, 1974; Sherman, 1978; Diab and Garstang, 1984; Rohatgi and Nelson, 1994; Frank *et al.*, 2001) though seldom in the context of wind climatology.

Regional climate models were developed in response to the climate modeling community needs for physically-based dynamical models of the atmosphere that were capable of running on a much finer resolution grid than general circulation models (Williamson *et al.*, 1995; Henderson-Sellers and McGuffie, 1997). These regional climate models, or RCMs, are often nested in the grids of coarser scale general circulation models (GCM) and cover a region that may span only a few thousand square kilometers. As a result, the output from RCMs provides estimates of meteorological variables that potentially are able to resolve some of the small-scale variability inherent in mesoscale meteorological processes and landscapes (*e.g.*, the influence of heterogeneous land cover) that are not available directly from GCM output.

A number of regional climate models have been developed over the past two decades. Most notable are the Regional Atmospheric Modeling System (RAMS) model developed by the National Centers for Atmospheric Research (NCAR) (Pielke *et al.*, 1992), and the 5th Generation Mesoscale Model (MM5), developed by the Pennsylvania State University and NCAR (Haagenson *et al.*, 1994). These models operate by ingesting either observed or modeled data as initialization input and then approximating the mass, energy, and momentum transfer of the atmosphere (on a regular grid) using the so-called primitive equations (Pielke *et al.*, 1992). The grid is three-dimensional and consists of several layers arrayed logarithmically in distance from the surface. Such a grid structure is designed to provide a detailed analysis of the mixed layer near the surface. The application of the primitive equations produces iterative estimates of meteorological variables at each grid point (time steps are often around 15-30 seconds). Temporal averaging is used to generate hourly values for these estimates at each of the layers in the grid. The output of the RCM is a synthetic time series of the variable of interest at each grid point of interest. To that end, an RCM is capable of producing estimates of the wind resource over a region at a relatively high resolution. In fact, it is likely that the density of grid points in an RCM far exceeds the density of the instrumental network in the area.

He

oth

on

ex

m

a

(

S

(

(

However, despite much success in the use of RCMs for the analysis and prediction of other meteorological variables (*i.e.*, temperature, precipitation, cloud cover, pressure), only recently has extensive work been focused on the ability of an RCM to accurately estimate wind speeds over a region.

The most concentrated application of numerical weather prediction (NWP) models to wind energy research has been in the area of wind speed prediction. Although a great deal of work has been done to forecast wind speeds using stochastic methods (*e.g.*, Nielsen, 1998; Alexiadis *et al.*, 1999; Nielsen, 1999; Landberg, 1998, 2001; Sfestos, 2000, 2002), these studies have met with limited success largely due to their empirical nature. Early work using NWP in wind forecasting was performed by Diab and Garstang (1984) who predicted coastal wind speeds with the University of Virginia Mesoscale Model. Draxler (1990) coupled a boundary-layer model to the output from the U.S. NOAA Nested Grid Model (NGM) with limited predictive success. Whiteman and Doran (1993) nested a hydrostatic mesoscale numerical model in a GCM to better predict valley winds. Petersen *et al.* (1998b) outlined the use of NWP models to estimate winds at specific wind farm locations in Denmark, the UK and Greece by dynamically downscaling GCM output to the surface via the High Resolution Limited Area Model (HIRLAM) run by the Danish Meteorological Institute and then accounting for local topography with WAsP.

However, despite the interest in mesoscale numerical models for forecasting winds over a region, few investigations have explored the use of RCMs for wind resource evaluation. An early investigation into RCM wind climatology estimation was Pielke *et al.* (1983), who used a mesoscale numerical model to evaluate pollutant transport over the Chesapeake Bay region. At that time, they felt the method held promise but would require improved model specifications of boundary layer processes. Frank and Landberg (1997) used the Karlsruhe Atmospheric Mesoscale Model (KAMM) to provide input to WAsP and estimate the wind resource over Ireland. Frank *et al.* (2001) covered a larger portion of Europe using the same method. Both Frank and Landberg (1997) and Frank *et al.* (2001) met with moderate success, but agreed that further refinement was necessary to achieve desired levels of accuracy. Unfortunately, none of these investigations evaluated the RCM wind speed distribution estimates directly in the context of the overall wind climatology of the region. It is this point that this research seeks to address by answering the question of whether or not an RCM is directly capable of reproducing the wind climatology over a region with sufficient accuracy such that the climatological statistics produced from the model output can be used effectively by wind farm developers for site selection.

Whereas stochastic and probabilistic models are generally limited in scale to that which can be resolved by the observation network, dynamic models allow spatial and temporal resolution to be identified by the modeler. Thus, scale represents a significant challenge to models attempting to characterize wind vectors for wind energy conversion systems. Critical temporal scales range from decadal periods with climatological information to hourly forecasts. In a spatial sense, wind farm developers often use coarse resolution wind data to identify regions of interest, but then are keen to have a high resolution regional wind map from which to identify prime WECS locations within that region. On the forecast side, point forecasts are desirable for single turbines and wind farms may desire a spatial resolution of less than 10 km. However, several contradictory studies raise questions as to whether or not an increase in spatial resolution will result in a corresponding increase in forecast accuracy (*e.g.*, McQueen *et al.*, 1995, Buckley and Leslie, 2000, Mass *et al.*, 2002). The identification of optimal spatial resolutions for RCMs in the context of wind estimation is something that has to date been largely ignored, even in investigations utilizing RCMs for forecasting wind speeds. The question of what spatial resolutions are optimal is one that is addressed by this research.

2.4 Model Comparison and Validation

Although thousands of models have been developed for climatological analysis and of those hundreds address the wind resource, only a handful of procedures exist that provide robust and reliable evaluations of a model's performance. While some of these procedures can be quite complex, in most cases only simple measures are truly necessary to determine the utility of any given model.

Fox (1981) identifies three groups of data that ought to be compiled to facilitate model evaluation in air quality modeling. Of those, two are applicable to a broad spectrum of models and permit subsequent evaluative measures. These two groups are paired observed and estimated observations for a particular location at a particular time, and

Wi

me

be

es

an

ah

un

ag

no

m

t

(

(

and the empirical frequency distributions of both the observed and estimated data. Willmott (1981, 1982, 1984) and Willmott *et al.*, (1985) present a suite of statistical measures by which a robust and confident appraisal of the performance of a model may be conducted. The measures are the means and standard deviations of the observed and estimated data, the Pearson product moment correlation coefficient (r), the intercept (b_0) and slope (b_1) of a linear regression of the estimated data on the observed, the mean absolute error (*MAE*), the root mean squared error (*RMSE*), the systematic (*RMSEs*) and unsystematic (*RMSEu*) components of the root mean squared error, and an index of agreement (d_2) developed by Willmott (1982). While this set of evaluative statistics is by no means exhaustive, the majority of comprehensive model evaluations in the literature include all or at least some of these measures.

In addition, Wilks (1995) and Murphy (1988) discuss the use of skill scores for the evaluation of forecasting models. Skill scores are used extensively in the evaluation of model forecasts of many and diverse meteorological variables. However, as Murphy (1988) correctly notes, many of these so-called skill scores are based upon the mean square error and, when decomposed reveal the correlation coefficient and measures of the systematic and unsystematic bias in the estimates. Thus, while skill scores can be a useful measure for forecast model evaluation, they are in essence redundant to the more readily interpretable statistics presented by Willmott (1981), which can therefore be considered sufficient for the evaluation of any model concerned with producing estimates of a wind resource climatology as opposed to individual forecast wind speeds.

Chapter 3. Study Area, Data and Methods

3.1 Study Area

The Great Lakes region of North America has seen moderate wind energy development over the past several decades. Commercial wind turbines are operating in all of the states and provinces surrounding the lakes, and the lakes themselves are estimated to have a substantial wind resource (Elliott *et al.*, 1987). As noted in the previous chapter, wind resource potential over much of the land surface portions of the region was originally categorized as low by the United States Wind Atlas, but a number of factors including reanalysis of the wind resource, recognition of localized wind speed enhancements, and advances in turbine technology and siting practices have recently combined to make wind energy conversion in the Great Lakes region an economically viable possibility (Schwartz and Elliott, 2002). In particular, the relatively low surface roughness over the water areas of the region contributes to the generation of stronger winds along coastal and near-coastal areas of the region than had been estimated earlier.

However, despite the promising nature for wind energy development in the region, a major hurdle remains the relative sparseness of wind observing stations. The low number and irregular placement of existing station series limits the quality of any interpolated estimates of the wind at uninstrumented locations. Established meteorological observation stations in the region with recorded wind speeds and direction are, on average, over 100 km apart. Robeson and Shein (1997) showed that in the Central United States, the decay of nearest-neighbor wind correlations becomes evo

circ

sub

res

an

th

de

A

o

U

a

(

exceedingly high over relatively short distances. A dynamically-based regional circulation model-based simulation of winds over the region may therefore provide a substantial improvement in the accuracy of wind speed estimates.

To that end, the Great Lakes region has been chosen as the study area of this research (Figure 3.1). The region of interest extends from 76° W to 97° W Longitude and from 41° N to 50° N Latitude. Within this area lie the majority of the open waters of the Great Lakes and the adjacent coastal areas that are of potential interest to wind farm developers. For reference, all maps in this study are displayed using an Albers Equal-Area Conic projection that was produced using a suite of mapping algorithms, collectively called M_map, developed for Matlab by Dr. Rich Pawlowicz at the University of British Columbia (Pawlowicz, 2004). Matlab itself is a commercially available numerical analysis, simulation and graphical representation software (MathWorks, 2005). Matlab version 5.11 is used exclusively in this research due to its versatility in permitting a user to create unique code, the ability to efficiently handle very large data sets by virtue of matrix-based processing algorithms, and its generally excellent graphical display properties. All processing, analysis and display routines were subsequently written by the researcher in Matlab with the exception of M_map. The Albers Equal-Area Conic projection was chosen because, of the projections offered by M_map, a conic projection is best suited for a region the extent of the study area, providing a minimum of geographic distortion.

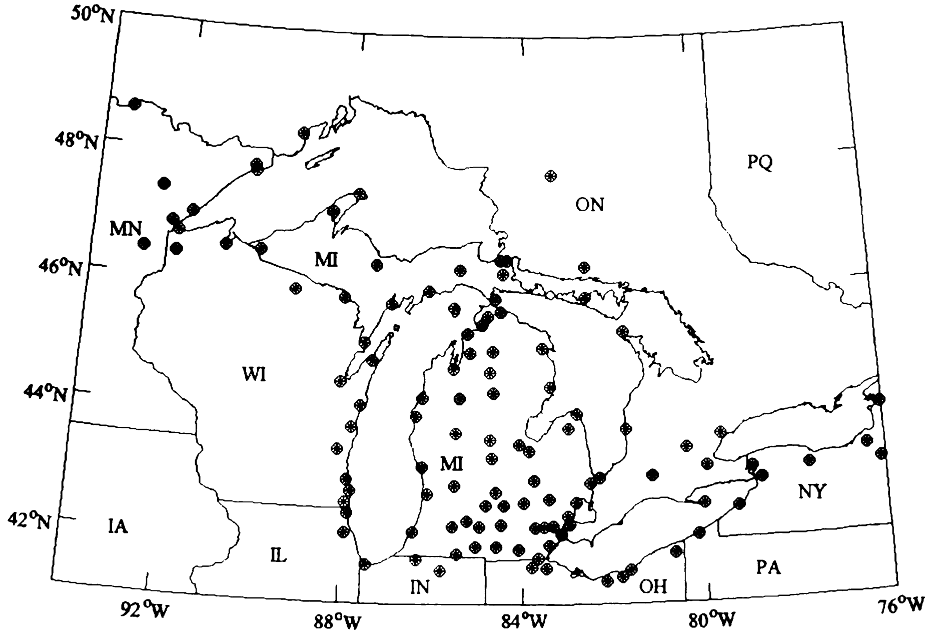

Figure 3.1 A map of the study area, which includes the majority of the Great Lakes region of North America. The dots represent the ASOS/AWOS stations used in this study.

3.2 Observational Data Types and Sources

Accurate observational records of meteorological conditions are a critical component of assessing the performance, accuracy, sensitivity and validity of any meteorological model. The assessment of the MM5 model in this research is no exception. Observational data for this research were obtained from the network of automated surface observing systems (ASOS) and automated weather observing systems (AWOS) installed at a number of airports throughout the study region.

The ASOS/AWOS network provides the most abundant available source of meteorological data within the study region. Because the areas of primary interest are the coastal regions surrounding the Great Lakes, many of the ASOS stations selected for inclusion lie in close proximity to one or more of the lakes themselves. The remaining stations (primarily in the interior of Michigan's Lower Peninsula) were included to retain a spatial coherence across the region. This criterion resulted in the identification of 115 ASOS and AWOS stations that would be used to provide the majority of observational wind data to this study. Of the 115, two were subsequently omitted due to data issues (as described further on). The listing of these stations along with the station type (ASOS/AWOS) is given in Appendix A and is displayed graphically in Figure 3.2.

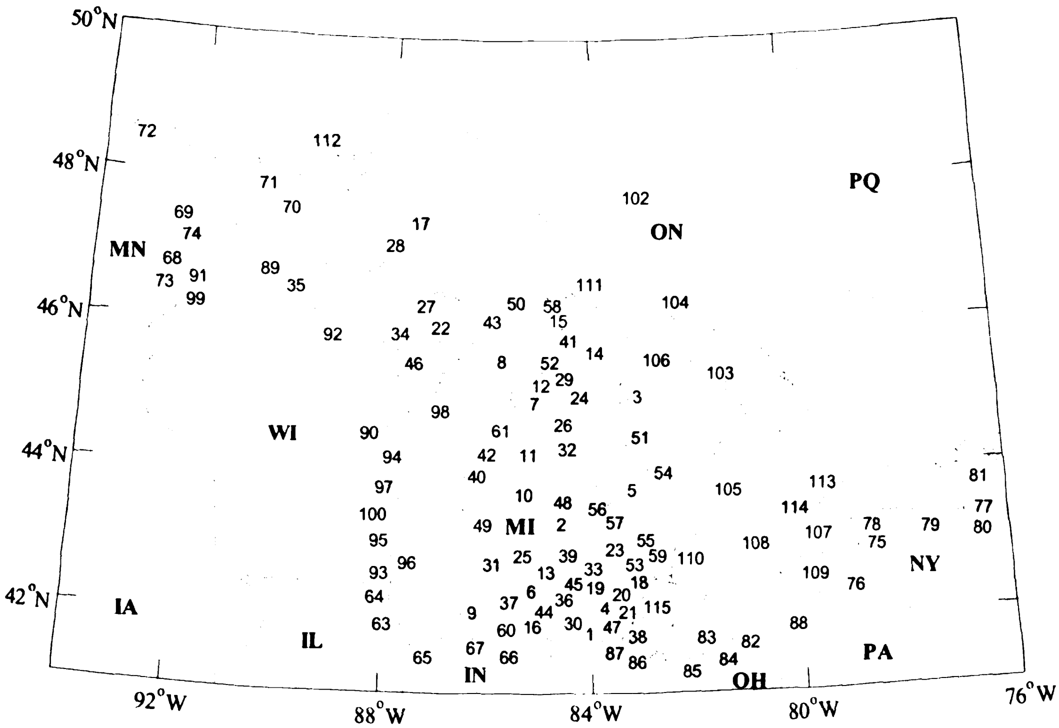

Figure 3.2 ASOS/AWOS stations used in this research. Each number corresponds to the list of stations in Appendix A. Stations may also be referenced by their geographic coordinates, also in Appendix A.

The ASOS/AWOS network is an international network of airport-based stations designed to provide regular, automated, instantaneous meteorological observations in support of aviation activities (FAA, 1999). In the United States, the Federal Aviation Administration (FAA), in conjunction with the National Weather Service (NWS), and the Department of Defense (DOD) sponsor the ASOS/AWOS network. In Canada, the network is operated by the Meteorological Services (MSC) division of Environment Canada. In the United States, all ASOS and numerous AWOS stations are installed and maintained by the Federal government. In addition, a number of the AWOS systems have also been installed and maintained by non-federal entities such as airport authorities, state, local or private organizations. Normally, non-federal AWOS systems that are linked to the NWS reporting network have been installed with the assistance of the FAA's Airport Improvement Program (AIP), and as such are subject to federal meteorological observation standards as well (FAA, 1999).

Of the 113 ASOS/AWOS stations used in this study, 43 were identified as being maintained by the FAA, 22 by the NWS, 33 by non-federal entities, 2 by the US Department of Defense, 1 by a private Canadian entity, and 12 by MSC. Appendix A contains a breakdown of station responsibility as well as references for several sources from which the aforementioned information was obtained.

All regular and special ASOS and AWOS reports from the United States are transmitted to the NWS Systems Monitoring and Coordination Center (SRRS) where they are then disseminated to non-aviation interests and an archive tape is sent to the

National Climatic Data Center (NCDC). In addition, data from elsewhere in the world (including Canada) are retrieved and processed for dissemination by the National Weather Service.

3.2.1 ASOS/AWOS wind sensors and siting

As wind information is commonly acknowledged to be a critical meteorological component of near surface aviation activities, accurate and timely reporting of wind vector information is key to ASOS and AWOS system operations (hereafter referred to collectively as ASOS). Although a number of configurations for AWOS systems exist (of which ASOS is the most advanced), all observe wind speed and direction at a 10 m height with identical performance standards (NOAA, 2001), which are set forth in the Federal Meteorological Handbook (OFCM, 1995). Furthermore, Federal and non-Federal AWOS systems installed in the United States, as well as those installed in Canada have been provided by one of three vendors certified by the FAA and Transport Canada. These vendors are SMI, Inc., Qualmetrics and Vaisala/Artais. Both SMI and Qualmetrics are subsidiaries of All Weather, Inc. All AWOS sensors manufactured by these vendors have been certified to meet or exceed the standards of the FAA, Transport Canada, International Civil Aviation Organization, and the World Meteorological Organization (All Weather, 2004). In fact, according to All Weather (2004) the wind sensor resolution (<1 kt, < 1°), accuracy (± 0.5 kt, ± 2°), and threshold (0.5 kt) for non-federal and Canadian AWOS systems are considered to be superior to the stated performance standards of the US Federal ASOS arrays (discussed next; NOAA, 2000) and to the resolution of the observations that are disseminated (1 kt and 10°). Although other AWOS systems may be operational in the study area, observations from uncertified systems are not available from the NWS and are not considered in this study. Based on the published ASOS/AWOS instrument and network operational specifications, the researcher judged wind observations to be of sufficient accuracy and quality for use in the study.

The ASOS wind sensor array (see Figure 3.3) consists of a cross-arm support that holds a separate anemometer transducer and wind vane transducer (the Bellfort 2000 sensor array). A wind sensor electronics enclosure is housed separately. Wind speed is measured by a 3-cup anemometer that measures rotation with a photo-interrupt transducer. Wind direction is measured by a wind vane attached to a precision potentiometer (NOAA, 1998). The specified accuracy of the wind vane is ±5° when wind speeds exceed 5 knots. Anemometer specified accuracy is given as ±2 knots or 5% of the wind speed whichever is greater. The resolutions are 1° and 1 knot respectively. These tolerances fall within U.S. federal guidelines for meteorological observation instrumentation (OFCM, 1995).

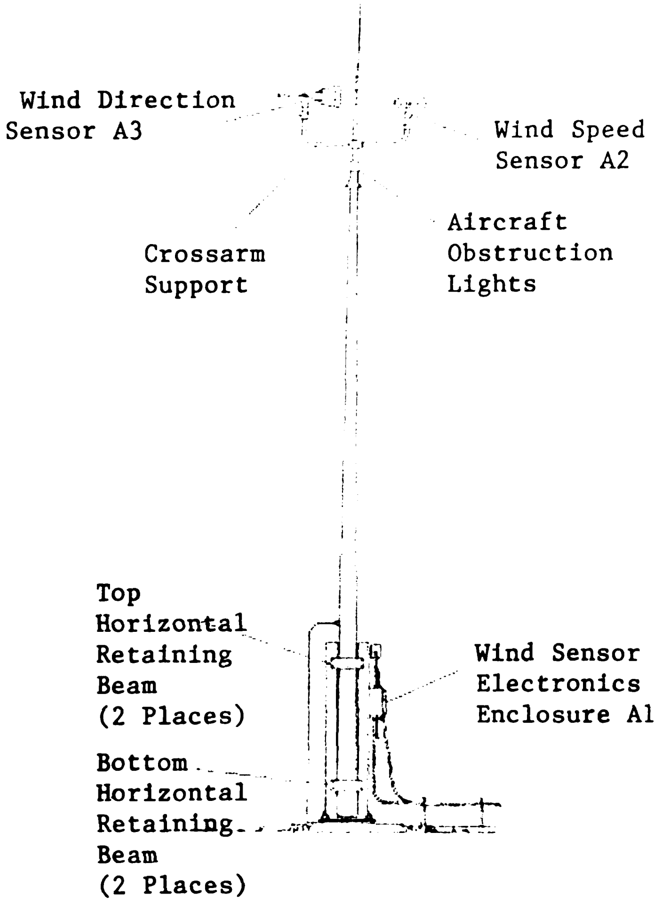

Figure 3.3 An ASOS wind sensor array (from NOAA, 2000).

The establishment of ASOS stations is prescribed in the Federal Standards for Siting Meteorological Sensors at Airports (OFCM, 1994). Typically, stations are located near the touchdown zone of the primary instrument runway or, if conditions preclude this siting, the station may be located at center field (NOAA, 1998). In either case, the station is sited in an area of ample, low roughness fetch. At a typical medium size airport (*e.g.*, one capable of supporting commercial air traffic), such a station would generally be at least a kilometer from the nearest major obstructions (*e.g.*, a terminal or hangar buildings) if wind observations are to be considered to be representative of the surrounding 1-2 km as outlined in OFCM (1994). Additionally, federal standards direct wind measurements to be taken at a height of 10 meters above ground level (10 m AGL). However, for reasons that could not be established by the researcher, winds are typically measured at either 27 or 33 feet (8.23 m or 10.06 m). Given the relatively low surface roughness, and, that the incongruity in speeds due to the height difference was assumed not to exceed the 2 knot error tolerance of the instrument, observations from these differing heights were included in the study without adjustment.

Unfortunately, in many mid-latitude locations, occasional ice accretion may artificially slow or even stop an anemometer, leading to underreporting of wind speeds. While equivalent AWOS wind sensor arrays offered optional heat, the aforementioned ASOS wind sensor arrays were unheated and as a result suffered operational degradation when experiencing ice buildup during super-cooled droplet precipitation events (NOAA, 2003). In response, the NWS undertook efforts to replace the wind sensor array with one that would remain relatively ice free. In 2002 the Vaisala 425NWS Ice Free Wind Sensor (IFW), a 2-dimentional ultrasonic anemometer, was adopted. ASOS anemometers were scheduled to be changed over to the IFW sensors at all 313 NWS systems by 01 October, 2002, and all of the 569 FAA-operated ASOS systems during the period 2003-2005. However, as of 15 May, 2003 (the latest date for which information was available), of the ASOS stations used in this study, only Hancock, MI (on 26 November, 2002) had been changed (NOAA, 2003). Although continuity testing from the old to the new anemometers was undertaken by the NWS, the tests have not yet been completed and results are not available. However, as the majority of the series from Hancock was observed with the IFW anemometer, series discontinuities due to instrumentation changeover were eliminated by truncating the start of the series to 26 November, 2002. The IFW sensor also complies with the observing standards of OFCM (NOAA, 2003).

3.2.2 ASOS/AWOS wind observation and reporting

In order to obtain what the FAA and the NWS consider to be a representative wind observation for the surrounding area of interest (identified as a radius 1-2 miles around the station; NOAA, 1998), several post-measurement processing algorithms are employed operationally in the networks. The ASOS software is programmed to collect observations from the sensor every second (1 Hz). Every 5 seconds, the previous 5 1-second observations are averaged and stored. For wind direction, every minute, a 2-minute moving average of 5-second average wind directions is calculated and reported. These 1-minute averages are rounded to the nearest 10 degree increment. It is this measurement that becomes the wind direction observation at the time the METAR or SPECI report is issued. The wind speed determination is similar. Wind speeds are a 2-minute moving average, updated every 5 seconds, and reported once every minute. Although wind gusts, peak winds, variable wind directions, wind shifts and even squalls are reported by ASOS, their only role in this research is as a modifier in extracting the wind speed and direction observations. This will be discussed further in a subsequent section on quality control (QC).

Although the network provides high quality meteorological observations over a geographically dispersed array of stations, research activities are not considered to be a primary data use or application. For this reason, sources for obtaining archived data are limited in number. The NCDC receives a daily archive tape from the NWS SRRS, but due to cost recovery efforts by NCDC, the cost of obtaining such a volume of data would have been prohibitively expensive. Therefore, as soon as the station site series needed for the study was identified in early January, 2003, an alternate source was sought from which to retrieve the data. The most expedient source was determined to be the Internet site of US Weather, Inc. (http://www.uswx.com).

Access to all ASOS observational reports (hereafter referred to as METARs) was provided without charge by US Weather, Inc. via their Internet site. However, the data displayed by the US Weather, Inc. site was limited to the most recent 1440 observations. Due to this limitation, the earliest date for which data exist at any of the study stations is late October, 2002. As data from most of the stations were available as of 01 November, 2002, this date was chosen as the starting date of this research. The ending date was set to be 30 June, 2004, which was chosen to allow appropriate time for data analysis and the dissemination of the results.

Although the METAR reports are available from US Weather, Inc. in both raw (*i.e.*, encoded) and decoded formats, the researcher chose to archive and extract the necessary information from the raw reports rather than relying on the decoded data. The reason for this choice was to maintain better control over the decoding and processing algorithms rather than relying on the quality of the undisclosed decoding algorithms used by US Weather, Inc.

Current meteorological observations are available instantaneously to pilots via VHF radio frequencies; however, standard METARs are only issued to non-flying interests on either an hourly or special issue basis. Standard observations are identified by the term METAR preceding the report. If meteorological conditions change beyond the limits of thresholds prescribed in the ASOS software, or if an operational observer feels conditions warrant mention, a special report is issued. Such irregular reports are preceded by the 'SPECI' report identifier (FAA, 1999). As such, there is no consistent number of reports for a specific period of time. However, the majority of ASOS stations in the research network appeared to report with a frequency such that 1440 observations comprised at least a two week period. Thus, for each ASOS station used in this study, the appropriate US Weather URL was accessed every two weeks (see Appendix A for a complete list of URLs). The resulting Web page displayed the 1440 raw METARs issued prior to the web page access. The entire Web page was saved as an ASCII text file. After all ASOS station reports were saved, all extraneous information (*e.g.*, graphics, HTML, advertisements) was removed, leaving only the observation reports.

3.3 Observational Data Quality Control

After retrieving the raw METAR reports, it was necessary to extract the time stamp and wind vector information from each report. Each METAR or SPECI report includes a number of schedule-driven elements (*i.e.*, observations for continuous variables) and, depending on conditions event-driven variables (*e.g.*, precipitation, lightning). The overall format of a METAR report is outlined in numerous publications (*e.g.*, NOAA, 1998, FAA, 1999), therefore only report information relevant to this research will be subsequently discussed.

Each report follows a predetermined format that begins on the left with the type of report (METAR or SPECI), the station identifier, the time stamp (Day, Hour and Minute) in Universal Time Coordinated (UTC, also known as Zulu (Z) time), a modifier if applicable (*e.g.*, corrected or automated reports), wind, visibility, weather phenomena, sky coverage, temperature and dew point, pressure, and remarks if applicable. Thus, a typical report may resemble:

METAR KLAN 031152Z AUTO 30013KT 5SM –RA OVC025 20/19 A2990 RMK A02

The preceding report is a routine (METAR) report for Lansing, MI (KLAN) issued on the 3rd day of the month at 11:52 Z, or UTC, and it was issued without an observer logged onto the system (AUTO). Winds were from 300° at 13 knots (30013KT), 5 statute miles visibility (5SM) in light rain (-RA) with an overcast ceiling at 2500 feet (OVC025), a temperature of 20° C and a dew point of 19° C (20/19) and a sea level pressure of 29.90" Hg (A2990). The remarks (RMK) indicate that the station is an automated station with a precipitation discriminator (A02). To highlight the format of the METAR data files received from U.S. Weather, Inc. every two weeks, a sample of the raw data is provided in Appendix B.

A problem with a standardized extraction procedure arises however, because ASOS and AWOS networks are designed so that missing meteorological elements are neither estimated nor listed as missing in the recorded observation. If less than 75% of the observations that comprise the value of an element at a given reporting time are missing, that element is simply omitted from the observation. All subsequent elements in the observation are shifted to the left to eliminate the space left by the missing element. As the report type element (METAR vs. SPECI) and station identifier element are always present and always of the same length (RRRRR SSSS), extraction of the time stamp is straightforward (simply the 12th to 17th characters in the report, followed by the letter "Z" to denote Zulu time or UTC). The event-driven inclusion of a report modifier and of several possible wind modifiers, however, makes it more difficult to extract the wind element as will be discussed shortly.

In order to identify the appropriate month and year of the report, the date of the last entry in the record file was compared against the date on which the file was saved. If they were not the same, it was assumed that the station had not been reporting for an undetermined period of time prior to the date of file saving. This station file was then flagged and manually checked to identify the month and year of the last valid report. In two instances it was determined that the ASOS station had ceased reporting during the study period. The first site was Meigs Field in Chicago, IL USA (KCGX). On 04 April, 2003 the ASOS station ceased operation when the airport was closed without warning by the Mayor of Chicago. The other station was Caribou Island, Ontario (CWCI), which ceased reporting on 28 May, 2003. The researcher was not able to determine an explanation for the failure of this station. For these two stations, the observational series were substantially shorter than the other series (642 and 3957 observations respectively), so they were omitted from the study. For stations other than KCGX and CWCI, observational reports were largely available throughout the study period of 01 November, 2002 to 30 June, 2004.

Once the observation time stamps in each downloaded file were verified for continuity the time stamp, wind speed and direction of each observation was extracted.. The time stamp was simply the 12th through 17th characters in the report. These data were parsed into day, hour and minute (Z, or UTC time). After all extraction was completed, the month and year of the report were added to the time stamp. The extraction of wind speed and direction presented more of a challenge.

Before the winds could be extracted, it was necessary to determine if a report modifier element was included. There are two basic types of modifier that may be added to a METAR report. The first is AUTO to signify that the report was generated without an observer being logged onto the system. The second is COR to alert that the report is a correction to a previously issued report. A number may be added to the COR element (*e.g.*, COR1, COR2) to signify the sequence of corrections issued to the original report. If a COR flag was encountered, it was necessary to determine if the subsequent wind element had been changed. If the wind element in the corrected report differed from that in the original report, the original value was discarded in favor of the corrected value. In all cases, the presence and length of the modifier element determined the report position of the wind element for extraction.

In METAR observation reports there are several variations in the way winds are reported. Winds are reported based on continuous observation in the 5 minutes preceding the report issuance. This 5-minute observation is described in the previous section and in NOAA (1998) and FAA (1999). When winds are relatively steady during the 5 minutes prior to the observation, they are simply reported in the format DDDSSKT, where DDD represents the compass direction in tens of degrees from true North, SS represents the wind speed and KT indicates the measurement units of the wind speed. Because METAR observations are collected and disseminated worldwide and do not need to adhere to a standard reporting unit for wind speed, the addition of the unit identifier is necessary. In the US and Canada, nautical miles per hour, or knots is the chosen unit of wind speed (1 knot = 0.5148 m s^{-1}).

If winds during the 5 minutes prior to the observation exhibit a strong fluctuation in speed, the wind observation will reflect that by adding a gust observation between the 5-minute average wind speed and the unit identifier (*e.g.*, DDDSSGssKT). The addition of "G" indicates a gust measurement, followed by a two-digit gust speed value (ss). This gust observation is the highest wind speed observed during that 5-minute period.

Additionally, should the wind direction vary by more than 60 degrees during the 5 minutes preceding the observation, the wind direction will be identified as variable. If wind speeds are less than 6 knots, the wind direction is replaced by the code VRB (and thus no directional wind information is available). If the wind speed exceeds 6 knots and the wind is variable by the aforementioned definition, an average wind direction is given in the wind observation, and the entire wind observation is followed by a variability observation that reports the extremes of the wind direction separated by the letter V (*e.g.*, 180V310).

Although there may be additional information regarding the wind in the remarks section of the METAR observation, such remarks are generally limited to either the time of peak wind occurrence should the wind report exceed 25 knots sustained or the time of a significant wind shift (NOAA, 1998, FAA, 1999). For the purposes of this research, only the 5-minute average wind speed and direction were extracted. Gust values were ignored. Where winds were of variable direction and less than 6 knots, the extracted wind direction value was flagged as missing. For variable direction winds exceeding 6 knots, the average wind direction was extracted from the two wind directions given by the variability report. Additionally, no wind information was extracted from the remarks section of the reports (*i.e.*, peak winds).

One additional problem that arose during the extraction of time stamps and wind data from the METAR reports was the occasional occurrence of keystroke errors. While rare, computer data transfers and operator errors can and do lead to the deletion, addition, or reformatting of data bits. On occasion, characters were added or omitted on the report modifier element (*e.g.*, AUTO became AUT, UTO, or AUTOO), in the time stamp (the Z was occasionally omitted), and even in the wind element (KT became K, G became K, VRB became VR or RB, etc.). For this reason, careful attention was paid to the error checking algorithms in the extraction program such that any potential keystroke errors could be detected, recorded, and flagged for later manual examination. Ultimately, of all observations at all the station sites considered in the study, only 28 so-called keystroke errors were encountered.

The result of the extraction process was a series of records with time steps and corresponding wind direction and speed observations. In many instances, the original reports had been duplicated anywhere from two to five times in the record files. While it would have been straightforward to simply eliminate all duplicate report entries from the series, a number of observations were out of order, and thus it was necessary to identify which of the duplicate entries, if any, were in the right location in the series. This involved iteratively processing each of the observation series files to place the observations in their correct temporal order, then eliminating any duplicate entries from the series. Each file subsequently contained a series of sequential wind observations with no duplicate entries. All series files corresponding to a particular ASOS/AWOS station were then appended to each other, removing any overlapping reports so that one file containing all available observations available between 01 November, 2002 and 30 June, 2004 was created for each station.

Lastly, in terms of quality control, all wind observations of zero knots were flagged. This determination was made because whenever observed 5-minute average wind speeds were below 2 knots, the wind was reported by ASOS/AWOS as calm, and the recorded observation given a speed value of 0 and a direction value of 0 degrees (NOAA, 1998). While the direction is not confused with northerly winds (northerly winds are recorded as 360°), the flag permits a zero wind speed report to be separated when comparisons are made with model estimates of winds (which do not have a 2 knot threshold) at those times. Wind directions described as variable were treated as missing data and not included in the analysis.

Despite the ASOS operating agencies' collection of quality, standardized wind data, it must be remembered that these data are intended for instantaneous aviation operations rather than for research purposes. Therefore, prior to their use, the data had to be transformed into a series that was more compatible with the goals of this research. This post-processing involved two steps. First, the observations, which are reported at various times within an hour, had to be adjusted to generate a series with data either as an hourly average, or interpolated to the top of the hour of record. This step was necessary to create series that could be compared to subsequent model output. Secondly, as the observational series comprise a short period of record relative to the average expected lifespan of a wind turbine, some assessment of the longer-term representativeness of the observational data had to be made. While assessing the representativeness of the observational data is a necessary step in this research, it is outside the realm of the analysis of evaluating model performance. Rather it is an integral part of the observational data collection and use. Therefore, these steps are discussed in the following sections rather than in Chapter 4.

3.3.1 Data homogenization and aggregation

Once the ASOS data had been extracted and quality controlled, it was necessary to generate series that would pair with wind estimates generated by the MM5 model. The MM5 used in this research generates estimates of instantaneous wind speed and direction on an hourly basis at the top of the hour. Therefore, an attempt was made to adjust the observational data to match the time steps of the MM5 data. In most instances, the ASOS stations issued hourly automated reports. However, these varied from station to station in terms of the time of the hour in which they were issued. Unfortunately, several of the stations did not regularly issue reports within 10 minutes of the top of the hour. As a result, the number of total observations in some of these top-of-the-hour adjusted series was much less than the potential total.

In addition to the routine reports, when an operator was logged on to the ASOS system, additional observation reports were sometimes issued at 15 or 20 minute intervals. Therefore, in many cases, several observations were available for a given hour. Lastly, special (SPECI) reports are issued whenever conditions warrant. During rapidly changing weather conditions, SPECI reports may outnumber routine reports and several may be present during a given hour.

Thus in order to pair observed wind data with modeled estimates, and to ensure that each station would have a representative series that was not unduly truncated, two hourly-resolution time series for each station were created and compared. First, the time stamp of each report was analyzed and if found to be within 10 minutes of the top of a given hour, was used as the wind observation for that hour. In cases where two or more observations occurred within 10 minutes of the top of the hour, the observation closest to the top of the hour was used, and where two observations were equally close to the top of the hour (*e.g.*, 0:55 and 0:05), the average speed and direction of the two was taken. If there was no observation within 10 minutes of the top of a particular hour, that hour was assigned a missing value. In this way, an hourly series of more-or-less instantaneous wind observations was created, referenced to the top of each hour. Due to generally strong temporal autocorrelation in hourly wind speeds (Brett and Tuller, 1991, Robeson and Shein, 1997), it is not anticipated that the hourly mean values would differ substantially from an instantaneous wind speed or direction value within that hour, except for the occasional instance where a weather event (*e.g.*, frontal passage or thunderstorm) occurs near the top of the hour. Thus, the second hourly time series was generated by averaging all observations between 30 minutes prior to and 29 minutes after the top of an hour. In cases where all observations for the hour in question were missing, the average for the hour also was set to missing. This processing resulted in an hourly resolution time series of averaged hourly values.

The resulting observational time series for each station have a total potential size of 14,617 hours (00:00Z 01 November, 2002 – 23:00Z 30 June, 2004). However, when missing values were not counted the series length at each station varied. The number and percentages of valid hourly values are presented in Table 3.1.

	Non-missing observations [n (%)]				
	Mean	**Median**	**Std. Dev.**	**Max**	**Min**
Top of hour	11,861 (81%)	12,312 (84%)	1,832 (13%)	14,154 (97%)	642 (4%)
Hourly Average	12,041 (82%)	12,298 (84%)	1,657 (11%)	13,843 (95%)	2,298 (16%)

Table 3.1 Statistics of the counts (and percentages) of non-missing values (out of 14,617 possible observations) from series constructed with top-of-the-hour observations and with hourly averaged values.

From Table 3.1 it is evident that the differences between the instantaneous and averaged series are rather small. The biggest difference was associated with sample reductions from each of several stations that did not consistently report observations within 10 minutes of the top of the hour. This is evident in the less peaked distribution of non-missing observations by station in Figure 3.4. If indeed the hourly-average series would present a larger and more consistent regional data pool, it is preferable to utilize these data over the less homogeneous instantaneous series. However, in order to rely solely upon the hourly-average series, it is first necessary to establish that these data are not significantly different from the instantaneous data.

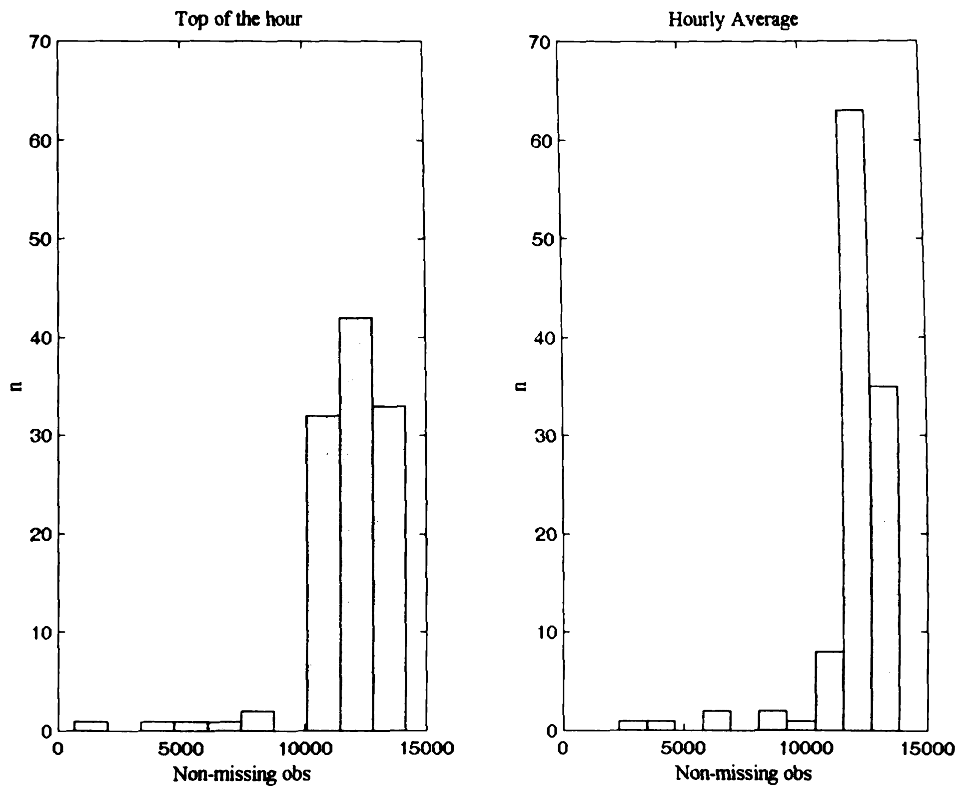

Figure 3.4 Histograms of the number of non-missing observations at the stations in the study region. Top-of-the-hour observations were those taken within 10 minutes of the top of the hour, while hourly averaged observations included an average of all observations from within 30 minutes of the top of the hour.

To establish the similarity of the two data sets, the two series from each station were subjected to a Student's paired two-tailed T-test for difference of means (Rogerson, 2001). In order to ensure that the assumption of independent, randomly distributed data was not violated by the properties of the wind speed distributions, 1000 random, pair-wise observations were selected to be used in the T-test. In all 113 instances, the calculated T score remained below the critical value at an alpha level of 0.05, indicating that the differences in the means of the instantaneous and averaged series were not statistically significant. Overall, a comparison between the two series is best done graphically. Figure 3.5 illustrates, over all stations, the similarity in mean values.

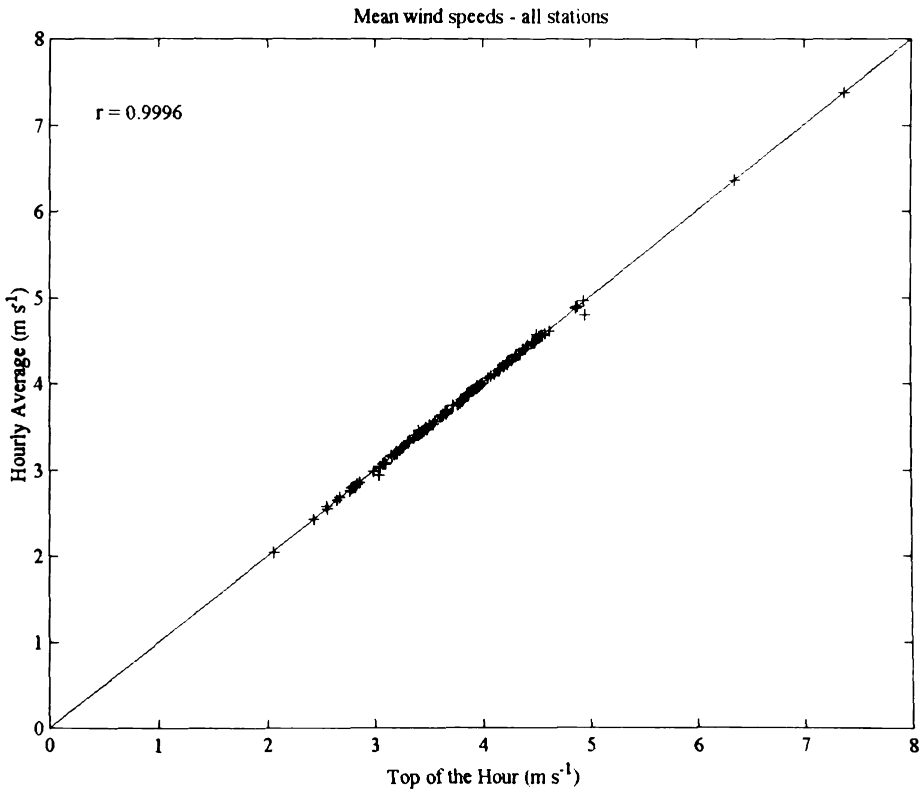

Figure 3.5 A comparison of observed mean wind speeds when using only the observation closest to the top of the hour (x) or the average of all observations for that hour (y).

Over the 113 stations, the average correlation between the instantaneous and averaged series was 0.96 with a standard deviation of just 0.04 and a minimum correlation of 0.8. To that end, it was decided that in the interest of maximizing observations and data homogeneity in this analysis, only the hourly average series would be carried forward.

3.3.2 Representativeness of ASOS data

An important issue regarding the observational ASOS data series is whether or not the data are representative of the long-term wind resource over the region. A number of previous works (*e.g.*, Corotis, 1977; Justus *et al.* 1979; Barros and Estevan, 1983; Barthelmie and Pryor, 2003) have concluded that characteristics of an annual wind series do not differ substantially from the long-term statistics at a given location, especially in the U.S. Midwest. However, it is generally acknowledged that at least a year of data, and preferably more than two or three years, is most desirable when evaluating the long-term wind resource of a location or region (Hannah *et al.*, 1996). To that end, the observational data used in this study were subjected to an analysis of representativeness in order to determine how well they could be expected to reflect the long-term wind resource over the study area.

In order to establish representativeness, 20 of the study stations were identified for which quality controlled, long-term data and metadata records were available. These stations are listed in Table 3.2. ASOS stations represent a relatively low cost investment in installation and maintenance and have been installed at a number of locations that previously were not included in the National Weather Service's pre-ASOS station network. Only 20 of the stations used in this research existed under the pre-ASOS station network (Table 3.2).

Stations having long-term data								
					ASOS		SAMSON	
ID	**Name**	**Lat (N)**	**Lon (W)**	**Elev (m)**	**u**	**s**	**u**	**s**
ANJ	Sault Ste Marie, MI	46° 28'	84° 22'	218	3.48	2.11	3.93	2.17
APN	Alpena, MI	45° 04'	83° 34'	210	3.42	2.20	3.77	2.09
BUF	Buffalo, NY	42° 56'	78° 44'	211	4.53	2.59	5.01	2.63
CLE	Cleveland, OH	41° 25'	81° 51'	233	4.38	2.44	4.58	2.30
CMX	Hancock, MI	47° 10'	88° 29'	326	4.48	2.82	4.08	2.10
DET	Detroit, MI	42° 24'	83° 01'	190	3.80	2.17	4.64	2.42
DLH	Duluth, MN	46° 51'	92° 12'	435	4.61	2.44	4.71	2.30
ERI	Erie, PA	42° 05'	80° 11'	222	4.35	2.48	5.20	2.53
FNT	Flint, MI	42° 58'	83° 45'	233	4.08	2.36	4.40	2.31
GRB	Green Bay, WI	44° 29'	88° 08'	208	4.06	2.39	4.32	2.32
GRR	Grand Rapids, MI	42° 53'	85° 31'	237	4.48	2.52	4.37	2.32
INL	International Falls, MN	48° 34'	93° 24'	360	3.59	2.15	3.88	2.18
LAN	Lansing, MI	42° 47'	84° 35'	264	4.13	2.49	4.46	2.54
MKE	Milwaukee, WI	42° 47'	87° 54'	206	4.57	2.47	4.99	2.43
MKG	Muskegon, MI	43° 10'	86° 14'	191	4.45	2.62	4.82	2.53
ROC	Rochester, NY	43° 07'	77° 41'	178	4.21	2.61	4.43	2.46
SBN	South Bend, IN	41° 42'	86° 19'	237	4.23	2.49	4.49	2.39
SYR	Syracuse, NY	43° 07'	76° 06'	127	3.78	2.52	4.18	2.49
TOL	Toledo, OH	41° 35'	83° 48'	210	3.92	2.66	4.20	2.23
TVC	Traverse City, MI	44° 44'	85° 34'	190	3.14	2.26	3.95	2.34

Table 3.2 20 NWS weather stations that existed in the study area prior to the ASOS transition during the mid-1990s. Each station corresponds to an ASOS station used in this study and is used to compare the study period data to the long-term (1961-1990) wind climate at the station. Mean wind speeds (u) and standard deviations (s) are based on wind speeds (including zeros) given in m s^{-1}.

In addressing whether pre- and post-ASOS installation data from these stations would indeed be comparable, stations were examined to determine whether they existed in the same physical location before and after the ASOS installation. Initially it appeared that 19 of the 20 stations had been relocated (although all were on airport grounds and remain so), however, NCDC (2002) indicated that the stations had not actually been relocated, but rather that a more precise GPS method of positioning had been used to determine the position of the station. Pre-GPS geographical positioning had been obtained by traditional survey methods and the resulting position often was rounded or truncated. The re-measurement of position resulted in a more precise assessment of geographic position and elevation that accounts for the differences between pre- and post-ASOS installation position measurements for the 20 stations under investigation.

At the 20 stations listed in Table 3.2, hourly wind data were available to the researcher for the period 1961-1990 as part of the National Renewable Energy Laboratory (NREL) Solar and Meteorological Surface Observation Network 1961-1990 (hereafter called SAMSON) data set (NREL, 1993). As noted by Shein (1995), SAMSON data have not been standardized or homogenized for the height of observation. Therefore, it was first necessary to adjust all of the wind speeds to a 10-meter height so as to permit comparison with the ASOS data series. This adjustment was accomplished using methods outlined in Shein (1995) and Robeson and Shein (1997). With the exception of Traverse City (KTVC) and Houghton (KCMX), anemometer heights were identified from station histories (NCDC, 1994a and b) and the speeds observed at those heights adjusted to 10 meters by applying the wind speed power law:

$$U = U_r \left(\frac{z}{z_r} \right)^{\alpha} \tag{3.1}$$

where U is the wind speed at level z, U_r is the wind speed at reference level z_r, and α is an exponent, which was assumed to be 1/7. Counihan (1975) and others (*e.g.*, Touma, 1977, Petersen and Hennessey, 1978) have concluded that although empirically derived for neutral stability conditions, an exponent value of 1/7 provides reasonably accurate estimates for the profile of wind speeds up to several hundred meters within the boundary layer. Because their anemometer heights could not be identified, KTVC and KCMX data were left unadjusted.

Once the SAMSON data were adjusted to a standard 10-meter height, characteristic statistics (*i.e.*, mean, standard deviation, probability distribution) were calculated for both the SAMSON and ASOS data (Table 3.2). The aforementioned statistics were calculated for the overall series as well as for each year and by aggregate season (*e.g.*, all winter observations). These statistics were subsequently evaluated graphically and statistically for goodness-of-fit and correspondence.

A Student's T-test for difference of means was conducted to determine whether or not the two samples (SAMSON and ASOS) came from the same population (Rogerson, 2001). To ensure independence of the sample observations, 1000 observations were randomly selected (without replacement) from each series. At a significance level of 0.05 (2-tailed) that there was no difference in the means of the two data sets, the null hypothesis was rejected at all 20 stations. Seasonally, the same analysis was conducted and again, for all of the 20 stations, there was no statistically significant difference in their means and it was therefore concluded that regionally, the winds observed between November, 2002 and June, 2004 likely came from the same population that produced the winds observed between 1961 and 1990.

Wind speed frequency distributions have long been used in providing a measure of wind power potential for a location, and in particular, the Weibull distribution has been found to provide an excellent fit to wind speed data in the middle latitudes (*e.g.*, Justus *et al.*, 1976, Corotis *et al.*, 1977, Hennessy, 1977, Conradsen *et al.*, 1984, Troen and Petersen, 1989). As the empirical distribution of wind speeds at the stations used in this study most widely appear to graphically approximate the shape of a Weibull distribution (Figure 3.6), its selection as a theoretical distribution for the data was not unreasonable.

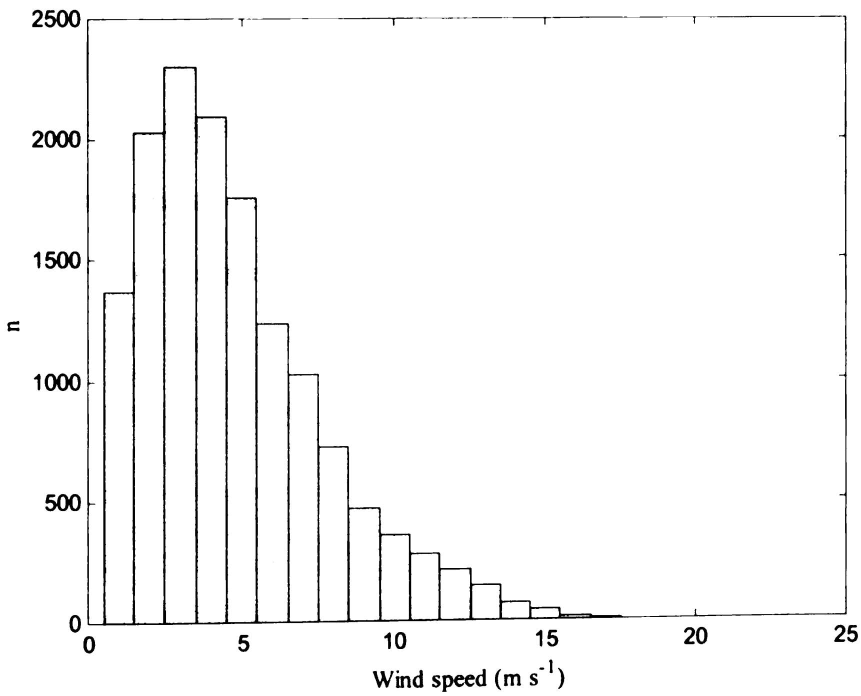

Figure 3.6 A wind speed distribution (with calms removed) from KP59 (Copper Harbor, MI). While the distribution may vary from one station to another, all stations in the study exhibit a similar distribution shape, supporting the use of a Weibull distribution for wind speed description.

Therefore, the Weibull probability distribution function was estimated for the same subset of stations as before and compared graphically and statistically for goodness of fit. Analysis of Weibull distributions took two forms. First, it was necessary to determine whether the selection of a Weibull distribution was an appropriate fit to the data from which it was estimated. Second, the interchangeability between SAMSON derived and ASOS derived distributions had to be assessed (*i.e.*, could the ASOS data be drawn from a distribution empirically derived from the SAMSON data) as statistical testing has suggested.

A Weibull distribution is a variation of the classic gamma distribution. It has two parameters describing shape and scale. A third parameter, location, may also be included to shift the distribution along the abscissa. However, as winds are a zero limited variable, the location parameter can be set to zero and its inclusion becomes irrelevant to the distribution. The Weibull probability density function (from Weibull, 1951) takes the form:

$$f(U) = \frac{k}{c}\left(\frac{U}{c}\right)^{k-1} e^{-\left(\frac{U}{c}\right)^{k}} \tag{3.2}$$

where k is the shape parameter, and c is the scale parameter (in units of the variable U). The Weibull cumulative distribution function is

$$F(U) = 1 - e^{-\left(\frac{U}{c}\right)^{k}} \tag{3.3}$$

The parameters of the Weibull distribution (k and c) can be estimated in one of two ways. The first is via maximum likelihood estimation (MLE), and the second is by ordinary least squares (OLS) regression. There does not appear to be a preference in the literature for one method over the other, and previous work (Justus *et al.*, 1976) has shown that parameters estimated by the OLS technique do not differ greatly from those estimated by MLE. To be certain, Weibull parameters were estimated using both MLE and OLS techniques at 20 stations within the study area. Overall, the OLS technique provided slightly more conservative parameter estimates. Also, the greatest difference in k was 0.8 and for c, just 0.3 m s^{-1}. As the OLS technique is much less computationally intensive, it was chosen here for the remainder of the stations. In the OLS method (see Justus *et al.*, 1976, Rohatgi and Nelson, 1994, Romeu, 2003a), Equation 3.3 can be rearranged by taking the double natural log of both sides as such

$$\ln[-\ln\{1 - F(U)\}] = k \cdot \ln(U) - k \cdot \ln(c) \tag{3.4}$$

Functionally, Equation 3.4 now takes the form of the standard linear regression equation:

$$y = b_0 + b_1 x \tag{3.5}$$

where, for the variable $ln(U)$, k is equal to the slope of the line (b_1), and the intercept (b_0) occurs at $-k\ ln(c)$.

Based on the OLS estimation procedure, a theoretical Weibull distribution was fit to each set of the data from the 20 evaluation stations. The shape parameters ranged from 1.67 to 3.29, with a mean of 2.12 and a standard deviation of 0.41. The scale parameter ranged from 4.04 m s^{-1} to 5.86 m s^{-1}, with a mean of 4.96 m s^{-1} and a standard deviation of 0.45 m s^{-1}. To establish the goodness of fit, each data set was binned and plotted against both the probability and cumulative Weibull density functions (Figures 3.7 and 3.8). This graphical procedure has been well established (*e.g.*, Nelson, 1982, Rohatgi and Nelson, 1994, Romeu, 2003a).

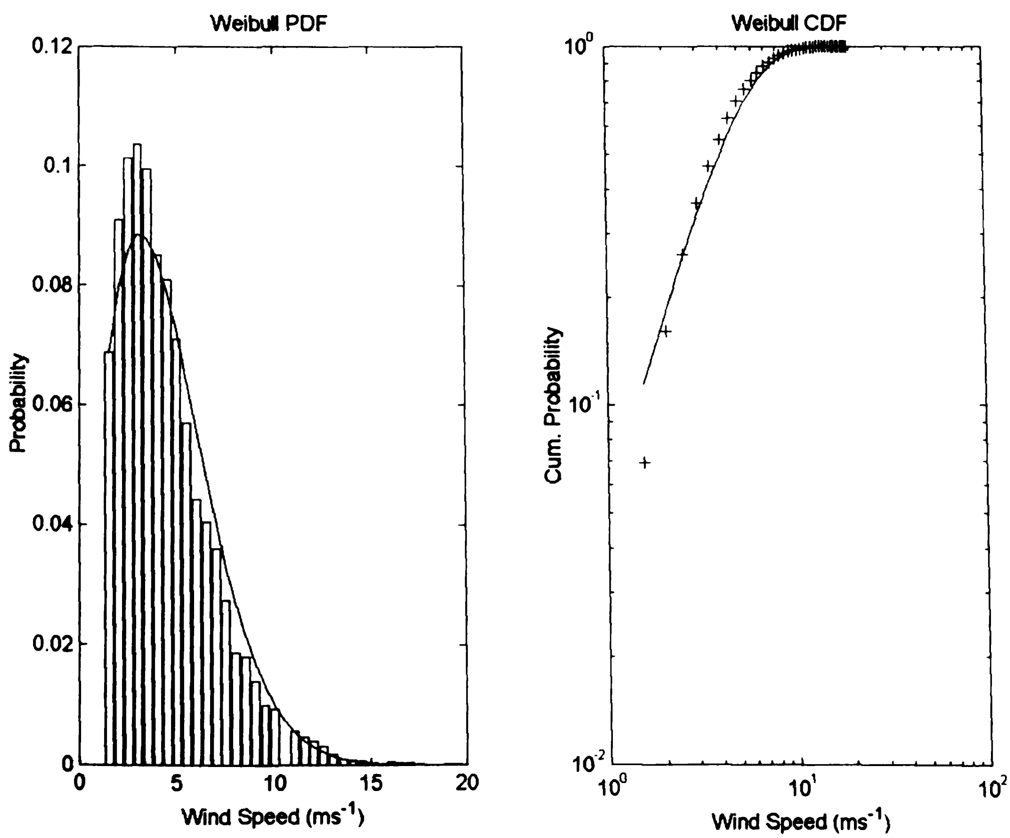

Figure 3.7 Wind speed frequency distribution (r) and cumulative frequency distribution (l) at Rochester, NY (KROC) for ASOS data. Theoretical Weibull distributions are shown as solid lines.

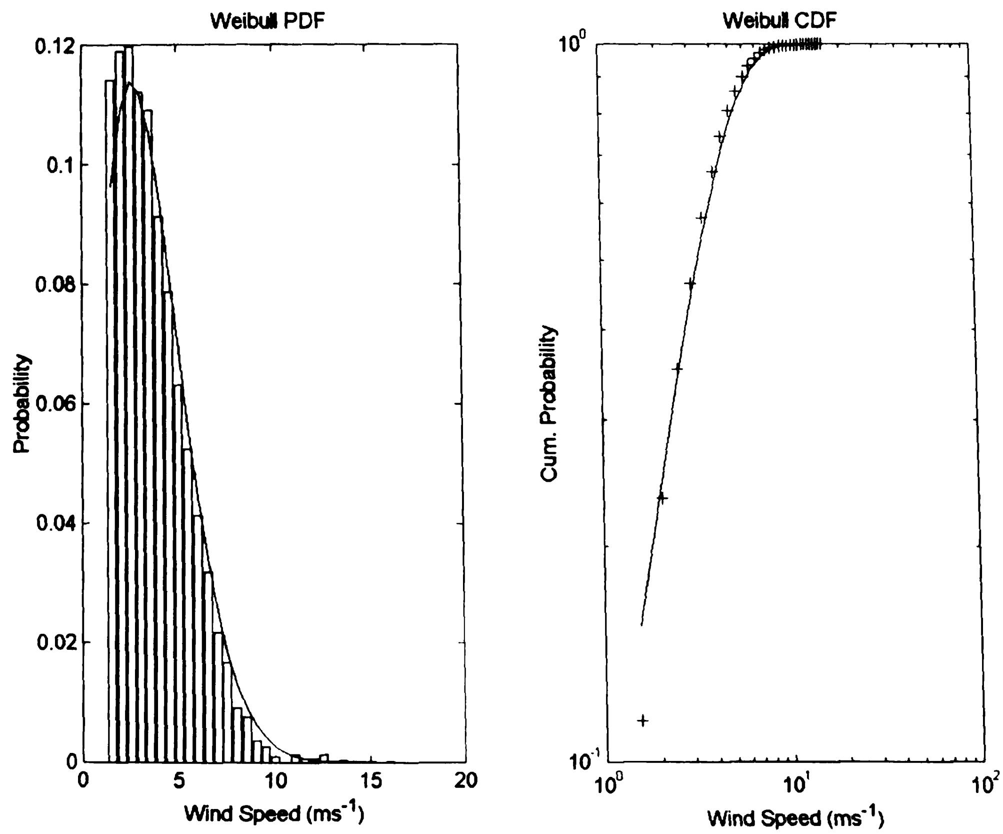

Figure 3.8 Wind speed frequency distribution (r) and cumulative frequency distribution (l) at Traverse City, MI (KTVC) for ASOS data. Theoretical Weibull distributions are shown as solid lines.

As expected, given empirically derived shape and scale parameters, the two-parameter Weibull distribution provided a good fit to the majority of wind data from all series. Figure 3.7 is the distribution of wind speeds at Rochester, NY, and represents what appears, graphically, to be the worst Weibull fit of any of the 20 stations. Conversely, Figure 3.8 is the wind speed distribution at Traverse City, MI, arguably the best Weibull fit of the 20 stations. It should be noted that most of the 20 stations more closely resembled the Traverse City fit than the Rochester fit. Even so, the Rochester fit does not appear to be inappropriate to the data.

While the ASOS data have already been determined to be representative of the long-term wind regime over the study area and the Weibull distribution was found to be a good visual fit for the ASOS data, it was still necessary to determine statistically whether Weibull is an appropriate choice of distribution, and if so, could the ASOS data be drawn from the Weibull distributions of the long-term SAMSON data as might be assumed given the results of the T-test. To that end, the Weibull distribution that had been empirically fit to the SAMSON series was applied to the ASOS data. One tendency in ASOS wind data noted by an earlier study is a general reduction of ASOS-observed wind speed data relative to pre-ASOS observations (Powell, 1993). The ASOS data used in this study were found to follow the same pattern (see Table 3.2), in most cases, with the distribution of ASOS wind speeds, while similar to SAMSON counterparts, shifted to a lower mean wind speed (see Figure 3.9). Again, a graphical approach for the goodness-of-fit was used to determine whether ASOS data could come from a distribution empirically specified by the long-term SAMSON data. While graphics showed some degradation in fit (Figure 3.9), overall, it appeared that the ASOS data could be derived from the SAMSON Weibull distributions, especially if the systematic shift of the wind speed distribution were accounted for as instrument discrepancy.

The final step in determining the appropriateness of a Weibull distribution to the ASOS data was to statistically test the goodness-of-fit. Although several methods for testing the goodness-of-fit of a distribution to data exist, the Anderson-Darling test (Anderson and Darling, 1954) was selected as the most appropriate.

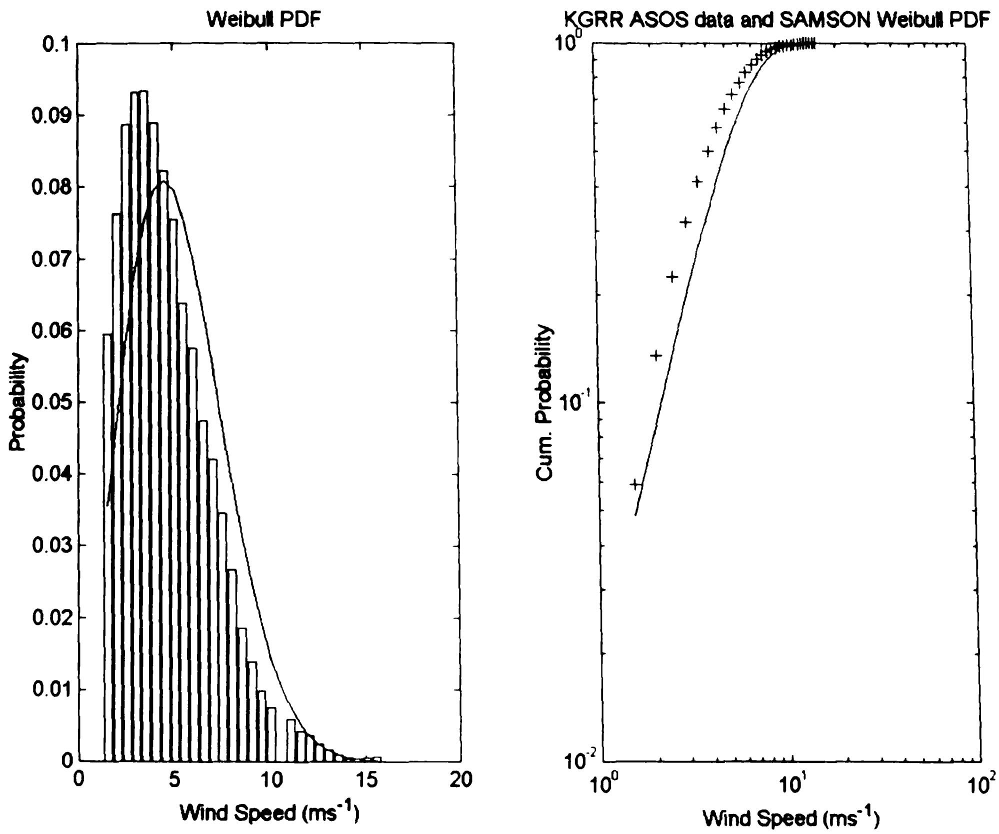

Figure 3.9 Weibull pdf (r) and cdf (l) (solid lines) at Grand Rapids, MI (KGRR) derived from 30-year hourly data (1961-1990) applied against the ASOS observed (11/2002 - 6/2004) wind speed distribution [bars (l) and + (r)].

A number of so-called distribution free goodness-of-fit tests exist to evaluate how well a chosen probability distribution fits to a sample of data. The most common of these tests are the Chi-square and Kolmogorov-Smirnov tests. Such tests are referred to as distribution free, or empirical distribution functions (EDFs) in the sense that their critical values do not depend upon the specific theoretical distribution function being tested and the parameters of the distribution may be empirically derived from the data itself (Birnbaum, 1953). The X^2 test is among the most commonly used tests in that it is relatively easy to calculate (Davis, 1986, Snedecor and Cochran, 1989). However, the X^2 test is of low statistical power and requires relatively large bin counts to ensure the robustness of results (Snedecor and Cochran, 1989). A slightly more powerful test is the Kolomogorov-Smirnov, or K-S test (Davis, 1986). One major advantage of the K-S test over the X^2 test is that it is considered an exact test as it does not require the data to first be binned as with the X^2 test, thus increasing its power (Davis, 1986). However, the K-S test has several important limitations. First, it tends to be less sensitive to data in the tails than near the center of the distribution. Secondly, and perhaps most importantly, the distribution being tested must be fully specified. In other words, the distribution cannot be evaluated against the data from which the distribution parameters were empirically estimated. In such cases, the critical region is no longer valid and must be estimated by repeated simulation (Fillibin and Heckert, 2003). Furthermore, both the X^2 and K-S tests suffer from the limitation of requiring continuous, rather than discrete distributions (Fillibin and Heckert, 2003).

The Anderson-Darling test is a special case of the Kolmogorov-Smirnov test that is more sensitive in the tails of the distribution (Stephens, 1974, Romeu, 2003b). In addition, the distribution in question does not need to be fully specified. That is, the parameters of the distribution can be estimated from the data being evaluated without invalidating the critical region of the test (Anderson and Darling, 1954, Fillibin and Heckert, 2003). Strictly speaking, however, the Anderson-Darling test, while an EDF, is not distribution free. Its critical values are dependent upon the distribution being evaluated (Lewis, 1961, Stephens, 1976). While the specification of a distribution makes the Anderson-Darling (A^2) test more powerful and sensitive than the K-S test, it also means critical values must be calculated for the specific distribution. Fortunately, because the Weibull distribution is used extensively in engineering, failure and lifetime studies, critical values of A^2 have already been specified (Stephens, 1974, 1976).

The disadvantage of a more powerful statistical test tends to manifest itself in the complexity of its calculation. The Anderson-Darling test is no exception, and is more complex than either the X^2 or K-S tests. For asymptotic distributions the test statistic, A^2 is given by Anderson and Darling (1954) as

$$A^2 = -n - \frac{1}{n}\sum_{i=1}^{n}(2i-1)\left[\ln U_i + \ln\left(1 - U_{n-i+1}\right)\right] \tag{3.6}$$

where n observations of x are ordered and U_i is the function $F(x_i)$. Substituting the Weibull distribution for the standard normal distribution, the A^2 equation becomes (corrected from Romeu, 2003b)

$$A^2 = -n - \frac{1}{n}\left[\sum_{i=1}^{n}(2i-1)\left[\ln\left(1 - \exp\{-Z_i\}\right) - Z_{n-i+1}\right]\right] \tag{3.7}$$

where

$$Z_i = \left[\frac{x_i}{c}\right]^k \tag{3.8}$$

and where k and c are the empirical estimates of the Weibull shape and scale parameters respectively. For small samples, the test statistic is modified by Equation 3.9.

$$A^{2*} = \left(\frac{1 + 0.2}{n^{0.5}} \right) A^2 \tag{3.9}$$

However, there are no set guidelines as to what constitutes a small sample and critical values are calculated such that they must be compared with this modified test statistic (Stephens, 1974, 1976). Because small sample size tends to lead to a more conservative critical value, this only strengthens the results of the test. Therefore, all test statistics were calculated for small samples (and subsequently both the notation A^2 and A^{2*} refer to the small sample statistics interchangeably in this research).

The null hypothesis of the Anderson-Darling test used in this study states that the data were drawn from the specified Weibull distribution. The alternative hypothesis therefore is that they were not. Rather than continually refer to calculated tables to assess the test outcomes, the observed significance level (OSL) of the modified test statistic (A^{2*}) was calculated empirically using

$$p = 1 / \left\{ 1 + \exp\left[-0.1 + 1.24 \ln\left(A^{2*}\right) + 4.48\left(A^{2*}\right) \right] \right\} \tag{3.10}$$

as described by Romeu (2003b). The observed significance level is the probability (*p*) of the null hypothesis being true. Unless the OSL is smaller than the critical probability level (*i.e.*, alpha level), the null hypothesis may not safely be rejected without an undue risk of committing a Type I statistical error.

Like any statistical hypothesis test, certain assumptions must be met. For the outcome of the Anderson-Darling test to be considered statistically valid, the data being evaluated must be independent and come from a Weibull distribution (Romeu, 2003a). In order to meet the assumption of independence, 100 wind speed observations were randomly selected without replacement from the ASOS data for each station. Anderson-Darling has been used with n as small as 6 with robust results (Romeu, 2003a) and thus an n of 100 is assumed to be sufficiently large. This procedure was repeated 100 times for each station. Because the Weibull distribution is mathematically unable to accommodate calm (0 m s^{-1}) values, only wind speeds above the 2 knot threshold were included in the random selection. However, the exclusion of these calm wind speeds does not necessarily invalidate the assumption of independence of the selected wind speed observations because the randomization ensures that each sampled speed is unrelated in time to every other sampled speed in the subset. The A^2 test was applied to each of the 100 random series for a given station using the empirically derived Weibull shape and scale parameters from the 30-year SAMSON record of wind speed at the same stations, and the results are presented in Table 3.3.

Weibull and A^2 statistics at selected stations						
		ASOS			SAMSON	
ID	Name	k	c	A^{2*}	k	c
ANJ	Sault Ste Marie, MI	2.01	4.03	2.6142	2.15	5.5
APN	Alpena, MI	2.31	4.18	2.1210	1.85	4.29
BUF	Buffalo, NY	1.98	5.16	1.9197	2.46	7.00
CLE	Cleveland, OH	2.16	5.14	1.7692	2.56	6.53
CMX	Hancock, MI	1.77	5.30	2.1641	1.92	6.53
DET	Detroit, MI	2.07	4.46	2.3177	1.73	6.66
DLH	Duluth, MN	2.03	5.34	2.1491	2.70	6.69
ERI	Erie, PA	2.10	5.01	1.7748	2.32	7.93
FNT	Flint, MI	1.97	4.82	2.2716	1.83	6.38
GRB	Green Bay, WI	3.23	5.86	2.1550	2.46	6.23
GRR	Grand Rapids, MI	2.06	5.11	1.6503	2.23	5.91
INL	International Falls, MN	3.29	5.53	2.0812	2.59	5.99
LAN	Lansing, MI	2.06	4.99	1.9886	2.40	6.52
MKE	Milwaukee, WI	2.04	5.32	2.1747	2.25	6.39
MKG	Muskegon, MI	2.00	5.28	1.8537	2.59	6.36
ROC	Rochester, NY	1.80	4.96	2.4818	2.07	5.83
SBN	South Bend, IN	2.12	4.93	1.8412	2.43	7.02
SYR	Syracuse, NY	1.67	4.56	3.2709	2.13	5.83
TOL	Toledo, OH	1.80	4.89	2.4188	2.37	5.76
TVC	Traverse City, MI	1.85	4.04	3.3116	2.58	6.25

Table 3.3 Wind data distribution and goodness-of-fit statistics for 20 ASOS stations in the study area with long-term (1961-1990) wind records. Weibull shape (*k*) and scale (*c*) parameters are given for short (ASOS) and long-term (SAMSON) speeds. Average Anderson-Darling (A^{2*}) test statistics based on 100 trials of 100 observations are given for the ASOS data.

At a significance level of $p = 0.01$, the results were mixed and in general inconclusive. The null hypothesis (that the ASOS data came from the SAMSON-derived Weibull distribution) was accepted about half the time when averaged across all 20 stations. While the most of the stations were able to accept the null in more than 50% of the trials, a few stations were unable to accept the null more than a few times. The overall average was reduced by the results from Traverse City, MI (KTVC) at which the null was rejected in all cases. Overall, however, for all stations the distribution of test statistics was negatively skewed toward more conservative values (Figure 3.10), and it appears that the average test statistics were by-and-large skewed by a few large outliers.

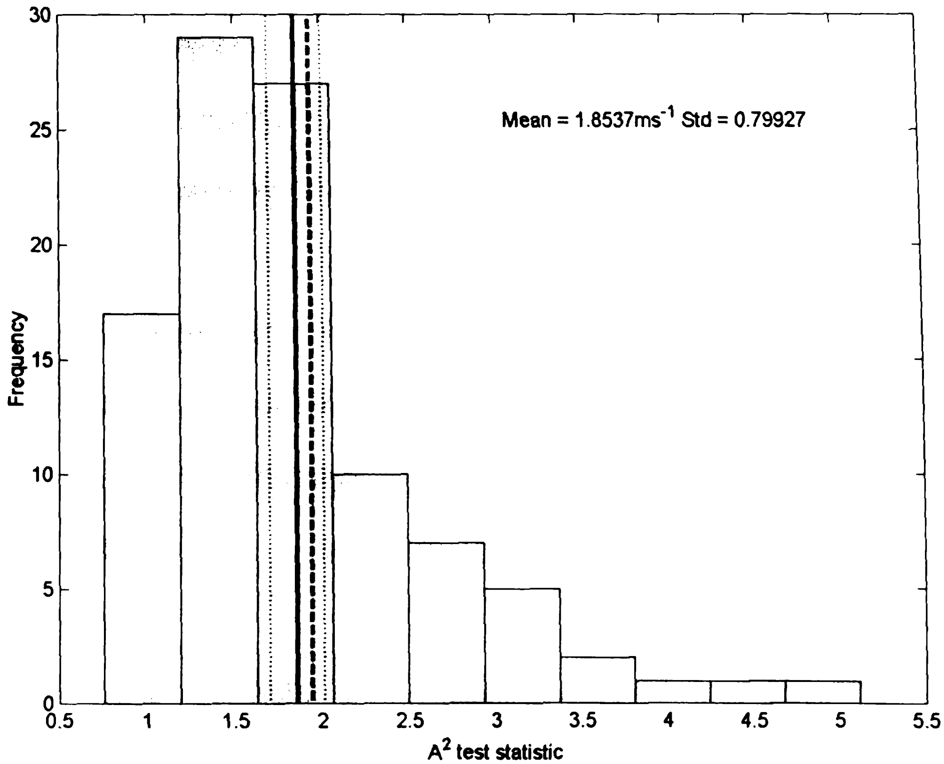

Figure 3.10 The distribution of Anderson-Darling (A^2) test values from 100 random samples of 100 ASOS wind speed observations at Muskegon, MI (MKG). The critical value (dashed) of 1.943 is shown, as is the mean test statistic (solid) and 95% confidence intervals (dotted). This station accepted the population Weibull distribution 66/100 times.

This behavior corresponds with the results of Shein (1995) who demonstrated that significant variation in empirically-derived Weibull parameters may occur from one year to the next, but that even though one year's distribution may vary from another, both are drawn from the same long-term population, both fit a Weibull distribution, and both are representative of the long-term wind speeds at a station. Therefore, the results of this representativeness analysis suggests that while the statistical summary of trial samples

(ASOS) may not have agreed with the long-term Weibull parameters (SAMSON), the preponderance of null-acceptance trials coupled with the graphical and statistical similarity between the two data distributions were enough for the researcher to conclude that the ASOS data are, in general drawn from a population that is distributed according to a Weibull function, and that it appears the ASOS data are, in general representative of the long-term wind speed climatology of the region.

Once the general goodness-of-fit of the Weibull distribution for data within the region and confidence that the data were not materially different from the long-term wind regime had been established, OLS was used to estimate the Weibull parameters for the ASOS data at the remainder of the 113 stations. The shape parameters ranged from 0.96 to 4.89, with a mean of 1.76 and a standard deviation of 0.41. The scale parameter ranged from 2.19 m s^{-1} to 7.48 m s^{-1}, with a mean of 4.10 m s^{-1} and a standard deviation of 0.98 m s^{-1}. This relatively low variation with respect to the parameter means suggests that wind speed distributions across the region do appear to exhibit some spatial coherence. Station values of shape and scale are presented in Appendix C.

3.4 Spatial and Temporal Behavior of Observational Data

3.4.1 Non-seasonal assessment

Prior to evaluating the estimative ability of a model, it is necessary to develop an understanding of the properties and behavior of the variable to be modeled. The Wind

Energy Atlas of the United States (Elliott *et al.*, 1987) indicated that, with the exception of the over-water and coastal zones, the Great Lakes region has a relatively low wind power potential, based in large part on the relatively low observed mean wind speeds over land in the area (Figure 3.11). Despite the increase in the number of stations in the study area in recent years relative to when the Atlas was compiled, wind statistics from the study period suggest that the results of the Atlas were not in great error.

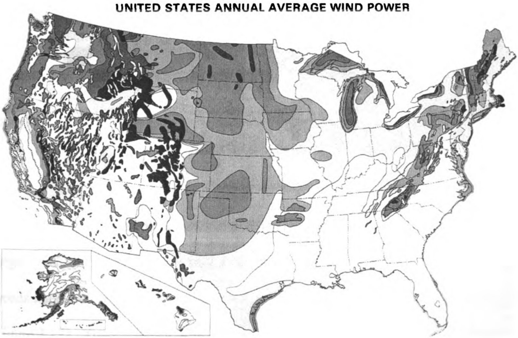

Figure 3.11 Average wind power map (at 50-m) of the contiguous United States from Elliott *et al.*, (1987). Darker areas represent greater wind energy potential. Values (as found in Elliott *et al.*, 1987) are based upon wind speed observations from lower heights, and many of the over-water estimates are of low confidence due to limited data availability. A substantial portion of the over-land parts of the study area are listed as category 2, or very low wind speed potential.

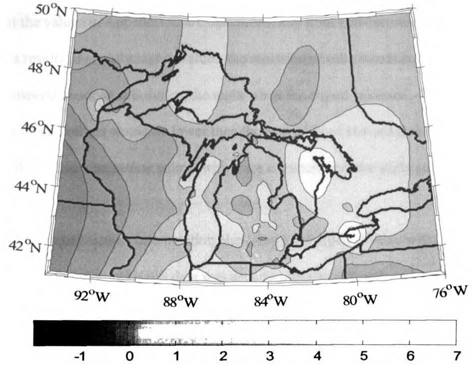

Figure 3.12 Annual mean wind speeds (in m s^{-1}) for the period of record across the study region. Negative values are invalid byproducts of interpolation and should be ignored.

Over the Great Lakes region the mean wind speeds from the period of record range from 2.06 to 7.10 m s^{-1} with a mean regional speed of 3.77 m s^{-1}. The strongest speeds appear to be concentrated near Long Point, ON with the weakest in SE Michigan (Figure 3.12). There appears to be a fair amount of variability about the means at a number of stations. Stationwise standard deviations range from 1.60 m s^{-1} to as much as 3.77 m s^{-1}, with a mean standard deviation of 2.38 m s^{-1}. Regionally, however, variability is much less. The standard deviation of station means over the region was just 0.75 m s^{-1}, indicating that there appears to be some degree of homogeneity in the regional wind field, and that much of the variability is the result of local scale influences. Means and standard deviations of all stations are presented in Appendix C. However, it should be noted that the values in Appendix C are calculated only from non-zero wind speeds. While this results in slightly higher values, the omission of calm winds is because several stations suspend observations during the night when the airport is closed. Thus the means for these stations would be lower than those at 24-hour stations that are more greatly influenced by nighttime calms, which are common over the study region.

A biharmonic spline interpolation algorithm, developed by Sandwell (1987), originally for interpolating GOES data was used to generate the contour maps of each variable over the region. Figures 3.12 and 3.13 both employ this method, as do all subsequent contour maps. The choice of this interpolation method was based on a comparison of several available alternative methods such as standard linear interpolation, cubic interpolation, and nearest neighbor interpolation. Standard linear, cubic, and nearest neighbor interpolation methods are all based upon Delaunay triangulation. The linear method contains discontinuities at its first derivative, and the nearest neighbor at its zeroth derivative. The cubic, while producing a smooth surface, was not equipped to perform extrapolation over the region.

In addition to the mean wind speeds over the region, the prevailing winds also were examined (Figure 3.14). When averaged over the study period, a general southwesterly prevailing wind direction was found at most stations. Such behavior is expected as the overlying synoptic scale flow at these latitudes is largely westerly, often with a southerly component when a trough resides over the Great Plains region

(Eichenlaub *et al.*, 1990). It is interesting to note that several stations do not conform to this pattern, instead demonstrating southeasterly prevailing winds. It is likely that these stations are more greatly influenced by high levels of localized flow modification, due either to mechanical (terrain) or thermal (sea breeze) factors or a combination of both.

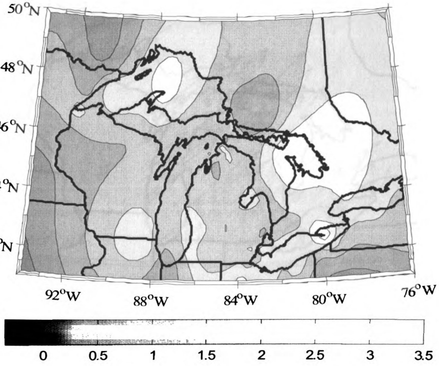

Figure 3.13 Standard deviations (m s^{-1}) about mean annual wind speeds over the study region for the period of record.

From the wind roses produced for each station, overall annual prevailing wind directions were identified at each station. The majority of stations exhibited prevailing winds from westerly directions. However, although a prevailing direction could be established for each station, most stations exhibited a multimodal wind rose and the prevailing direction was not clearly dominant when non-seasonal (all data) were used (Figure 3.15; Appendix D).

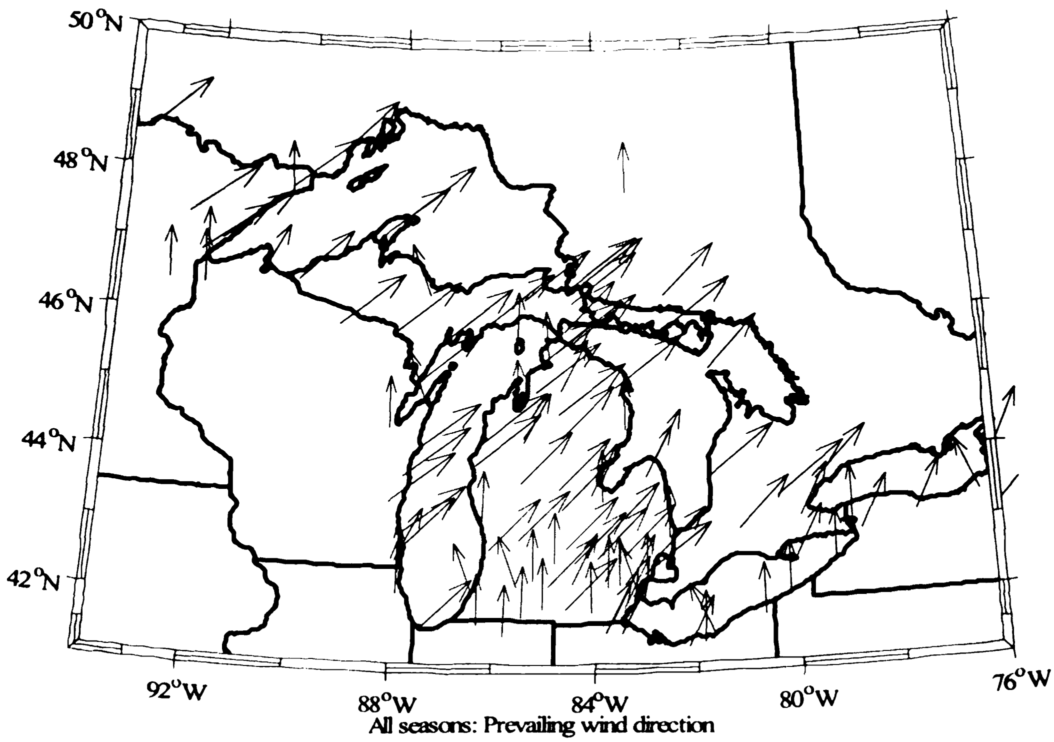

Figure 3.14 Prevailing wind directions (arrows are scaled by mean speed) at the stations used in this study. Prevailing winds are derived from all available data from all seasons in the period of record.

Furthermore, most stations exhibited a great deal of diversity in their wind rose distributions, both seasonal and overall. This suggests that the region is influenced by different flow regimes at different times of year, each contributing to the overall behavior of the wind field at each station. It also suggests that localized influences may play a larger than expected role in determining the behavior of the wind field at a given station site, which may complicate the wind field estimation of a non-local scale physically-based model.

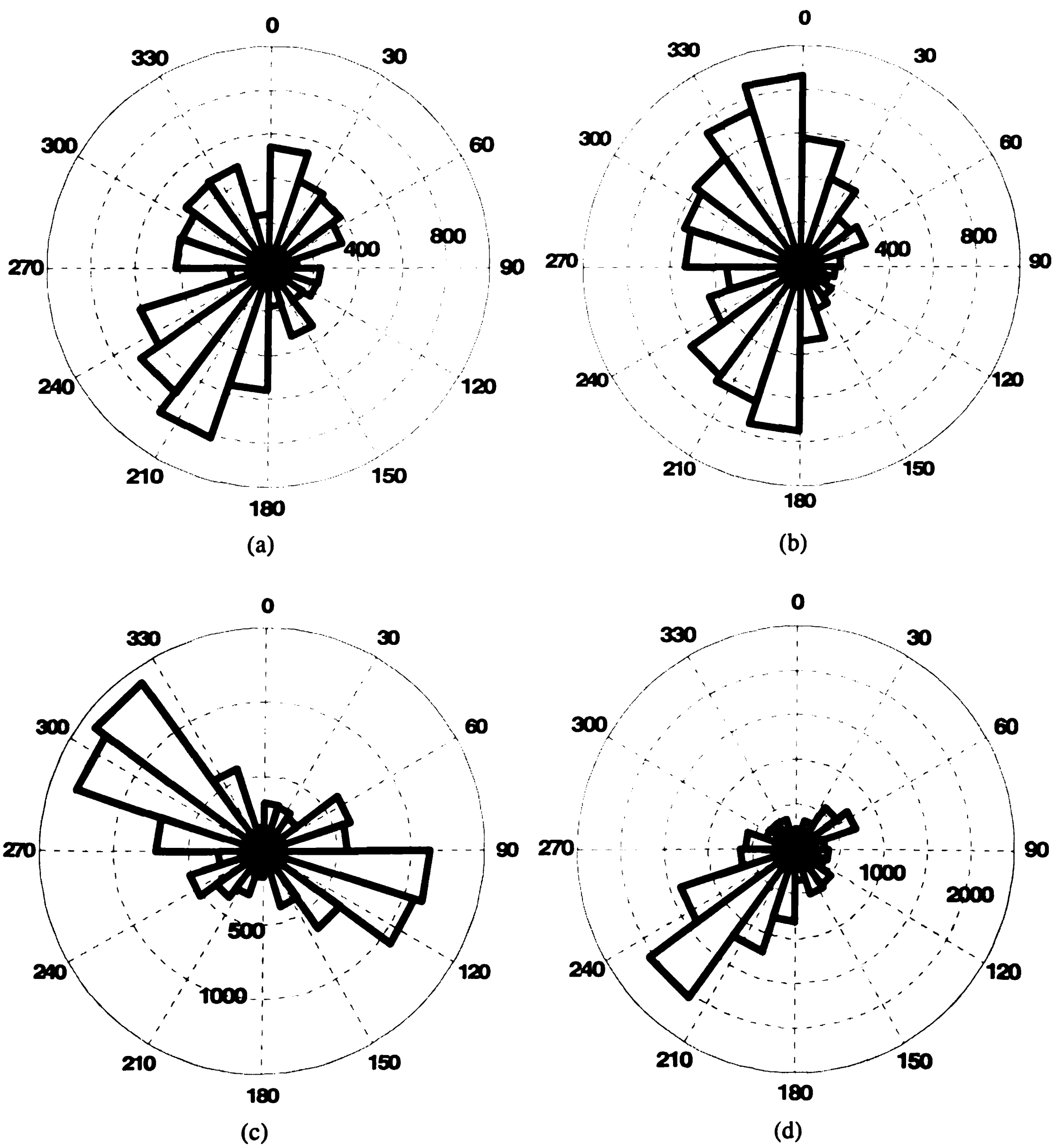

Figure 3.15 Annual wind roses at four stations across the study area [(a) Chapleau, ON, (b) Bellaire, MI, (c) Sault Ste. Marie, MI, and (d) Buffalo, NY]. Wind regimes over the study region are very diverse over the period of record (see Appendix D).

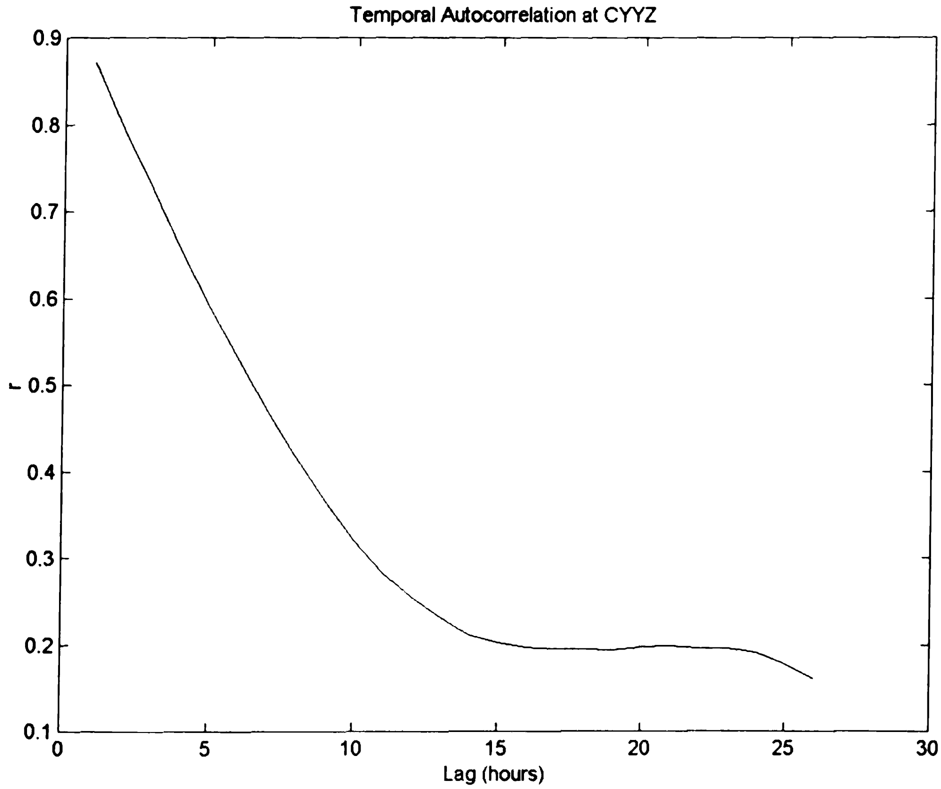

Figure 3.16 Temporal autocorrelation of non-seasonal wind speeds at Toronto, ON (CYYZ) over the period of record. This autocorrelation behavior is typical of wind speeds across the Great Lakes.

It is commonly accepted that wind speeds tend to exhibit a strong degree of temporal autocorrelation. An autocorrelation function was applied to the data in this study at each station and the results for the first 26 hour lags are plotted in Figure 3.16. Distinct autocorrelation was found at all locations, necessitating steps to minimize this behavior when statistically assessing the data. At a lag of one hour, autocorrelations ranged from 0.93 to 0.78, with a regional mean of 0.88 and a standard deviation of 0.03. The majority of strong lag-1 autocorrelations appear to come from stations that extend into the water regions of the Great Lakes (Figure 3.17). This suggests that the relatively low roughness of the lakes limits localized influences on the wind regime and may facilitate the success of autoregressive type models for wind speed forecasting over the water. However, given a correlation of 0.36 between the standard deviation of wind speeds and the autocorrelation coefficient, it does not appear that an increase in station speed variability necessarily results in decreased autocorrelation.

In addition to the temporal autocorrelation of the hourly wind speed observations, it is also noteworthy to describe additional patterns that may be present in the data. These include the possibility of both diurnal and seasonal (annual) patterns. Neither signal is inappropriate for the region. Near surface wind speeds tend to reach their zenith during the afternoon hours, when maximum local insolation has generated the strongest thermal gradients and turbulence over an area. Nighttime generally brings the slowest speeds as thermal activity is minimized and the boundary layer may decouple from the free atmosphere. This behavior also is manifested in an annual signal, but in reverse. Strongest winds over the Great Lakes tend to be exhibited in winter, at the time of the greatest hemispherical pressure gradients, and weakest in summer, when the polar front migrates well north of the region (Eichenlaub, 1979, Eichenlaub *et al.*, 1990).

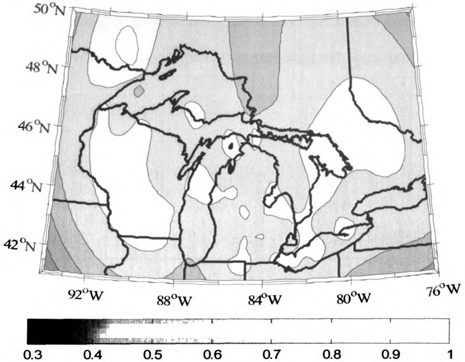

Figure 3.17 First order (lag 1) autocorrelation coefficients over the study area for the period of record. Although all stations are strongly autocorrelated, the highest autocorrelations appear to occur at stations most isolated from major land regions.

The seasonal signal is demonstrably recognizable in a time series of wind speeds at any station within the study area (Figure 3.18) and can also be visualized in a comparison between summer and winter wind speeds as will be discussed in the next sub-section. Several stations were found that did not exhibit a pronounced annual cycle. These stations tend to be relatively exposed (*e.g.*, Erie, PA) or in complex terrain (*e.g.*, Ironwood, MI) and as such may have a seasonal signal that is damped by local effects.

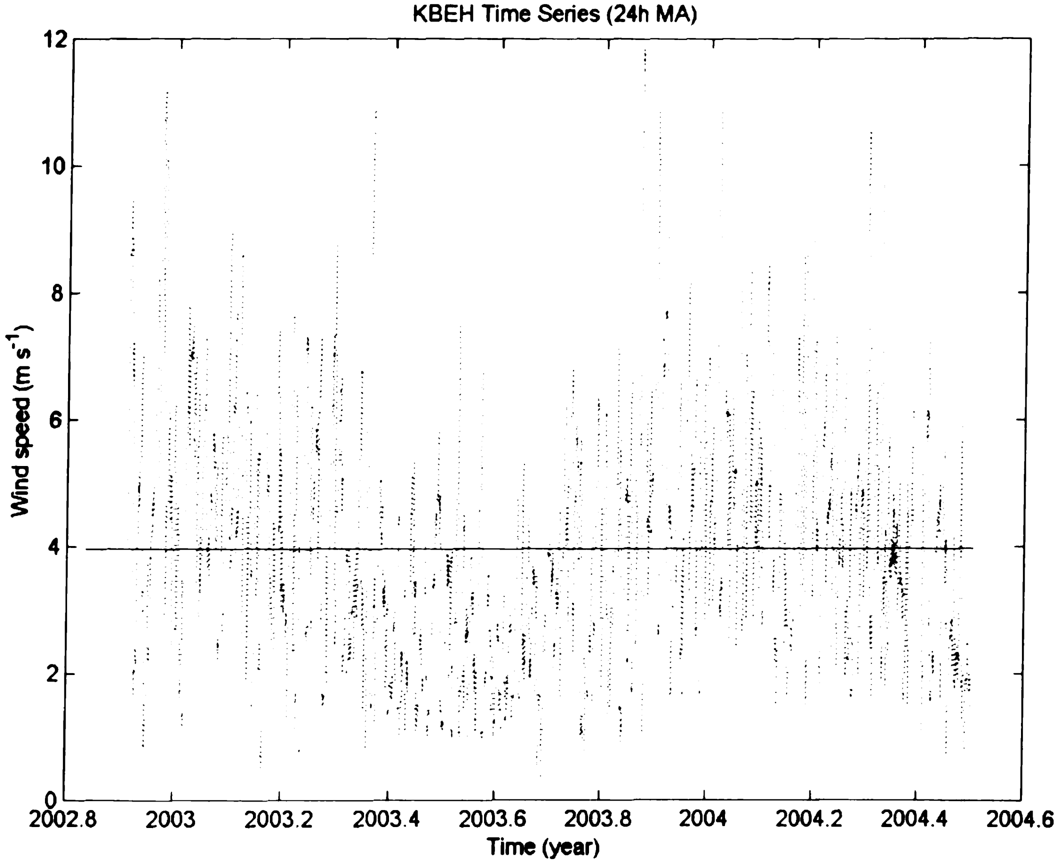

Figure 3.18 A 24-hour moving average time series of wind speeds at Benton Harbor, MI (KBEH) over the period of record. Lowest wind speeds are found during the summer months, while strongest winds are experienced in winter. All seasons appear to exhibit substantial variability about the station mean.

The diurnal cycle of wind speeds tends to be more difficult to visualize than the longer annual cycle. However, by decomposing the time series of hourly wind speed observations into its component cycles, the dominance of a diurnal cycle quickly manifests itself at most stations in the study region. The transition of data from the time domain to the frequency domain was accomplished by employing a Fast Fourier Transformation on the data at each station. The results of the transformation highlight the relative importance of the diurnal signal (and thus the effects of local influences) to the behavior of the wind field at a given location (Figures 3.19 and 3.20). Somewhat surprising was the relative strength of the diurnal cycle, which was found to be fairly constant across the region, indicating that lake breeze circulations along the coasts may not have as much of an influence on diurnal wind speeds as had been previously thought.

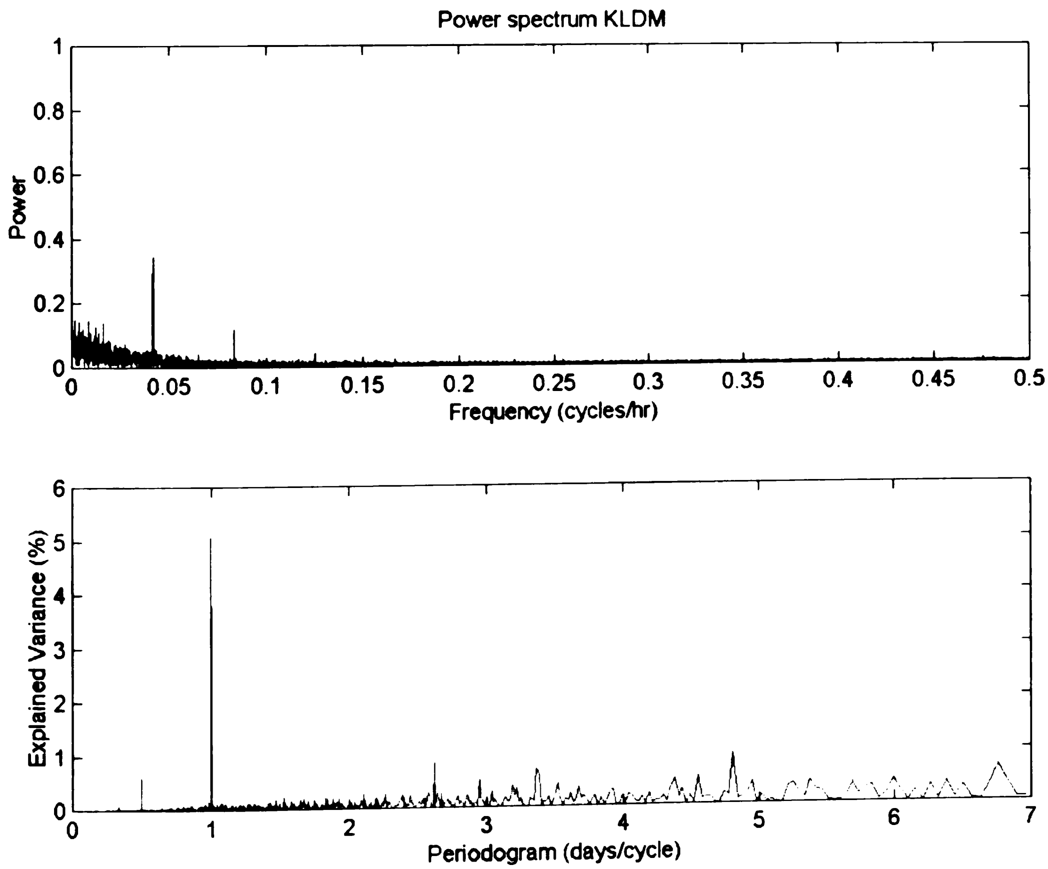

Figure 3.19 Power spectrum of wind speed at Ludington, MI (a coastal location) from 11/02 to 6/04. The diurnal cycle near 0.04 cycles/hr is dominant, accounting for 5% of the explained variance in the data.

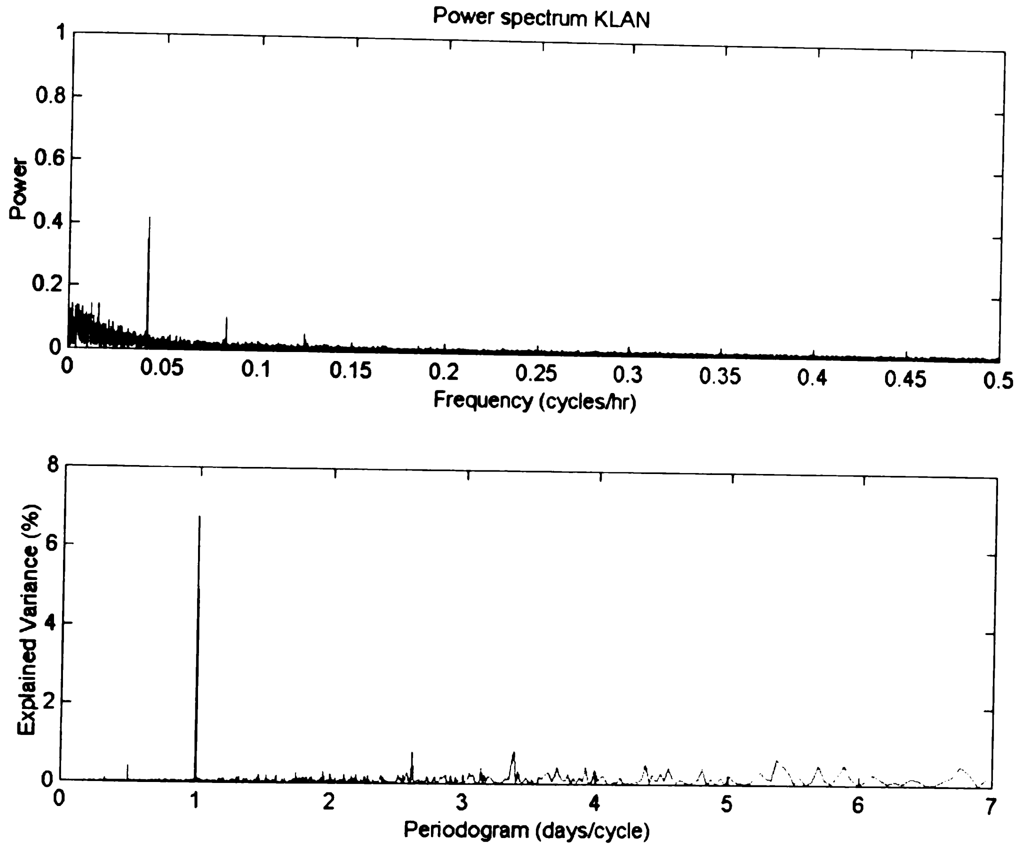

Figure 3.20 Power spectrum of wind speed at Lansing, MI (an inland location) from 11/02 to 6/04. The diurnal cycle near 0.04 cycles/hr is dominant, accounting for 7% of the explained variance in the data.

The annual distribution of wind speeds at the stations in the study area has already been discussed earlier in this chapter. However, while the frequency distributions of wind speeds over the study region appear to be well approximated by a two-parameter Weibull distribution, there was some variability in the parameters of the distribution over the region. The shape parameter (k) appears to be the least spatially variable (Figure 3.21). This is the parameter that controls the peakedness of the distribution (Figure 3.22). The larger the value of the shape parameter, the lower the variability about the mean, or stated another way, the greater the probability of experiencing a wind speed observation near the mean speed. From the data in Figure 3.21, it appears that the least variable winds (largest shape values) occur systematically toward the southern areas, centered about the tip of Lake Michigan. A lack of spatial variability in the Weibull shape parameter indicates that the variability of wind speeds about their mean does not vary appreciably over the region.

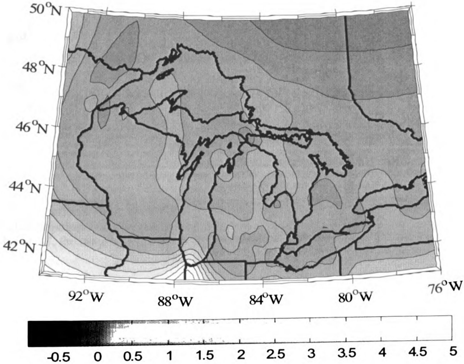

Figure 3.21 Annual Weibull PDF shape parameters over the study area for the period of record. Highest values indicate highest probabilities of winds near the mean wind speed.

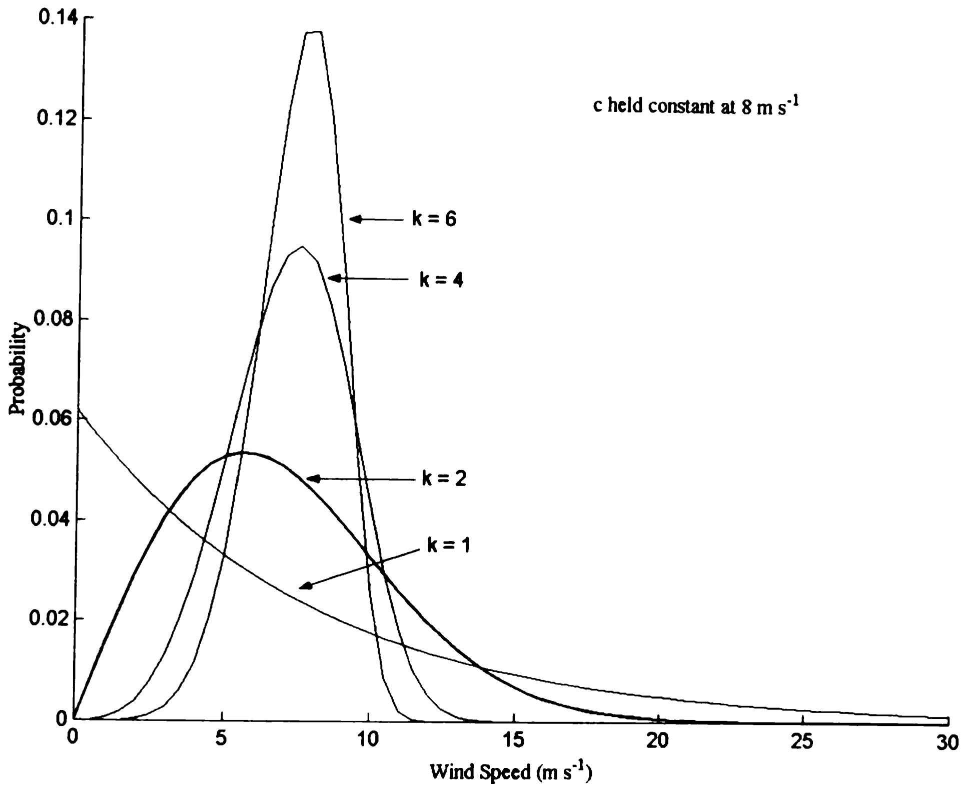

Figure 3.22 The influence on a Weibull PDF when the shape parameter is varied. A shape value of 1 is an exponential distribution, 2 is a Raleigh distribution, and 3.7 approximates a normal distribution. Below a shape value of 3.7, the distribution is right skewed, and above it left skewed.

Annually, the Weibull scale parameter (c) appears to be much less systematic in its behavior (Figure 3.23). However, one must remember, that the scale parameter is largely a measure of the first and second moments of the distribution (mean and standard deviation). The scale parameter value represents approximately the 63rd percentile of the distribution. Thus, as scale increases, the distribution is necessarily stretched toward the right tail because the distribution is bounded by zero on the left. Conversely, as scale decreases, the distribution is squeezed toward zero (Figure 3.24). Over the region, the highest scale parameters tend to occur in locations with high mean wind speeds. This is logical as a higher mean moves the distribution away from the lower zero bounds, thus stretching the distribution toward the right tail.

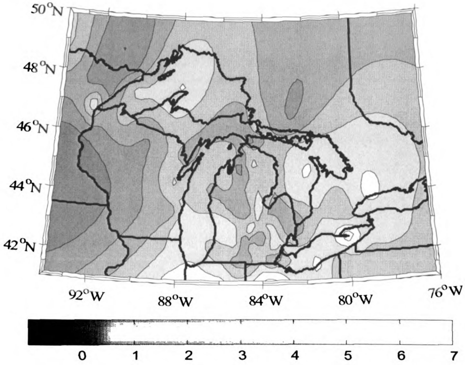

Figure 3.23 Non-seasonal (all data) Weibull PDF scale (*c*) parameters over the study area. It is clear that as with the shape, the distribution parameters cannot be considered regionally constant.

An alternative way in which to visualize and compare the distribution of wind speeds over the region is through schematic plots. Because schematic plots utilize more robust and resistant statistical measures (*e.g.*, median and IQR), such plots are arguably more robust than graphics that employ moment-based (*e.g.*, mean and standard deviation) measures (Wilks, 1995; Tukey, 1977). Additionally, more information can often be captured and presented in a schematic plot than in a standard frequency distribution histogram. For example, not only is the median presented, but additionally, it demonstrates the degree of spread of data about that median value; whether or not the data are symmetrically distributed and if high or low values are legitimately part of the main body of the distribution or whether they are outliers.

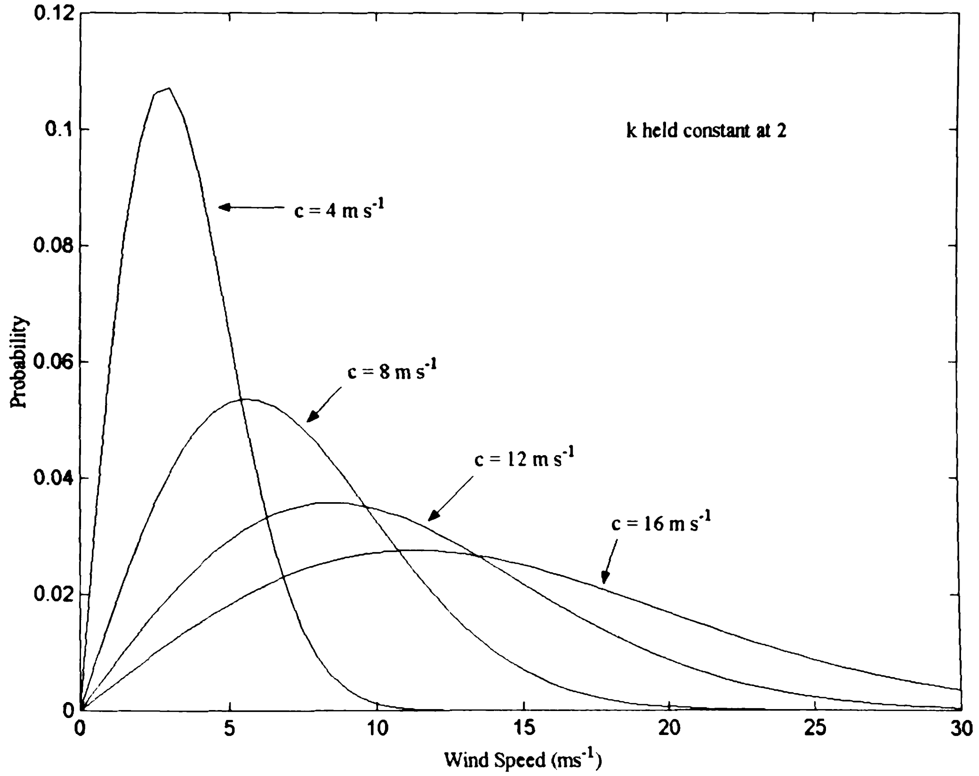

Figure 3.24 Variations in the Weibull scale parameter result in a stretching or squeezing of the distribution and reflect the behavior of the mean and standard deviation of the wind speed distribution.

Schematic plots of the wind speed series at each station were constructed as a notched box and whiskers plot, whereby the lower and upper bounds of the box are the lower and upper quartile respectively. The median bisects the box, and the notch represents a robust estimate of the uncertainty about the median value for comparison with other plots. The so-called whiskers that extend from the box ends represent the outer fences of the data, or 1.5 times the interquartile range (IQR). The whiskers help to illuminate the extent of the more unusual data within the distribution. Lastly, outliers, or those values that exist beyond the outer fences are illustrated independently as points on the plot. Overall, the schematic plots allow a great deal of information regarding the distribution to be presented and graphically compared to other distributions. Three example schematic plots are presented in Figure 3.25. Schematic plots for all stations can be found in Appendix D.

Surprisingly, when the outliers are clearly identified and excluded, it appears that there is not a great deal of variation between stations. This clearly illustrates the dependence of the mean wind speed on extreme outlier values. In general, most plots show a median value of between 4 and 5 m s^{-1} and an IQR of only about 2-3 m s^{-1}, with much of the higher winds constrained to the upper outer fence region and but a few extreme outliers. Unfortunately, it appears that, based upon these distributions, very few of the stations would have wind speeds sufficient to economically support wind energy conversion as the entire IQR resides below the peak power thresholds (the lower bounds of rated power output) of most turbines (about 9 m s^{-1} when adjusted to 10-m height). As expected, however, it was the distributions at stations extending into the lakes or along the windward shores in which the peak power threshold occurred within the upper whisker region of the plot.

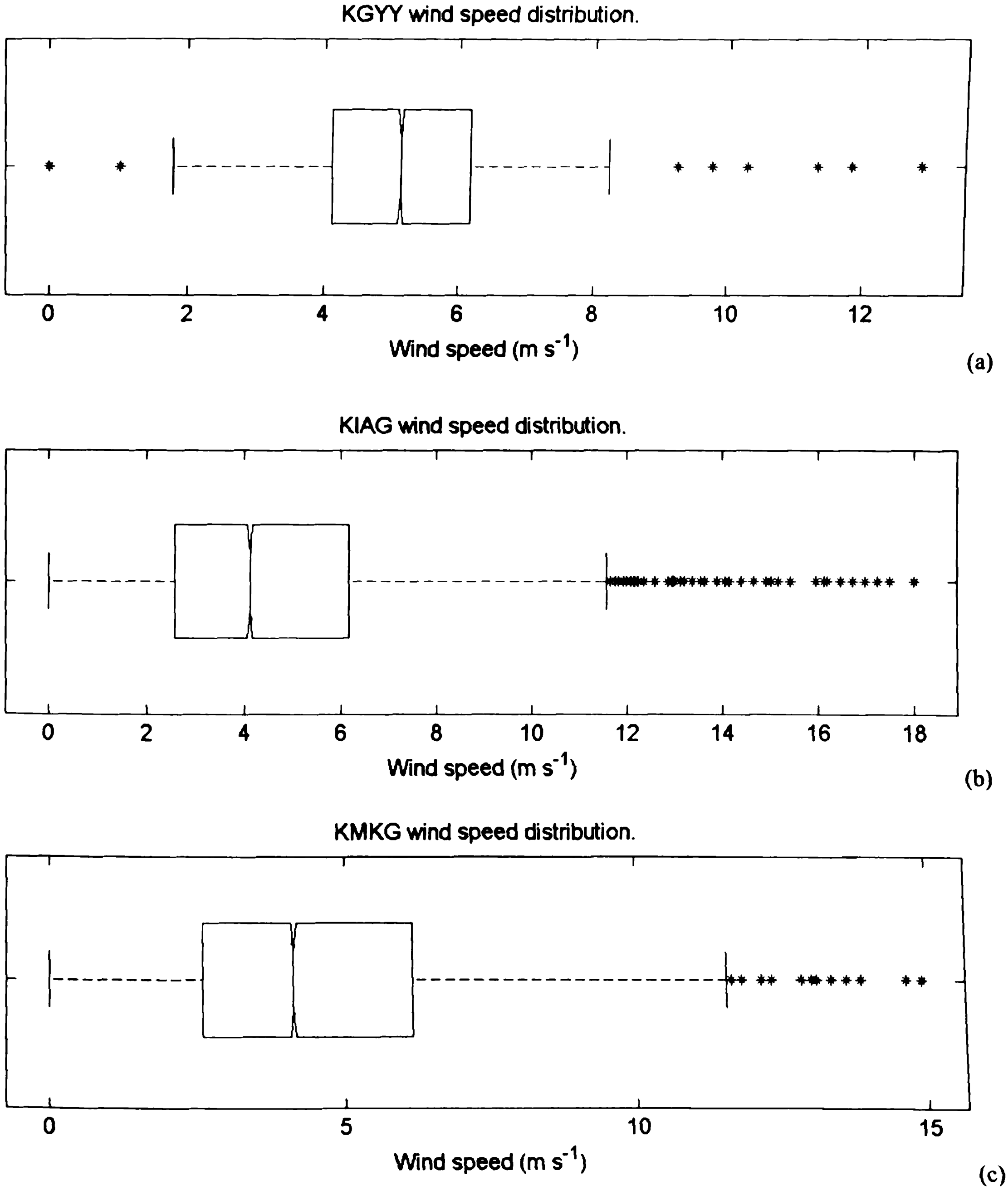

Figure 3.25 Schematic plots of non-seasonal wind speed distributions at 3 stations [(a) Gary, IN, (b) Niagara Falls, NY, and (c) Muskegon, MI] for the period of record. Most of the variability appears to be not in the main body (IQR) of the distribution, but rather in the presence of high wind speed outliers. This information likely skews both the mean and standard deviation of the distributions toward higher values. See Appendix D for plots for all stations.

To further examine the wind power potential of the region, a power analysis was undertaken. This involved examining two factors. First was the amount of time a turbine would experience winds in the range at which it would produce its maximum (or rated) power. This amount of time is called TARP, or time at rated power (Shein, 1995) and, for this study area is largely dependent on the winds in the upper whisker region of the aforementioned schematic plots. The rated power calculations were based upon an idealized turbine with a rated wind speed range of 12 to 25 m s^{-1} at a hub height of 50 meters. The results of this analysis are presented in Figure 3.26. It appears that, as expected, the overall percentage of time that the wind speeds fall within the rated power portion of the turbine power curve is relatively low; under 20% for the entire region.

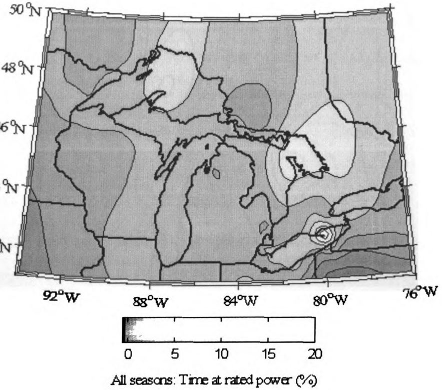

Figure 3.26 Percent time at rated power (TARP) over the study area for the period of record. This is a ratio of the total time a wind turbine might be expected to be producing its rated (maximum) power. Calculations are based on a 50 m turbine hub height with a rated power range at 50 m of 12 to 25 m s^{-1}.

As expected, the greatest TARP percentages were over Lakes Superior and Erie, as well as Georgian Bay. However, TARP does not include those wind speeds at which the turbine would be producing power at less than its rated capacity. Thus, an estimation of total actual power potential was called for. This power estimate was obtained by adjusting the wind speeds to 50 meters using the wind speed power law (Equation 3.1) with the $1/7^{th}$ exponent, and using the actual power curve of a moderate sized wind turbine that might reasonably be installed in the study region. The turbine used was a Vestas 850 kW with a 50-m hub height. By translating 50-m wind speed estimates into estimated turbine power output, a realistic measure of wind power potential over the region could be obtained (Figure 3.27).

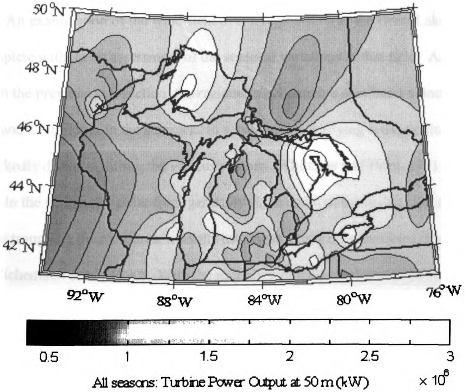

Figure 3.27 Power output in kilowatts over the period of record from a Vestas 850 kW wind turbine.

From Figure 3.27 it is rather clear that coastal regions that can be expected to have a substantial over water fetch appear also to be the most productive in terms of power output from a turbine placed at those locations. In particular, Long Point and Georgian Bay in Ontario as well as the Lake Michigan shoreline and Keweenaw Peninsula in Michigan would be most appropriate for WECS development. This spatial pattern of Figure 3.27 appears to share some similarity over the region with the U.S. wind power map in Figure 3.11 (Elliott *et al.*, 1987).

3.4.2 Seasonal assessment

An examination of the wind field over a region such as the Great Lakes would not be complete without an assessment of the seasonal variations in that field. As has been noted in the previous sub-section, the regional winds reach a maximum velocity in the winter and a minimum in the summer. In addition, the overlying synoptic flow patterns are markedly different during the various seasons (Whittaker and Horn, 1981, Harman, 1987). In the winter, the polar front generally shifts south of the region, and so, with frequent troughing over the area, a northwesterly wind might be expected (Eichenlaub, 1979, Eichenlaub *et al.*, 1990). With the migration of the polar front to the northern reaches of the study area, summertime is expected to bring a shift to a more southwesterly flow over the region, and, with a decreased pressure gradient over the region, a weakened velocity structure. While strong summer winds do occur, they tend to be inconsistent, occurring in coincidence with frontal passage and convective activity rather than a strong upper-level flow as is present in the winter. Overall, the year was divided up into four parts of three months apiece to represent each of the seasons. Winter was comprised of December, January and February. Spring was March, April and May. Summer was June, July and August. Fall was September, October and November.

As the variation in mean wind speeds has been discussed in the previous sub-section it is not necessary to repeat it here. However, an examination of differences in seasonal variability is in order. Although it was thought that perhaps the transitional seasons of Spring and Fall would experience the greatest variability of wind speeds about the mean, this was not found to be the case (Figure 3.28). Rather, winter, with its highest mean speeds also had the highest standard deviations. Summer, in contrast, with its low speeds tended to also have the lowest variation in speeds.

In addition to differences in variability of wind speed, it is also expected that there exists a variation in prevailing wind direction from one season to the next. The prevailing winds therefore were plotted over the region and examined by season. Figure 3.29 shows the transition from a summer regime to a winter one in terms of shifts in the prevailing winds.

(a) Spring

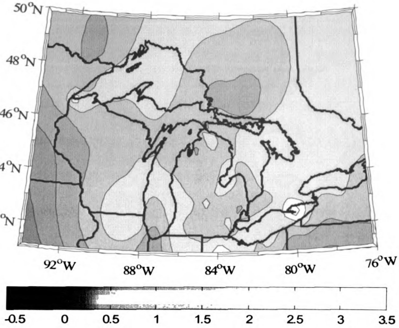

(b) Summer

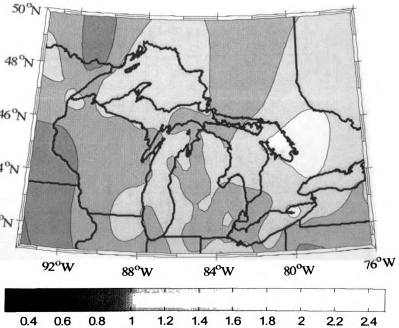

Figure 3.28 Standard deviation (in m s^{-1}) of wind speeds by season (11/2002 - 6/2004). While the highest wind speeds occur in the winter, so does the greatest variability in wind speeds. As expected, summer, with the lowest mean speeds also has the smallest variation.

(c) Fall

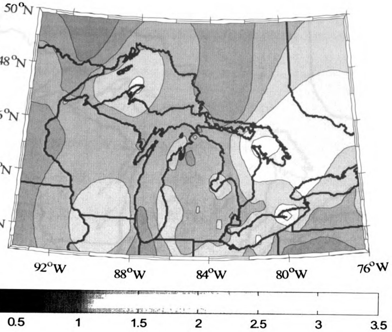

(d) Winter

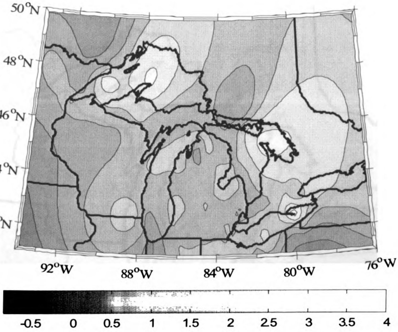

Figure 3.28 Continued.

(a) Spring

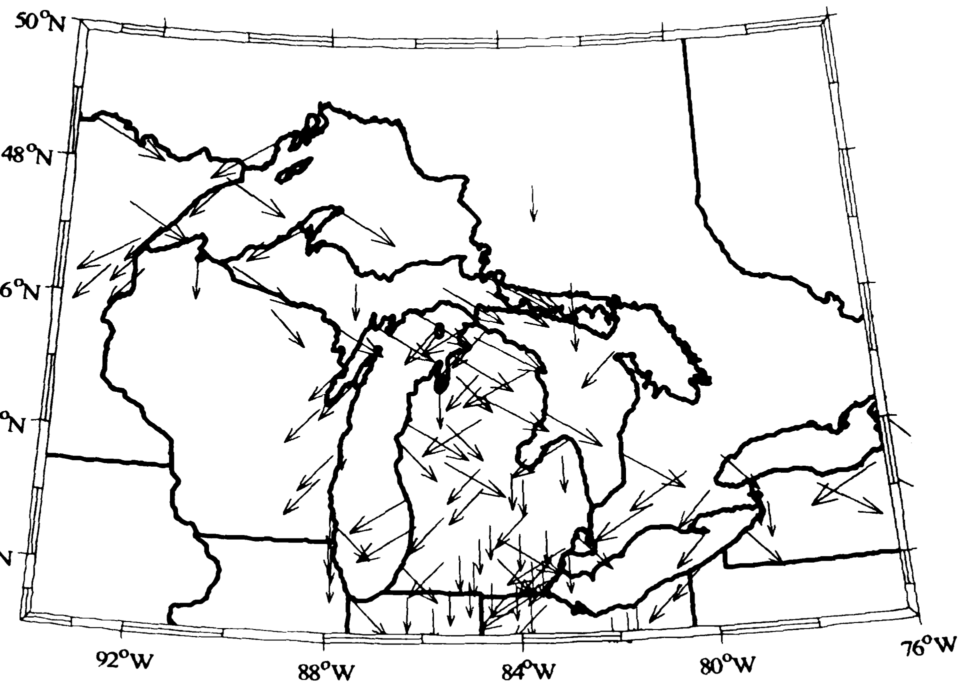

(b) Summer

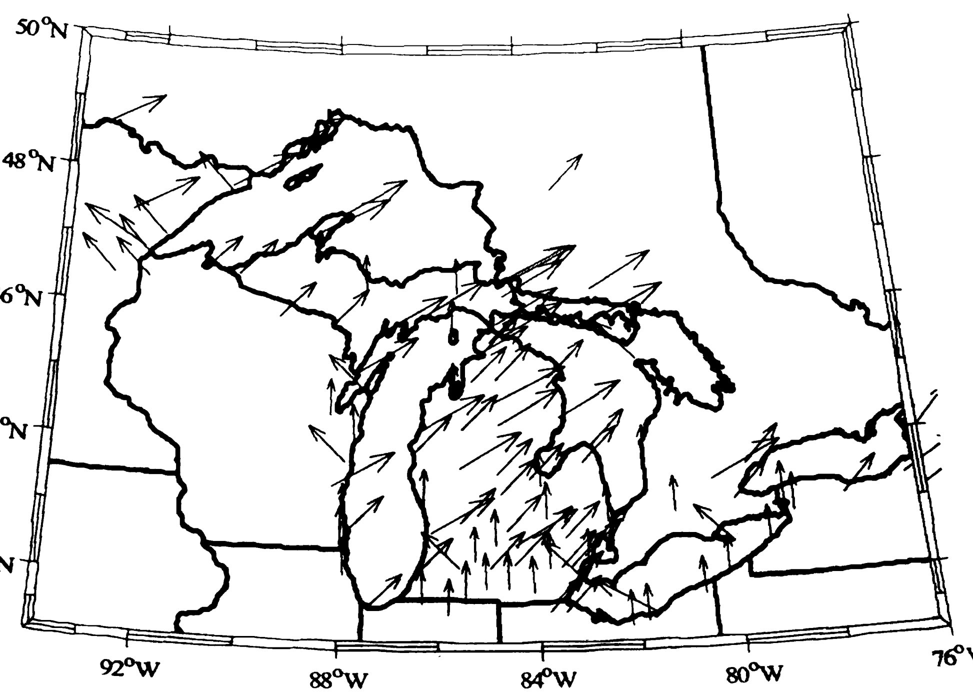

Figure 3.29 Prevailing winds during each season (11/2002 - 6/2004) at the stations in the study area. The dominant direction in all seasons except Spring is southwesterly. Spring is characterized by predominantly northerly and northwesterly winds. Station wind arrows are scaled by seasonal mean wind speed.

(c) Fall

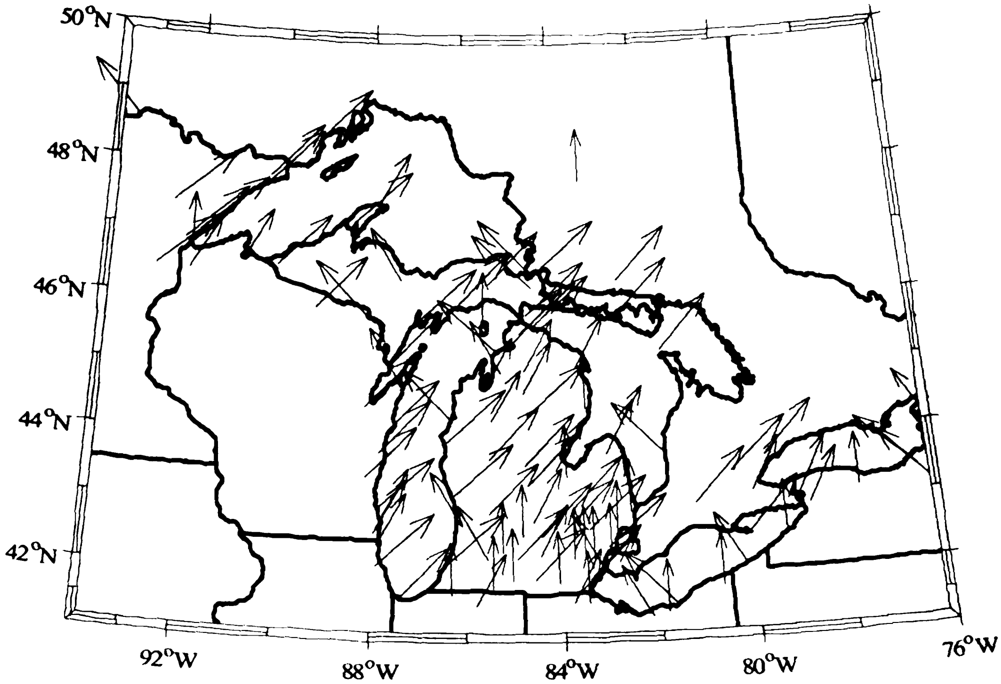

(d) Winter

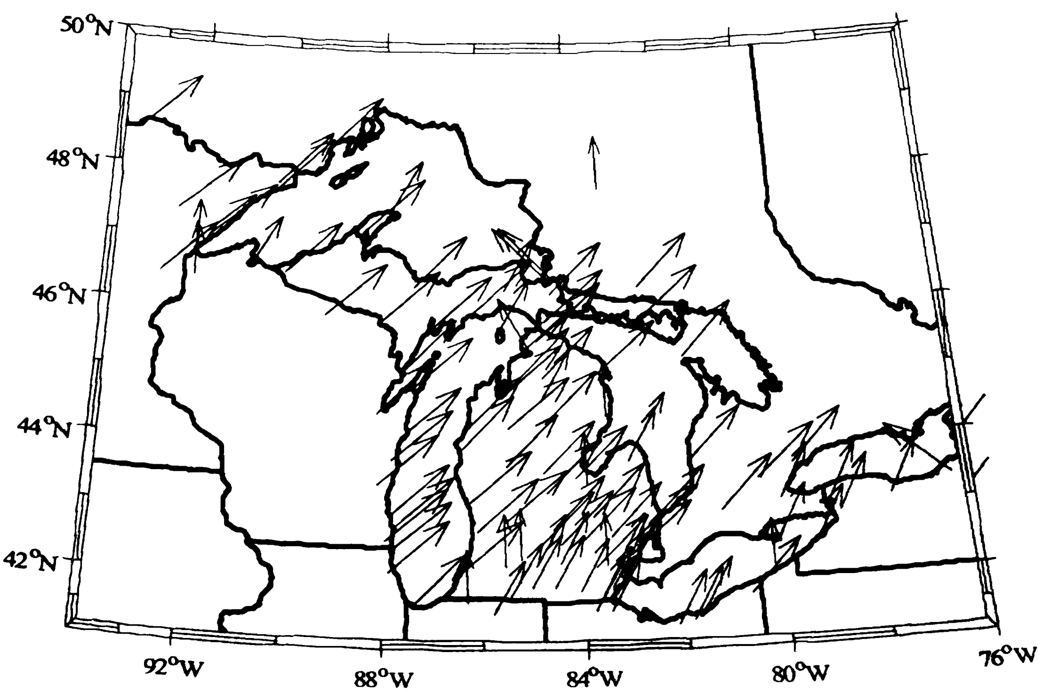

Figure 3.29 Continued.

Interestingly, the expected northwesterly flow of a wintertime mid-latitude wind field did not materialize. Instead, this northerly flow was restricted to the Spring months. It is possible that a deviation from the regular winter synoptic patterns over the region during the period of record led to this inconsistency. In addition, winter was the most consistently southwesterly. In the Fall and Summer, a number of stations had prevailing wind directions that did not adhere to the general regime of the region, likely the result of a dominant local flow pattern. Indeed, it is during these months that insolation is maximized, and as a result the thermal lake breeze is strongest. This is evident in that the stations having deviant prevailing winds all appear to be located in close proximity to a coast, and the direction is largely perpendicular to the coastline. Winter shows the least amount of variability from the prevailing southwesterly flow.

Based on this seasonal variation, seasonal wind roses at the stations were examined. The seasonal wind roses highlighted two important characteristics of the regional wind field. First, it was confirmed that the majority of stations exhibited seasonal wind roses that were consistent with the regional pattern (Figure 3.30). However, the seasonal wind roses also demonstrated that in most cases there was a great deal of variability in wind directions, and that the prevailing wind direction was not dominant. In general, it appeared that Fall, closely followed by Winter exhibited the greatest variability in wind direction. With a few exceptions, Summer was the least variable in terms of wind direction. In addition, Summer wind roses at many of the coastal stations exhibited a fair degree of bimodality, suggesting at least some local thermal influences.

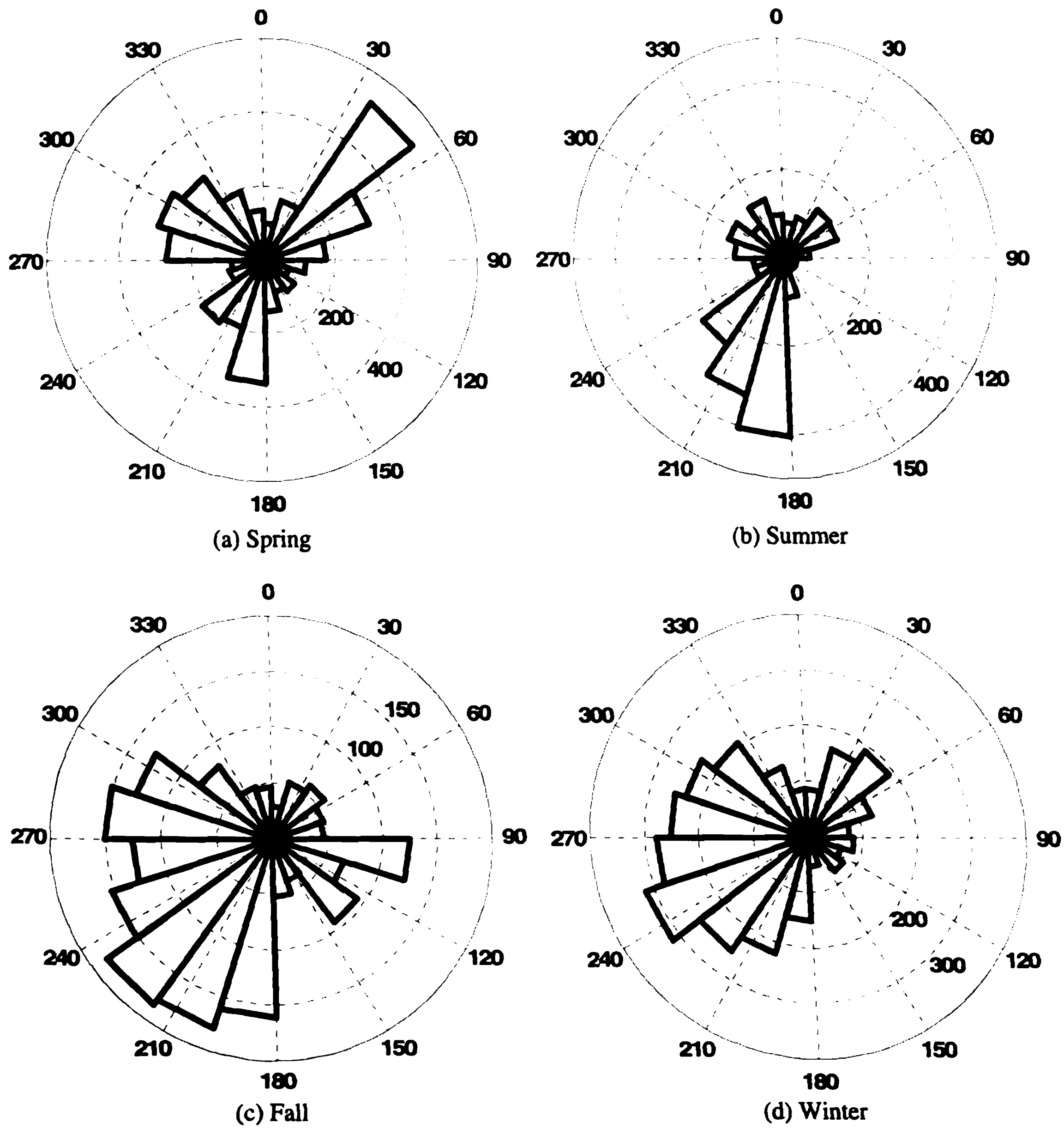

Figure 3.30 Seasonal wind roses at Beaver Island, MI (KSJX) for the period of record. This station is consistent with the regional prevailing flow regime.

Secondly, at station sites where it could be assumed that local terrain or local thermal flow regimes might substantially affect the wind field, a corresponding signal was found in the wind roses (Figure 3.31). As mentioned earlier, a thermally induced lake breeze circulation appeared to be commonly manifested in Summer wind roses as a bimodal distribution of low variability. In other instances, such as the sheltered bay surrounding Traverse City, MI, the wind flow appears to be dominated by thermal circulation guided by the orientation of the bay during the Spring and Summer, and dominated more by the overlying westerlies the remainder of the year.

To better address some of the influences on the local station winds at different times of year, it is perhaps advantageous to examine the dominant signals in each of the seasonal wind speed series (Figure 3.32). In particular, three signals are of interest. The first is the diurnal signal, which may indicate a dominant thermally induced pattern of winds (diurnal heating/cooling). At coastal locations in the Summer, a half-day signal might also appear, the result of a lake breeze circulation. Lastly, cycles with periods of 3 to 7 days are of interest. This is approximately the frequency with which mid-latitude synoptic systems pass over the region (Eichenlaub, 1979, Harman, 1987).

The behavior of the data in the frequency domain is exactly as expected for the region. There is a diurnal cycle present at all stations. The diurnal signal also varies by season. The diurnal signal has its most power in the Summer. For example, at Holland, MI (Figure 3.32), the power of the daily cycle is nearly three times stronger than in either the Spring or Fall. The daily cycle is at its lowest power during the Winter months.

Secondly, at stations near a coastline, such as Holland, MI, there is a distinctive half-day cycle that is present in all seasons, but is weakest in the Winter (Figure 3.32). The half-day cycle is of more-or-less equal power in the Summer and Fall, and only slightly weaker in the Spring. It is likely that the half-day cycle during winter is more the result of aliasing from the diurnal cycle than an actual thermally induced lake breeze circulation. The cycle's presence at predominantly coastal locations during months of heightened insolation appears to confirm the presence of a lake breeze circulation, as aliasing is unlikely to account for the entire signal to that magnitude.

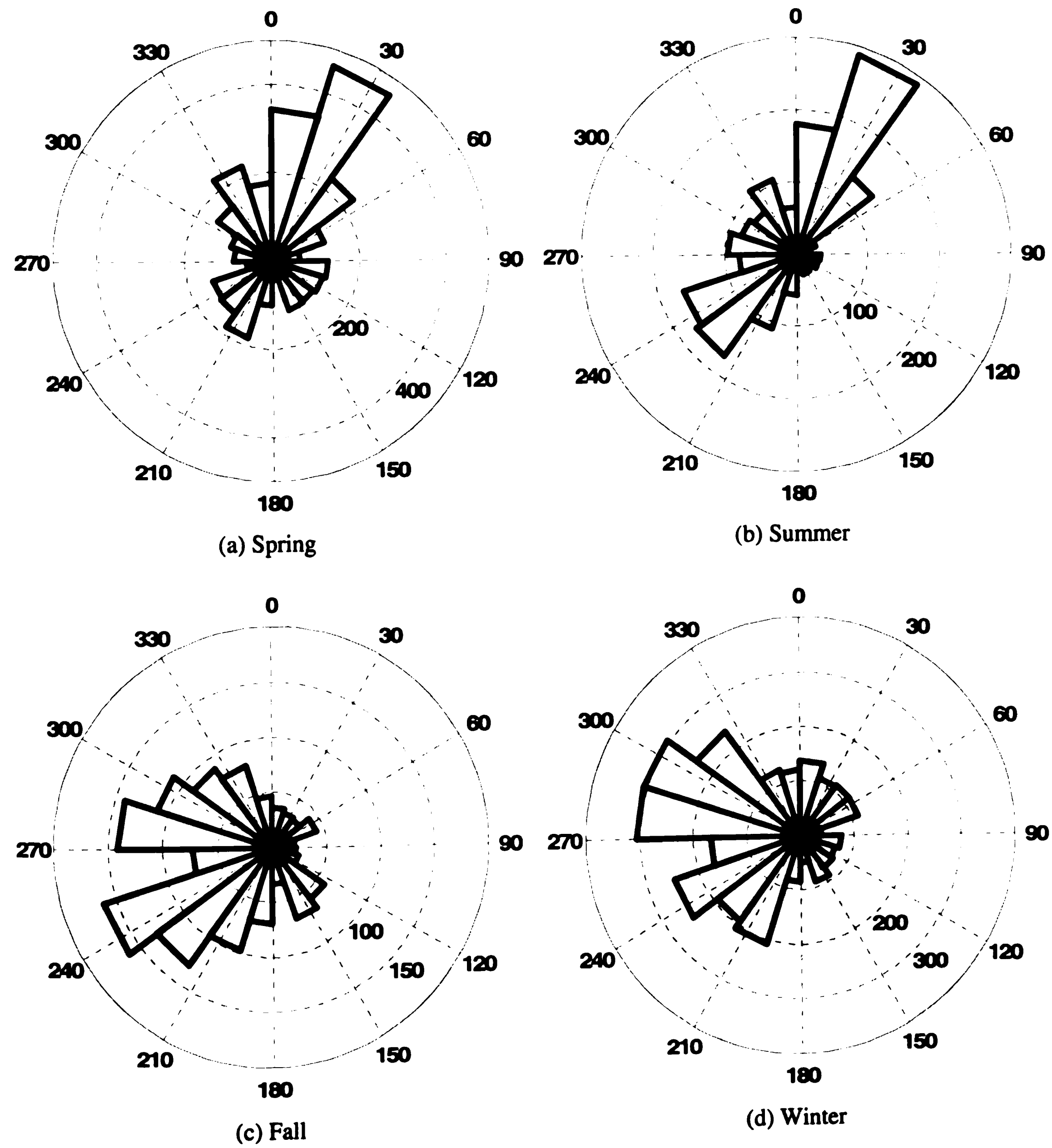

Figure 3.31 Seasonal wind roses at Traverse City, MI for the period of record. In its bay location, lake breeze circulation and localized flow predominates, especially in Spring and Summer.

(a) Spring

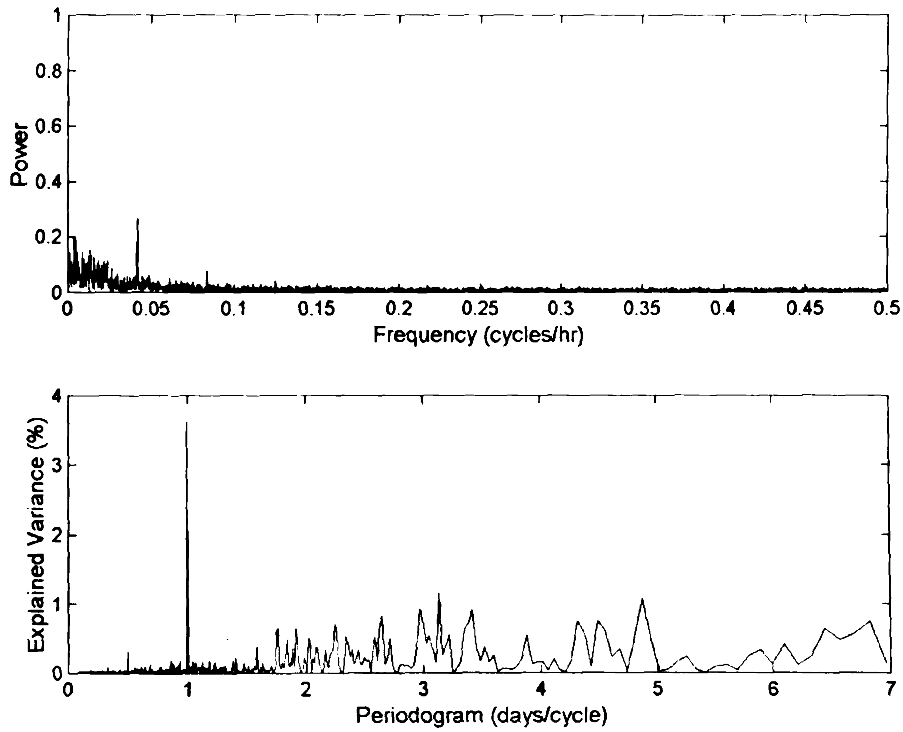

(b) Summer

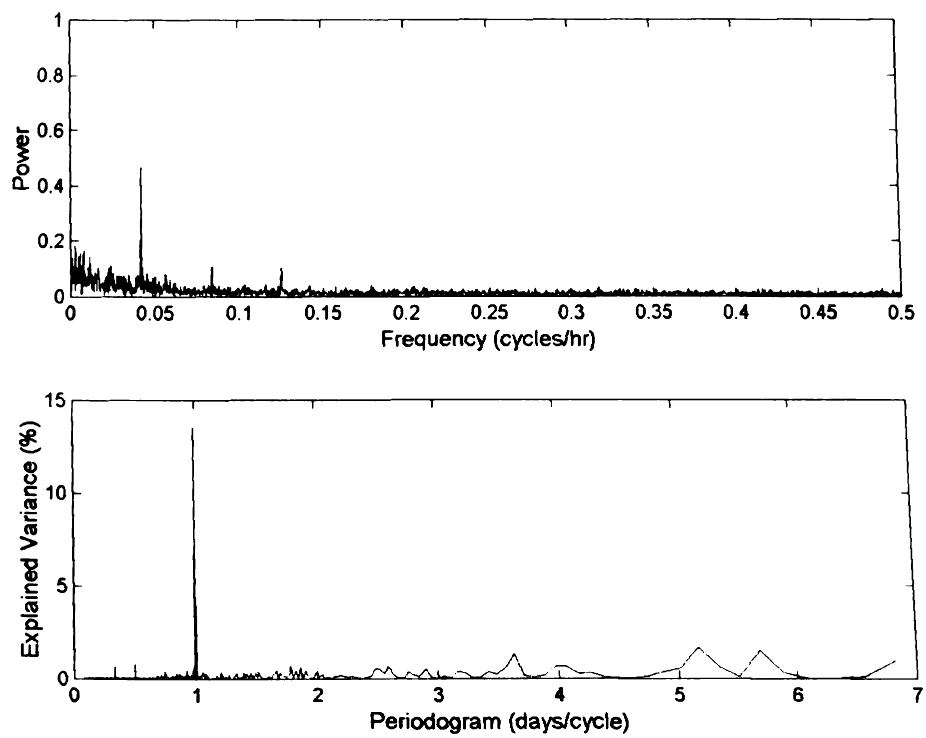

Figure 3.32 FFT seasonal power spectra at Holland, MI for the period of record. Upper figures indicate the power of the signal at any given frequency. Lower figures translate the power into a percentage of explained variance of each signal relative to its periodicity.

(c) Fall

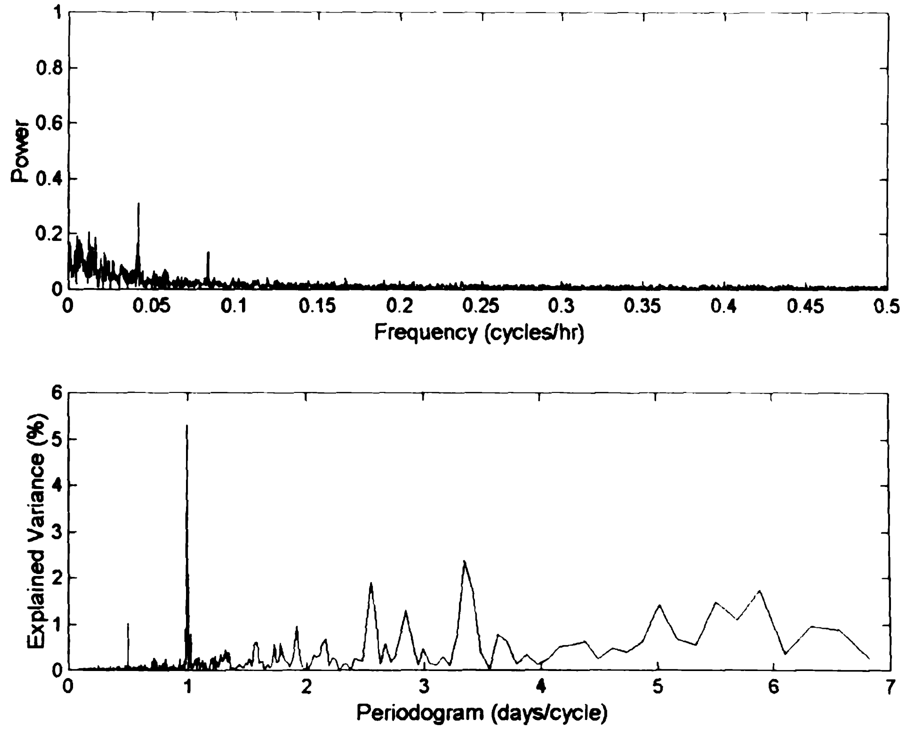

(d) Winter

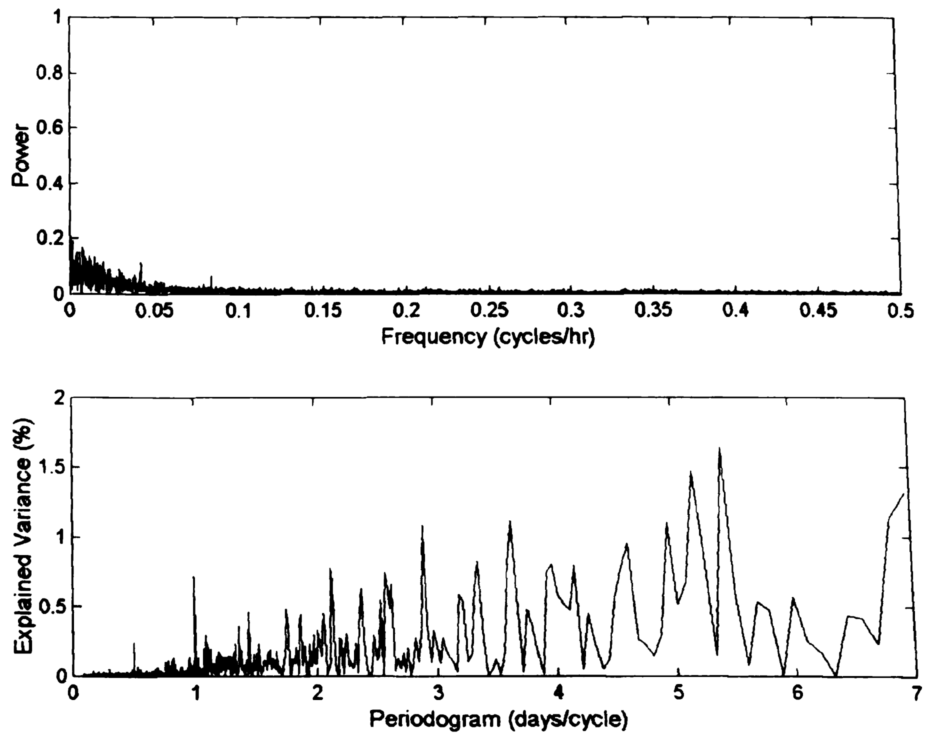

Figure 3.32 Continued.

Lastly, as expected, all stations exhibited relatively strong signals between 2 and 7 days per cycle, but not equally in all seasons (Figure 3.32). This so-called synoptic signal is most likely the result of mid-latitude synoptic systems traversing the region. As expected, these signals were strongest in the Winter and weakest in the Summer. More moderate synoptic signal strength was encountered in the Spring and Fall.

In summary, the wind field in the region is characterized by two dominating influences. There is a distinct influence by the overlying synoptic circulation of the mid-latitudes. This is manifested in the predominance of a regionalized prevailing wind direction and the fundamental similarity in mean wind speeds across the region. It is likely that a regional scale, numerically driven climate model may capture this influence with a high degree of confidence. The other influence however, is a local component that is the result of both differential heating from variations in land cover, and of terrain that may channel the flow. As this is a study primarily of coastal regions of the Great Lakes, much of both influences is due to the land – water transition. From a thermal perspective, the differences in specific heat between the lakes and the land adjoining them is quite strong, but also can be variable depending on the land cover along the coast. From a mechanical perspective, the land – water transition zone often represents one of the most acute changes in surface roughness in a region. It is likely that even the most well specified dynamical models may have difficulty fully parameterizing these localized effects, and it is likely that here is where much of the model error will occur.

3.5 FSMM5 Model and Wind Estimates

The major objective of this study is to evaluate the performance of the regional-scale numerical climate model known as MM5 for use in identifying areas with wind energy potential, and to identify techniques that may improve the performance of the model. In order to accomplish this goal, MM5 estimates of the near-surface wind field were obtained over the region at a number of spatial resolutions. Because the implementation and oversight of MM5 requires a substantial investment in both computer and operator time, the performance of MM5 was also compared to estimates of the wind field derived from several other popular stochastic model approaches, such as Measure-Correlate-Predict (Derrick, 1992). Each of the comparison models represents a technique that has been used in wind energy research and is less complex than MM5. This chapter discusses MM5 and the comparison models and outlines the methods for model evaluation and comparison.

3.5.1 Model implementation and domains

Simulated wind data for the study were obtained from version 3.4 of the non-hydrostatic 5th Generation Mesoscale Model (MM5), developed at the Pennsylvania State University and NCAR (Haagenson *et al.*, 1994). This version of MM5 (hereafter FSMM5) has been implemented for operational and research use by the U.S. Forest Service North Central Research Station in East Lansing, MI (USDA, 2002). FSMM5 has been run operationally since the summer of 2002 and produces 48-hour hourly forecasts of several meteorological indices of importance to forest fire risk and mitigation (Charney *et al.*, 2003, Heilman *et al.*, 2003). FSMM5 is run at 36 vertical sigma layers (non-spectral) on a 36-km grid that covers much of eastern North America and a 12 km domain that extends from 31.9° N, 101.9° W (lower left) to 51..9° N, 63.7° W (upper right). Within the 12-km domain a 4-km grid is nested to provide greater spatial resolution (Figure 3.33). The distribution of grid points over the study area is presented in Figures 3.34 to 3.36. The domain layers are variably distributed according to pressure, with the lowest at around 2 meters (surface) and the top layer at approximately 12 km (100 mb). Within the vertical domain, near surface layers are more closely spaced (corresponding to vertical pressure gradients), gradually increasing from about a 10 meter spacing between the bottom layers to about 1500 meters of spacing between the uppermost layers (In *et al.*, 2004).

Each of the domains is specified using a Lambert Conformal projection with true latitudes at 40 and 60 degrees (Charney, 2004 *personal comm.*). The study area (Figure 3.1) is fully enclosed by the 36 and 12 km domains (Figures 3.33, 3.35 and 3.36), and partially by the 4 km domain (106 of the 113 ASOS stations are situated therein – the stations outside the domain are omitted from analysis at this resolution) as shown in Figure 3.34. Based on these grid domains, FSMM5 is capable of producing estimates of the wind resource over a region at a relatively high resolution.

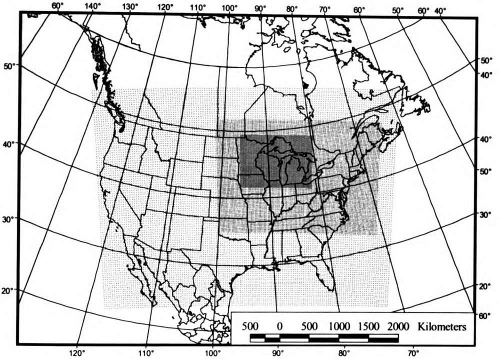

Figure 3.33 Spatial coverage of the 3 domains of FSMM5. The coarsest resolution (36 km) covers the contiguous United States, some of Canada and Mexico. The intermediate (12 km) covers the east-central portion of North America. The finest resolution (4 km) includes most of the Great Lakes region.

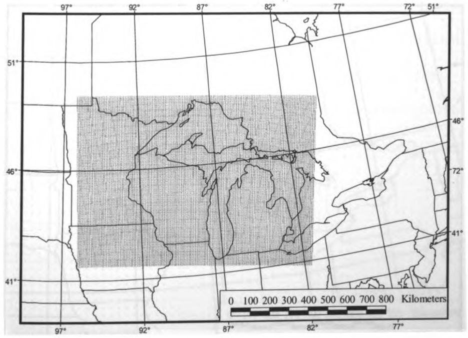

Figure 3.34 Spatial coverage of the 4-km (West) domain of FSMM5 over the study region (41° - 50° N by 76° - 97° W). This is the finest resolution domain run by the model and covers much of the Great Lakes. Each dot represents a domain grid cell corner point.

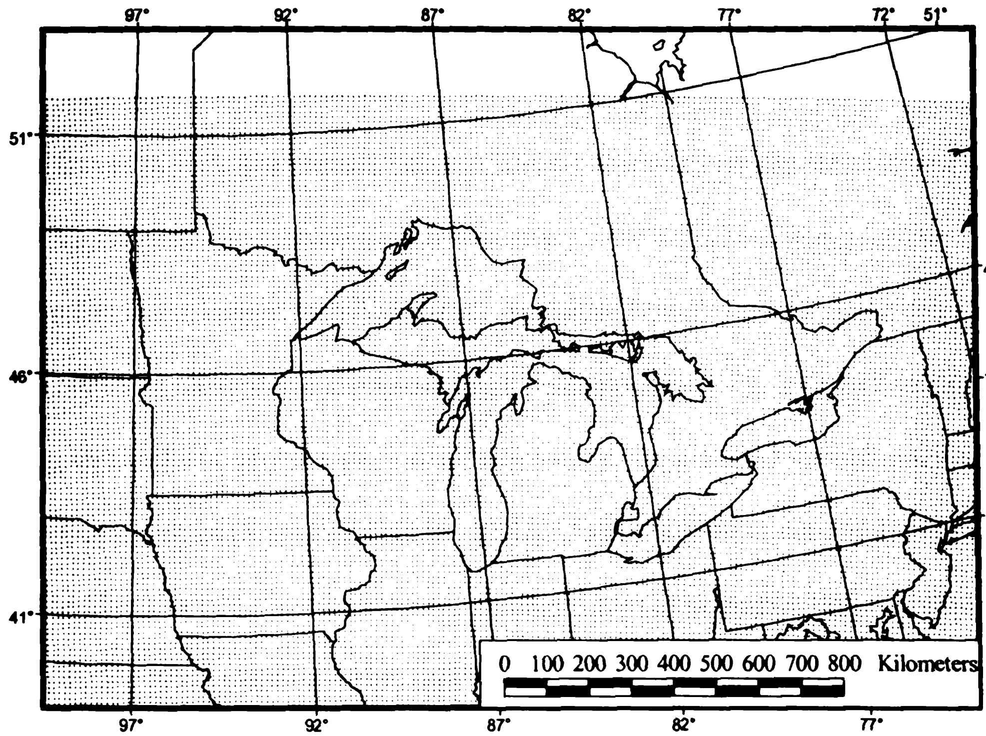

Figure 3.35 Spatial coverage of the 12-km FSMM5 domain over the study area (41° - 50° N by 76° - 97° W). Each dot represents a domain grid cell corner point.

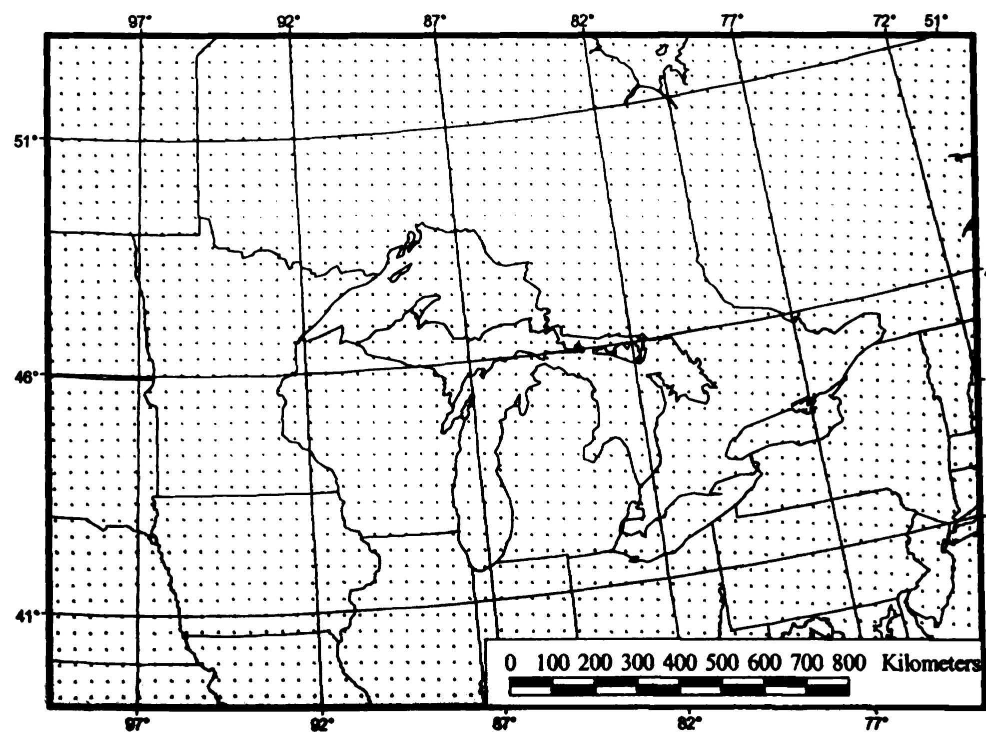

Figure 3.36 Spatial coverage of the FSMM5 36-km domain over the study area (41° - 50° N by 76° - 97° W). Each dot represents a domain grid cell corner point.

Within FSMM5, a 5-minute (5-9 km grid) digital elevation model (DEM) obtained from the U.S. Geological Survey (USGS) characterizes the land surface of a region. The FSMM5 model runs used in this study were initialized using 40-km resolution Eta (now known as NAM; North American Meso) model initialization analysis from the National Centers for Environmental Prediction (NCEP). FSMM5 employs the following atmospheric physics parameterizations: the Kane-Fritsch cumulus scheme for simulating convection (Kain and Fritsch, 1990), Dudhia's (1989) cloud radiation model, the Mellor-Yamada turbulent kinetic energy model for the boundary layer (Mellor and Yamada, 1974, 1982, Gerrity, 1994) and Reisner et al's (1998) mixed phase cloud microphysics model. These parameterizations and schemes have been used with success in a wide variety of MM5 implementations (Dudhia, 2004).

FSMM5 is run operationally on a Linux based Beowulf cluster (Adams and Vos, 2002) comprised of 16 individual processor nodes and is capable of producing a 48-hour 12 km simulation in 1 hour and a nested 24-hour 4 km simulation in 4 hours (Charney, 2002 *personal comm.*). Computational schematics of FSMM5 are discussed in detail by Heilman *et al.* (2003).

3.5.2 Model output

FSMM5 estimates the *u* and *v* components of wind at each vertical level for each grid point location. Unlike precipitation and temperature, which are calculated by MM5 at dot points (grid cell center points), wind components are estimated directly at grid cross points (the grid cell corners). The four estimation levels that were available for this study were the surface (2 meters), 30 meters, 50 meters and 80 meters and are the mean height of the level. As MM5 performs its calculations on spectral levels an interpolation to physical altitudes was subsequently necessary. The aforementioned wind speed altitudes were confirmed by Forest Service personnel (Bian, 2004 *personal comm.*) at the time of data transfer. Wind speeds were estimated by MM5 as *u* (zonal) and *v* (meridional) wind vectors in meters per second (m s^{-1}) at each grid point (and are not grid cell averages) within the aforementioned domains. Although the computational time step for the 36, 12 and 4-km spatial resolution domains is 90, 30, and 20 seconds respectively, the output wind vectors were estimated as instantaneous values for a given time, rather than an aggregate over the entire preceding time step (Charney, 2004 *personal comm.*). Thus, a wind vector estimate for 0000 UTC, for example, was the instantaneous estimate at that time, rather than an average of prior time-step estimates. Such model behavior must be noted when any comparison with observed values is attempted as most observed values are temporally-averaged over some specified period.

The wind vector output available for this study included hourly estimates of the wind vectors at each grid cross point of each domain for either a 48-hour lead (36 and 12 km), or 24-hour lead (4 km). The FSMM5 model is run twice each day at 0000 and 1200 Z, but only the 0000 Z analyses output was available for this research. Furthermore, output from several model runs were not available to the researcher, resulting in approximately one to three missing days of estimates per month. In particular, 10 days of model output was missing from the month of December, 2002. In order to maintain a continuous series that matched the ASOS data, these days' estimates were indicated with missing number flags (NaN in the data coding). Ultimately, each model run provided 62,245 grid point estimates in the 4-km West domain, 34,118 estimates in the 12-km domain, and 13,500 in the 36-km domain for each hour time step. Overall, for the study, and including all missing or unavailable output, a total of 14,617 hourly estimates were available at each grid point in each domain during the period of record.

3.5.3 FSMM5 wind estimates

Wind estimates generated from the FSMM5 model had to be extracted from the domain grids in order to create meaningful and coherent time series of estimates for each station. To generate paired comparison data sets for model evaluation where one data set is gridded and the other is an irregularly spaced network of points, two approaches are available. Either the data from the irregular network must be interpolated to nearby grid points, or the gridded data must be interpolated to the network locations. This research selected the latter method as the networked data was the observational data. In model evaluation, it must necessarily be assumed that the observational data being used for the evaluation are free from error (Willmott, 1981). Interpolating estimates to observation locations preserves this status, whereas interpolating the observational data from their collection locations would unnecessarily introduce bias into the observed data, and the resulting model evaluation would have been comparing model estimates to observational estimates, where the bias could not be assumed to reside in the model estimates.

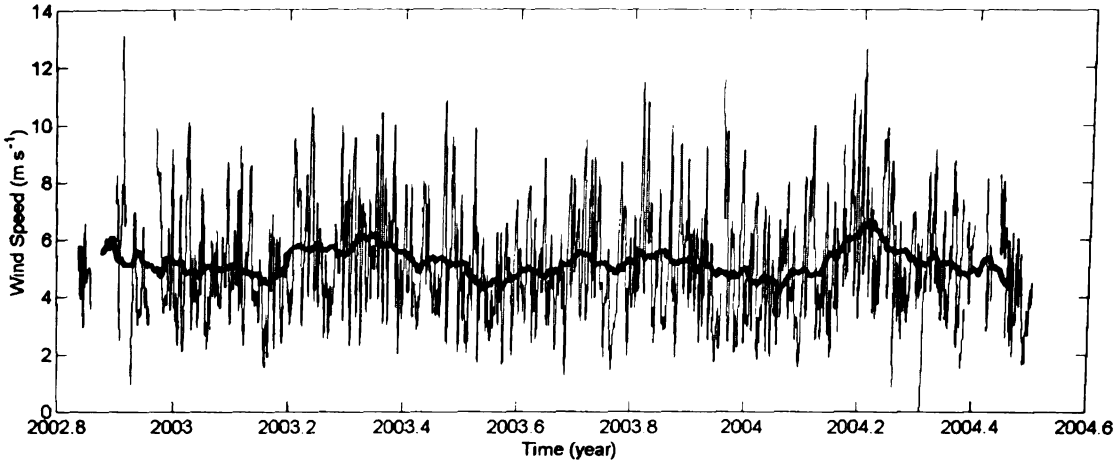

Figure 3.37 Mean daily (thin line) and mean monthly (thick line) 10-m wind speeds at Toronto, ON (CYYZ) from the 12-km run of FSMM5 and using an inverse distance weighting of estimates from the nearest 4 grid cross points.

As a critical issue surrounding the performance of a numerical model is the possibility that systematic spatial bias may exist, a number of different interpolation methods were used to generate the series used for model evaluation in order to evaluate the potential spatial systematic component of model estimative error. First, a series was created that simply assigned the wind estimates from the grid point nearest a station location to that station's file. Given the rapid distance decay of correlations (Robeson and Shein, 1997), this series represents only a "first guess" estimate of the wind around the station location. The second and third series were derived by taking the 4 grid points nearest a station location and assigning an unweighted average of the wind vector to the second series, and for the third series calculating an inverse-distance weighted average (Figure 3.37). In recognition of the possibility of potential systematic spatial bias (as discussed in the preceding chapter), unweighted average series were also generated from the 16 and 36 grid points nearest to a given station. If a systematic spatial bias exists, it is likely that the coarser 16 and 36 point average series will show significantly less of this bias than the 1 or 4 point series. The degree of difference in performance is also an indicator of the magnitude of this spatial bias.

Once the aforementioned estimate series were generated for each station, it was necessary to estimate the winds at the standard observational height of 10 meters for comparison with the observed series. This was accomplished by fitting an exponential curve to the 2-, 30-, 50-, and 80-meter estimates in order to generate an exponent that can be used in the wind speed power law (Equation 3.1). Whereas the SAMSON data used in the previous chapter provided wind speed information at only one height and an exponent of 1/7 was assumed (Touma, 1977, Petersen and Hennessey, 1978, Counihan, 1975), FSMM5 data were given at 4 levels. Thus the wind speed power law (Equation 3.1) was simply reversed and used to explicitly derive an exponent that fits each hour's data. Thus, from the hourly data at the four FSMM5 levels, the empirically derived exponent facilitated the interpolation of wind estimates at 10 meters for each station location.

Although Holton (1979) felt that Ekman spiraling was not great in the lowest few meters of the atmosphere and Klink (1999) chose to ignore it in directional height corrections, there was a noticeable shift in wind direction from one FSMM5 level to the next based on 100 random samples of the 4-level wind estimates. Thus, as it was not computationally intensive, wind direction at 10 meters was estimated in this study with a process utilizing the concept of Ekman spiraling. Resulting 10-meter wind direction was non-linearly interpolated from 2 meters using the same exponential profile function earlier derived for the wind speed to produce altitude weights that were subsequently applied to the 2-meter wind directional shifts. This adjustment simply created a directional shift in proportion to the level at which the estimates could be compared with the observations.

One critical issue of note in this analysis is that the data from the FSMM5 model are forecasts of wind speed and direction, which are based upon a set of initial meteorological conditions. The model is run twice each day, and for the 12 and 36-km grid domains, forecasts are generated hourly at lead times up to 48 hours (24 hours for the 4-km domain) beyond the model initialization time. Thus, although the physical basis of the equations do not change from one forecast time to a subsequent time, the laws of entropy dictate that the model error and potential bias in the forecasts will increase with greater lead times. To that end, model estimates at each hourly time step (*e.g.*, all 00Z data, 01Z data) were interpolated to the location of each station and examined. No appreciable increase in estimation bias for longer lead times versus short lead times was found at any of the station locations (Figure 3.38). As a result, all model estimates were weighted equally in the subsequent analysis of model performance, regardless of their lead time.

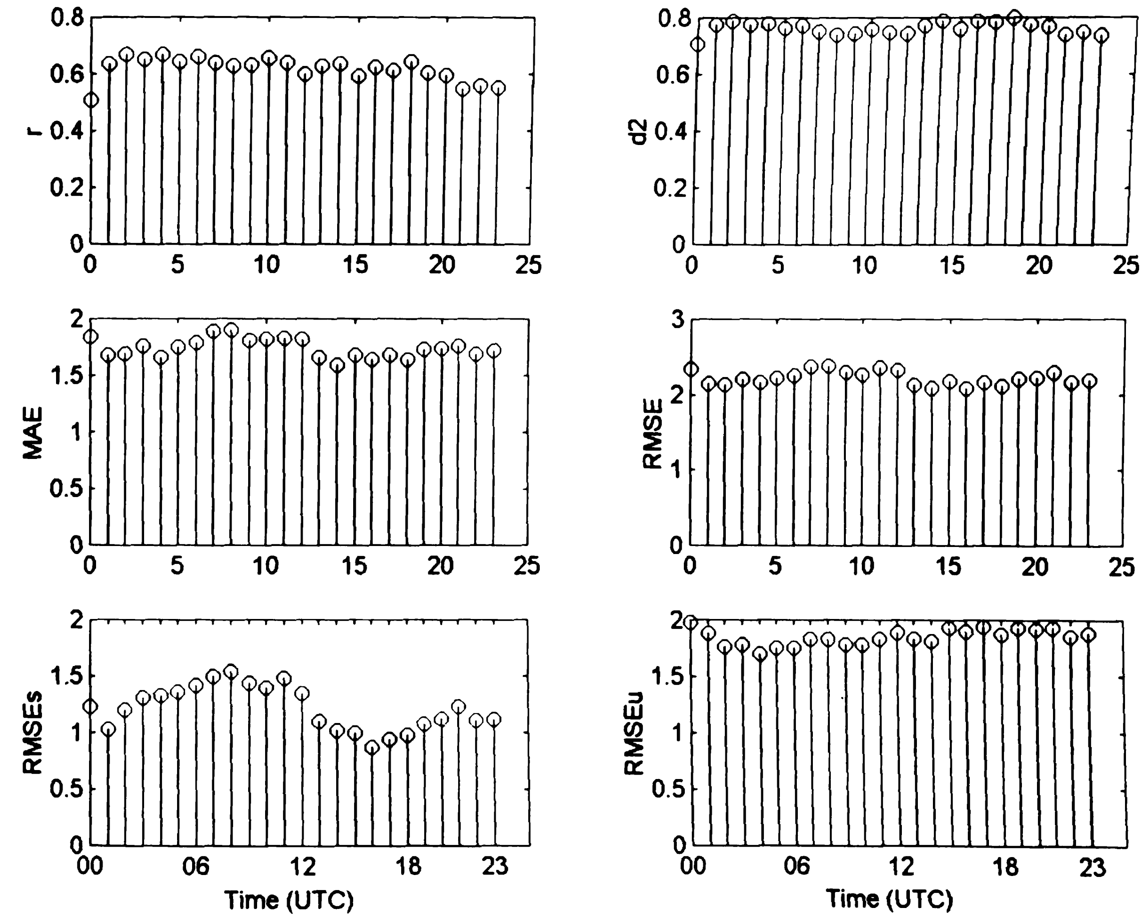

Figure 3.38 Examination of model estimates of wind speed versus observed wind speeds at Grand Rapids, MI (KGRR) from the 4 km domain over the period of record. There is little degradation of estimation with departure from initialization time. Similar results were obtained at all stations and grid resolutions. RMSE is root mean squared error (m s^{-1}), with RMSEs and RMSEu being the systematic and unsystematic components. MAE is mean absolute error (m s^{-1}), while r is the correlation coefficient and d2 is Willmott's (1982) index of agreement.

3.6 Statistical Model Identification and Construction

One of the objectives of this research is to determine whether or not a numerically-driven regional climate model might out-perform traditional stochastic and probabilistic methods for wind resource estimation. To that end it is necessary to construct and test established wind estimation techniques and compare their performance to the estimates derived by the MM5 model. The majority of wind resource estimation techniques are statistical in nature and take advantage of the common geographic assumption that objects in close proximity are more related to one another than are distant objects (*i.e.*, Tobler's First Law of Geography; Tobler, 1970). Thus, all statistical models for wind resource estimation at a location rely upon establishing a statistical relationship with nearby locations having long wind records.

Because of the aforementioned fundamental similarity of statistical wind resource estimation techniques, three representative statistical estimation methods were selected for evaluation. These include two stochastic models and one probabilistic model. Of the two stochastic models, while both are nearest neighbor-type functions, the first involves point source relationships whereas the second takes advantage of regionalized geographic behavior. The first of the stochastic models is a Measure-Correlate-Predict function as described in Chapter 2. The second is a Krige model similar to that described by Haslett and Raftery (1989). Lastly, the third model is a probabilistic model based on the joint probability of winds at two locations.

3.6.1 Measure-Correlate-Predict

One of the most straightforward stochastic approaches to wind resource estimation is the use of nearest neighbor interpolation. As discussed in the previous chapter, this method involves the spatial interpolation to a location from one or a set of neighboring locations for which data exist. Nearest neighbor interpolation can range from simple (unweighted, linear, low sample size) to highly complex (distance and roughness weighted, non-linear, high sample size).

The Measure-Correlate-Predict (MCP) model is a variation on nearest neighbor interpolation that has been used extensively in wind energy resource estimation (Derrick, 1992, Barthelmie *et al.*, 1999). The goal of the MCP scheme is to effectively estimate the long-term wind speed record at a location by linearly correlating a short record at that location with a long-term series from a nearby reference location. It is assumed that the reference anemometer record is representative of winds at both sites as a function of the overlying non-local wind field.

The MCP model is derived by first extracting from the reference record a series of wind speed and direction observations corresponding to the short record at the location of interest (hereafter called the short location). These paired observations are subsequently binned according to the wind direction at the reference location. The number of directional bins is entirely arbitrary, though a set of 12 or 16 bins is commonly employed (Derrick, 1992).

Once the short, paired records have been binned according to direction, a simple linear equation of the form:

$$U_{sl} = b_0 + b_1 U_{ref} \tag{3.11}$$

is applied to the paired wind speed data for each of the directional bins. In Equation 3.11, U_{ref} is the wind speed at the reference location, U_{sl} is the corresponding wind speed observation at the short location, b_1 is the slope of the equation and b_0 is the intercept. While this method is identical to that of fitting an ordinary least squares regression to the reference speed data, the MCP makes no assumptions regarding causality and is therefore not considered a regression from a statistical standpoint.

A synthetic long-term series at the short location is subsequently generated in two steps. First, the entire long-term series from the reference location is binned by direction. Second, the directionally-based linear relationships between the reference speeds and short location speeds (defined by Equation 3.11) are applied to each directional bin of the long-term series wind speed data to estimate the long-term wind speed record at the short location.

While it may seem that the linear relationships assumed by MCP may not be appropriate, Derrick (1992) and others have shown that for most non-complex terrain, such an assumption is not unreasonable. Furthermore, if it becomes clear that a linear relationship is not appropriate for a particular bin (*e.g.*, local influences may exhibit an exponential influence on increasing wind speeds), the MCP is highly modifiable by simply fitting an appropriate non-linear function to that particular directional bin, or by further categorizing the bin by wind speed.

As this research is designed to explore the relative success of wind resource estimation techniques over a large region, the decision was made to apply the same MCP technique, as described above, to all stations in the study area. While the MCP method has a number of challenges, as discussed in the previous chapter, for the purposes of this model and this research over this study area, the relationships between nearest neighbor wind speeds are assumed to be linear, regardless of local surface differences. Furthermore, the problems of representativeness due to seasonality, runs autocorrelation and anisotropy in the short location record were overcome by randomly selecting 1500 (approximately two months) pairwise observations from each station and its nearest neighbor. The random selection process resulted in a theoretically de-seasonalized and stationary distribution. The random short record from each station and its nearest neighbor was used to create estimations of the long-term record at the station of interest. The climatology and biases of the synthetic series were then assessed relative to the complete observational series at the station of interest and to the results of the other models. The results are presented in the next chapter.

3.6.2 Krige model

One of the primary limitations of the simple nearest neighbor interpolation model is that the relationship between the wind speeds at the two locations may vary quite strongly with wind direction. That is, the relationship exhibited when the wind vector is parallel with the station-to-station azimuth may be entirely different than when it is perpendicular. In fact, from certain directions, it is entirely possible that the wind speeds, even at stations in close proximity with one another, may exhibit no coherent relationship at all. Thus another method must be sought; one that accounts for the winds over the entire region surrounding the location of interest.

While the concept of a regionalized variable is not new, with a few notable exceptions discussed in the previous chapter, it has not enjoyed wide use in wind resource estimation with the exception of Haslett and Raftery (1989). However, near surface wind is a spatially continuous variable that is driven by a coherent overlying circulation structure and is normally highly correlated over short distances. As such, wind exhibits a behavior that exists between truly random and entirely deterministic. Therefore, the near surface wind can quite legitimately be considered a regionalized variable and lends itself quite well to a spatially driven interpolation scheme (Davis, 1986). The researcher has chosen a universal kriging function as an appropriate wind resource estimation model.

Kriging is a method by which the value of a regionalized variable can be estimated at any location within a specified region based on values observed at discrete locations within the region. While a simple linear interpolation using all observations within the region regardless of relevance could produce estimates of a regionalized variable, such a methodology would be highly inefficient and would not easily yield measures of statistical certainty. Because of the method by which a kriged surface is obtained, one can be assured that measures of uncertainty are inherent to the model and that only an optimal set of nearest neighbor stations is used in the construction of the model. The optimal set of neighbors, and their corresponding bias-minimizing weights is derived from a semivariogram. A much more detailed description of kriging can be found in Davis (1986).

It has already been established that near-surface wind suffers varying degrees of anisotropy. Therefore, it is necessary to employ a universal, rather than punctual kriging. Universal kriging not only assumes drift in the observations, but calculates and removes it as well. The drift is then returned to the estimates once derived.

For this research, the universal krige model was specified as follows. The first step in the analysis was to obtain semivariances for each station. Semivariance is a measure of spatial dependence between observations separated by a distance (*h*). It is computationally identical to finding the sum of squared differences between observations at two points separated by distance *h*. The semivariance is given by the equation,

$$\gamma_h = \sum_{i}^{n-h} (O_i - O_{i+h})^2 / 2n \tag{3.12}$$

where O_i is the observation at location i, O_{i+h} is the observation at a point h distance away, and n is the number of points (from Davis, 1986). Using the semivariance for a location, a distance can be established beyond which further increasing the distance has little effect on increasing the semivariance value. Graphically this analysis is called a semivariogram, an example of which is presented in Figure 3.39.

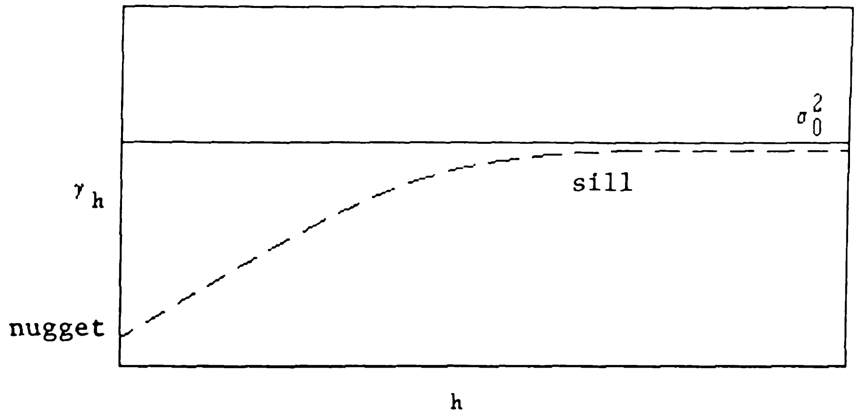

Figure 3.39 An idealized example of a semivariogram. The solid horizontal line represents the variance of the data interest, while the dashed line is the semivariance (γ_h) at any given distance interval (h). The nugget represents the minimum achievable semivariance due to localized effects.

Two portions of the semivariogram were of interest in the krige analysis. The first is the portion of the semivariogram known as the sill. This is the region where increasing distance from the location of interest no longer has much of an effect on the value of the semivariance, and theoretically has leveled off at the autocovariance (the variance of the original data). Stations existing beyond the distance marking the beginning of the sill are extraneous to the analysis and can be safely omitted (Davis, 1986).

As with the MCP model, in order to reduce the effects of non-stationarity and seasonality, a set of 1500 random times were selected and extracted from each station as a subset. This pairwise subset was used to generate the semivariances and ultimately the krige model. Once the semivariance was calculated for each station relative to all its neighbors, the semivariogram was analyzed to find the approximate distance to its sill.

This was accomplished computationally by fitting a second-order polynomial to the semivariances and establishing when the value of the semivariance first came within 95% of the autocovariance. This distance was then deemed to be the furthest distance from the station that an observation from a neighbor station could be correlated. Thus, only neighbor stations falling within the estimated relevant distance were used in subsequent calculations. Once the sill distance for each station was established, the sill distances were used to determine how many nearest neighbor stations should be used in the krige model. To ensure uniformity over the region, this number was then averaged over all stations. This analysis determined that on average 5 nearest neighbors were sufficient to account for most of the variance in the station. Thus, the five nearest neighbor stations were used to construct the krige model.

The other region of interest in the krige analysis is the so-called nugget. Theoretically, the semivariance at a distance of zero should equal zero. However, in real-world instances where there exist localized influences operating beneath the resolution of the data points, local noise may be introduced into the semivariance and, according to Davis (1986) the semivariogram will almost instantaneously track from zero to the nugget point over a distance shorter than the sampling interval. For wind speed, the nugget is an important piece of information. It provides revealing evidence of the magnitude of localized influences (*e.g.*, terrain roughness, obstructions and obstacles to the flow). As the nugget increases, the ability of any regionalized model to accurately estimate the wind at that location will decrease proportionally.

Once the representative number of nearest neighbors had been established, the problem became one of a more straightforward weighted spatial average. The universal krige model was applied to determine the optimal weights for each station used in the subsequent interpolation. By optimal, it is meant that kriging produces a set of weights for each station that will result in a minimization of the estimation error, or error variance,

$$s_{\varepsilon}^{2} = \frac{\Sigma\left(\hat{Y}_p - Y_p\right)^2}{n} \tag{3.13}$$

where Y_p is the estimate and Y_p is the actual observation. The determination of the optimal weights for the 5 nearest neighbors was accomplished by solving a set of eight simultaneous equations (3.14). The first 5 equations are used to determine the actual weights, while the 6[th] equation determines the coefficient for the constraint (λ) of weight unity (*e.g.*, a Lagrange multiplier), and the last two equations solve the coefficients of the drift of the surface.

$$\begin{aligned}
W_1\gamma(h_{11}) + W_2\gamma(h_{12}) + W_3\gamma(h_{13}) + W_4\gamma(h_{14}) + W_5\gamma(h_{15}) + \lambda + \alpha_1 X_{11} + \alpha_2 X_{21} &= \gamma(h_{1p}) \\
W_1\gamma(h_{12}) + W_2\gamma(h_{22}) + W_3\gamma(h_{23}) + W_4\gamma(h_{24}) + W_5\gamma(h_{25}) + \lambda + \alpha_1 X_{12} + \alpha_2 X_{22} &= \gamma(h_{2p}) \\
W_1\gamma(h_{13}) + W_2\gamma(h_{23}) + W_3\gamma(h_{33}) + W_4\gamma(h_{34}) + W_5\gamma(h_{35}) + \lambda + \alpha_1 X_{13} + \alpha_2 X_{23} &= \gamma(h_{3p}) \\
W_1\gamma(h_{14}) + W_2\gamma(h_{24}) + W_3\gamma(h_{34}) + W_4\gamma(h_{44}) + W_5\gamma(h_{45}) + \lambda + \alpha_1 X_{14} + \alpha_2 X_{24} &= \gamma(h_{4p}) \\
W_1\gamma(h_{15}) + W_2\gamma(h_{25}) + W_3\gamma(h_{35}) + W_4\gamma(h_{45}) + W_5\gamma(h_{55}) + \lambda + \alpha_1 X_{15} + \alpha_2 X_{25} &= \gamma(h_{5p}) \\
W_1 + W_2 + W_3 + W_4 + W_5 + 0 + 0 + 0 &= 1 \\
W_1 X_{11} + W_2 X_{12} + W_3 X_{13} + W_4 X_{14} + W_5 X_{15} + 0 + 0 + 0 &= X_{1p} \\
W_1 X_{21} + W_2 X_{22} + W_3 X_{23} + W_4 X_{24} + W_5 X_{25} + 0 + 0 + 0 &= X_{2p}
\end{aligned} \tag{3.14}$$

In the set of equations (3.14), $\gamma(h_{ij})$ is the semivariance for the distance between two control points, i and j. X_{1i} is simply the East-West coordinate for the control point, i, while X_{2i} is the North-South coordinate. Both coordinates were given in degrees (Longitude or Latitude respectively). The coefficients, α_1 and α_2 are the coefficients of the linear drift equation,

$$D_p = \alpha_1 X_{1i} + \alpha_2 X_{2i} \tag{3.15}$$

where D_p is the linear drift at point p. To find the drift and the weights, the simultaneous equations were solved using matrix algebra, whereby the components of the equations were rearranged according to the matrix equation 3.16.

$$\begin{bmatrix} \gamma(h_{11}) & \gamma(h_{12}) & \gamma(h_{13}) & \gamma(h_{14}) & \gamma(h_{15}) & 1 & X_{11} & X_{21} \\ \gamma(h_{12}) & \gamma(h_{22}) & \gamma(h_{23}) & \gamma(h_{24}) & \gamma(h_{25}) & 1 & X_{12} & X_{22} \\ \gamma(h_{13}) & \gamma(h_{23}) & \gamma(h_{33}) & \gamma(h_{34}) & \gamma(h_{35}) & 1 & X_{13} & X_{23} \\ \gamma(h_{14}) & \gamma(h_{24}) & \gamma(h_{34}) & \gamma(h_{44}) & \gamma(h_{45}) & 1 & X_{14} & X_{24} \\ \gamma(h_{15}) & \gamma(h_{25}) & \gamma(h_{35}) & \gamma(h_{45}) & \gamma(h_{55}) & 1 & X_{15} & X_{25} \\ 1 & 1 & 1 & 1 & 1 & 0 & 0 & 0 \\ X_{11} & X_{12} & X_{13} & X_{14} & X_{15} & 0 & 0 & 0 \\ X_{21} & X_{22} & X_{23} & X_{24} & X_{25} & 0 & 0 & 0 \end{bmatrix} \bullet \begin{bmatrix} W_1 \\ W_2 \\ W_3 \\ W_4 \\ W_5 \\ \lambda \\ \alpha_1 \\ \alpha_2 \end{bmatrix} = \begin{bmatrix} \gamma(h_{1p}) \\ \gamma(h_{2p}) \\ \gamma(h_{3p}) \\ \gamma(h_{4p}) \\ \gamma(h_{5p}) \\ 1 \\ X_{1p} \\ X_{2p} \end{bmatrix} \tag{3.16}$$

Multiplying by the inverse of the semivariance matrix thus solves the weights matrix. Once the weights and drift for each station were determined, they were applied to the observational series of each of the 5 nearest neighbor control points to generate a synthetic series of wind speeds at the station of interest. Climatological differences between the observed and estimated series are presented in the next chapter.

3.6.3 Joint probabilistic model

As has been discussed in Chapter 2, probability density functions have long been used to describe the wind resource at a location. While wind speeds may vary a great deal over short distances, spatial variations in the overall distributions of wind speeds are much lower because while the magnitude of the wind speed itself may be governed by boundary layer characteristics (*e.g.*, roughness, zero-plane displacement, eddy diffusivity), the relative, overall distribution of speeds are governed more by the overlying synoptic flow. Thus, if the boundary layer modification of surface winds can be known (*i.e.*, surface roughness), the overlying probability distribution of the wind resource can be adjusted to properly estimate the wind speed distribution at an uninstrumented location. This method has been used with great success by the developers of WAsP, and the resulting Danish and European Wind Atlases (Troen and Petersen, 1989).

In addition, as with the linear interpolation model and the MCP model, the probabilistic model seeks to estimate the resource at one location using information derived from its nearest neighboring station. Such modeling may, at its most simplistic be accomplished by assuming the wind at the location of interest possesses a probability density function identical to the wind at its nearest instrumented location. In regions where the terrain is relatively homogeneous and not overly complex, and obstacles to the near-surface flow are few and far between, such a model may indeed produce plausible

However, where terrain is more heterogeneous or frequent obstacles disorganize or impede the near-surface flow, a more complex variation on the probabilistic model is suggested. Such a model would be better served if the distribution assumed to exist at the location of interest was one that was regionally representative. To obtain a more regionalized distribution function, it would be necessary to construct a synthetic long-term series derived from all neighboring stations within a given distance of the location of interest. The distribution of this synthetic series could then be applied to the location of interest with greater confidence. With the exception of WAsP, the researcher knows of no studies that have explored regionalized probability density functions in any detail with respect to near-surface winds.

Garcia-Rojo (2004) suggests an alternative to the aforementioned probability models. The alternative is a joint-probability model that, like MCP, makes use of a short wind record at the location of interest paired with a longer series at a nearby reference station. In addition, like the MCP approach, and unlike more simplistic probability models, Garcia-Rojo's (2004) joint-probabilistic approach makes use of the directional information to refine in greater detail the estimates obtained from the model. In the case of the joint probability approach, it is the probability of joint occurrence of wind speeds at the reference site and the site of interest that is assessed, rather than the linear correlation between speeds within the two series (Garcia-Rojo, 2004). It is this joint-probabilistic model, named JPWIND by Garcia-Rojo, that will be used in this research to assess the performance of a probabilistic wind model relative to MM5.

The joint probability mass function, or the probability that two sets of meteorological events, in this case wind direction and speed at each location, occur simultaneously is defined by Garcia-Rojo (2004) as:

$$0 \leq f(d_{ref}, U_{ref}; d_{site}, U_{site}) \leq 1 \tag{3.17}$$

Where d_{ref} and U_{ref} refer to the direction and speed at the reference location, and d_{site} and U_{site} are for the site of interest. The function sums over all of the probability space as:

$$\sum_{\{d_{ref}, v_{ref}\}} \sum_{\{d_{site}, v_{site}\}} f(d_{ref}, U_{ref}; d_{site}, U_{site}) = 1 \tag{3.18}$$

Thus, the probability of measuring an event (d_{site}, U_{site}) at the location of interest independently of what is measured at the reference location can be determined from the marginal probability mass of events (Garcia-Rojo, 2004):

$$P(d_{site}, v_{site}) = \sum_{\{d_{ref}, v_{ref}\}} f(d_{ref}, U_{ref}; d_{site}, U_{site}) \tag{3.19}$$

Similarly, once the marginal probabilities have been determined from the short, paired records for each event (d_{site}, U_{site}) at the site of interest, it is then possible to use these probabilities to derive their probability of occurrence given an independent event occurring at the reference location.

As with the other models, 2000 wind speed and direction observation times were randomly selected for each station / nearest neighbor pair. Wind speed and direction data corresponding to those observation times were extracted from both the station and its nearest neighbor to create a deconvoluted "short" time series of paired observations of approximately two months in length. These short series were used to obtain the joint probability function for the station. The function was subsequently applied to the full record from the nearest neighbor station to generate a synthetic full series for the station of interest. The results of this analysis are presented in the next chapter and compared with the results from the other models.

3.7 Model Evaluation

Model evaluation is critical to the acceptance of any model and any comparison between models. Many of the important issues related to model evaluation are succinctly advanced by Beck *et al.* (1993) and as such will be only briefly outlined forthwith. The evaluation of each of the aforementioned models is accomplished using several standard evaluative procedures. With respect to this research, the evaluation of model performance falls into two categories, probabilistic and deterministic.

3.7.1 Probabilistic evaluative statistics

Probabilistic performance measures seek to evaluate the legitimacy of the statistical properties of the distribution of estimated data against those of corresponding observed data. Unlike deterministic methods, probabilistic methods are stochastic in nature in that they are not concerned with the exact replication of the variable being modeled, but rather the replication of the distribution of the data, or the internal behavior of the system (Beck *et al.*, 1993). As this research is primarily concerned with the ability of FSMM5 to provide accurate estimates of the regional wind climatology, rather than the hour-to-hour accuracy of actual forecast values, probabilistic performance measures are given the most weight of the evaluative techniques employed herein.

There are a number of techniques available to the researcher seeking to evaluate the probabilistic performance of a model. Among the most widely used are comparisons of means and of variances. These two statistics represent the first and second moments (respectively) of the distribution of the data in question and therefore, provide perhaps the most powerful assessment of the similarity of two distributions of data.

$$\overline{U} = n^{-1} \sum U_i \tag{3.20}$$

$$s^2 = n^{-1} \sum \left(U_i - \overline{U}\right)^2 \tag{3.21}$$

where U is the sample mean and s^2 is the sample variance. In both Equation 3.20 and 3.21, Roman letters, rather than Greek, are used to symbolize that these statistics are derived from a sample, rather than from the unknown population. Unfortunately, because it has been squared, the variance does not have units of the original data. Thus it is more common to report the square root of the variance, or standard deviation, as the measure of spread of the data about the mean value.

Comparison of means is often conducted by using the Student's T test. This method is adequately described in a number of reference works (*e.g.*, Davis, 1986, Wilks, 1995, Rogerson, 2001) and thus only a synopsis is presented here. Student's T-test is a procedure by which the distributional statistics of a sample may be compared against a hypothetical population, or more importantly for this research, the statistics of two samples can be compared to determine whether they are derived from the same population. The T distribution is a statistical modification of the Gaussian Z distribution, and the T-test has been made more conservative than the Z-test to account for a lack of knowledge about the parameters of the population in question. In order to examine the null hypothesis that the means of the populations, from which both the observed and estimated data sets were drawn, are identical. The two-sample T statistic is calculated as,

$$t = \frac{\overline{U}_E - U_O}{s_e} \tag{3.22}$$

where U_E is the mean of the estimated sample, U_O is the mean of the observed sample, and s_e is the standard error of the mean (after Davis, 1986). Because two samples are used, s_e must necessarily be a function of both samples.

$$s_e = s_p \left(n_E^{-1} + n_O^{-1} \right) \tag{3.23}$$

In Equation 3.23, s_p is the pooled standard deviation as determined by,

$$s_p = \left[\frac{(n_E - 1)s_E^2 + (n_O - 1)s_O^2}{n_E + n_O - 2} \right]^{0.5} \tag{3.24}$$

When the t-statistic has been calculated from Equation 3.22, it is compared against a critical value that has been obtained based on the number of degrees of freedom of the test and the proportional level of rejection of the null hypothesis to determine whether the populations from which the two samples were drawn do indeed have the same mean.

Additionally, the parameters of empirical distribution functions derived from both the observational and the model-produced synthetic series may be evaluated for differences by using simple comparisons and more complex statistical methods such as the Chi-Square, Kolmogorov-Smirnov or Anderson-Darling test statistics outlined previously (Anderson and Darling, 1954). These methods illuminate the so-called goodness-of-fit of a set of data to a distribution function defined by the data from which the candidate series is suspected to have come. In doing so, they also provide valuable information about the similarity of variance between the two sample distributions. In the case of this research, it is assumed that the observational data were drawn from a population comprising all possible wind speeds and directions at a given location. Thus, theoretically, the statistics of these sample observations represent the overall statistical parameters of the population from which the data were sampled. Furthermore, it is hypothesized the estimated data have been drawn from the same population. If this is indeed the case, then the aforementioned goodness-of-fit methods will reflect that both the observed and estimated data are not derived from different populations, and therefore, the estimated data can be deemed a surrogate for the observed. Additionally, the degree of fit, in the form of the magnitude of the test statistic can be used as a simple way to determine which of the models provides the best general fit to the data.

Graphical methods and the Anderson-Darling goodness-of-fit tests were described in great detail earlier in the chapter and so are not discussed here. However, the Kolmogorov-Smirnov and Chi-squared tests were only cursorily mentioned and so deserve elaboration. While these latter methods are statistically less powerful than the Anderson-Darling test, they nevertheless contribute a meaningful support for the confirmation or denial of fit of a particular sample of data to an expected distribution.

The Chi-squared test is the least powerful of the goodness-of-fit statistical tests. It simply divides a sample into discrete probability bins, and compares the observed frequencies of occurrence to those that would be expected if the sample data were drawn from a given distribution. The null hypothesis is that the sample data does indeed come from the population distribution. The test statistic (X^2) is calculated as,

$$X^2 = \sum_{j=1}^{z} \frac{(O_j - E_j)^2}{E_j} \tag{3.25}$$

Where O_j is the observed frequency and E_j is the expected frequency for the value range bin j out of z possible bins (from Davis, 1986). The calculated X^2 statistic is compared against a critical value, again based on the degrees of freedom of the test and a pre-determined critical probability level for the rejection of the null hypothesis.

The Kolmogorov-Smirnov, or K-S test is an alternative, non-parametric goodness-of-fit method to the Chi-square test. The K-S test statistic is exceedingly straightforward. It is simply the maximum difference between the cumulative probability levels of the observed frequency distribution and the expected frequency distribution. The difference is the test statistic and is compared against a critical level in the same manner as other hypothesis tests. The null hypothesis is that the discrete distribution of the data is equal to the distribution to which it is being compared. Normally, the K-S test, like the Chi-squared test or other goodness-of-fit methods is used to evaluate the hypothesis that a particular sample distribution is derived from a theoretical parent distribution function where the parameters are either known (parametric) or not (non-parametric). That is, these tests evaluate whether or not a sample "fits" a particular distribution, as was accomplished in the prior chapter. However, in the comparison of models, the observed data is, in effect, the population whose distribution forms the basis for the goodness-of-fit.

To adequately address the probabilistic evaluation of FSMM5 and compare it to the other models, this research has calculated, reported and interpreted the mean, standard deviation, and empirical distribution statistics for each of the model estimated data sets as well as for the observed data (as described in the previous chapter). The veracity of both the estimative probabilistic statistics and the empirical distribution parameters was determined through the use of a bootstrap resampling procedure as outlined by Efron and Gong (1983). In this case, 10,000 bootstrapped series of 1000 estimated values each were sampled with replacement from the entire model-estimated series. From these samples, confidence limits were generated for estimated data statistics.

3.7.2 Deterministic evaluative statistics

Deterministic evaluation methods seek to evaluate the performance of the model in terms of its ability to replicate reality (*i.e.*, the observed data). Such measures are more appropriately termed model validation methods as they seek to determine the validity of the model estimates themselves by examining the properties of the residual differences between the estimated and observed data (Beck *et al.*, 1993). Methods for the validation of models are normally used to determine how well a model has been able to replicate the variables it is estimating, and a model is generally not considered validated unless all systematic behavior in the residuals had been eliminated and/or accounted for within the model proper (*i.e.*, residuals are independent and normally distributed with a mean of zero). While the goal of this research is not to assess the forecasting abilities of MM5 or any of the other models evaluated, a thorough analysis of the residual bias of all models was conducted. The rationale for performing a deterministic evaluation is that a model's ability to accurately approximate actual values and minimize the systematic bias in its residual values are measures of how comprehensively the model has been specified, and how reliable is its output for generating an overall climatology. While it cannot necessarily be assumed that a model that performs well is correctly specified (small, non-systematic residuals could be obtained by random chance), an appropriate model construction is most likely. Such behavior is preferential to a model that performs poorly (large, or systematic residuals) and likely has been, in some way, incorrectly specified. As a variable's climatology is a function of the individual observations (or estimates of those observations), a model that produces small, randomly-distributed residuals can be expected to also produce a plausible climatology of the variable being investigated.

Each model's residuals were used to determine the validity of the specific model, and are further compared with the residuals behavior of the other models. The measures that are used in this analysis include MAE, RMSE, Pearson's *r*, and the index of agreement (d). These measures are detailed in Willmott and Wicks (1980), Willmott (1982), Willmott *et al.*, (1985), and Wilks (1995) but also are outlined below.

By far the most widely used measure of the performance of a model is Pearson's product moment correlation coefficient (*r*).

$$r = \frac{\sum OP - \frac{\sum O \sum P}{n}}{\left[\left(\sum O^2 - \frac{\{\sum O\}^2}{n}\right)\left(\sum P^2 - \frac{\{\sum P\}^2}{n}\right)\right]^{0.5}} \tag{3.26}$$

where O and P are two series of data of length n. Pearson's r is thus a measure of the degree of covariance of the two variables, or how linearly related their behavior appears to be. From equation 3.26 it is clear that if the series O and P vary identically, r will equal 1.0, or -1.0 if they vary perfectly inversely. If there is no similarity between the variances of the two series, the correlation coefficient will equal zero. Theoretically, if a model is perfectly specified (*i.e.*, observations are perfectly reproduced), the model-estimated series would be identical to the observational series, and the correlation would equal 1.0. Practically, however, all models contain some estimation error, supposedly reducing the value of r. Unfortunately, because Equation 3.26 does not take into account the magnitude of the differences between the observed and estimated values, it ultimately fails to capture much of the model's true ability to reproduce reality, nor does it provide any measure of how much of the model's error is systematic, and is thus correctable. Figure 3.40 highlights some of the drawbacks of relying solely on Pearson's correlation coefficient for model evaluation. An alternative, the index of agreement, is presented further on. Despite the limitations of Pearson's r, it remains a widely recognized measure of the correspondence between to variables, and as such will be reported in this research.

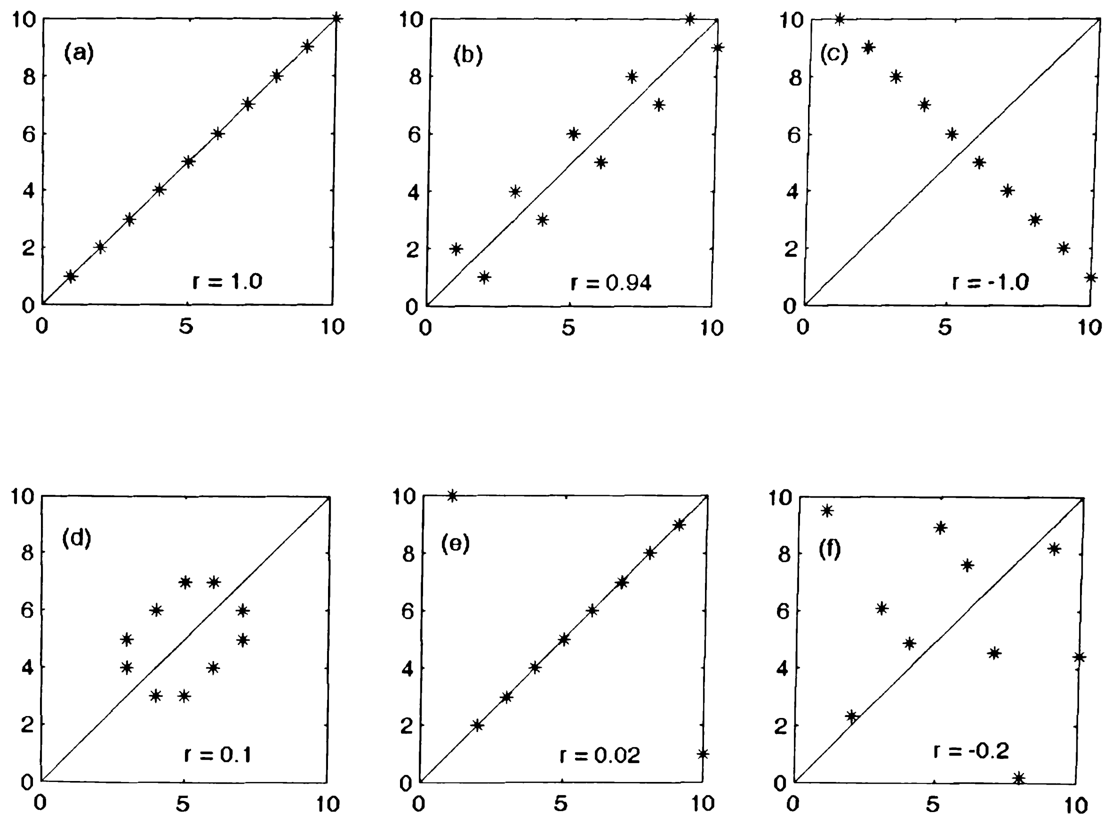

Figure 3.40 Idealized relationships between two variables and their corresponding Pearson's correlation coefficients. Of the top row, each of which exhibits a perfect or near-perfect correlation between the two variables, only the first (a) would represent a truly error-free model, whereas (b) and (c) exhibit systematic error not taken into account. On the bottom row are three idealized examples of variables that show little or no correlation. However, like (b) and (c), (d) is a function of systematic bias. Figure (e) shows the influence of two extreme outliers. Only (f) represents a randomly generated data set where no correlation is expected.

Because of the limited ability of Pearson's r to adequately assess the performance of a particular model, it is more telling perhaps to assess the magnitude and behavior of the actual differences, or residuals, between observed values and those estimated by the model.

$$O_i = P_i + e_i \tag{3.27}$$

In Equation 3.27, the observation O of a variable at a point i in either space or time (or both) can be replicated precisely from the model estimate P of that variable for the same point and a resultant error e, also known as model bias, or the residual of the model. From this point forward, the model estimated variable is defined as P (for predicted; even though it is not truly a prediction), because the use of E might needlessly confuse the estimated variable with the error term e. Because it must be assumed that no error exists in the observed variable (otherwise it would have been corrected prior to analysis), it follows that the error e is solely a product of the model (Willmott *et al.*, 1985). It is the series of model-introduced bias terms that is ultimately evaluated in an effort to discover the utility of the model.

Because the model bias exists for each observation/estimate pair, the residuals themselves form a series of values that can be evaluated statistically. Of the statistics that summarize the behavior of the residuals, the means of the residual series are most commonly used in the Geo and Atmospheric sciences (Fox, 1981; Willmott, 1982). In particular, the mean absolute error (*MAE*) and to a lesser extent the mean squared error (*MSE*) and root of the mean squared error (*RMSE*) are widely used to evaluate the performance of a model against a set of observations.

$$MAE = n^{-1}\sum\left|P_i - O_i\right| \tag{3.28}$$

$$MSE = n^{-1}\sum(P_i - O_i)^2 \qquad (3.29)$$

$$RMSE = MSE^{0.5} \qquad (3.30)$$

Such measures as *MAE*, *MSE* and *RMSE* provide a clear assessment of the overall performance of a model in that they provide a first moment statistic for the differences between the observed and estimated variables. Of the three measures, *MAE* and *RMSE* are most used because they report the error in units of the variable. Furthermore, these measures are more greatly mathematically tractable than is the simple mean error. In fact, the reporting of the mean of the observed values and the mean of the estimated values is generally preferred to the simple mean error because the former are more easily understood, and they provide greater versatility in computing additional statistical measures than does the mean error (Willmott, 1982).

What is more, the *MSE* (and therefore also the *RMSE*) has certain properties that allow it to be mathematically parsed into measures of the degree of systematic (correctable) and unsystematic (random) error contained within the overall residual values. The systematic (MSE_s) and unsystematic (MSE_u) components of the bias of a model are given as,

$$MSE_s = n^{-1}\sum\left(\hat{P}_i - O_i\right)^2 \qquad (3.31)$$

$$MSE_u = n^{-1}\sum\left(P_i - \hat{P}_i\right)^2 \tag{3.32}$$

In Equations 3.31 and 3.32, $\hat{P}$ represents an estimated series derived from the least-squares regression of the model-predicted variable on the observed variable. The *RMSE* versions simply take the square root of equations 3.31 and 3.32, and are preferred as they retain the units of the original variable. However, in their *MSE* form, Equations 3.31 and 3.32 are conservative.

$$MSE = MSE_s + MSE_u \tag{3.33}$$

The relationship expressed in Equation 3.33 means that the relative proportions of systematic and unsystematic bias may also be calculated by dividing MSE_s or MSE_u by the *MSE*. Measures of systematic and unsystematic bias are quite important as measures of the veracity of the model. As a model's performance is improved, the systematic component of its bias must tend toward zero, while the unsystematic, or random component ($RMSE_u$) is minimized toward the value of the overall *RMSE* (Willmott, 1982).

In addition to the mean values of the residuals, Willmott (1981) recommends the calculation, reporting, and interpretation of a set of "summary measures" that will aid in standardizing the comparison of performance between models. These measures include the mean of the observed variable (*O*), the mean of the predicted ($\overline{P}$), the standard deviations of both series (s_o and s_p), and the slope and intercept parameters (m and b) from an ordinary-least squares fit of the observed to the predicted variable (Willmott, 1981). The researcher is in agreement with Willmott (1982), who feels that such measures are readily recognized and understood by the scientific community, and that these measures form the basis for many higher-level statistical measures such as skill scores. As such, these measures are reported along with *MAE* and *RMSE* in the next chapter for each model.

Given the aforementioned limitations surrounding the meaning and interpretation of Pearson's product moment correlation coefficient (r), a more statistically meaningful and descriptive expression is desirable. One such alternative is the so-called Index of Agreement proposed by Willmott and Wicks (1980).

$$d = 1 - \left[\frac{\sum (P_i - O_i)^2}{\sum \left(|P_i'| + |O_i'| \right)^2} \right], \quad 0 \le d \le 1 \tag{3.34}$$

From Equation 3.34, the Index of Agreement (d) is a function of the *MSE* and of two difference series P' and O', where $P_i' = P_i - \overline{O}$ and $O_i' = O_i - \overline{O}$. Unlike Pearson's r, Willmott and Wicks' Index of Agreement (d) is not a measure of association. It does not attempt to explain the degree to which the observed and estimated variables co-vary. Instead, d is "a measure of the degree to which a model's predictions are error free" (Willmott and Wicks, 1980). As it is bounded between 0 and 1, a perfect, error free model would obtain a value of 1, whereas a purely random model would be expected to have $d = 0$. Furthermore, because it is bounded, d can be used as a relative measure, comparing the performance of one model against another. As such, it is a powerful assessment tool and is reported in the suite of evaluative statistics for each model. Because this research reports the index of agreement based on the *RMSE* rather than *MSE*, it is noted as d_2 rather than d to avoid confusion.

Thus, in the next chapter, the results from each model are reported as a suite of statistical measures as outlined in this section. The use of a standard set of statistics not only permits a thorough evaluation of the performance of an individual model, but additionally sets a standard measure that permits the performance of one model to be compared against the performance of other, perhaps disparate models.

3.7.3 Spatial analysis of model evaluation

Evaluation of model performance in this study was complicated by the spatial character of the analysis, with comparative statistics derived at over 100 individual stations sites. In fact, the primary goal of this analysis is to illuminate the relative ability of FSMM5 to estimate wind climatology across the region. One of the primary benefits of utilizing a numerically-based regional climate model is its perceived ability to generate representative values of meteorological variables in locations where few data observations exist, such as in complex terrain or in coastal zones. As such, it is highly desirable to identify not only differences between observed and estimated wind values at individual stations, but also evaluate these differences with respect to their position within the study region.

3.7.3.1 Trend surface analysis

Geographic analysis provides several methods by which the spatial behavior of the model residuals may be assessed. Two of these methods were employed in this study, trend surface analysis and isopach analysis. Trend surface analysis is widely used in the Earth sciences as a means of apportioning the spatial behavior of a variable into a regional component of variability and a local component at any given location in space. In this respect it is similar to the division of the bias of a temporal series into its conservative systematic and unsystematic components. In trend surface analysis, a surface is empirically fit to the data occurring over a region. Numerical description of the fitted surface can range from a simple first-degree linear plane to an *n*-degree non-linear surface, with the choice of equation complexity dictated by deference to parsimony, the spatial scale of the data, and its spatial behavior. Due to their simplicity of calculation, low degree (*e.g.*, 2^{nd} or 3^{rd} order) polynomials are commonly chosen for this type of analysis. These levels of complexity offer a balanced alternative to purely stationary planar surfaces and higher-order non-linear equations, neither of which easily lend themselves to meaningful interpolation.

Davis (1986) offers an excellent description of the construction and interpretation of trend surfaces for geographical analysis applications and a discussion on the selection of parsimonious trend surface equations. As near surface winds are spatially continuous and partially governed by a relatively coherent overlying geostrophic flow, a second-order polynomial trend surface was deemed to be most appropriate for the analyses used in this study, and was subsequently applied to both observed and model estimates. The equation took the form,

$$\hat{O} = b_0 + b_1 X + b_2 Y + b_3 X^2 + b_4 Y^2 + b_5 XY \tag{3.35}$$

where the regional estimate of the observation $\hat{O}$ is a function of the geographic coordinates, X and Y (Longitude and Latitude respectively), their squares and their cross product (Davis, 1986).

Surfaces calculated with this equation provide an estimation of the regional component of the spatially distributed variable. The difference between the value of the surface at a location and the measured (or estimated) value of the variable at that same point can therefore be interpreted as a measure of the proportion of the variable's value that is not explained by a regional behavior. Instead, this spatial residual value is assumed to reflect the degree of localized influences that have shifted the value away from the regionally influenced surface (Chorley and Haggett, 1965).

The analysis of trend surfaces for both the observed and model estimated values lends insight to the degree the model reproduces the regional wind field, in that it can act as a low pass filter. That is, when only the trend surfaces are compared, the high frequency, or localized behavior has been removed, leaving an estimate of the regional wind field relative to the observed regional wind field, which has been calculated in the same manner. Furthermore, if the differences between the two trend surfaces (*i.e.* observed and model estimated) are mapped, a spatial behavior of the accuracy of the model can be obtained. On the other hand, the localized wind, as represented by the difference of the trend surface and the actual data or estimates (acting as a high pass filter), can be assessed spatially and used to evaluate a model's ability to account for local influences in generating estimates.

3.7.3.2 Isopach analysis

The second geographical method for the spatial analysis of data that has been employed in this research is known as isopach analysis (Davis, 1986). An isopach is simply a contour map of differences of a variable over space. The variable being mapped can be anything, and as such, isopach analysis is ideally suited for the evaluation of spatially-based model output. As was discussed in the previous paragraph, maps of the differences in trend surfaces are actually a form of isopach analysis. Many of the model evaluative statistics that were produced for the observed data and each series of model estimates were subsequently subjected to isopach analysis to highlight the magnitudes and spatial distribution of observed-estimated differences across the study region. In particular, isopach maps often are able to graphically illustrate geographic patterns in spatial bias. A variety of isopach maps therefore are presented in the next chapter and used to assist in identifying the spatial variability of overall model performance.

Chapter 4. Results

The ability of a numerical climate model (FSMM5) to accurately estimate the wind resource of the Great Lakes region was the primary goal of this study. To that end, potential near surface winds over the study area were estimated by the FSMM5 model and evaluated for accuracy. Due to the complexity of numerical models relative to established statistical techniques, it was necessary to compare the relative performance of each type of model. This was accomplished by constructing and applying three statistical models (two stochastic and one probabilistic) to estimate the wind resource at the same geographical locations as FSMM5-derived output estimates. A comparison of relative model accuracy is subsequently presented. The final objective of this study was to evaluate the bias of the FSMM5 model estimates and determine the degree of systematic error that could potentially be removed from the model estimates in order to increase accuracy.

4.1 FSMM5 Model Performance

The statistics used to evaluate model performance were chosen to quantify differences and similarities between model-estimated and observed wind fields. The mean and standard deviation of both observational data and model estimates (hereafter noted as o, s_o, e and s_e respectively) describe the basic similarity of both distributions. The Pearson product moment correlation coefficient (r) describes the degree of covariation between the observed and estimated data. The mean absolute error (*MAE*) and root mean squared error (*RMSE*) are measures of the magnitude of the overall bias contained in the estimates, and *RMSEs* and *RMSEu* are the systematic and unsystematic components of the root mean squared error. The percentage of the total bias that was systematic (hereafter *SB%*) was included to help lend clarity to the interpretation of the results. Lastly, Willmott's Index of Agreement (d_2, based on *RMSE*) is presented as a measure of the non-biased proportion of the estimate. While often useful where the systematic bias of the model estimation error results in a consistency of under or over estimation, the mean error (*ME*) was unfortunately of limited use in this analysis because the variability of the unsystematic bias resulted in both under and over estimates, generating mean series errors near zero over much of the study area.

Additionally, two sets of evaluative statistics are presented. The first is an evaluation of model-derived estimates at individual time steps, hereafter referred to as forecast accuracy. The second is the evaluation of the estimates of the distributional parameters of the wind resource, referred to as resource accuracy. While the evaluation of forecast accuracy is important, it is not as critical to wind resource estimation as is the resource accuracy. A model can, for example, exhibit low forecasting skill in that it never precisely estimates the observed wind speed at a given time or place, but that same model may be of exceedingly high skill in estimating a distribution of wind speeds that closely approximate the observed distribution at a given location. In this study, relatively greater emphasis was therefore placed on evaluating resource accuracy to determining the level of model skill.

Overall, the performance of FSMM5 in describing wind fields over the Great Lakes was variable, and in many cases, poor. Evaluative statistics of forecast accuracy from all implementations of the model are given in Table 4.1. Evaluative statistics of the resource accuracy of the same model implementations are given in Table 4.2. As was discussed in the previous chapter, wind estimates obtained from FSMM5 were disseminated into 15 model variations. Wind estimates from each of the three domain resolution (36-km, 12-km, and 4-km) runs were interpolated from the domain grids to the station sites using unweighted 1, 4, 16, and 36 km nearest neighbor schemes and a 4 point inverse distance weighted procedure.

FSMM5 Performance evaluation (forecast accuracy)				
	x_{min}	$\bar{x}$	s_x	x_{max}
o **(m s^{-1})**	*2.05*	*3.76*	*0.70*	*7.05*
e **(m s^{-1})**	*3.05*	*5.26*	*1.51*	*8.12*
s_o **(m s^{-1})**	*1.63*	*2.41*	*0.30*	*3.88*
s_e **(m s^{-1})**	*1.52*	*2.49*	*0.69*	*4.09*
r	*0.00 (-0.11)*	*0.17*	*0.20*	*0.72*
MAE **(m s^{-1})**	*1.57*	*2.99*	*0.96*	*5.19*
RMSE **(m s^{-1})**	*2.01*	*3.72*	*1.12*	*6.24*
RMSEs **(m s^{-1})**	*1.10*	*2.84*	*0.98*	*5.07*
RMSEu **(m s^{-1})**	*1.46*	*2.38*	*0.64*	*3.79*
SB% **(%)**	*20.95*	*57.84*	*8.91*	*71.38*
d_2	*0.27*	*0.44*	*0.11*	*0.79*

Table 4.1 Evaluative statistics of FSMM5 model performance obtained from wind estimates of 15 variations (X_i) of the model over the period of record . The -0.11 value for minimum r is the lowest negative correlation obtained (0.00 was the lowest absolute correlation obtained).

FSMM5 Performance evaluation (resource accuracy)				
	x_{min}	$\bar{x}$	s_x	x_{max}
o (m s^{-1})	*2.05*	*3.76*	*0.70*	*7.05*
e (m s^{-1})	*3.05*	*5.26*	*1.51*	*8.12*
s_o (m s^{-1})	*1.63*	*2.41*	*0.30*	*3.88*
s_e (m s^{-1})	*1.52*	*2.49*	*0.69*	*4.09*
k_o	*1.21*	*1.94*	*0.38*	*4.81*
k_e	*1.07*	*1.98*	*0.38*	*2.70*
c_o	*2.70*	*4.53*	*0.89*	*7.52*
c_e	*2.61*	*5.55*	*1.61*	*9.08*
r	*0.01*	*0.78*	*0.21*	*0.97*
MAE (n)	*54.44 (0.48)*	*228.46 (2.02)*	*118.19 (1.06)*	*535.85 (5.27)*
RMSE (n)	*96.80 (0.81)*	*401.60 (3.55)*	*159.81 (1.44)*	*843.71 (7.80)*
RMSEs (n)	*0.13 (0.00)*	*183.57 (1.64)*	*175.75 (1.57)*	*661.10 (6.80)*
RMSEu (n)	*87.55 (0.73)*	*335.19 (2.96)*	*99.46 (0.89)*	*588.24 (6.41)*
SB% (%)	*0.00*	*21.32*	*22.15*	*79.30*
d_2	*0.34*	*0.86*	*0.14*	*0.98*

Table 4.2 Evaluative statistics of FSMM5 model performance obtained from wind estimates of 15 variations (X_i) of the model over the period of record. The mean error statistics are given in bin counts and the numbers in parentheses in the mean error rows are the percentage of total n. k and c are Weibull shape and scale parameters respectively.

It is clear from Table 4.1 and from Figure 4.1 that FSMM5 is of somewhat limited utility as a model for forecasting hourly wind resources for wind energy production at a given location, Minimum bias is on the order of just over 1 m s^{-1}. While this level of accuracy may be acceptable for other applications, given the sensitivity of turbine power output to wind speed (see Figure 1.1), even a 1 m s^{-1} deviation from actual values could mean an exponentially larger error in power output, which would in turn become even larger when multiplied by a number of turbines in a wind farm reliant upon that wind speed. Unfortunately, errors in the 1 m s^{-1} range are limited to just the best of the model variants, and even then only at certain locations within the study area. On average over the study area and across all FSMM5 variants, MAE and RMSE were on the order of 3 to 4 m s^{-1}, which is unacceptable accuracy within the realm of wind power forecasting.

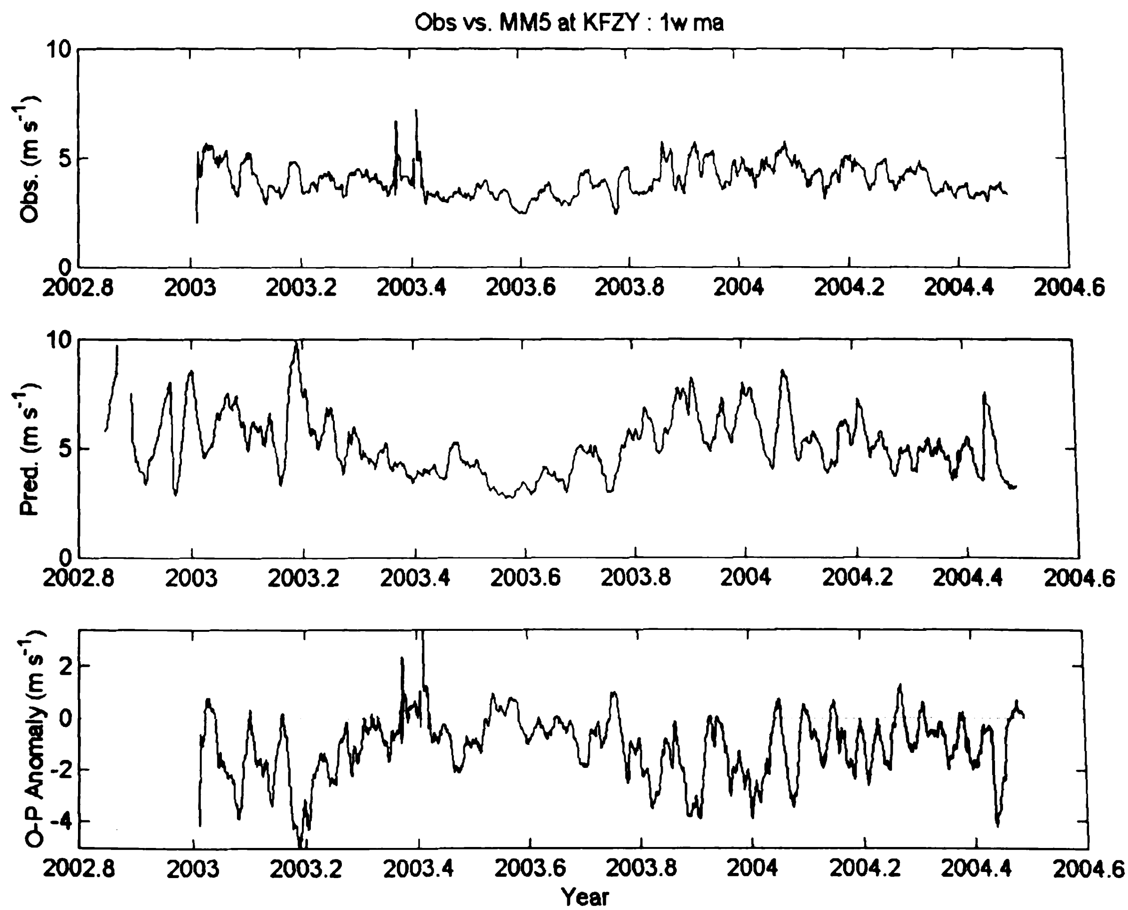

Figure 4.1 One week moving averages of the ASOS observed (top) and FSMM5 forecast (middle) wind speeds at Fulton, NY (KFZY) for the period of record. The bottom figure is a 1-week moving average applied to the hourly differences (O-P) between observed and predicted wind speeds. The moving average was used to more clearly illustrate the degree of variability that exists. All stations exhibit similar variability.

Furthermore, an assessment of correlation indicates a very low degree of covariance between model-estimated and observed wind speed values over the study area. The best correlation obtained was 0.72, with a mean correlation of just 0.2 and several occurrences of nearly perfect non-correlation (0.00). These low correlations and relatively large errors (with respect to the mean speeds) are corroborated by the low index of agreement (d_2) scores. A mean d_2 of 0.44 indicates that, on average only about 44% of the model estimate is error free.

Fortunately, it appears that a great deal of the bias residing in the FSMM5 estimates is systematic in nature. Based on the calculation of the systematic component of the *RMSE*, anywhere from 21% to 72% of the bias in the model estimates can potentially be accounted for within the model. However, that is beyond the scope of this research.

Rather, the focus of this study is in the ability of the model to accurately estimate the overall (not time dependent) distribution of the wind resource over the study region. In this respect, FSMM5 performs notably better (see Table 4.2). To perform this assessment, observed and estimated wind speed values were sorted into 1 m s^{-1} histogram bins. The bin counts of the observed and estimated wind speed distributions were then assessed for differences. While mean absolute and root mean squared errors still appear to be rather large (they are presented in terms of bin frequencies), they actually represent a very small proportion of the number of observations from which the histograms were obtained (on average 11,396 values). Thus, in fact the *MAE* and *RMSE* are relatively low (on average just 2 and 3.5% of total sample size respectively).

Additionally, the mean correlation (*r*) jumps from 0.17 for the forecast estimation to 0.78 for the resource estimation (with similar standard deviation). Despite this improvement, very low resource estimate correlations were observed at some stations and model variants, ,while exceptional correlations were observed at others. The overall good agreement is further reinforced by the noticeably increased index of agreement, with a mean of 0.86 (or 86% error-free estimate).

While the means of the observed and model estimated distributions do not appear to readily agree, there is still remarkable similarity of the shape (*k*) and scale (*c*) parameters of the Weibull density functions that had been empirically fit to the observed and estimated data. Furthermore, it appears that while some stations or model variants exhibit a great degree of systematic bias (a maximum of 79% was encountered), the mean systematic bias was just 21%, indicating that most of the variability between the observed and model estimated wind speed distributions was not associated with the model.

While an evaluation of the overall performance of FSMM5 reveals a substantial amount of systematic bias and a relatively large variability in the error, it does not address the causes of that bias. To more appropriately evaluate the performance of the FSMM5 variants, a more detailed analysis of model performance is warranted. First, the relative performance of the three model domain resolutions (*i.e.*, 4 km, 12 km and 36 km) is compared, followed by the influence of spatial aggregation on model performance. This evaluation will largely determine which of the model variants exhibits the lowest resource estimation error.

4.1.1 Performance based on grid resolution

For each FSMM5 domain, 5 variants were considered (based on aggregation resolution as discussed in Chapter 3). The statistics presented in this subsection for each domain were derived from a grouped analysis of those 5 variants. Table 4.3 describes the relative performance of the model variants within each grid domain. The evaluation statistics are based upon the observed versus estimated resource distributions and not on the individual time-step model estimates (*i.e.*, forecasting evaluation).

From Table 4.3 several patterns are evident. In particular, mean differences between the observed and estimated mean wind speeds tend to decrease with decreasing spatial resolution. Furthermore, the mean standard deviation of estimated speeds also decreased appreciably. Despite the general agreement between first and second moments of the distributions, given the large *n*, they were all found to be significantly different ($t_{2,0.99}$ - *note:* statistical tests are identified with the number of tails and significance level as a subscript). However, the mean of the 36 km domain distribution is significantly lower than that of the 12 km domain ($t_{1,0.90}$) This improvement in estimative accuracy is borne out in the parameters of the theoretical Weibull pdf. While the parameters of all domains appear to be in good agreement, it is only with the 36 km domain that neither mean estimated shape nor mean estimated scale are significantly different from those fit with the observed data ($t_{2,0.99}$).

FSMM5 Evaluation Statistics by Domain						
	4 km		12 km		36 km	
	$\bar{x}$	s_x	$\bar{x}$	s_x	$\bar{x}$	s_x
o (m s^{-1})	3.76	0.70	3.77	0.70	3.76	0.70
e (m s^{-1})	5.80	0.95	5.93	1.88	4.04	0.37
s_o (m s^{-1})	2.41	0.30	2.41	0.30	2.40	0.30
s_e (m s^{-1})	2.76	0.54	2.77	0.80	1.94	0.28
k_o	1.94	0.38	1.94	0.38	1.94	0.38
k_e	1.90	0.29	1.93	0.31	2.12	0.47
c_o	4.53	0.89	4.54	0.89	4.53	0.89
c_e	6.03	1.04	6.20	2.09	4.41	0.59
r	0.76	0.17	0.69	0.27	0.89	0.07
MAE (n)	252.02 2.23 %	102.96 0.91 %	262.92 2.34 %	152.90 1.36 %	170.44 1.50 %	53.49 0.49 %
RMSE (n)	419.33 3.71 %	147.31 1.32 %	436.77 3.89 %	193.76 1.74 %	348.71 3.06 %	114.48 1.04 %
RMSEs (n)	228.79 2.03 %	155.94 1.40 %	239.34 2.15 %	220.97 1.97 %	82.58 0.73 %	65.17 0.62 %
RMSEu (n)	336.65 2.97 %	86.92 0.76 %	334.92 2.98 %	100.36 0.90 %	334.01 2.93 %	109.90 0.98 %
SB% (%)	29.22	19.91	27.18	27.02	7.74	8.59
d_2	0.85	0.12	0.80	0.19	0.93	0.04

Table 4.3 Evaluative statistics of FSMM5 model performance obtained from the 5 variants (X_i) of the model within each of the 3 model domains over the period of record. The mean error statistics are given in bin counts and are followed by the percentage of total *n*. *k* and *c* are Weibull shape and scale parameters respectively.

The measures of agreement also demonstrate improvement of skill with decreasing domain resolution. The 36 km domain again was associated with the lowest overall bias, which is significantly lower than both the 12 and 4 km domain ($t_{1,0.95}$). However, interestingly the 12 km domain exhibits higher model bias than the 4 km domain. Additionally, while there is no statistically significant difference in unsystematic bias between model domains, there is a significant improvement in systematic bias with the 36 km domain over both other domains ($t_{1,0.95}$). Furthermore, the systematic error becomes a much smaller proportion of the overall error as coarser domains are selected, as evidenced by the drop in systematic bias percentage (*SB%*) from around 30% at 4 km to just 8% at 36 km. Thus, not only do modeled resource estimates appear to improve significantly at coarser resolutions, but their systematic component also decreases, indicating that perhaps there is spatial bias inherent in the domain itself.

The behavior of the model over the three domain resolutions can be better illustrated by graphical methods. Two graphical analyses in particular demonstrate the behavior of the FSMM5 model bias. The first, Figure 4.2, is a representative plot of the goodness of fit between the observed data and the Weibull pdf obtained from the FSMM5 estimates that were interpolated from each domain to the locations of the ASOS stations using the nearest 4 grid points and an inverse distance weighting technique (the same technique is applied to all comparisons in this subsection).

From this figure (especially from the cdf) it is clear that the 36 km domain did the best job estimating the wind speed distribution. The primary reason for the overestimation of speeds near the mean is because FSMM5 had not estimated enough high wind speeds to shift the scale parameter to the right and "stretch" the distribution. Although Figure 4.2 represents just one station, similar behavior exists at most stations in the study area. Alternatively, model bias may be viewed with respect to the distribution of wind speeds by graphically assessing the variability of bin frequencies (Figure 4.3).

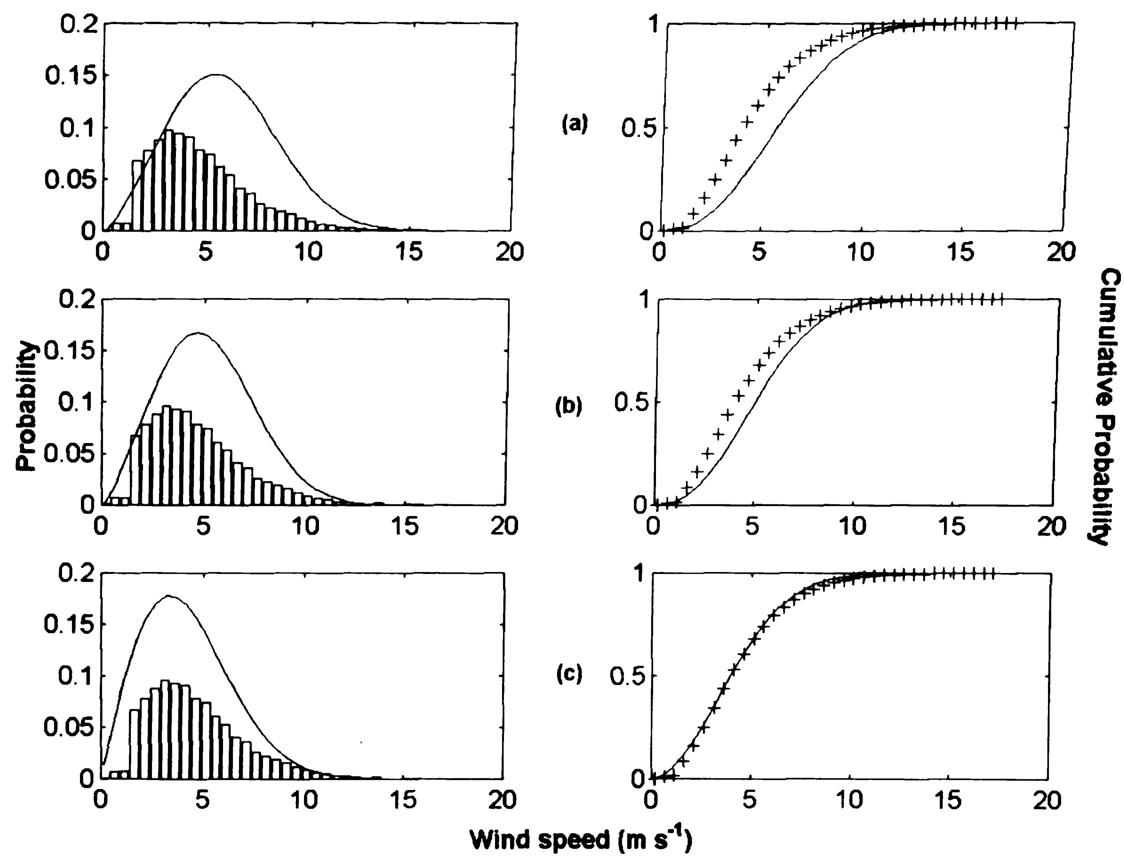

Figure 4.2 Comparison of the FSMM5 estimated Weibull pdf (left, line) and cdf (right, line) at Holland, MI (KBIV) and the observed wind speed distribution (left, bars; right, crosses) for each of the three domains, (a) 4 km, (b) 12 km and (c) 36 km using the 4 weighted nearest neighbors, over the period of record.

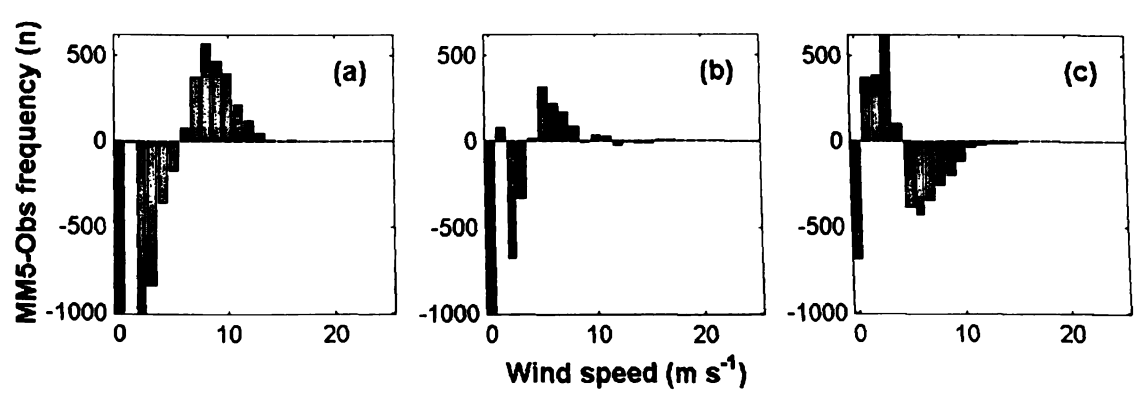

Figure 4.3 Wind speed distribution frequency differences (FSMM5 - ASOS) at Holland, MI (KBIV) for the (a) 4 km, (b) 12 km and (c) 36 km domain using 4 weighted nearest neighbors, over the period of record.

Figure 4.3 illustrates several issues regarding the estimation of wind speed distributions by FSMM5. First and foremost, the model greatly under represents the frequency of calm periods (*i.e.*, < 1 m s^{-1}). This under-representation is systematically present over all domains and decreases only slightly over the 36 km domain. The second issue appears to be a systematic under and over estimation of wind at certain speeds. At the coarsest resolution, low wind speeds appear to be over-estimated while higher speeds are under-reported. Over the 4 and 12 km domains, this relationship appears to be reversed, where the frequency of low wind speeds is systematically under-estimated while the frequency of stronger winds is over-estimated. As with the overall distributions highlighted in Figure 4.2, this systematic behavior is present throughout the study region.

The systematic bias observed in Figure 4.3 is also present when wind directions are examined. Figure 4.4 presents the observed and estimated wind roses at Holland, MI, while Figure 4.5 shows the differences in directional frequency observed at that same station. As with previous figures, statistics from the Holland, MI (KBIV) location are displayed because the behavior of model estimated winds relative to ASOS observed winds are representative of the results across the study area. As displayed in Figure 4.4, there is a fair amount of dissimilarity between observed and model estimated wind direction distributions. Once again, much of this dissimilarity appears to be systematic (Figure 4.5). In general, winds from the northeast appear to be consistently over-estimated whereas the frequency of winds out of the southwest (the prevailing direction) is most often under-estimated.

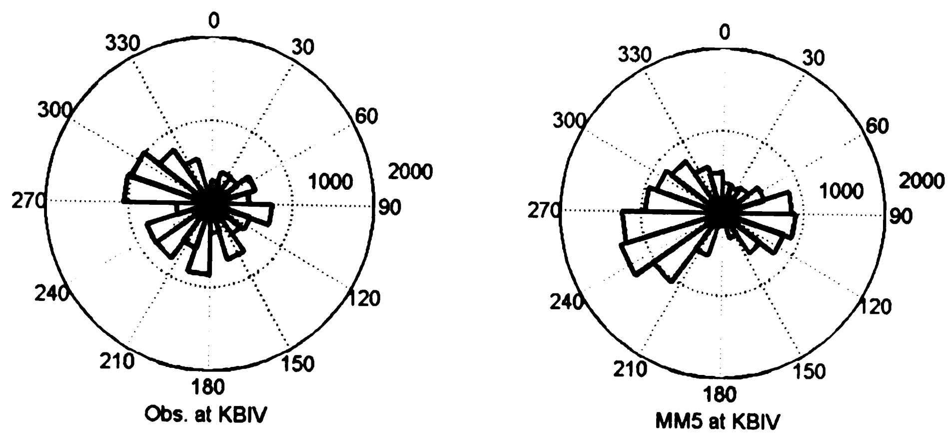

Figure 4.4 Wind roses at Holland, MI (KBIV) from the 12 km FSMM5 domain showing the observed wind direction distribution (left) and the FSMM5 estimated direction distribution (right) from 11/02 - 6/04.

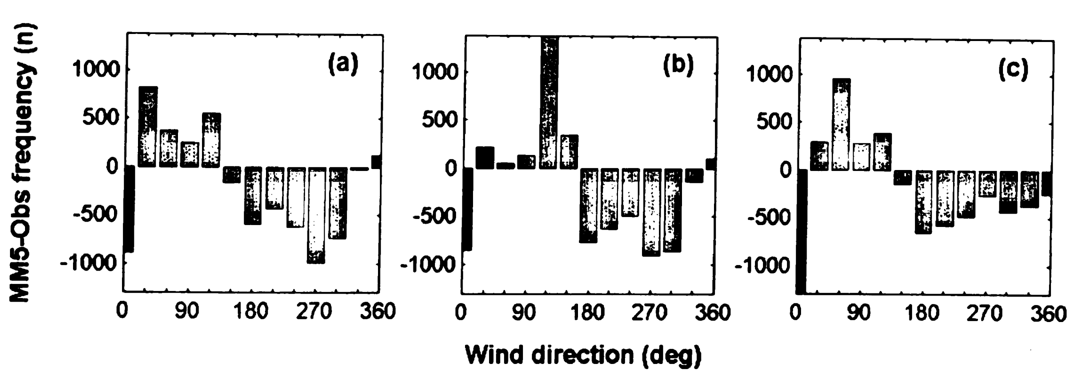

Figure 4.5 Frequency differences between FSMM5 and ASOS observed wind directions at Holland, MI (KBIV) for the (a) 4 km, (b) 12 km and (c) 36 km domains for the period of record.

Given the apparent systematic bias inherent in the wind regimes estimated by FSMM5 over the study region, an examination of the spatial variability of the resource estimates is in order. For example, the spatial variability of the model estimates of mean wind speed over the three domains is demonstrated in Figure 4.6. It is clear from Figure 4.6 that substantial differences exist in the model's calculation of wind speeds at the different domain resolutions.

(a) 4 km

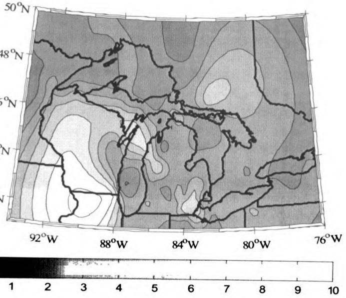

(b) 12 km

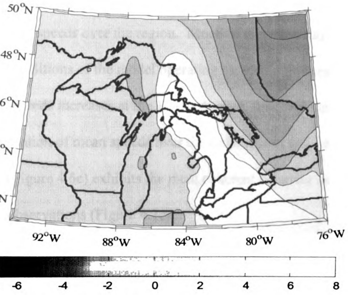

Figure 4.6 FSMM5-estimated mean wind speeds (in m s^{-1}) over the study region over the three model domains using an inverse distance weighting technique on the nearest 4 grid points to a station from 11/02 to 6/04. The negative mean speeds in (b) are a function of the spatial interpolation scheme extrapolating beyond the observation network and should be ignored.

(c) 36 km

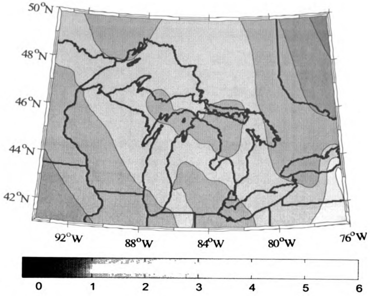

Figure 4.6 Continued.

As expected, the 4 km domain estimates appear to produce the most spatial variation in mean wind speeds over the region. Much of this variability is likely due to the boundary layer conditions of the model operating on such a fine resolution. Coherence of mean speeds increases at the 12 km domain, however there appears to be a systematic over estimation of mean speeds over the Lake Huron and Lake Erie regions. The 36 km domain (Figure 4.6c) exhibits the most coherent behavior as well as the most agreement with the observations (Figure 4.7c).

(a) 4 km

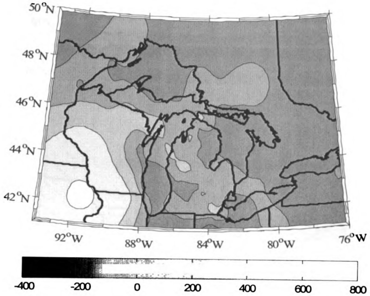

(b) 12 km

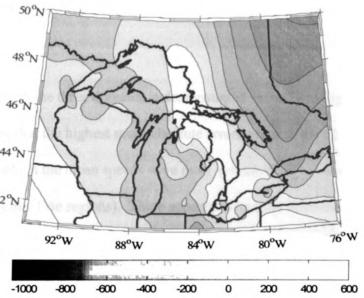

Figure 4.7 Mean Absolute Error (in bin counts: n) of wind speed histogram frequencies between FSMM5 and observed data over the study area on the three model domains from 11/02 to 6/04. All estimates were interpolated to stations using an inverse distance weighting technique on the nearest 4 grid points. Negative MAE values are the result of the biharmonic spline procedure extrapolating beyond the range of the stations and should be ignored.

(c) 36 km

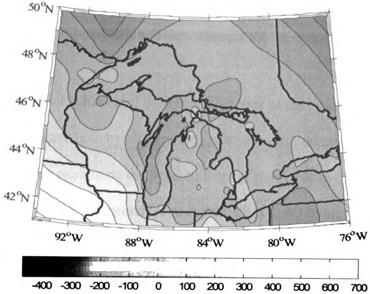

Figure 4.7 Continued.

Model bias in the three domains is demonstrated spatially in Figure 4.7. In general, it appears that the highest mean absolute errors occur in the 12 km domain in the same areas over which the mean speeds were most systematically over-estimated (*i.e.*, Lake Huron and Lake Erie regions). There appears to be little difference in the magnitude of the errors between the 4 and 36 km *MAE*, but in general, the 36 km domain appears to exhibit more spatial coherence in bais (*i.e.*, more spatially systematic).

The spatial component of the degree of bias in the model estimates of the wind resource can perhaps be best described by variations in the index of agreement (d_2) over the region. This is presented for each model domain in Figure 4.8. As expected, FSMM5 exhibits its most spatially coherent model bias at the coarsest (36 km) domain. The 12 km and 4 km domains both exhibited consistently lower indexes of agreement over the study area and are dichotomous in their behavior. The 12 km domain is very spatially systematic in the distribution of index values, whereas the 4 km domain is not.

Lastly, the spatial behavior of the systematic error of the model estimated wind resource can be visualized both by plotting the systematic error component of *RMSE* over the region as well as by examining the trend surfaces of the residuals of the mean wind speed. The systematic *RMSE* is presented in Figure 4.9, and the trend surface analysis in Figure 4.10.

The spatial patterns of systematic bias over all domains closely mirror the behavior of the overall bias presented in the preceding figures. The 36 km domain exhibits the most spatial consistency in systematic bias whereas the 4 km domain is the most spatially inconsistent. Again, the greatest systematic bias over the 12 km domain was coincident with locations where the model substantially over-estimated the mean speeds.

(a) 4 km

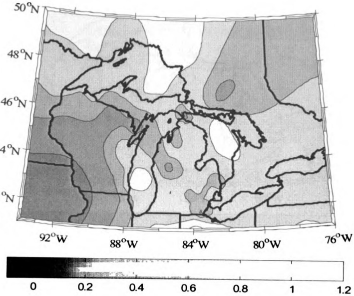

(b) 12 km

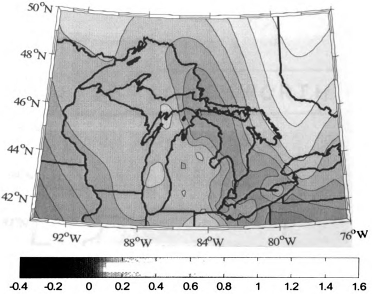

Figure 4.8 Index of agreement (d_2) for FSMM5 estimates of the wind resource over the (a) 4 km, (b) 12 km and (c) 36 km domains from 11/02 to 6/04. Values outside the range 0 - 1 are extrapolation artifacts and should be ignored.

(c) 36 km

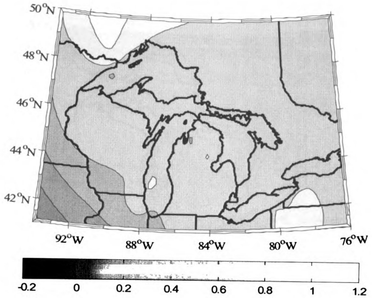

Figure 4.8 Continued.

(a) 4 km

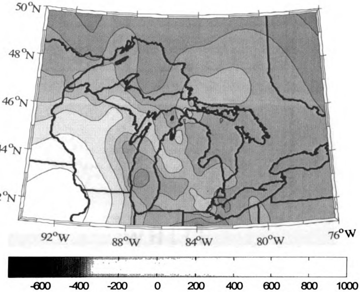

Figure 4.9 Systematic component of the Root Mean Squared Error (*RMSEs*) over the study region from the (a) 4 km, (b) 12 km and (c) 36 km FSMM5 domains from 11/02 to6/04. Negative values are an extrapolation artifact and should be ignored.

(b) 12 km

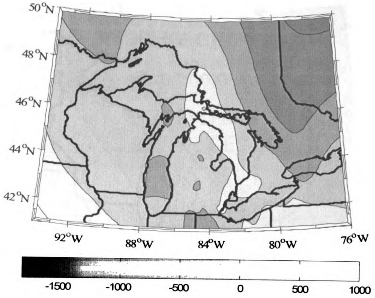

(c) 36 km

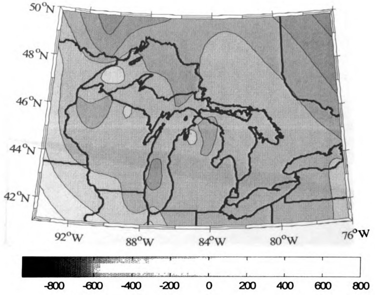

Figure 4.9 Continued.

(a) 4 km contour

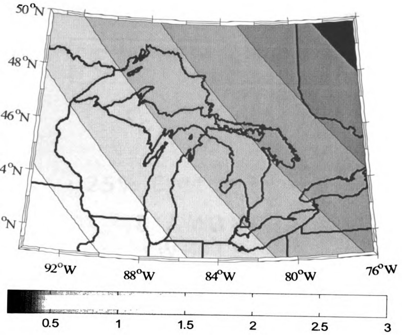

(b) 4 km surface

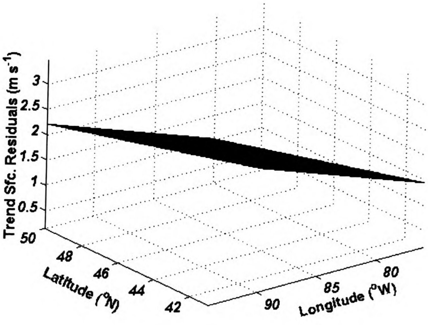

Figure 4.10 Fitted trend surfaces of FSMM5-Observed histogram residuals (m s^{-1}) over the study area from the (a-b) 4 km, (c-d) 12 km and (e-f) 36 km domains from 11/02 to 6/04. The lower figures are 3-dimensional representations of the first-order trend surfaces that are contoured in the upper figures.

(c) 12 km contour

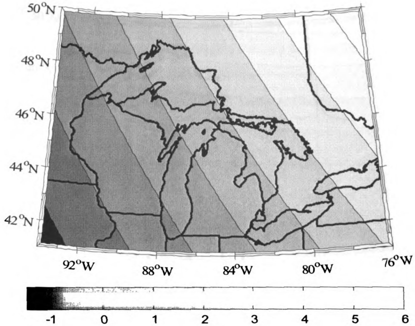

(d) 12 km surface

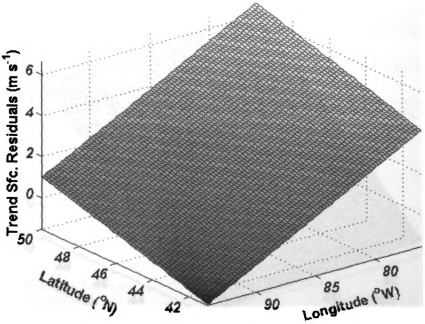

Figure 4.10 Continued.

(e) 36 km contour

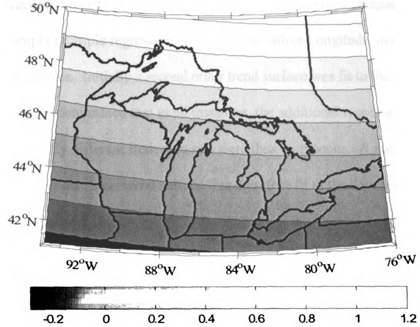

(f) 36 km surface

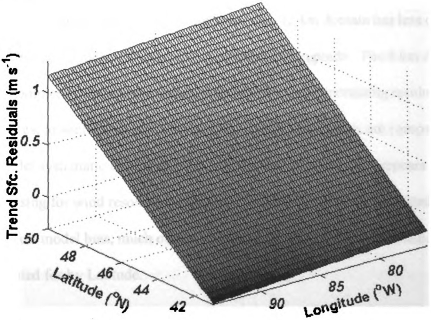

Figure 4.10 Continued.

The use of trend surface analysis was discussed in the preceding chapter as a means of extracting information regarding the behavior of a variable in space. Trend surfaces are simply multiple regression equations that utilize Longitude and Longitude as the regressor variables. Initially a second order trend surface was fit to the data, however, it was subsequently determined that in all instances, the additional regression coefficients were not significantly different from zero and were thus extraneous. A more parsimonious first order linear trend surface was therefore fit to the data and the results are presented in Figure 4.10.

The presence of a strong trend, both latitudinally and longitudinally reveals the relative link between geographical location and model bias. Figure 4.10 demonstrates that the coarsest resolution domain (36 km) appears to exhibit a distinctly latitudinal trend, but only slightly dependent on longitude. The 12 km domain has less of a latitudinal trend, but more pronounced dependence on longitude. The 4 km domain pattern is completely the reverse of the 12 km domain, with increasing residual values from northeast to southwest across the region.. When these trends are compared with the overall model systematic error over each domain, the 36 km domain appears to be the most promising for wind resource estimation. In addition to being associated with the overall lowest model bias, much of that systematic bias might be spatial in nature and was accounted for by Latitude.

4.1.2 Performance based on spatial aggregation resolution

The FSMM5 was also evaluated to determine which of the 5 interpolation schemes yielded the best wind estimates at the site locations. In review, wind estimates were calculated at each station locations within the study network using interpolated grid point estimates from each model domain with five different interpolation schemes. In the first method the location of interest simply assumed the value from the nearest model grid point. The second estimated each location value as an unweighted average of the nearest 4 grid points. The third used a linear inverse distance weighting scheme on those same 4 points. The fourth and fifth methods produced an unweighted average of the nearest 16 and 36 grid points respectively. The increasing number of nearest neighbor grid points was considered in order to investigate the influence of spatial aggregation, and perhaps uncover the degree of spatial bias inherent in the different model domains. Some of the results of the third interpolation method were presented in the preceding chapter. All five are assessed here and are limited to the 36 km domain which was found to be superior to the other domain resolutions.

An analysis of the model evaluation statistics is presented in Table 4.4. Based upon these statistics, there does appear to be a trend in the behavior of the various interpolation schemes. It was initially suspected that the estimates calculated with the greatest number of grids (and from the greatest areas) would provide the best results in that they would be largely devoid of any localized influences. This was not the case, however, as the larger sample estimates were found to be associated with the poorest performance. This may imply that the localized component of the wind resource at a location is a substantial portion of the overall wind regime. Larger aggregation intervals would tend to mask that influence.

Model evaluative statistics for 5 interpolation schemes on the 36 km domain										
Nearest neighbors	**1**		**4**		**4 (IDW)**		**16**		**36**	
	$\bar{x}$	s_x	$\bar{x}$	s_x	$\bar{x}$	s_x	$\bar{x}$	s_x	$\bar{x}$	s_x
o (m s^{-1})	3.76	0.70	3.76	0.70	3.76	0.70	3.76	0.70	3.76	0.70
e (m s^{-1})	4.03	0.46	4.02	0.39	4.03	0.43	4.04	0.29	4.07	0.26
s_o (m s^{-1})	2.40	0.30	2.40	0.30	2.40	0.30	2.40	0.30	2.40	0.30
s_e (m s^{-1})	2.11	0.30	1.99	0.25	2.04	0.27	1.84	0.19	1.73	0.16
k_o	1.94	0.38	1.94	0.38	1.94	0.38	1.94	0.38	1.94	0.38
k_e	2.14	0.17	1.94	0.14	1.52	0.25	2.27	0.30	2.76	0.26
c_o	4.53	0.90	4.53	0.90	4.53	0.90	4.53	0.90	4.53	0.90
c_e	4.62	0.51	4.26	0.47	3.81	0.61	4.52	0.41	4.85	0.31
r	0.91	0.07	0.89	0.08	0.90	0.07	0.88	0.07	0.87	0.08
MAE (n)	151.17 1.33%	52.72 0.50%	164.61 1.45%	53.70 0.50%	**157.72** 1.39%	52.56 0.50%	182.39 1.60%	48.10 0.44%	196.31 1.72%	47.74 0.43
RMSE (n)	**296.43** 2.61%	106.11 1.00%	335.75 2.95%	110.17 1.03%	**314.51** 2.77%	107.68 1.03%	**380.14** 3.33%	103.35 0.94%	416.72 3.64%	102.75 0.88%
RMSEs (n)	71.17 0.64%	67.49 0.66%	73.79 0.66%	65.70 0.64%	71.85 0.65%	67.30 0.66%	89.03 0.79%	57.44 0.54%	107.03 0.94%	60.99 0.53%
RMSEu (n)	**282.64** 2.48%	98.25 0.90%	322.80 2.83%	104.53 0.94%	**301.18** 2.65%	100.67 0.61%	365.47 4.52%	102.07 0.41%	397.97 4.85%	103.38 0.31%
SB% (%)	8.28	10.01	7.31	8.67	7.77	9.35	7.85	7.72	9.17	8.02
d_2	0.95	0.04	0.94	0.04	0.94	0.04	0.93	0.04	0.92	0.04

Table 4.4 Evaluative statistics of 5 spatial aggregation schemes applied to the FSMM5 36 km domain wind speed estimates over the period of record. Percentage values in the error statistic cells are the error (bin frequency) as a percentage of the overall number of estimates. Bold values are statistically significant improvements over the next higher model ($t_{1,0.99}$).

Initially, even though there appears to be a trend toward better model performance with smaller spatial aggregation intervals, the differences between aggregation schemes do not appear to be substantial. Statistical testing confirmed this observation. A one-tailed t-test with an alpha level of 0.01 was applied to the data to evaluate the statistical significance of the relationships in the data. Except where indicated, all statistical tests in this section are one-tailed t-tests with an alpha of 0.01. With respect to the observed and estimated means, significant differences were found for all model variants.

Another set of variables examined for statistically significant differences were the parameters of the observed and estimated Weibull density functions. With a T-test, no significant differences were found between the observed and estimated shape (*k*) or scale (*c*), with the exception of the scale parameter in the 36 nearest neighbor variant which was significantly different at the critical level of 99%. Furthermore, there appears to be a strong correlation between observed and estimated wind speed histograms, as evidenced by the high, and statistically significant *r* values ($t_{1,0.99}$). However, with the correlation coefficients, differences in the model variants begin to appear. Although the differences between variants are not statistically significant, the highest correlation is exhibited by the lowest-order aggregation scheme (one nearest neighbor).

It was therefore necessary to evaluate the behavior of the estimation bias. With the exception of the 4 nearest neighbors variant, the models all tended to exhibit decreasing error as the level of spatial aggregation was reduced. Most of the improvements in *MAE* or *RMSE* were not, however statistically significant, with the exception of those indicated in bold in Table 4.4. Notably, the most improved model variant was the 4-neighbor inverse distance weighting (IDW) scheme, with statistically significant improvements in all but systematic error. In fact, no aggregation model significantly improved the systematic bias of the 36 km domain.

Given the lack of distinctiveness between the 5 aggregation variants over the 36 km domain, it was apparent that while any of these approaches would provide a reasonable estimate of the wind resource at a location over the region, the one nearest neighbor variant is the most parsimonious from a spatial standpoint and as such, there is no reason to prefer the more complex aggregation approaches.

At 8.28% of overall model error (with a standard deviation of about 10%), the mean systematic resource bias of the 36 km, 1 nearest neighbor model variant is relatively low. Furthermore, the reduction of this bias would result in an improvement in the model estimation of the resource. However, given the low proportion of bias that is systematic, it is unlikely that any adjustment would be regionally significant. Still, if the first order trend surface of the residuals is examined, there does appear to be a strong latitudinal component that might permit a systematic improvement in model accuracy (Figure 4.11).

Based upon the results discussed in this section, it appears that the 36 km domain, using a one nearest neighbor aggregation scheme provided the best model performance of the 15 variants evaluated. It is therefore this variant that will be compared with the three aforementioned statistical models for wind resource estimation.

(a) Trend surface contour

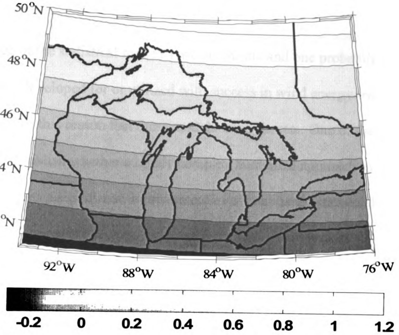

(b) Trend surface

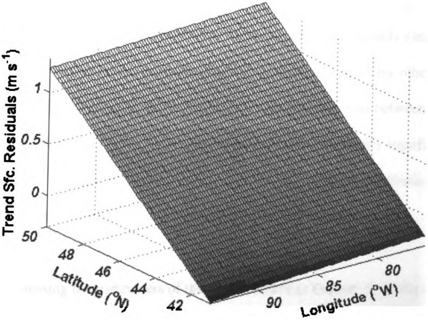

Figure 4.11 First-order trend surface of residuals (mean FSMM5 - mean Obs, in m s^{-1}) over the study area from the 36 km domain, 1 nearest neighbor FSMM5 variant from 11/02 to 6/04.

4.2 Model Comparison

All three of the statistical models (two stochastic and one probabilistic) have been either previously developed for or utilized with success in wind energy resource estimation. It is for this reason that these models were chosen. One of the goals of this research was to establish whether a highly complex numerical approach to wind resource estimation represents a significant improvement over established statistical methods.

4.2.1 Statistical model performance

As with the 15 FSMM5 variants in the previous section, the performance of the three statistical models can be evaluated statistically. Statistics describing the relative performance of the models are presented in Table 4.5. It is immediately clear from the statistics that the Krige model does not appear to perform as well as the other two statistical models. Even so, in an evaluation of difference of means between model estimates and observed values, none of the models have a statistically significant difference from the observed mean ($t_{2,0.99}$). Additionally, all have distribution correlations that are significant at the same level ($p = 0.99$).

In assessing the parameters of the Weibull density function fit to the observed data, again there were no statistically significant differences between any of the parameters with the exception of the shape (k) parameter of the Krige model. This indicates that in general, at least two of the models are providing an excellent estimate of the observed wind speed distribution. This is corroborated by the correlation of the distributions, all of which are significantly high, but the joint probabilistic model appears to correlate best with the observed data.

Evaluative statistics for three statistical wind estimation models						
Model	**JP**		**MCP**		**Krige**	
	$\bar{x}$	s_x	$\bar{x}$	s_x	$\bar{x}$	s_x
o (m s^{-1})	3.77	0.69	3.77	0.69	3.78	0.69
e (m s^{-1})	3.79	0.67	3.74	0.70	3.71	1.02
s_o (m s^{-1})	2.40	0.28	2.40	0.29	2.40	0.29
s_e (m s^{-1})	2.12	0.24	2.02	0.29	2.63	1.19
k_o	1.94	0.39	1.94	0.38	1.94	0.37
k_e	1.83	0.42	1.81	0.62	1.56	0.44
c_o	4.54	0.88	4.54	0.88	4.52	0.88
c_e	4.14	1.02	3.81	1.12	4.19	1.92
r	0.92	0.07	0.88	0.14	0.76	0.18
MAE (n)	130.14 1.17%	43.99 0.39%	114.15 1.03%	44.80 0.42%	116.89 1.25%	81.94 0.87%
RMSE (n)	313.18 2.80%	133.45 1.17%	270.99 2.42%	131.02 1.17%	247.34 2.62%	161.38 1.72%
RMSEs (n)	57.61 0.52%	50.39 0.46%	52.63 0.48%	44.13 0.42%	81.34 0.88%	92.15 1.00%
RMSEu (n)	305.75 2.73%	128.71 1.13%	263.45 2.35%	128.42 1.14%	226.09 2.39%	145.01 1.53%
SB% (%)	4.41	5.15	5.81	6.64	12.37	15.11
d_2	0.94	0.05	0.95	0.04	0.93	0.11

Table 4.5 Evaluative statistics over the period of record for three statistical wind resource models, a joint probabilistic model (JP), a measure-correlate-predict model (MCP), and a Krige model (Krige). Error values are in bin count differences (n), and the percentages are relative to overall record length.

Although the Krige model fitted values appear to have the worst agreement with the observed data, it is helpful to consider the error statistics. Between the mean absolute error and the root mean squared error there is minor disagreement between error measures. In terms of absolute frequency, the MCP model has the lowest *MAE*, but the Krige model appears to have a lower absolute *RMSE*. This is, however rectified by examining the errors relative to the overall frequency count. When viewed as percentages of total, the MCP model has the lowest *MAE* and *RMSE*. However, it should be noted that at $p = 0.99$, a 2-tailed t-test failed to identify any statistically significant difference in the errors between the MCP model and either of the other models. In fact, all three models have indexes of agreement over 0.90 indicating that the majority proportion of their estimates are error free.

Thus, we must turn to the distribution of error among systematic and unsystematic to determine whether one model outperforms the others. In all instances, the systematic component of the *RMSE* was less than 1% of the length of record. Of the *RMSEs* values however, the MCP model, with the lowest score was significantly lower than the Krige model ($t_{1,0.99}$). There was no corresponding significance with the joint probabilistic model. In fact, the joint probabilistic model actually has a lower percentage of systematic bias relative to overall bias than does the MCP model. The bias in the Krige model on the other hand is around 12%, nearly three times as high as the other models.

Overall, it appears that while the Krige model does perform reasonably well over the region, its complexity relative to the other models would likely preclude its use. Therefore, the model has been removed from further consideration and comparison with the selected FSMM5 model variant.

4.2.2 Comparison of FSMM5 to statistical models

The question that must now be asked is whether the best performing variant of the FSMM5 model can perform better than established statistical wind energy resource models. To assess this question, Table 4.6 and 4.7 are presented. Table 4.6 contains the evaluative statistics for the resource estimation and Table 4.7 holds the statistics for the forecast estimation from each of the models. The three models that are compared are the joint probabilistic model, the measure-correlate-predict model and the 36 km FSMM5 with one nearest neighbor aggregation.

Evaluative statistics for three wind resource estimation models						
Model	**JP**		**MCP**		**FSMM5**	
	$\bar{x}$	s_x	$\bar{x}$	s_x	$\bar{x}$	s_x
o (m s^{-1})	3.77	0.69	3.77	0.69	3.76	0.70
e (m s^{-1})	3.79	0.67	3.74	0.70	4.03	0.46
S_o (m s^{-1})	2.40	0.28	2.40	0.29	2.40	0.30
S_e (m s^{-1})	2.12	0.24	2.02	0.29	2.11	0.30
k_o	1.94	0.39	1.94	0.38	1.94	0.38
k_e	1.83	0.42	1.81	0.62	2.14	0.17
c_o	4.54	0.88	4.54	0.88	4.53	0.90
c_e	4.14	1.02	3.81	1.12	4.62	0.51
r	0.92	0.07	0.88	0.14	0.91	0.07
MAE (n)	130.14 1.17%	43.99 0.39%	114.15 1.03%	44.80 0.42%	151.17 1.33%	52.72 0.50%
RMSE (n)	313.18 2.80%	133.45 1.17%	270.99 2.42%	131.02 1.17%	296.43 2.61%	106.11 1.00%
RMSEs (n)	57.61 0.52%	50.39 0.46%	52.63 0.48%	44.13 0.42%	71.17 0.64%	67.49 0.66%
RMSEu (n)	305.75 2.73%	128.71 1.13%	263.45 2.35%	128.42 1.14%	282.64 2.48%	98.25 0.90%
SB% (%)	4.41	5.15	5.81	6.64	8.28	10.01
d_2	0.94	0.05	0.95	0.04	0.95	0.04

Table 4.6 Evaluative statistics for the performance of three wind resource estimation models, joint probabilistic (JP), measure-correlate-predict (MCP), and FSMM5 running on a 36 km domain and utilizing the one nearest neighbor scheme over the period 11/02 to 6/04. Error measures are given in bin count differences and the percentages are relative to overall record length.

Evaluative statistics for three wind forecasting models						
Model	**JP**		**MCP**		**FSMM5**	
	$\bar{x}$	s_x	$\bar{x}$	s_x	$\bar{x}$	s_x
o **(m s^{-1})**	*3.77*	*0.69*	*3.77*	*0.69*	*3.76*	*0.70*
e **(m s^{-1})**	*3.79*	*0.67*	*3.74*	*0.70*	*4.03*	*0.46*
s_o (m s^{-1})	*2.40*	*0.28*	*2.40*	*0.29*	*2.40*	*0.30*
s_e (m s^{-1})	*2.12*	*0.24*	*2.02*	*0.29*	*2.11*	*0.30*
r	*0.79*	*0.08*	*0.76*	*0.17*	*0.00*	*0.05*
MAE **(m s^{-1})**	*1.19*	*0.25*	*1.12*	*0.25*	*2.62*	*0.26*
RMSE **(m s^{-1})**	*1.56*	*0.33*	*1.45*	*0.31*	*3.32*	*0.35*
RMSEs **(m s^{-1})**	*0.78*	*0.29*	*0.79*	*0.32*	*2.55*	*0.31*
RMSEu **(m s^{-1})**	*1.34*	*0.23*	*1.19*	*0.20*	*2.11*	*0.30*
SB% **(%)**	*24.36*	*9.13*	*29.79*	*12.87*	*59.34*	*7.28*
d_2	*0.86*	*0.06*	*0.88*	*0.06*	*0.37*	*0.03*

Table 4.7 Evaluative statistics for the performance of three wind forecasting models, joint probabilistic (JP), measure-correlate-predict (MCP), and FSMM5 running on a 36 km domain and utilizing the one nearest neighbor scheme for the period 11/02 to 6/04.

Although not a focus of this study, Table 4.7 demonstrates that as a wind power forecasting model, it does not appear that on average the FSMM5 variant would be a good choice. On all counts it appears to lack the performance of the statistical models. From a statistical standpoint ($t_{1,0.99}$), all of the FSMM5 model error statistics were significantly higher than those of either statistical model. However, from a wind resource estimation standpoint, Table 4.6 demonstrates that perhaps the numerical FSMM5 is not as quite as erroneous, and performs on par with the other models.

In terms of mean wind speeds, the FSMM5 estimates were significantly different from the observed value ($t_{2,0.99}$). However, neither the estimated Weibull shape nor scale parameters were significantly different from the observed parameters. In terms of the shape (k) parameter, FSMM5 estimates the true values most closely more of the time versus the other models. Although it appears, too, that the scale parameter was best approximated by FSMM5, it was not consistent across the region and the statistical models proved more reliable in this regard. Error statistics proved more difficult to assess as the differences between the three models were not very great. The only statistically significant difference that existed was that the *MAE* for the FSMM5 was significantly larger than either of the statistical models ($t_{1,0.99}$). None of the instances where the FSMM5 exhibited lower error than the statistical models was determined to be a statistically significant improvement.

One of the goals of this research was also to determine if the FSMM5 model would have a significant advantage in estimative accuracy for remote locations where no nearby long-term records exist. Thus, the five stations in the study that were most distant from their nearest neighbors were selected for more specific model evaluation and comparison. The analysis for Chapleau Airport, ON (CYLD), the most remote of the 5 (its nearest neighbor is Sault Ste. Marie, ON, approximately 180 km distant) is presented in Table 4.8. The other 4 locations exhibited similar behavior and so are not discussed.

At Chapleau Airport (Table 4.8), both the joint probabilistic and FSMM5 models estimates of the mean speed were significantly different from the observed value ($t_{2,0.99}$). Although the evaluative statistics indicated that the MCP model demonstrated the best Weibull fit, a graphical analysis revealed that the joint probabilistic model was the most appropriate Weibull fit to the data and that the FSMM5 Weibull fit was the poorest (Figure 4.12). However, from Table 4.8 it is the MCP model that exhibits the lowest correlation between the observed and estimated histograms. The histogram differences are displayed in Figure 4.13.

Evaluative statistics for three wind resource estimation models. Chapleau Airport, Ontario (CYLD)			
Model	**JP**	**MCP**	**FSMM5**
o (m s^{-1})	3.07	3.09	3.01
e (m s^{-1})	3.18	3.14	4.50
S_o (m s^{-1})	1.99	2.00	1.99
S_e (m s^{-1})	1.48	1.15	2.36
k_o	1.61	1.64	1.56
k_e	2.19	2.09	2.28
c_o	3.72	3.69	3.50
c_e	3.76	3.29	4.90
r	0.90	0.17	0.88
MAE (n)	142 1.85%	150 1.90%	147 1.82%
RMSE (n)	289 3.76%	321 4.06%	245 3.05%
RMSEs (n)	95 1.23%	112 1.42%	115 1.43%
RMSEu (n)	274 3.56%	301 3.81%	217 2.70%
SB% (%)	10.68	12.23	21.90
d_2	0.93	0.92	0.93

Table 4.8 Evaluative statistics for model estimates of the wind resource at Chapleau Airport, Ontario (CLYD). The models are joint probabilistic (JP), measure-correlate-predict (MCP), and the 36 km domain, one nearest neighbor variant of FSMM5 (FSMM5) for the period 11/02 to 6/04. Error values are given in bin count differences and percentages are relative to the length of record.

Based upon the histogram differences, the influence of systematic error becomes clear. While all three models exhibit some systematic bias, the FSMM5 model appears to be the most systematic in its under-estimation of the occurrence of low wind speeds and its over-estimation of the frequency of higher speeds (relative to the mean). Both statistical models appear to over-estimate winds near the mean speed and under-estimate all others (Figure 4.13). Furthermore, as hinted at by its low histogram correlation, the MCP model greatly over-estimates winds near the mean observed speed at CYLD. This is corroborated by the extreme peakedness of the Weibull distribution estimated from the MCP model (Figure 4.12e).

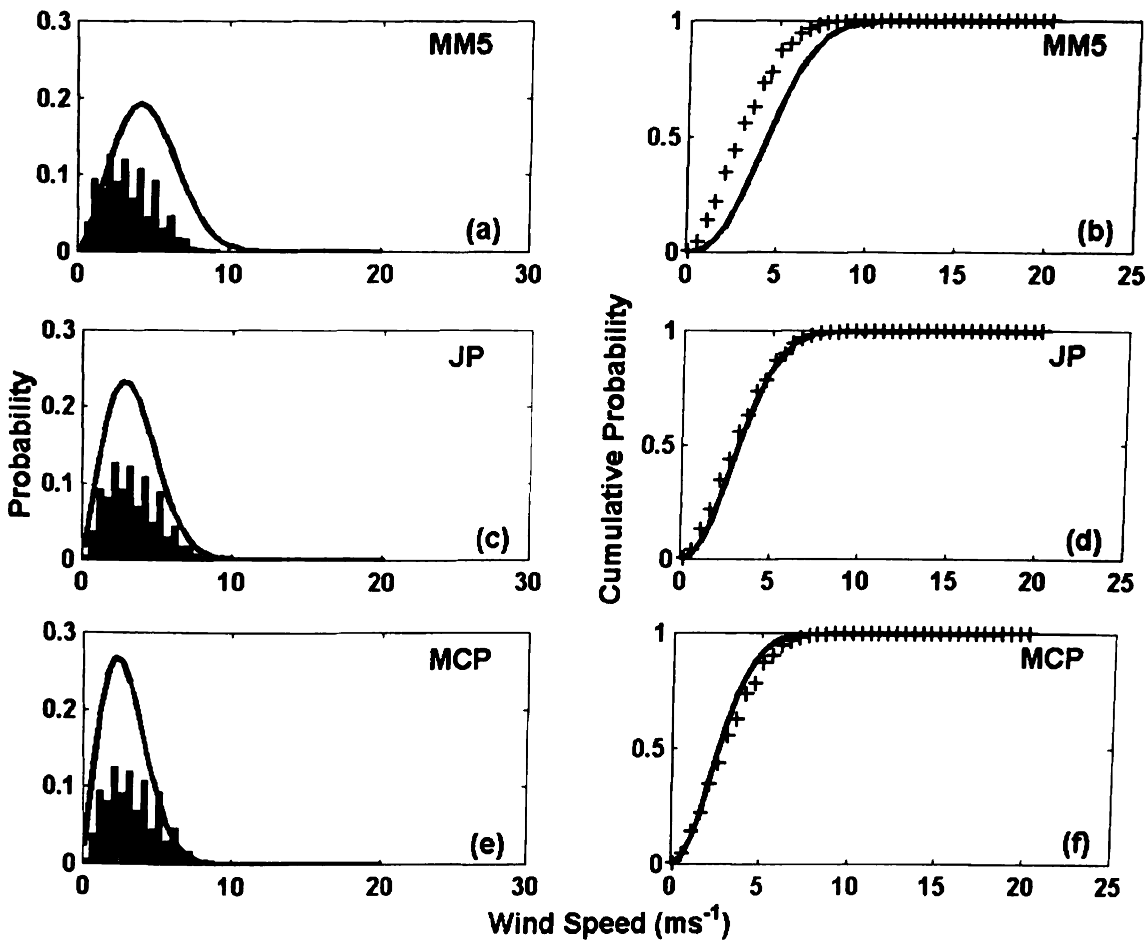

Figure 4.12 Fit of model estimated Weibull distribution (line) to observed wind speed data frequencies (left, bars; right, crosses) at Chapleau Airport, ON (CYLD) for the period 11/02 to 6/04. Left plots are the probability density function, and right plots are the cumulative density function. The models are: the 36 km domain, 1 nearest neighbor FSMM5 (a,b), the joint probabilistic model (c,d), and the measure-correlate-predict model (e,f).

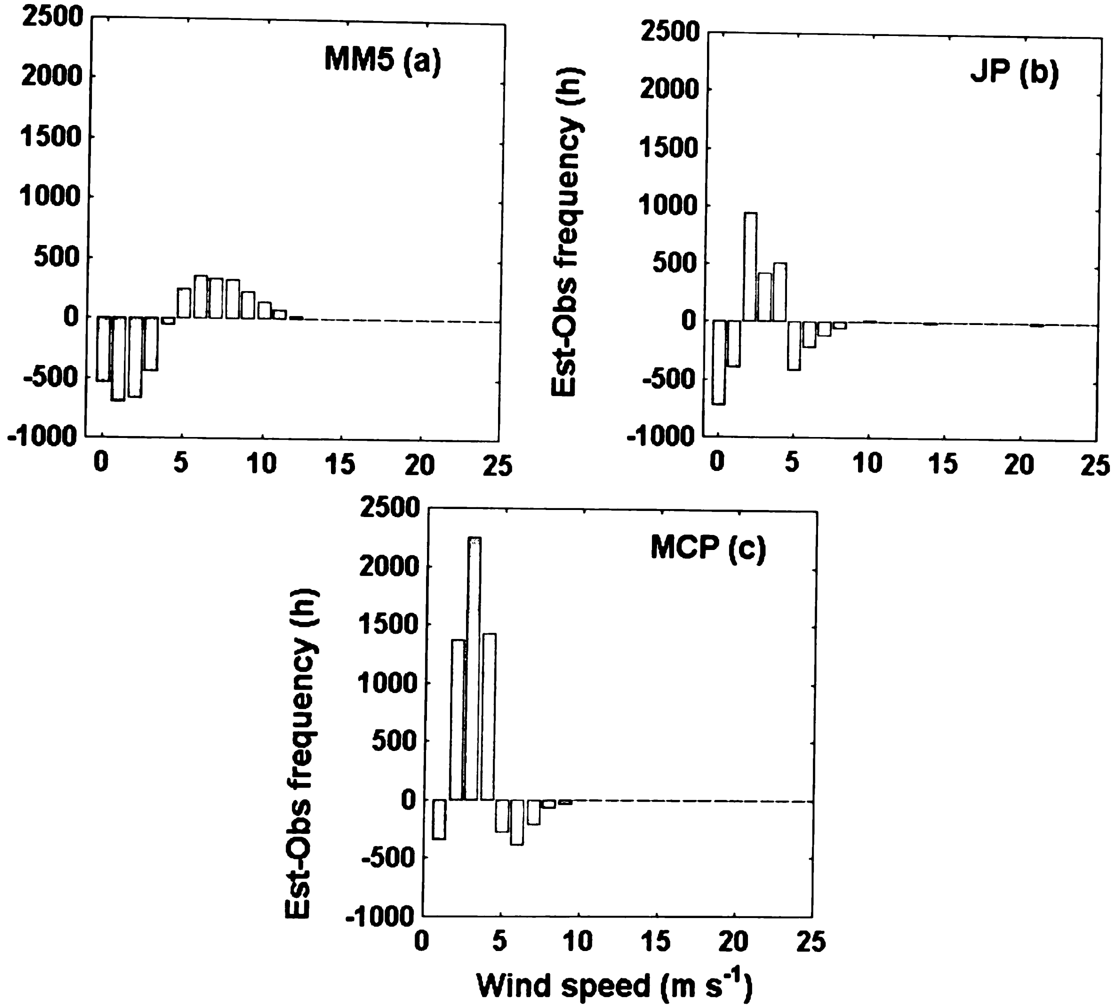

Figure 4.13 Wind speed frequency histogram differences (Estimated - Observed) for three wind models [(a) 36km/1 nearest neighbor FSMM5, (b) joint probabilistic, and (c) measure-correlate-predict] at Chapleau Airport, Ontario (CYLD) for the period 11/02 to 6/04.

This assessment of systematic bias is further supported by the percentage of systematic bias reported in Table 4.8. At CYLD, the FSMM5 model bias was approximately 22% systematic, compared to 11 and 12% for the joint probabilistic and MCP models respectively. Thus, while all three models appear to perform with similar accuracy, which in itself is remarkable, especially for the statistical models given the great distance between CYLD and its neighbors, a correction of the bias in the FSMM5 model may in fact result in a substantial improvement of the model's performance. Additionally, given the lower unsystematic bias of FSMM5, it could be expected that an adjusted model would outperform the two statistical models.

4.3 Accounting for spatial bias in FSMM5

A final goal of this research was to establish whether or not any of the resource estimation bias inherent to the FSMM5 model could be reduced. Given the aforementioned low levels of systematic bias, it is unlikely that a significant improvement could be made. However, with the small differences in model performance, it is possible that a reduction in FSMM5's systematic error could in fact result in its outperforming the statistical models. To that end, the resource estimates of the FSMM5 model (the estimated frequency distributions, Weibull shape and scale) were subjected to a multiple regression that took into account two factors that would appear to exert some influence on the model's estimates. The first is geographic location. Trend surface analyses of the residuals of the model estimates indicated a distinct relationship with both Longitude and Latitude. The second factor is terrain. Although FSMM5 contains a high resolution digital terrain model as part of its base information, it is possible that the processes associated with various terrain types have not all been properly specified. As such, certain types of terrain might be associated with higher errors than others. To examine this possibility, a terrain complexity index (*TCI*) was created for each station location (Figure 4.14). This index was calculated as the standard deviation of the elevations at the 16 grid nodes in the FSMM5 12 km domain nearest to a station location (Figure 4.15).

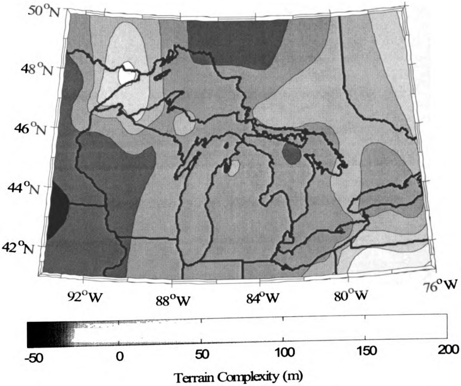

Figure 4.14 Terrain Complexity Index (TCI) obtained for the study area by calculating the standard deviation of elevation of the 16 grid points (12-km MM5 domain) surrounding each station location.

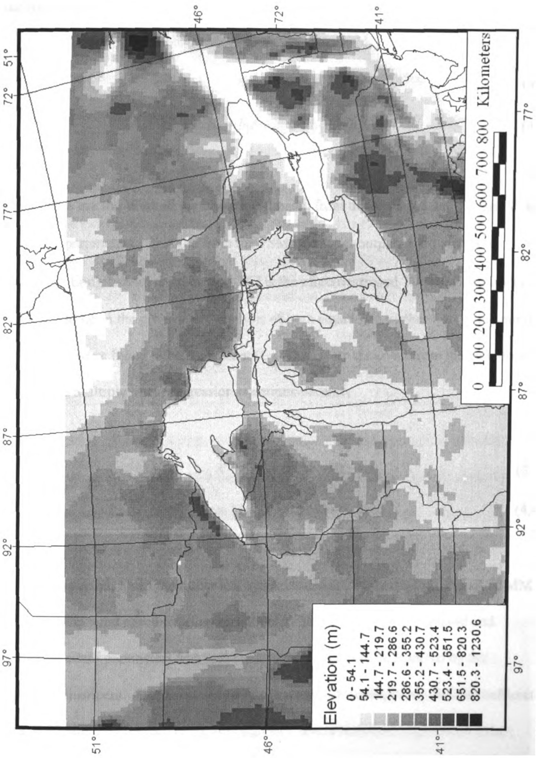

Figure 4.15 Surface elevation of the area encompassing the study region, from the 12-km domain of FSMM5.

Initial multiple linear regressions took the forms,

$$k = b_0 + b_1\hat{k} + b_2\phi + b_3\lambda + b_4TCI \tag{4.1}$$

$$c = b_0 + b_1\hat{c} + b_2\phi + b_3\lambda + b_4TCI \tag{4.2}$$

where *k* and *c* are the Weibull parameters estimated from the observed data, $\hat{k}$ and $\hat{c}$ are the Weibull parameters estimated from the FSMM5 model output, ϕ is Latitude in degrees, λ is Longitude in degrees, and *TCI* is the aforementioned Terrain Complexity Factor. Based upon the preliminary analysis of both equations, neither Longitude nor the *TCI* variables were found to be significant ($t_{2,0.9}$) and were removed from the equations. The resulting multiple linear regression equations became,

$$k = 4.55 - 0.11\hat{k} - 0.054\phi \tag{4.3}$$

$$c = 11.128 + 0.185\hat{c} - 0.169\phi \tag{4.4}$$

As expected, given the rather low systematic bias inherent in the original FSMM5 estimates of the wind speed distributions, much of the error between observed and estimated Weibull parameters was unsystematic and could not be resolved by the regression adjustment. This is borne out by the rather low multiple correlation coefficient values (0.27 and 0.35 respectively), although an F test reveals both regressions to be significant at the 0.01 level. Thus, Equations 4.3 and 4.4 were applied to the FSMM5 Weibull parameter estimates in an attempt to reduce the error between them and the observed parameters.

Indeed, the linear correction based upon Latitude generally improved the Weibull estimates across the region. For the shape (*k*) parameter an average 0.23 ms^{-1} *MAE* improvement over the original estimates was obtained at over 70% of the stations. Results were similar for the scale (*c*) parameter. An average *MAE* improvement of 0.46 m s^{-1} at 67% of the stations. In both shape and scale, this represented a statistically significant overall improvement in estimative accuracy from the original FSMM5 estimates as defined by *MAE* ($t_{1,0.95}$). However, it still remained to be seen whether or not the correction represented a significant improvement in estimates relative to the other two models.

Prior to the regression correction, there were no significant differences ($t_{2,0.95}$) between the *MAE* of the estimated shape parameters of any of the models. After the regression correction was applied to the FSMM5 estimates, the *MAE* of the new FSMM5 estimates of *k* was significantly lower than the *MAE* from the MCP estimates. Furthermore, prior to the regression, the *MAE* associated with the scale estimates from FSMM5 was significantly higher than that of the joint probabilistic model ($t_{1,0.95}$). However, after the regression, there was no longer any statistically significant difference in the *MAE* associated with the scale estimates from any of the models ($t_{2,0.95}$). Thus, it appears that a simple multiple linear regression, as was conducted in this research is able to substantially improve the estimative accuracy of the FSMM5 model over the Great Lakes region in terms of wind resource estimation.

Chapter 5. Discussion

Since the advent of commercially viable wind energy conversion systems (*i.e.*, wind turbines), there has been a great interest in the accurate point source or areal estimation of wind resources. Early methods utilized climatological reduction approaches, while later methods tended to be based on probability and correlation methods. However, while many of these methods have been successfully applied under a variety of atmospheric and geographical conditions, the degree of their success largely remains dependent on the network of wind observation stations that may be employed. Because many of the processes that govern the wind at a particular location are local or quasi-local (*e.g.*, a few meters to a few kilometers), most operational anemometer networks are of a spatial resolution that is too coarse to resolve such sub-network characteristics or behavior. As a result, a coarse instrumental network (*e.g.*, on the order of tens to hundreds of kilometers between stations) may only capture the regional coherence and behavior of the wind field unless local conditions between stations exhibit a high level of correspondence.

Over the past several decades, there has therefore been growing interest in the use of methods that are capable of addressing the localized component of near-surface atmospheric motion. This need has led primarily toward the use of process-based numerical models. Such models seek to account for local influences by incorporating the known physical properties of turbulence and momentum fluxes within the boundary layer. When applied at a fine spatial scale, it is hoped that behavior at that scale can subsequently be resolved and included in estimates of the near-surface wind field. The incorporation of numerically-based localized boundary layer conditions into wind resource estimation models is not new. The WAsP system developed in Denmark has done so for several decades with success (Petersen *et al.*, 1988, Troen and Petersen, 1989).

One area of process-based modeling that has received increased attention is regional-scale climate models. RCMs occupy a middle scale between boundary layer models and coarser general circulation models. Such models operate on a scale and resolution that make them ideally suited to estimating the wind resource over a given area on the order of a few thousand kilometers at a resolution of use to wind farm developers (*e.g.*, < *10 km*). However, until recently, because of their complexity and computational needs, generating longer-term (*e.g.*, > 1 or 2 years) series of estimates for wind resource assessment has meant a large time commitment. As a result, RCMs have been used primarily as a short-term (*i.e.*, < 48-h) point forecasting tool, and substantial research has been carried out regarding the ability of RCMs to estimate wind speeds at discrete locations over a span of a few days (*e.g.*, Nielsen, 1998, Alexiadis *et al.*, 1999, Landberg, 2001, Sfestos, 2002). Unfortunately, using RCMs to estimate a region's wind climatology has been largely overlooked in favor of less complex stochastic approaches. It is this gap in the science of wind field estimation that this research has addressed.

As the resources needed to run RCMs become less expensive and the models are more easily deployed, it has become apparent that such models may be able to provide accurate estimation of the general wind resource over a region, especially those regions that lack a dense network of observational locations. Such use has substantial implications for the accurate selection of optimal locations for future wind farm development. Unfortunately, until now the utilization of an RCM in this manner has received limited attention despite its potential benefit. Thus, it was not known how accurately an RCM might reproduce the wind field over a region of diverse geography. That was the goal of this research.

5.1 Summary of Research

The primary objective in this study was an assessment of the performance of the MM5 mesoscale numerical model over the Great Lakes region of North America, implemented and run by the U.S. Forest Service North Central Research Station. In this study, the gridded wind vector estimates from three model domain resolutions were utilized (36 km, 12 km and 4 km). These gridded wind estimates were used to estimate the wind speed and direction at the geographic coordinates of 113 automated wind sensors throughout the region using five interpolation schemes. The first utilized the grid value nearest the station as the estimate. The second and third estimated the wind at the location from the nearest four grid points using an unweighted and inverse distance weighted average respectively. The fourth used an unweighted average of the nearest 16 grid point estimates, and the fifth obtained the unweighted average of the surrounding 36 grid point estimates.

Based upon these 15 model variants (domain + interpolation scheme), estimates of the distribution of wind speeds at each of the anemometer locations were generated and compared to the distributions of the observed winds at these locations. It was determined that the 36 km resolution model domain was most adroit at reproducing the wind distributions at the stations in the study region. Furthermore, of the 5 grid-to-point estimation techniques, the nearest neighboring grid point option proved to be the most reliable estimator.

Additionally, while the FSMM5 model did perform well in reproducing the general wind resource over the region, it was important to compare its performance with more established and widely used wind resource estimation models. Three models were selected for comparative evaluation, two stochastic and one probabilistic. The stochastic models were a traditional measure-correlate-predict model (Derrick, 1992) and a Krige model (Haslett and Raftery, 1989, Davis, 1986). A joint probabilistic model (Garcia-Rojo, 2004) rounded out the three as the probabilistic selection.

Both the measure-correlate-predict (MCP) and the joint probabilistic (JP) models provided excellent results. From a forecasting standpoint it was determined that either of these two statistical approaches easily outperformed the FSMM5 model. But, from a resource estimation standpoint, all three models (FSMM5, MCP, and JP) performed more-or-less equally well. In one aspect, however, the FSMM5 model held promise. A substantially greater proportion of its model bias was found to be systematic, allowing for

a potential improvement of estimated wind resource over the region. To that end, a multiple linear regression model was applied to the FSMM5 model estimates. Based on earlier trend surface analysis, it was determined that geographic position could account for some of the systematic bias. Initially it also was felt that the complexity of terrain might be a systematic issue, however, that variable proved insignificant in the regressions and was omitted. With the final version of the multiple linear regression, estimates of the Weibull distribution parameters were adjusted solely as a function of Latitude.

The regression correction improved a majority of the FSMM5 estimates over the region to the point that in many instances, they exceeded the accuracy of those produced by the statistical models. However, while the improvements in the FSMM5 estimates were in many cases quite substantial, and represented a statistically significant improvement over the original estimates, they were not significantly better than the estimates produced by either of the statistical models.

5.2 Conclusions and Discussion

Several conclusions were reached as the result of this research. The primary conclusion is that while FSMM5 was able to adequately reproduce wind speed frequency distributions at most stations across the study region, it was not able to significantly outperform the more readily implemented statistical models, even at locations that were remote from their nearest neighbors in the anemometer network. While its use might be justified in regions where the observational data is considered to be of suspect quality or the network of wind sensors is deemed too sparse, if a sufficient network of quality observations exists in a region, the use of a RCM at this point in time represents perhaps an unnecessary addition of model complexity and resource utilization.

What this research suggests, however is that a numerical model approach to regional wind resource estimation does hold some promise, particularly in areas where few data exist and neighboring stations are distant (*e.g.*, over water). Although most of the bias encountered in the estimates of the wind distributions was unsystematic in nature, there was sufficient systematic bias to permit a simple linear model to improve those estimates. It is likely that the improvement based solely on geographic position is indicative of a spatial bias that is inherent to the model itself. One possibility is that as the grid points become longitudinally condensed with increasing latitude, the parameterizations that utilize the underlying terrain and land cover characteristics may experience a degradation of spatial accuracy. This issue has a number of associated aspects. One factor is the possible failure of the model to address the corresponding decrease in grid area with increasing Latitude relative to its non-atmospheric components. As a result, the terrain and land cover inputs may be systematically altered in space relative to the grid and may no longer be fully appropriate to the grid cell being modeled. Thus, momentum calculations within cells and transfers between grid cells may be inappropriately specified. Secondly, it is possible that the terrain and land use model projections differed slightly from that used to specify the model domain. If these data sets were subject to a projection calculation other than that which was applied to the model grid, the geographic coordinates (*i.e.*, Latitude and Longitude) would not match and substantial spatial bias, increasing with Latitude, would result. Both of the aforementioned issues are inherent to the model development and implementation itself, and thus were beyond the scope of this research. While it is possible that these issues have already been addressed by the model's developers, they would merit a closer examination as part of subsequent research.

An additional possibility behind the poor performance of the model at many locations is that there may be some misspecification in the surface parameterizations of the model. However, if this is the case, one would expect decreasing performance with increasing surface complexity in terms of terrain and land cover. Thus, the most accurate parameterizations should be expected over homogeneous terrain (*e.g.*, open water or flat grassland). Unfortunately, it did not appear that model estimates at locations of greater surface homogeneity consistently outperformed those at more heterogeneous sites. This is borne out by the insignificance of terrain complexity as a factor in the model correction algorithms. In order to more appropriately address this issue, future research might seek to classify each of the anemometer sites according to surface characteristics beyond simple terrain complexity and readdress this issue. Furthermore, as FSMM5 utilizes roughness look-up tables to determine surface roughness, a baseline assessment of model performance might be conducted using only those estimates produced for grid points over water where surface roughness is lowest according to the tables. These estimates could be compared against observed buoy data. If the model performs similarly, it is not likely that the surface parameterizations are to blame. However, substantial model improvement might suggest that more complex terrain may be incorrectly parameterized in the model. It is interesting to note that a recent independent analysis of FSMM5 wind forecasts over the Great Lakes region, though not focused on the evaluation of near surface winds *per se*, achieved bias statistics that were of similar magnitude to those calculated in this research and presented in Table 4.1 (Zhong *et al.*, 2005). This leads this researcher to believe that the bias is most likely a function of model misspecification, rather than of the observed data against which the model estimates were evaluated.

A tertiary conclusion concerns the spatial resolution and spatial aggregation of the FSMM5 model. Over the Great Lakes, the coarsest model domain (36 km) consistently produced the most accurate estimates of the wind resource. Interestingly, the 12 km (intermediate) resolution domain consistently produced the worst estimates. Additionally, the improved performance of the 4 km over the 12 km domain may actually be an artifact of the nesting of the former in the later and therefore the distribution of the spatial bias of the 12 km grid into smaller proportions on the 4 km grid. In the locations where the higher resolution domains did outperform the coarser resolutions, the differences were not statistically significant. This issue may be related to many of the same issues already mentioned regarding spatial or surface misspecifications. Thus, based on these results, an increase in horizontal resolution of the FSMM5 model cannot be justified in the modeling of near-surface wind distributions over the Great Lakes, especially given the exponential increase in computing resources necessary to produce estimates at the finer resolution domains.

Furthermore, the increased accuracy with increasing aggregation parsimony was of note. The use of a single nearest neighbor grid point proved a far more robust estimator than using averages from the surrounding $n > 1$ grid points. This speaks to the similarity of conditions over short distances throughout the region and that as more distant grid cells are included in the averaging, that similarity is noticeably degraded. It is therefore concluded that, at least over the Great Lakes region, the grid point nearest to a location is the best estimator of the winds at that location.

A fourth conclusion is again related to the primary conclusion in that a substantial portion of overall FSMM5 estimate bias is systematic. Much of this bias was reduced when a corrective measure was applied. Thus it is also concluded that the model estimates can be improved by a suitable model output statistics scheme, and that such a scheme is necessary for the most accurate estimation of the wind resource over a region. This conclusion is supported by numerous previous works (*e.g.*, Frank and Landberg, 1997, Petersen *et al.*, 1998b) that did not use RCM estimates of wind speed directly, but rather employed them as initial input to some form of stochastic adjustment procedure (*e.g.*, WAsP, MOS, downscaling) in order to produce satisfactory local-area wind estimates.

Lastly, although it was not a stated purpose of this research, the performance of either the measure-correlate-predict model or the joint probabilistic model was such that this research recommends either of these approaches for future estimation of the wind resources over the Great Lakes region. As has been demonstrated, the region has a relatively dense network of automated wind sensors that are collecting data of acceptable quality. Also, the wind field appears to be such that robust correlations in wind speeds and their probability distributions can be readily obtained. Thus, at least over this region, the increased complexity of a numerical climate model is not warranted at this time.

5.3 Future Directions

This research, while extensive, has only begun to address some of the issues of wind resource estimation accuracy regarding numerical models of the atmosphere. As of this writing, FSMM5 is being phased out in favor of the next generation Weather Research and Forecasting (WRF) model (Michalakes *et al.*, 2004). This new model corrects a number of issues that were present in earlier models such as FSMM5 (a discussion of which can be found in Michalakes *et al.*, 2004). It is possible that WRF has accounted for much of the systematic bias that existed in the FSMM5 wind fields and may produce more accurate wind resource estimates (although it should be noted that WRF uses the same boundary layer look-up tables as MM5). A potential direction of future research is therefore to evaluate the wind resource estimates of WRF at various resolutions relative to the estimates produced by FSMM5. If such research is performed for the same locations using the same initial conditions to produce wind speed estimates for the same period of time, the differences between FSMM5 and WRF can be compared. Changes in boundary-layer flow parameterizations can then be assessed for sensitivity and robustness as a function of the differences between WRF and FSMM5 estimates.

Additionally, while wind farm developers in the Great Lakes region are focused on land-based wind farms, it is likely that offshore developments may be explored in the future. Such developments are already operational in the offshore waters of Europe and are being planned for New England coastal waters in the US. Given the relative lack of wind observations over the Great Lakes themselves, a regional scale numerical model may produce superior estimates of the wind resource over these water regions relative to observation-based models such as MCP or JP. While this research has evaluated the wind resources at wind sensor locations on several islands in the lakes, subsequent research should evaluate the estimative ability of an RCM over open water through comparisons with buoy data. In addition to validating the RCM over open water, such research would be able to address variations in model error as a function of surface parameterizations.

Lastly, the primary goal of using an RCM for wind resource estimation is to produce a reliable estimate of the wind resource on a continuous fine-scale surface over a region such that suitable wind farm locations can be identified. Therefore, it remains to be seen whether such a surface can successfully be developed and incorporated as an automated decision-making criterion into a geographic information system (GIS). To that end, additional research is necessary to better understand the possible inter-grid point behavior of the wind field at whatever domain resolution is chosen. It is then imperative to develop a method of assessing model confidence over the region such that the wind resource estimate can be appropriately weighted in the decision making process.

In conclusion, this research has accomplished its stated goals in that it has evaluated the performance of FSMM5 over the study region with respect to the model's ability to estimate the regional wind climatology at various spatial resolutions. It identified that a coarser resolution domain was better able to estimate the wind resource and concluded that important systematic bias was present at all spatial resolutions, but that such bias could be accounted for. Finally, the research determined that in its present implementation, the FSMM5 model did not present a significant performance improvement for estimates of the wind resource at ASOS locations across the Great Lakes region compared with established statistical models. However, the FSMM5 model did perform satisfactorily in some respects over the region and therefore may be useful in the estimation of wind resources over more poorly instrumented portions of the Great Lakes (*e.g.*, offshore). As improvements are made in the parameterizations and specifications of regional-scale numerical models (*e.g.*, WRF), model resource estimations are likely to improve, perhaps to the point of outperforming established stochastic methods. Additionally, it is possible that the use of a sophisticated post-model corrective procedure (*e.g.*, WAsP) could substantially improve the estimates from FSMM5 or other RCMs over the region. Therefore, while the research cannot at present recommend the use of an RCM as a stand-alone tool for wind resource estimation over the Great Lakes region, that conclusion could easily change as newer RCMs are evaluated.

Appendix A. Automated Reporting Stations Used

Please note, this appendix consists primarily of information in a tabular format, and is therefore listed as "Appendix A" in the list of tables near the beginning of this document.

	Station ID*	State/ Prov	Station Name	Latitude (deg. N)	Longitude (deg. W)	Agency **	Type ***
1	KADG	MI	ADRIAN	41.867	84.083	FAA	ASOS
2	KAMN	MI	ALMA	43.317	84.683	NF	AWOS
3	KAPN	MI	ALPENA	45.067	83.567	NWS	ASOS
4	KARB	MI	ANN ARBOR	42.217	83.733	FAA	ASOS
5	KBAX	MI	BAD AXE	43.783	82.983	NF	AWOS
6	KBTL	MI	BATTLE CREEK	42.317	85.233	FAA	ASOS
7	KACB	MI	BELLAIRE	44.983	85.200	FAA	AWOS
8	KSJX	MI	BEAVER ISLAND	45.700	85.567	NF	AWOS
9	KBEH	MI	BENTON HARBOR	42.133	86.417	FAA	ASOS
10	KRQB	MI	BIG RAPIDS	43.717	85.500	NF	AWOS
11	KCAD	MI	CADILLAC/WEXFORD	44.267	85.417	NF	AWOS
12	KCVX	MI	CHARLEVOIX	45.300	85.267	NF	AWOS
13	KFPK	MI	CHARLOTTE	42.567	84.817	NF	AWOS
14	KSLH	MI	CHEBOYGAN	45.650	84.517	NF	AWOS
15	KCIU	MI	CHIPPEWA INTL	46.250	84.467	FAA	AWOS
16	KOEB	MI	COLDWATER	41.917	85.033	NF	AWOS
17	KP59	MI	COPPER HARBOR	47.467	87.883	NWS	AWOS
18	KDET	MI	DETROIT/CITY AIR	42.400	83.017	FAA	ASOS
19	KYIP	MI	DETROIT/WILLOW	42.233	83.533	FAA	ASOS
20	KDTW	MI	DETROIT/WAYNE	42.233	83.333	NWS	ASOS
21	KONZ	MI	DETROIT/GROSSE ISLE	42.100	83.150	NF	AWOS
22	KESC	MI	ESCANABA	45.750	87.017	FAA	AWOS
23	KFNT	MI	FLINT	42.967	83.750	NWS	ASOS
24	KGLR	MI	GAYLORD	45.017	84.683	FAA	ASOS
25	KGRR	MI	GRAND RAPIDS	42.883	85.517	NWS	ASOS
26	KGOV	MI	GRAYLING AFB	44.683	84.733	DOD	AWOS
27	KSAW	MI	GWINN/SAWYER AFB	46.350	87.400	FAA	AWOS
28	KCMX	MI	HANCOCK	47.167	88.483	FAA	ASOS
29	KMGN	MI	HARBOR SPRINGS	45.433	84.917	NF	AWOS
30	KJYM	MI	HILLSDALE	41.917	84.583	NF	AWOS
31	KBIV	MI	HOLLAND	42.750	86.100	FAA	ASOS
32	KHTL	MI	HOUGHTON LAKE	44.350	84.667	NWS	ASOS
33	KOZW	MI	HOWELL	42.617	83.967	NF	AWOS
34	KIMT	MI	IRON MOUNTAIN	45.817	88.117	FAA	ASOS
35	KIWD	MI	IRONWOOD	46.517	90.117	FAA	AWOS
36	KJXN	MI	JACKSON/REYNOLDS	42.267	84.467	FAA	ASOS
37	KAZO	MI	KALAMAZOO	42.233	85.550	FAA	ASOS
38	KDUH	MI	LAMBERTVILLE	41.733	83.650	NF	AWOS
39	KLAN	MI	LANSING	42.783	84.583	NWS	ASOS
40	KLDM	MI	LUDINGTON/MASON	43.967	86.400	NF	AWOS
41	KMCD	MI	MACKINAC ISLAND	45.850	84.633	NF	AWOS
42	KMBL	MI	MANISTEE	44.267	86.250	FAA	AWOS
43	KISQ	MI	MANISTIQUE	45.967	86.167	NF	AWOS

44	KRMY	MI	MARSHALL	42.233	84.950	NF	AWOS
45	KTEW	MI	MASON	42.567	84.417	NF	AWOS
46	KMNM	MI	MENOMINEE	45.117	87.617	FAA	AWOS
47	KTTF	MI	MONROE	41.933	83.417	NF	AWOS
48	KMOP	MI	MOUNT PLEASANT	43.617	84.733	NF	AWOS
49	KMKG	MI	MUSKEGON	43.167	86.233	NWS	ASOS
50	KERY	MI	NEWBERRY	46.300	85.450	NF	AWOS
51	KOSC	MI	OSCODA/WURTSMITH	44.450	83.400	NF	AWOS
52	KPLN	MI	PELLSTON	45.567	84.800	FAA	ASOS
53	KPTK	MI	PONTIAC	42.667	83.417	FAA	ASOS
54	KP58	MI	PORT HOPE	44.017	82.800	NWS	AWOS
55	KPHN	MI	PORT HURON	42.917	82.517	NF	AWOS
56	KMBS	MI	SAGINAW	43.533	84.083	FAA	ASOS
57	KHYX	MI	SAGINAW/BROWNE	43.433	83.867	NF	AWOS
58	KANJ	MI	SAULT STE MARIE	46.467	84.367	NWS	ASOS
59	KMTC	MI	SELFRIDGE ANGB	42.617	82.817	DOD	AWOS
60	KIRS	MI	STURGIS/KIRSCH	41.800	85.433	NF	AWOS
61	KTVC	MI	TRAVERSE CITY	44.733	85.567	FAA	ASOS
62	KCGX*	IL	CHICAGO/MEIGS	41.867	87.583	FAA	ASOS
63	KPWK	IL	PALWAUKEE	42.117	87.900	FAA	ASOS
64	KUGN	IL	WAUKEGAN	42.417	87.867	FAA	ASOS
65	KGYY	IN	GARY REGIONAL	41.617	87.417	FAA	AWOS
66	KGSH	IN	GOSHEN	41.533	85.783	FAA	ASOS
67	KSBN	IN	SOUTH BEND	41.700	86.317	NWS	ASOS
68	KDLH	MN	DULUTH	46.850	92.200	NWS	ASOS
69	KEVM	MN	EVELETH MUNI	47.383	92.500	NF	AWOS
70	KGNA	MN	GRAND MARAIS	47.750	90.350	NWS	AWOS
71	KCKC	MN	GRAND MARAIS	47.833	90.367	NF	AWOS
72	KINL	MN	INTERNTNL FALLS	48.567	93.400	NWS	ASOS
73	KMZH	MN	MOOSE LAKE	46.417	92.800	NF	AWOS
74	KTWM	MN	TWO HARBORS	47.033	91.750	NF	AWOS
75	KBUF	NY	BUFFALO/CHEEKTOW	42.933	78.733	NWS	ASOS
76	KDKK	NY	DUNKIRK	42.500	79.283	FAA	ASOS
77	KFZY	NY	FULTON	43.350	76.383	FAA	ASOS
78	KIAG	NY	NIAGARA FALLS	43.117	78.933	FAA	ASOS
79	KROC	NY	ROCHESTER	43.117	77.683	NWS	ASOS
80	KSYR	NY	SYRACUSE	43.117	76.100	NWS	ASOS
81	KART	NY	WATERTOWN	43.983	76.033	FAA	ASOS
82	KHZY	OH	ASHTABULA	41.783	80.700	FAA	ASOS
83	KBKL	OH	CLEVELAND	41.533	81.667	FAA	ASOS
84	KCLE	OH	CLEVELAND	41.417	81.850	NWS	ASOS
85	KLPR	OH	LORAIN/ELYRIA	41.350	82.183	FAA	ASOS
86	KTDZ	OH	TOLEDO	41.567	83.483	FAA	ASOS
87	KTOL	OH	TOLEDO	41.583	83.800	NWS	ASOS
88	KERI	PA	ERIE	42.083	80.183	NWS	ASOS
89	KASX	WI	ASHLAND	46.550	90.917	FAA	ASOS
90	KGRB	WI	GREEN BAY	44.483	88.133	NWS	ASOS
91	KDYT	WI	DULUTH SKY HARBOR	46.717	92.033	NF	ASOS
92	KEGV	WI	EAGLE RIVER	45.917	89.267	NF	AWOS
93	KENW	WI	KENOSHA	42.600	87.933	FAA	ASOS
94	KMTW	WI	MANITOWOC MUNI	44.117	87.667	FAA	AWOS
95	KMKE	WI	MILWAUKEE	42.950	87.900	NWS	ASOS
96	KRAC	WI	RACINE	42.767	87.817	FAA	ASOS

97	KSBM	WI	SHEBOYGAN	43.783	87.850	FAA	ASOS
98	KSUE	WI	STURGEON BAY	44.850	87.417	FAA	AWOS
99	KSUW	WI	SUPERIOR	46.400	92.050	NF	AWOS
100	KETB	WI	WEST BEND	43.417	88.133	FAA	AWOS
101	CWCI*	ON	CARIBOU ISLAND	47.317	85.817	MSC	AWOS
102	CYLD	ON	CHAPLEAU ARPT	47.817	83.333	MSC	CON
103	CWWX	ON	COVE ISLAND	45.317	81.717	MSC	CON
104	CYEL	ON	ELLIOT LAKE	46.350	82.567	PVT	PWS
105	CWGD	ON	GODERICH	43.767	81.717	MSC	AWOS
106	CYZE	ON	GORE BAY AIRPORT	45.867	82.567	MSC	AWOS
107	CYHM	ON	HAMILTON AIRPORT	43.167	79.933	MSC	CON
108	CYXU	ON	LONDON AIRPORT	43.017	81.150	MSC	AWOS
109	CWPS	ON	LONG POINT	42.567	80.033	MSC	CON
110	CYZR	ON	SARNIA AIRPORT	43.000	82.317	MSC	CON
111	CYAM	ON	SAULT STE MARIE	46.467	84.517	MSC	CON
112	CYQT	ON	THUNDER BAY	48.367	89.317	MSC	AWOS
113	CYYZ	ON	TORONTO/PEARSON	43.667	79.617	MSC	CON
114	CYKF	ON	WATERLOO WELL	43.467	80.367	MSC	AWOS
115	CYQG	ON	WINDSOR AIRPORT	42.267	82.967	MSC	CON

* The two grayed out stations (62 and 101) had insufficient data and although processed, were not used in this research.

** **Agency:** The entity, governmental or otherwise, responsible for the maintenance and/or dissemination of information gathered by the meteorological sensors deployed at the corresponding station.

FAA – Federal Aviation Administration (United States)
NWS – National Weather Service (United States)
DOD – Department of Defense (United States)
NF – Non-Federal entity; state, local or airport authority (United States)
MSC – Meteorological Services Canada (Canada)
PVT – Privately owned and operated (US and Canada)

*** **Type:** The type of sensor array deployed at the corresponding station.

ASOS – Automated Surface Observing System
AWOS – Automated Weather Observing System. A number of AWOS configurations exist, however, the wind sensor array in each performs to the same standards. Therefore no differentiation is made here (US and Canada).
CON – Contracted weather provider, station information unavailable (Canada).
PWS – Private Weather Station, station information unavailable (Canada).

Information on United States stations is derived from the following Internet resources:

Federal Aviation Administration ASOS Web page
(http://www.faa.gov/ASOS)
National Weather Service ASOS Operations and Monitoring Center
(http://www2.aomc.nws.noaa.gov/)

Information on Canadian stations is derived from the following Internet Resources:

US National Weather Service Aviation Digital Data Service
(http://adds.aviationweather.gov)

National Climate Data and Information Archive – Meteorological Services Canada - Environment Canada
(http://www.climate.weatheroffice.ec.gc.ca)

Observational data (METARs) were collected for each of the stations listed in the table by accessing the appropriate URL at US Weather, Inc. The URL for any given station can be obtained by placing the station identifier (e.g., KAPN) at the end of the following URL string:

http://www.uswx.com/us/stn/?code=c&n=1440&stn=

The preceding URL will retrieve the latest 1440 observations for that station in encoded format.

Appendix B. Raw METAR Report File

This appendix contains a sample of encoded METAR data via the U.S. Weather, Inc. Internet site. Data are from Lansing, MI (KLAN) covering the period 0055Z – 1355Z on 04 February, 2003. Wind data are marked in bold, and some remarks (RMK) not relevant to this research have been truncated for space.

METAR KLAN 040055Z **13007KT** 2SM -RA BR OVC003 03/03 A2925 RMK AO2 SLP911 P0004
SPECI KLAN 040119Z **VRB03KT** 3/4SM R28L/P6000FT -RA BR OVC003 03/03 A2924 RMK
METAR KLAN 040155Z **02004KT** 1/2SM R28L/2600V3500FT RA FG OVC003 03/02 A2921
METAR KLAN 040255Z **14005KT** 1/2SM R28L/P6000FT -DZ FG OVC003 04/04 A2918 RMK
SPECI KLAN 040338Z **16009KT** 1SM R28L/P6000FT -RA BR BKN003 BKN075 OVC100 06/06
METAR KLAN 040355Z **18010KT** 4SM BR BKN003 OVC070 07/07 A2910 RMK AO2
SPECI KLAN 040432Z **21012KT** 10SM BKN006 OVC010 08/07 A2910 RMK AO2 CIG 004V008
METAR KLAN 040455Z **23015KT** 3SM -RA BR OVC004 07/07 A2911 RMK AO2 RAB42 SLP864
SPECI KLAN 040516Z **22020G26KT** 1 3/4SM -RA BR BKN006 OVC010 06/06 A2913 RMK AO2 **PK WND 23027/0504** CIG 003V008 P0000
METAR KLAN 040555Z **23021G29KT** 10SM BKN010 OVC016 03/02 A2913 RMK AO2 **PK WND 25032/0538** RAE25 CIG 008V012 SLP871 P0000 60019 T00330017 10078 20028 55015
METAR KLAN 040655Z **24019G24KT** 10SM OVC010 02/00 A2914 RMK AO2 **PK WND 24033/0643** CIG 007V012 SLP875 T00170000
SPECI KLAN 040719Z **25024G32KT** 7SM -SN FEW008 BKN015 OVC022 01/M01 A2915 RMK AO2 **PK WND 25033/0707** RAB0657E10SNB10 P0000
METAR KLAN 040755Z **24016G24KT** 10SM UP BKN013 OVC020 01/M01 A2917 RMK AO2 **PK WND 25033/0707** RAB0657E10UPB21E24B50SNB10E21 SLP883 P0000 T00061011
SPECI KLAN 040813Z **25024G30KT** 10SM OVC015 01/M01 A2918 RMK AO2 **PK WND 25030/0810** UPE00 P0000
METAR KLAN 040855Z **25024G32KT** 10SM BKN017 OVC027 00/M02 A2919 RMK AO2 **PK WND 25032/0849** SLP893 P0000 60000 T00001022 53020
METAR KLAN 040955Z **28020G26KT** 10SM BKN020 OVC027 M01/M04 A2924 RMK AO2 **PK WND 27033/0927** SLP910 T10061039
SPECI KLAN 041018Z **27026G32KT** 10SM -SN SCT022 BKN030 OVC065 M02/M05 A2926 RMK AO2 **PK WND 28032/1017** UPB10E17SNB09E10B17 P0000
SPECI KLAN 041028Z **27024G33KT** 7SM -SN BKN022 BKN030 OVC047 M02/M06 A2927 RMK AO2 **PK WND 26033/1024** P0000
METAR KLAN 041055Z **26020G25KT** 1 3/4SM -SN BR BKN017 OVC023 M02/M04 A2928 RMK AO2 **PK WND 26033/1024** SLP924 P0000 T10221039
SPECI KLAN 041135Z **26018KT** 3SM -SN BKN017 OVC041 M02/M05 A2931 RMK AO2 **PK WND 26027/1103** P0000
METAR KLAN 041155Z **27017G23KT** 5SM -SN BR OVC017 M02/M04 A2932 RMK AO2 **PK WND 26027/1103** SLP938 P0000 60000 70023 T10221044 10033 21028 51044
METAR KLAN 041255Z **27018G24KT** 9SM -SN BKN021 OVC060 M02/M05 A2938 RMK AO2 **PK WND 28028/1226** SLP954 P0000 T10171050
METAR KLAN 041355Z **27018G27KT** 6SM -SN BLSN BKN020 OVC033 M01/M04 A2942 RMK AO2 **PK WND 27030/1343** SNE1257B17 SLP968 P0000 T10111044

Appendix C. Selected Statistics from ASOS Stations

Please note, this appendix consists entirely of information in tabular format, and is therefore listed as "Appendix C" in the list of tables near the beginning of this document.

	Station ID	Non-calm obs. (n) **	Mean ($m\ s^{-1}$) **	Std. Dev. ($m\ s^{-1}$) **	k ***	c ($m\ s^{-1}$) ***	Median A^2 ****	Avg. OSL ****
1	KADG	11168	4.14	2.03	1.84	3.81	1.319	0.052
2	KAMN	10499	3.75	2.09	1.57	3.24	1.577	0.054
3	KAPN	10736	4.03	1.81	2.03	3.91	1.141	0.071
4	KARB	10732	4.21	2.08	1.77	3.88	1.358	0.045
5	KBAX	10683	4.00	2.26	1.51	3.50	1.474	0.067
6	KBTL	12297	4.52	2.13	2.07	4.45	1.062	0.079
7	KACB	9097	2.88	1.53	1.43	2.38	1.962	0.038
8	KSJX	11407	4.08	2.07	1.75	3.86	1.215	0.082
9	KBEH	11036	4.57	2.21	1.58	4.20	1.467	0.051
10	KRQB	9625	3.47	1.95	1.42	3.02	1.480	0.061
11	KCAD	11132	3.83	2.04	1.74	3.45	1.479	0.065
12	KCVX	12005	4.12	2.33	1.63	3.91	1.059	0.100
13	KFPK	10777	3.56	1.95	1.47	3.10	1.583	0.058
14	KSLH	10857	3.64	2.13	1.41	3.21	1.330	0.072
15	KCIU	10108	4.18	2.28	1.57	3.90	1.215	0.074
16	KOEB	10678	3.76	2.14	1.44	3.34	1.410	0.064
17	KP59	10973	5.49	2.87	2.00	5.96	0.840	0.123
18	KDET	11309	4.22	1.90	2.16	4.26	1.012	0.092
19	KYIP	11325	4.65	2.27	1.83	4.82	0.921	0.094
20	KDTW	12096	4.53	2.26	1.85	4.76	0.880	0.103
21	KONZ	11183	3.78	2.00	1.64	3.60	1.154	0.084
22	KESC	11351	4.00	2.01	1.70	3.74	1.270	0.081
23	KFNT	11941	4.48	2.09	1.97	4.54	0.913	0.103
24	KGLR	9629	4.29	2.00	1.80	4.23	1.122	0.079
25	KGRR	12844	4.79	2.31	2.35	5.49	0.858	0.124
26	KGOV	9991	3.43	1.81	1.62	3.12	1.355	0.077
27	KSAW	10987	4.28	2.27	1.65	4.03	1.169	0.086
28	KCMX	11430	4.87	2.59	1.76	4.96	0.907	0.101
29	KMGN	10692	3.26	1.97	1.57	2.89	1.416	0.069
30	KJYM	10761	3.57	1.96	1.49	3.15	1.514	0.053
31	KBIV	12098	4.67	2.43	1.67	4.62	1.006	0.080
32	KHTL	11365	4.13	1.91	1.61	3.48	2.113	0.023
33	KOZW	10938	3.42	1.89	1.55	3.19	1.158	0.092
34	KIMT	10036	3.93	1.91	1.80	3.60	1.375	0.050
35	KIWD	10316	4.09	2.13	1.66	3.75	1.295	0.072
36	KJXN	10608	4.24	1.99	1.80	4.01	1.278	0.056
37	KAZO	11731	4.28	2.02	2.01	4.12	1.164	0.062
38	KDUH	10093	3.27	1.87	1.52	2.99	1.149	0.090
39	KLAN	12239	4.66	2.16	2.19	4.97	0.825	0.124
40	KLDM	11401	3.94	2.20	1.55	3.71	1.109	0.093
41	KMCD	9730	2.89	1.69	0.96	2.19	2.234	0.007
42	KMBL	11483	3.89	2.19	1.54	3.60	1.143	0.088
43	KISQ	11192	3.90	1.95	1.61	3.49	1.517	0.054
44	KRMY	9938	3.41	2.05	1.45	3.15	1.142	0.081
45	KTEW	10703	3.45	1.93	1.55	2.88	1.801	0.047

46	KMNM	10467	3.68	1.94	1.72	3.34	1.406	0.070
47	KTTF	10470	3.77	2.24	1.48	3.27	1.430	0.072
48	KMOP	10442	3.36	1.89	1.53	3.12	1.185	0.083
49	KMKG	12665	4.90	2.34	2.06	4.71	1.150	0.077
50	KERY	11335	3.68	1.96	1.54	3.24	1.485	0.061
51	KOSC	11074	4.07	2.28	1.53	3.84	1.071	0.095
52	KPLN	9832	4.52	2.24	1.64	4.26	1.215	0.064
53	KPTK	11503	4.41	2.07	1.96	4.71	0.872	0.107
54	KP58	9993	4.58	2.07	2.17	5.12	0.857	0.114
55	KPHN	10079	3.34	1.86	1.41	2.86	1.535	0.057
56	KMBS	12070	4.70	2.30	2.12	5.03	0.882	0.117
57	KHYX	11498	4.13	2.35	1.58	3.95	0.985	0.099
58	KANJ	11306	3.87	1.90	1.91	3.87	1.029	0.079
59	KMTC	9547	3.93	1.98	1.78	3.82	1.092	0.078
60	KIRS	10820	3.79	2.11	1.54	3.36	1.477	0.060
61	KTVC	9194	4.09	1.88	1.95	4.23	0.897	0.106
62	**KCGX***	2298	6.41	2.45	3.33	7.45	1.134	0.073
63	KPWK	10806	4.42	1.99	2.18	4.40	1.012	0.095
64	KUGN	11106	4.33	2.05	1.92	4.62	0.894	0.105
65	KGYY	7907	5.12	1.28	4.89	5.92	1.603	0.021
66	KGSH	11399	4.72	2.31	1.71	4.54	1.120	0.078
67	KSBN	11769	4.67	2.21	1.94	4.76	0.941	0.102
68	KDLH	12441	4.84	2.22	2.03	5.34	0.798	0.131
69	KEVM	10156	3.40	1.91	1.39	2.89	1.562	0.063
70	KGNA	8961	4.12	2.23	1.91	4.38	0.921	0.094
71	KCKC	11289	3.76	2.15	1.55	3.30	1.445	0.052
72	KINL	11507	4.06	1.85	2.05	3.85	1.273	0.058
73	KMZH	9920	3.20	1.73	1.47	2.68	1.831	0.051
74	KTWM	10693	3.24	1.99	1.30	2.85	1.261	0.065
75	KBUF	12252	4.79	2.43	1.89	5.11	0.805	0.121
76	KDKK	11171	4.75	2.39	1.77	4.80	0.943	0.103
77	KFZY	9793	4.05	2.13	1.68	3.98	1.026	0.079
78	KIAG	11452	4.97	2.60	1.89	4.97	0.945	0.101
79	KROC	11843	4.59	2.39	1.83	4.78	0.872	0.109
80	KSYR	11317	4.29	2.26	1.73	4.37	0.895	0.095
81	KART	10404	4.21	2.22	1.67	4.15	1.006	0.083
82	KHZY	10130	4.11	2.00	1.66	4.07	1.086	0.065
83	KBKL	11990	5.29	2.64	1.87	5.67	0.853	0.117
84	KCLE	12012	4.76	2.17	2.00	4.90	0.953	0.097
85	KLPR	11067	4.58	2.31	1.87	4.45	1.071	0.083
86	KTDZ	11452	4.56	2.31	1.74	4.52	1.010	0.078
87	KTOL	11132	4.58	2.32	1.88	4.46	1.054	0.087
88	KERI	11823	4.74	2.22	2.02	4.94	0.872	0.105
89	KASX	10674	3.99	1.99	1.72	3.63	1.386	0.050
90	KGRB	11787	4.48	2.12	1.86	4.41	0.961	0.085
91	KDYT	10865	4.38	2.77	1.43	3.91	1.220	0.089
92	KEGV	9643	3.27	1.79	1.45	2.76	1.637	0.059
93	KENW	12145	4.73	2.29	1.94	4.68	0.949	0.095
94	KMTW	10640	4.21	2.22	1.62	3.93	1.266	0.068
95	KMKE	12432	4.89	2.20	2.14	4.91	1.008	0.093
96	KRAC	12047	4.60	2.05	2.10	4.67	0.943	0.094
97	KSBM	11222	4.52	2.15	1.85	4.61	0.902	0.099
98	KSUE	11296	4.56	2.25	1.88	4.16	1.427	0.069

99	KSUW	10455	3.65	2.16	1.48	3.06	1.656	0.053
100	KETB	9439	3.89	2.10	1.58	3.31	1.809	0.052
101	**CWCI***	3953	7.39	3.77	1.85	7.48	0.925	0.109
102	CYLD	7901	3.35	1.82	1.26	2.56	2.391	0.018
103	CWWX	12038	5.60	3.24	1.74	5.81	0.867	0.119
104	CYEL	5660	3.17	1.70	1.38	2.48	2.255	0.024
105	CWGD	12291	4.91	2.71	1.45	5.30	0.878	0.106
106	CYZE	11690	4.50	2.46	1.53	3.80	1.702	0.044
107	CYHM	12422	4.39	2.60	1.53	4.04	1.139	0.078
108	CYXU	12411	4.22	2.35	1.61	4.37	0.839	0.128
109	CWPS	7627	7.16	3.85	2.00	7.37	0.932	0.104
110	CYZR	5974	5.04	2.65	1.75	4.73	1.241	0.080
111	CYAM	11253	3.82	2.02	1.53	3.44	1.314	0.057
112	CYQT	12075	3.64	2.22	1.75	3.54	1.050	0.086
113	CYYZ	12627	4.72	2.76	1.79	4.95	0.863	0.123
114	CYKF	11329	4.25	2.61	1.28	3.33	1.840	0.038
115	CYQG	12700	4.72	2.51	1.85	5.11	0.790	0.133

* Although statistics are displayed here, the two grayed out stations (62 and 101) were deemed to have insufficient data and were not used in this research.

** Non-calm Observations (n) are the number of observations at a station that exhibited a speed above zero. Mean0 is the mean wind speed (in m s-1) for all non-zero wind speed observations. Std. Dev. 0 is the standard deviation (in m s-1) nor all non-zero wind speed observations. These measures are reported here instead of measures based upon all valid observations (including calms) because at a number of stations, the airport is closed overnight and observations are suspended. Because nighttime represents a period where calm winds are common over the study region, 24-hour locations would experience a greater influence of calm winds in their average and standard deviation values. Therefore, to facilitate an equitable comparison of means and standard deviations, only those observations above zero meters per second (converted from knots) are utilized in these summary statistics.

*** Shape (k) and scale (c) parameters of the Weibull distribution were calculated for each station from all non-zero valid observations for the period of record (11/2002 - 6/2004) using the Ordinary Least Squares technique described by Rohatgi and Nelson (1994).

**** Median A^2 is the median value of the Anderson-Darling test statistic for small samples. This value was obtained from 1000 trials where samples of 100 wind speed values extracted from a station's full series with replacement were tested to see if they were obtained from the Weibull distribution specified by k and c (reported in the previous two columns). The median was used instead of the average, because the Anderson-Darling statistic has no upper bounds, and outlier values could exert undue influence. The average Observed Significance Level (Avg. OSL) is the average level of statistical significance from the 1000 trials. Where the OSL is smaller than a critical significance (or alpha) level (often 0.05) the null hypothesis that the data came from that particular Weibull distribution can be safely rejected (with 100 x (1-alpha) percent confidence). Unlike the test statistic itself, the OSL is bounded between 0 and 1 and thus is not likely to be unduly influenced by extreme outlier values. Therefore the average, rather than the median is shown. Based upon these OSL averages, wind speeds at locations in the study region can generally be well represented by a Weibull distribution. Of the 115 stations, only 10 rejected the Weibull distribution at 95% confidence, and only 1 rejected it at 99% confidence.

Appendix D. ASOS 10-m Wind Observations

The distribution of ASOS observed 10-m wind speeds at each station are displayed as a schematic (box and whiskers type) plot. As discussed in Chapter 3, the lower and upper bounds of the box are the lower and upper quartiles respectively. The median bisects the box, and the notch represents a robust estimate of the uncertainly about the median value for comparison with the other plots. The so-called whiskers extending from the box are the outer fences of the data, or 1.5 the interquartile range. Outliers are shown as points on the plot beyond the outer fences. ASOS observed 10-m wind directions are displayed as wind rose frequency histograms over the period of record indicated in Chapter 3.

Please note that the information in this appendix is in graphical tabular format, and is therefore listed as "Appendix D" in both the list of tables and list of figures near the beginning of this document.

Station	Schematic (box) plots of wind speed distribution
KADG	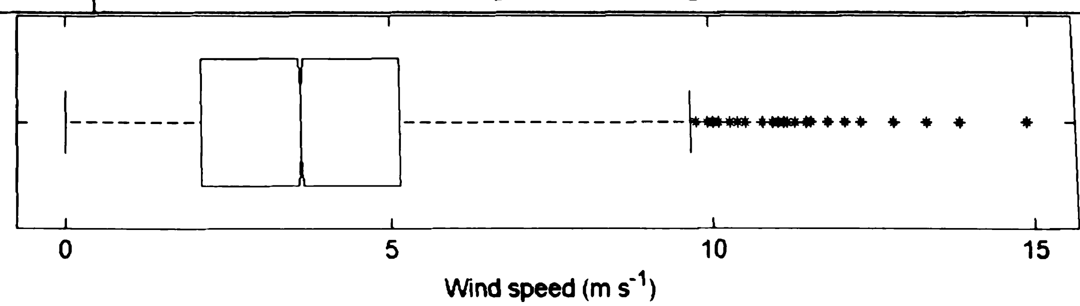
KAMN	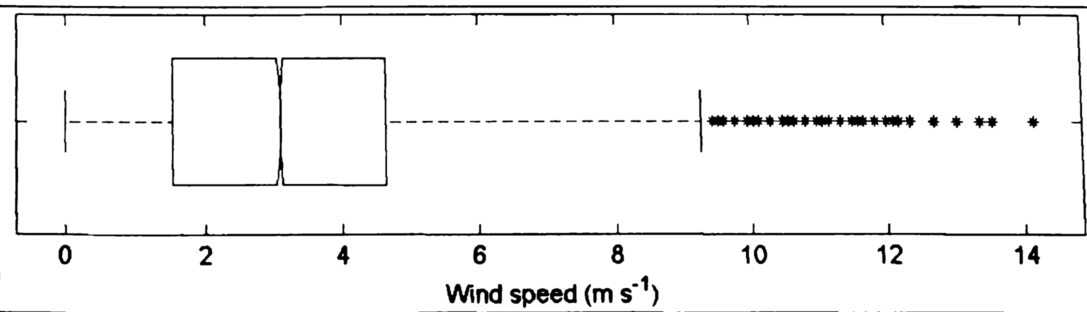
KAPN	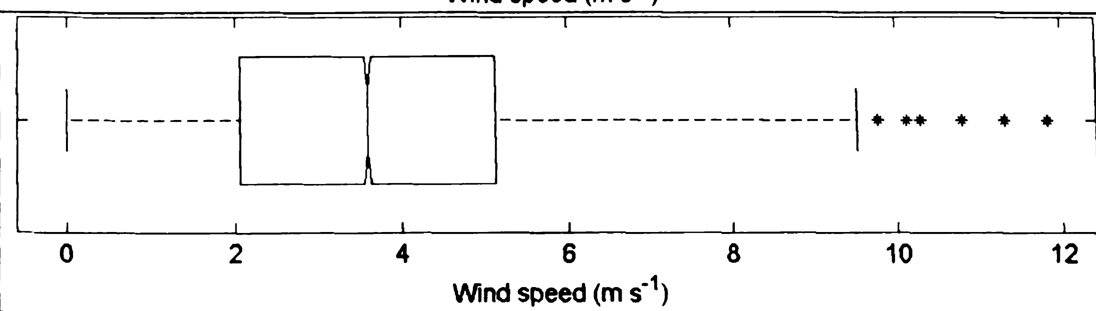

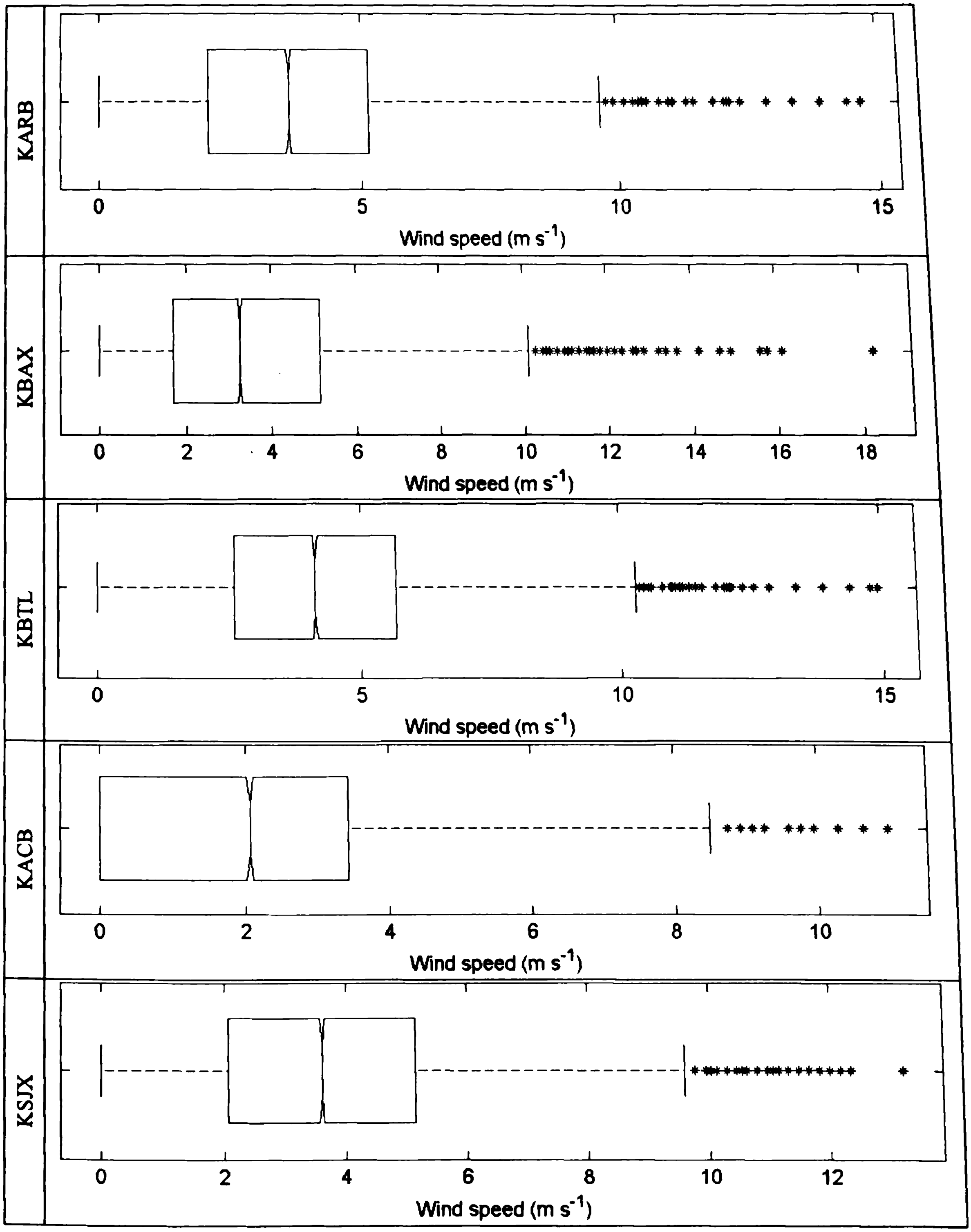
KARB
0
5
10
15
Wind speed (m s-1)
KBAX
0
2
4
6
8
10
12
14
16
18
Wind speed (m s-1)
KBTL
0
5
10
15
Wind speed (m s-1)
KACB
0
2
4
6
8
10
Wind speed (m s-1)
KSJX
0
2
4
6
8
10
12
Wind speed (m s-1)

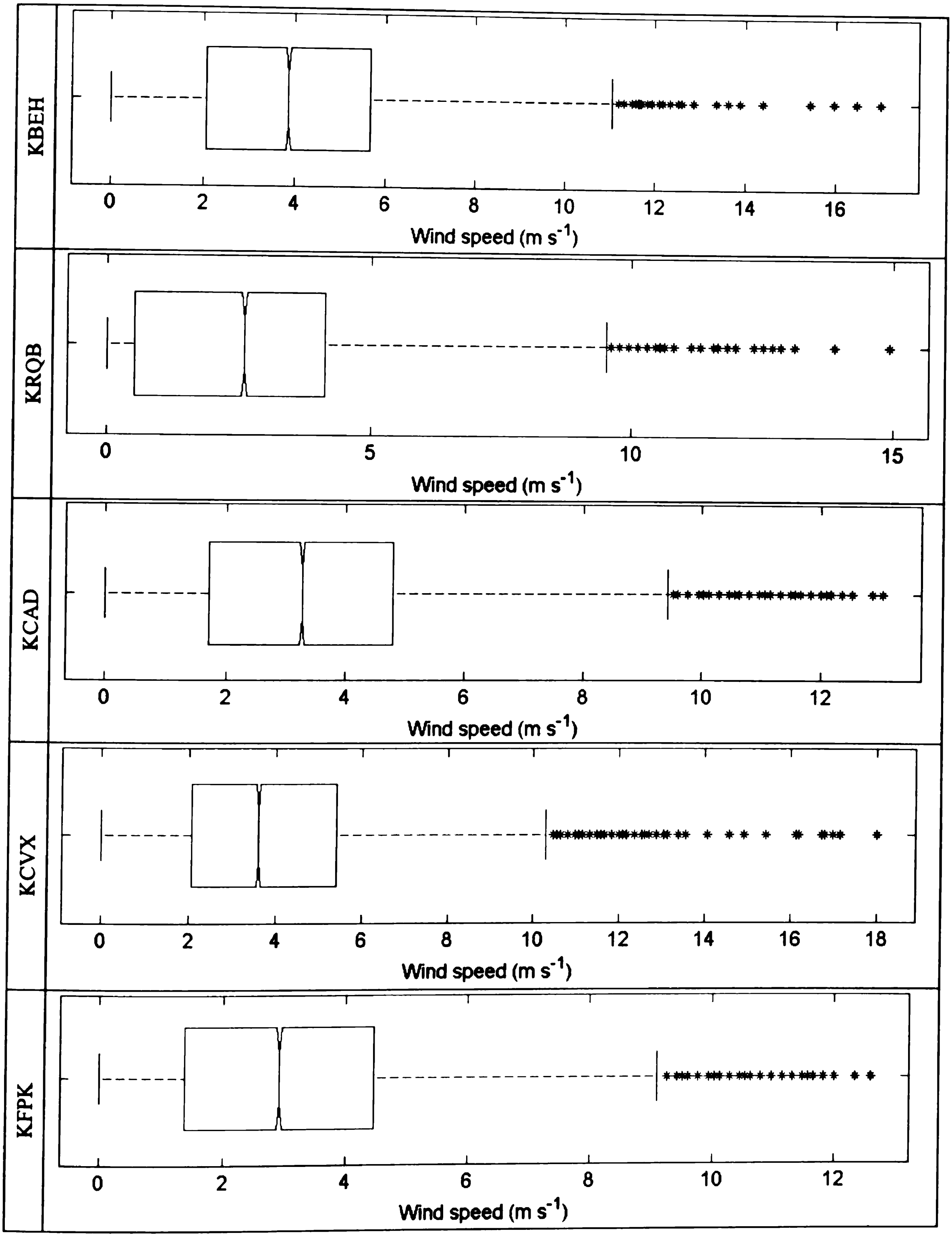
KBEH
0 2 4 6 8 10 12 14 16
Wind speed (m s-1)
KRQB
0 5 10 15
Wind speed (m s-1)
KCAD
0 2 4 6 8 10 12
Wind speed (m s-1)
KCVX
0 2 4 6 8 10 12 14 16 18
Wind speed (m s-1)
KFPK
0 2 4 6 8 10 12
Wind speed (m s-1)

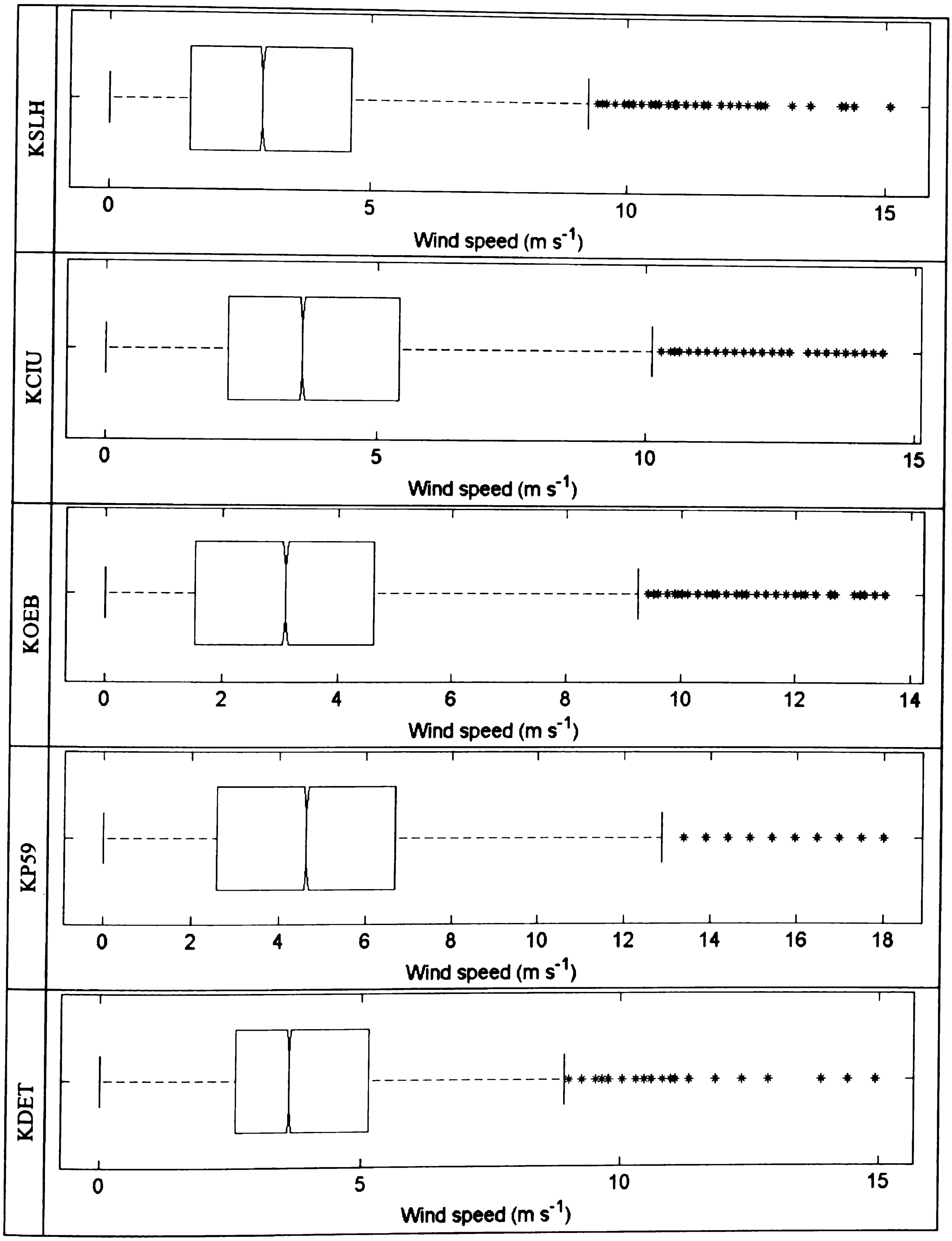
KSLH
0
5
10
15
Wind speed (m s-1)
KCIU
0
5
10
15
Wind speed (m s-1)
KOEB
0
2
4
6
8
10
12
14
Wind speed (m s-1)
KP59
0
2
4
6
8
10
12
14
16
18
Wind speed (m s-1)
KDET
0
5
10
15
Wind speed (m s-1)

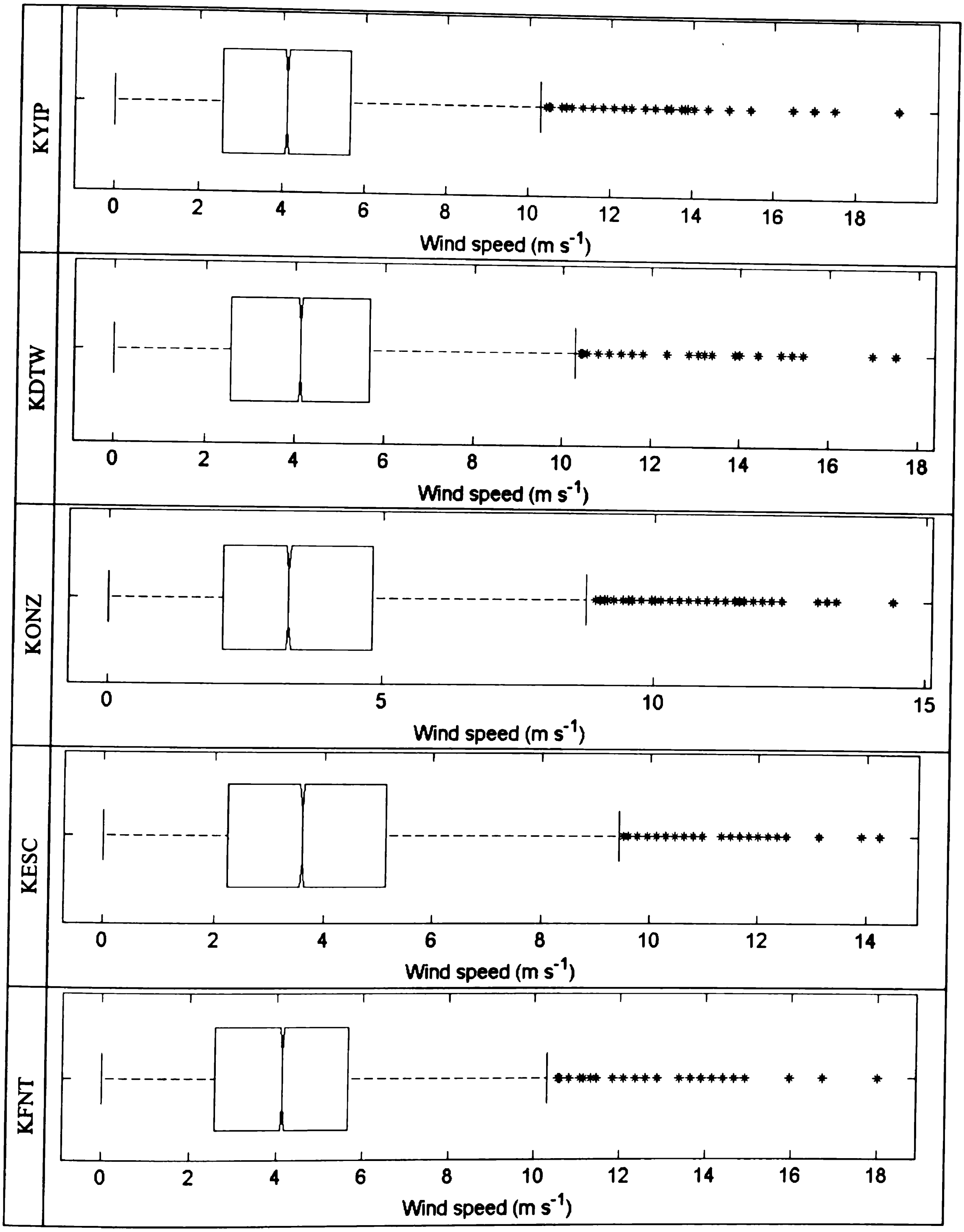
KYIP
0 2 4 6 8 10 12 14 16 18
Wind speed (m s-1)
KDTW
0 2 4 6 8 10 12 14 16 18
Wind speed (m s-1)
KONZ
0 5 10 15
Wind speed (m s-1)
KESC
0 2 4 6 8 10 12 14
Wind speed (m s-1)
KFNT
0 2 4 6 8 10 12 14 16 18
Wind speed (m s-1)

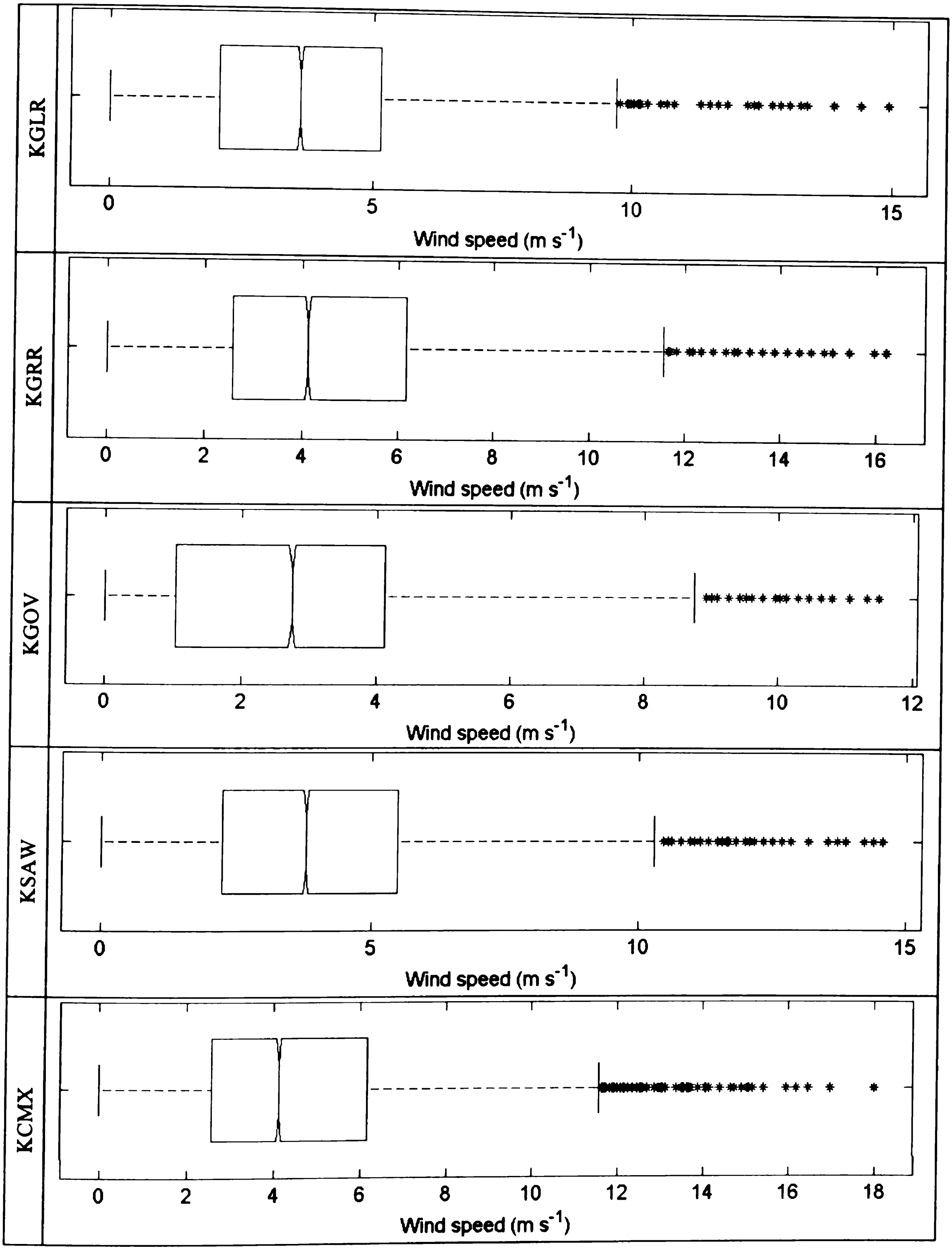
KGLR
0
5
10
15
Wind speed (m s-1)
KGRR
0
2
4
6
8
10
12
14
16
Wind speed (m s-1)
KGOV
0
2
4
6
8
10
12
Wind speed (m s-1)
KSAW
0
5
10
15
Wind speed (m s-1)
KCMX
0
2
4
6
8
10
12
14
16
18
Wind speed (m s-1)

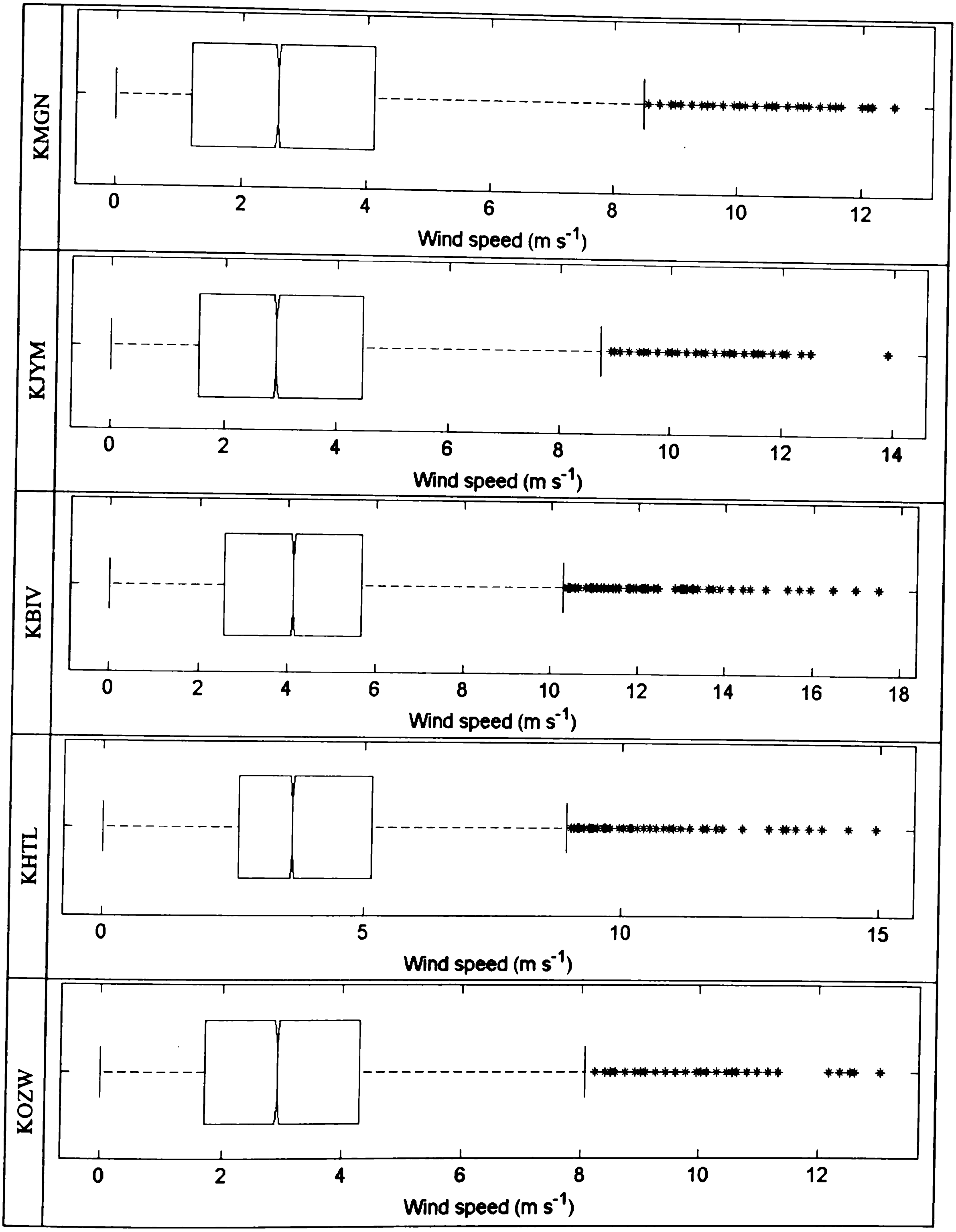
KMGN
0 2 4 6 8 10 12
Wind speed (m s-1)
KJYM
0 2 4 6 8 10 12 14
Wind speed (m s-1)
KBIV
0 2 4 6 8 10 12 14 16 18
Wind speed (m s-1)
KHTL
0 5 10 15
Wind speed (m s-1)
KOZW
0 2 4 6 8 10 12
Wind speed (m s-1)

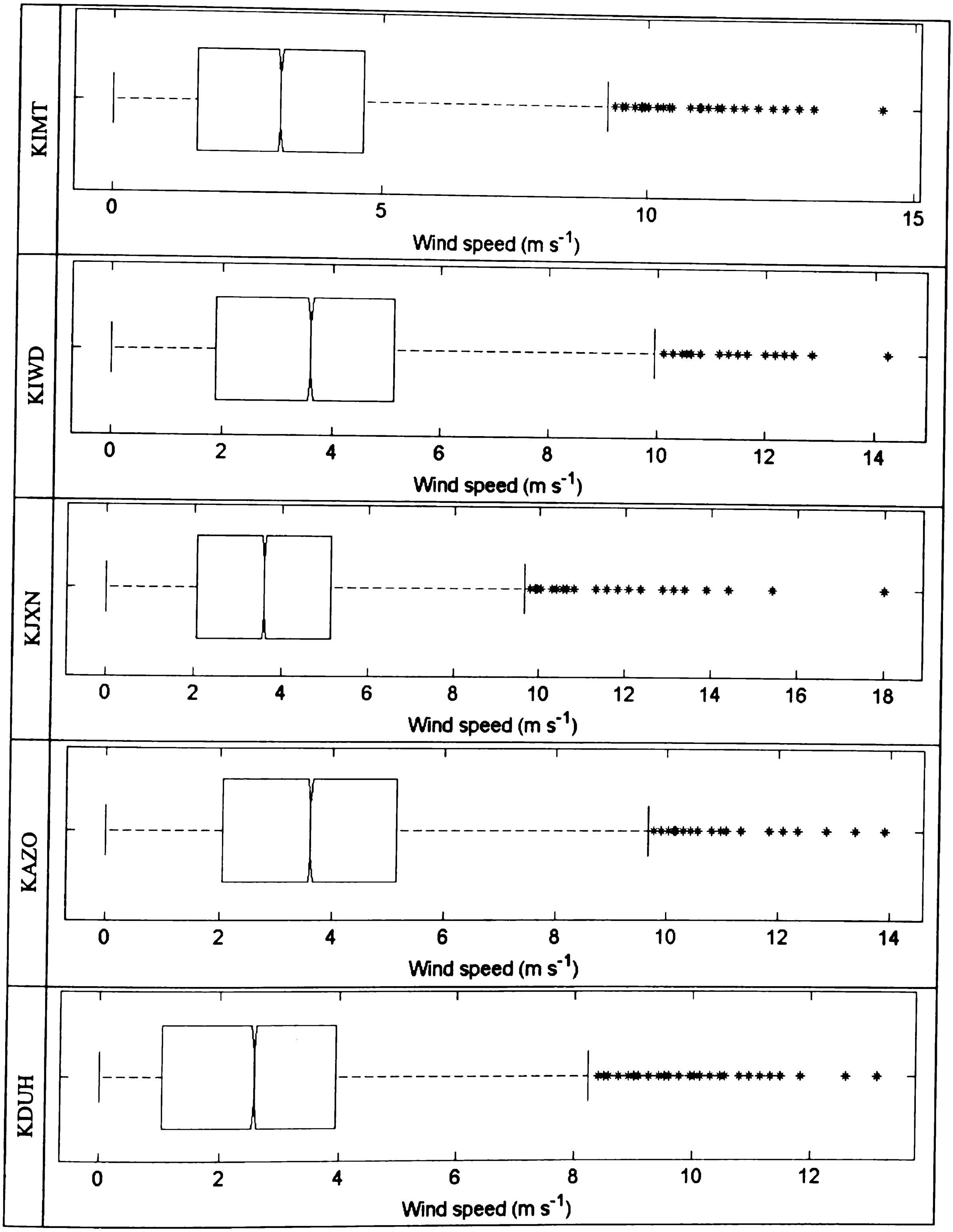
KIMT
0
5
10
15
Wind speed (m s-1)
KIWD
0
2
4
6
8
10
12
14
Wind speed (m s-1)
KJXN
0
2
4
6
8
10
12
14
16
18
Wind speed (m s-1)
KAZO
0
2
4
6
8
10
12
14
Wind speed (m s-1)
KDUH
0
2
4
6
8
10
12
Wind speed (m s-1)

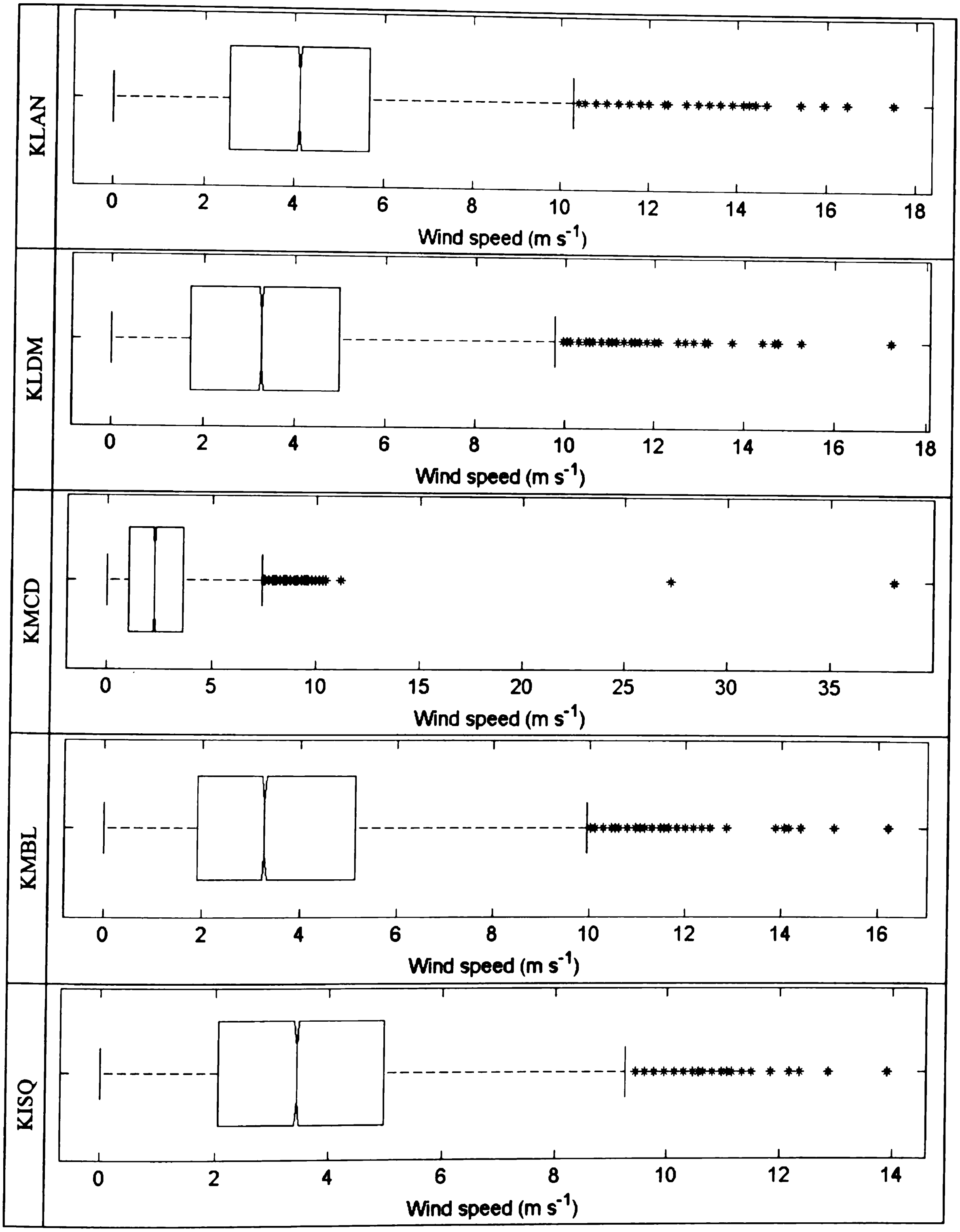
KLAN
0 2 4 6 8 10 12 14 16 18
Wind speed (m s-1)
KLDM
0 2 4 6 8 10 12 14 16 18
Wind speed (m s-1)
KMCD
0 5 10 15 20 25 30 35
Wind speed (m s-1)
KMBL
0 2 4 6 8 10 12 14 16
Wind speed (m s-1)
KISQ
0 2 4 6 8 10 12 14
Wind speed (m s-1)

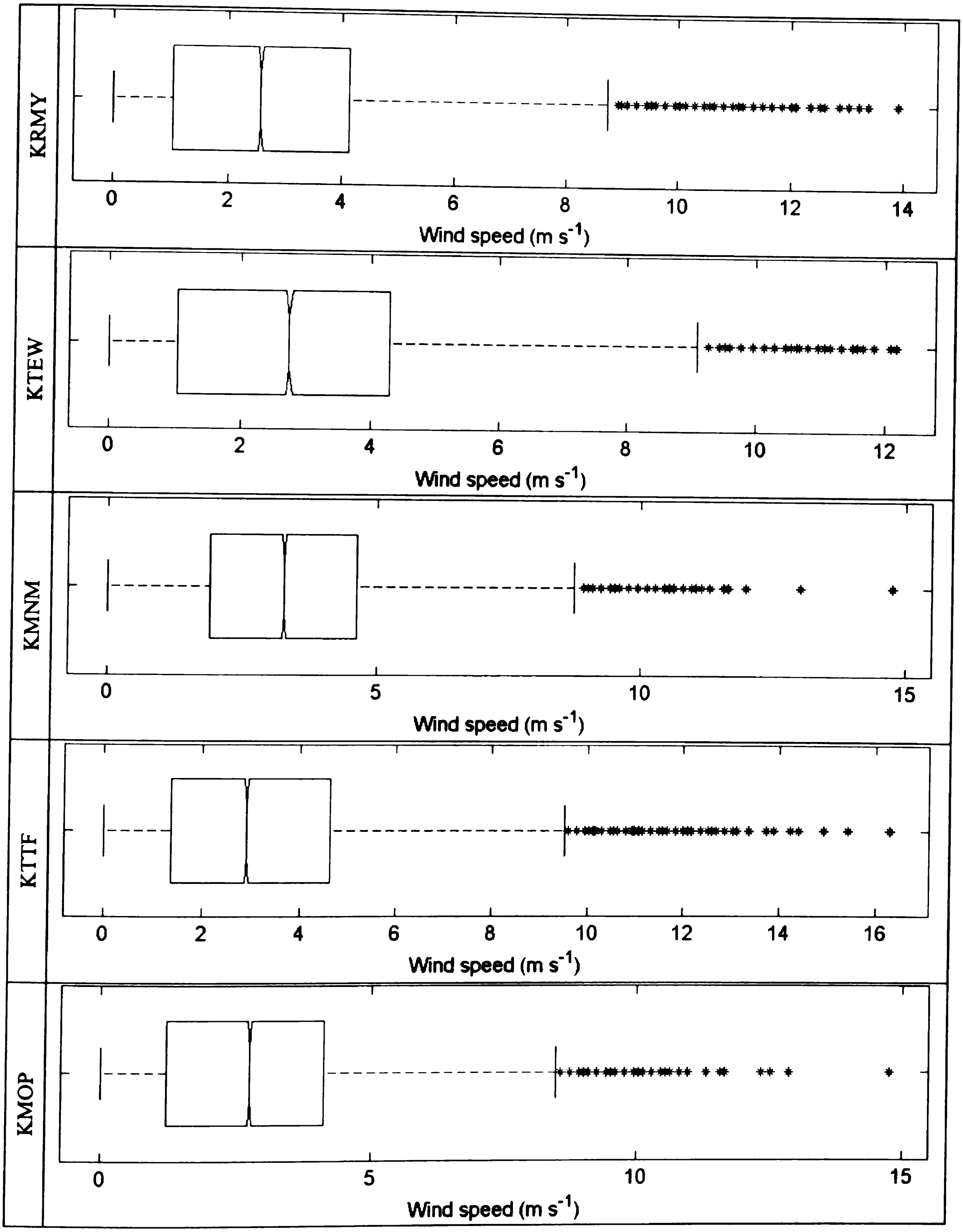
KRMY
0
2
4
6
8
10
12
14
Wind speed (m s-1)
KTEW
0
2
4
6
8
10
12
Wind speed (m s-1)
KMNM
0
5
10
15
Wind speed (m s-1)
KTTF
0
2
4
6
8
10
12
14
16
Wind speed (m s-1)
KMOP
0
5
10
15
Wind speed (m s-1)

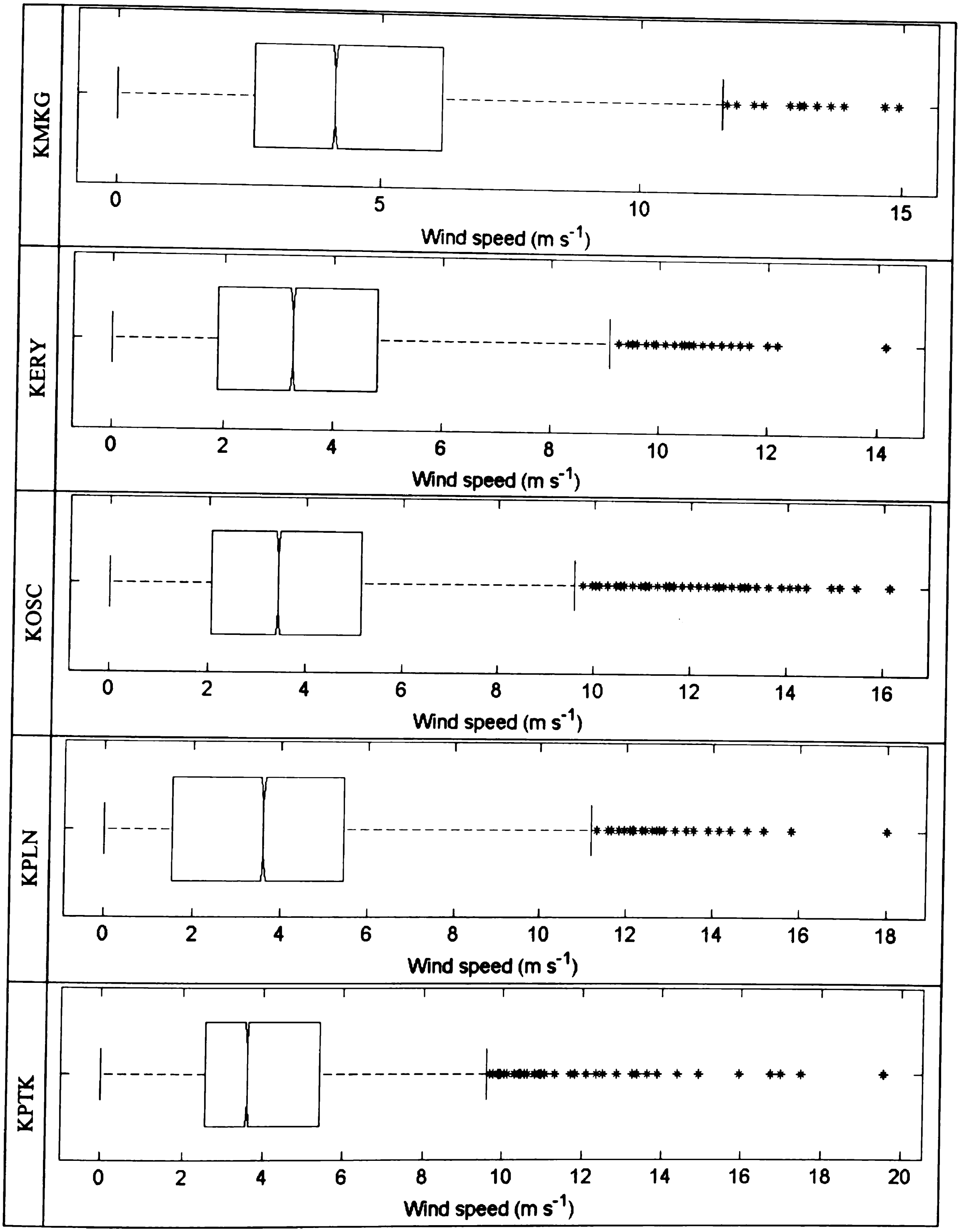

KMKG
0
5
10
15
Wind speed (m s-1)
KERY
0
2
4
6
8
10
12
14
Wind speed (m s-1)
KOSC
0
2
4
6
8
10
12
14
16
Wind speed (m s-1)
KPLN
0
2
4
6
8
10
12
14
16
18
Wind speed (m s-1)
KPTK
0
2
4
6
8
10
12
14
16
18
20
Wind speed (m s-1)

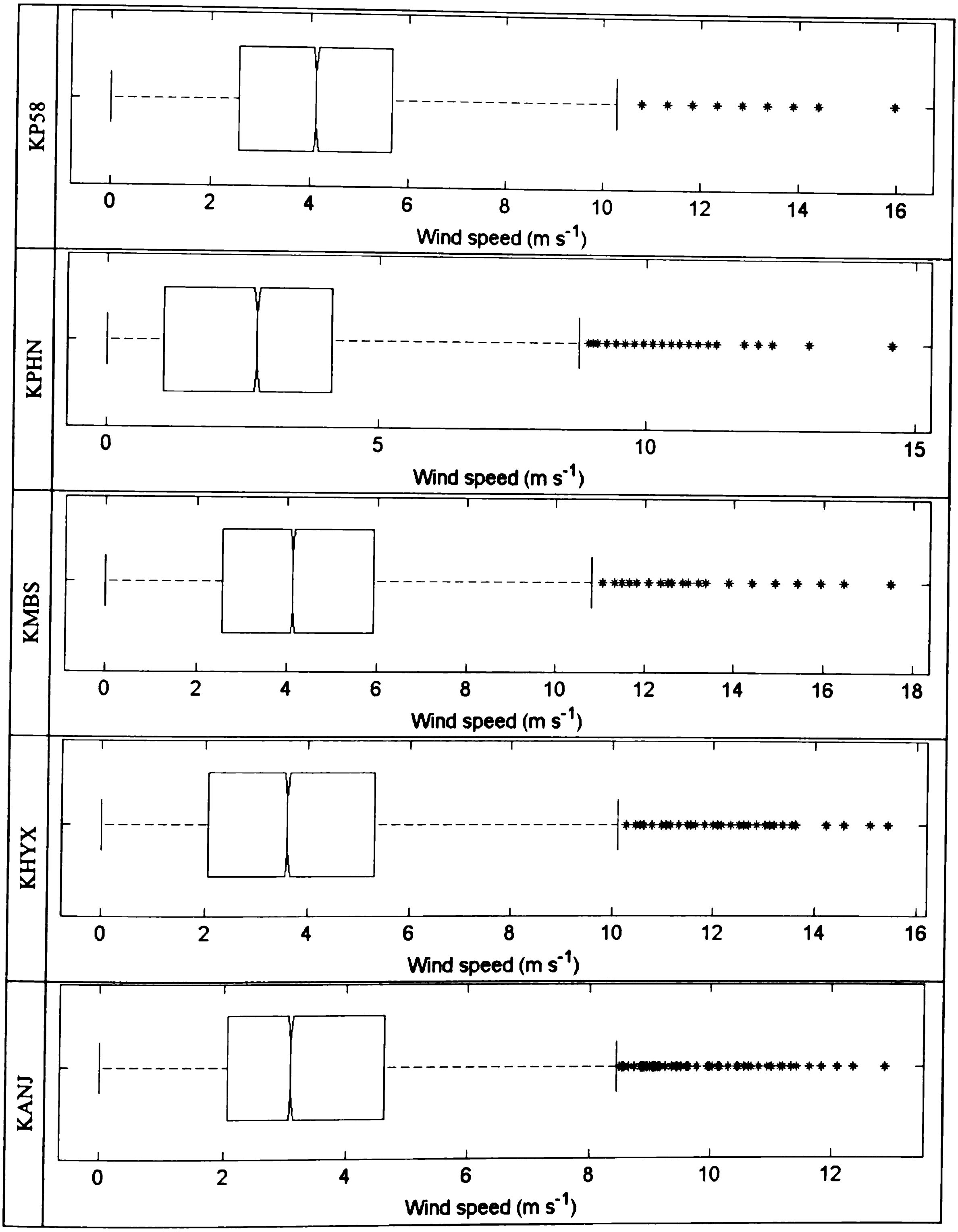

KP58
0 2 4 6 8 10 12 14 16
Wind speed (m s-1)
KPHN
0 5 10 15
Wind speed (m s-1)
KMBS
0 2 4 6 8 10 12 14 16 18
Wind speed (m s-1)
KHYX
0 2 4 6 8 10 12 14 16
Wind speed (m s-1)
KANJ
0 2 4 6 8 10 12
Wind speed (m s-1)

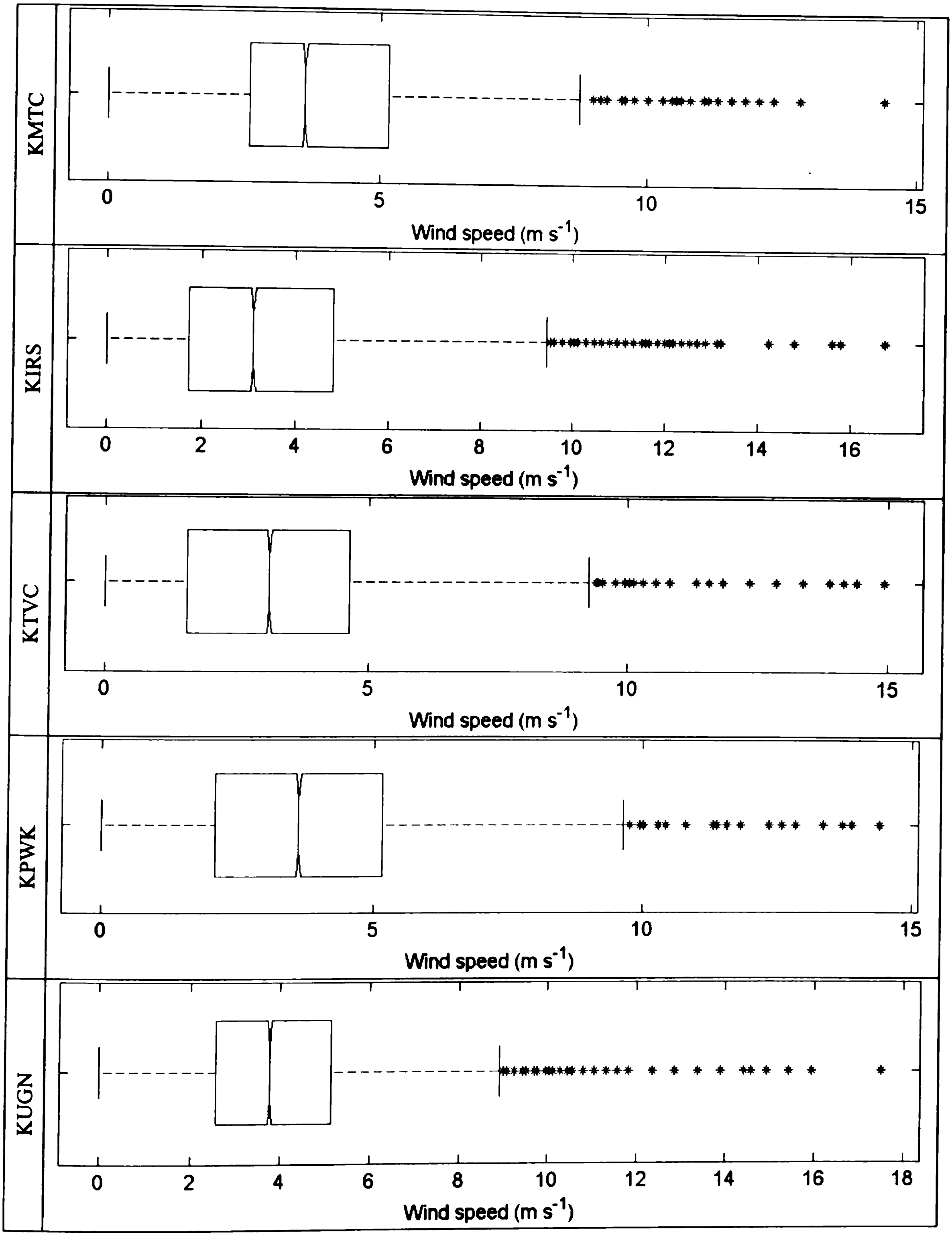

KMTC
0
5
10
15
Wind speed (m s-1)
KIRS
0
2
4
6
8
10
12
14
16
Wind speed (m s-1)
KTVC
0
5
10
15
Wind speed (m s-1)
KPWK
0
5
10
15
Wind speed (m s-1)
KUGN
0
2
4
6
8
10
12
14
16
18
Wind speed (m s-1)

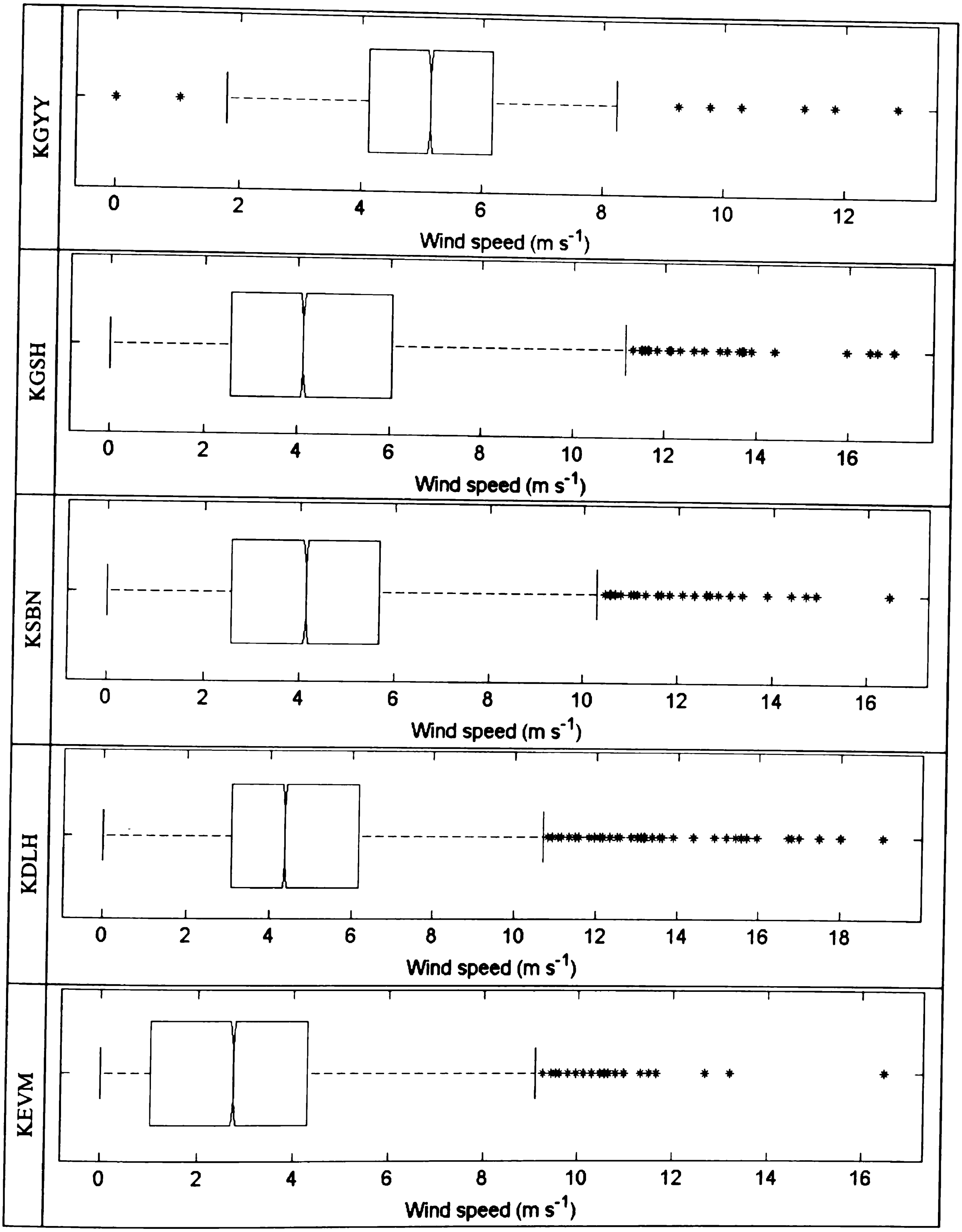
KGYY
0 2 4 6 8 10 12
Wind speed (m s-1)
KGSH
0 2 4 6 8 10 12 14 16
Wind speed (m s-1)
KSBN
0 2 4 6 8 10 12 14 16
Wind speed (m s-1)
KDLH
0 2 4 6 8 10 12 14 16 18
Wind speed (m s-1)
KEVM
0 2 4 6 8 10 12 14 16
Wind speed (m s-1)

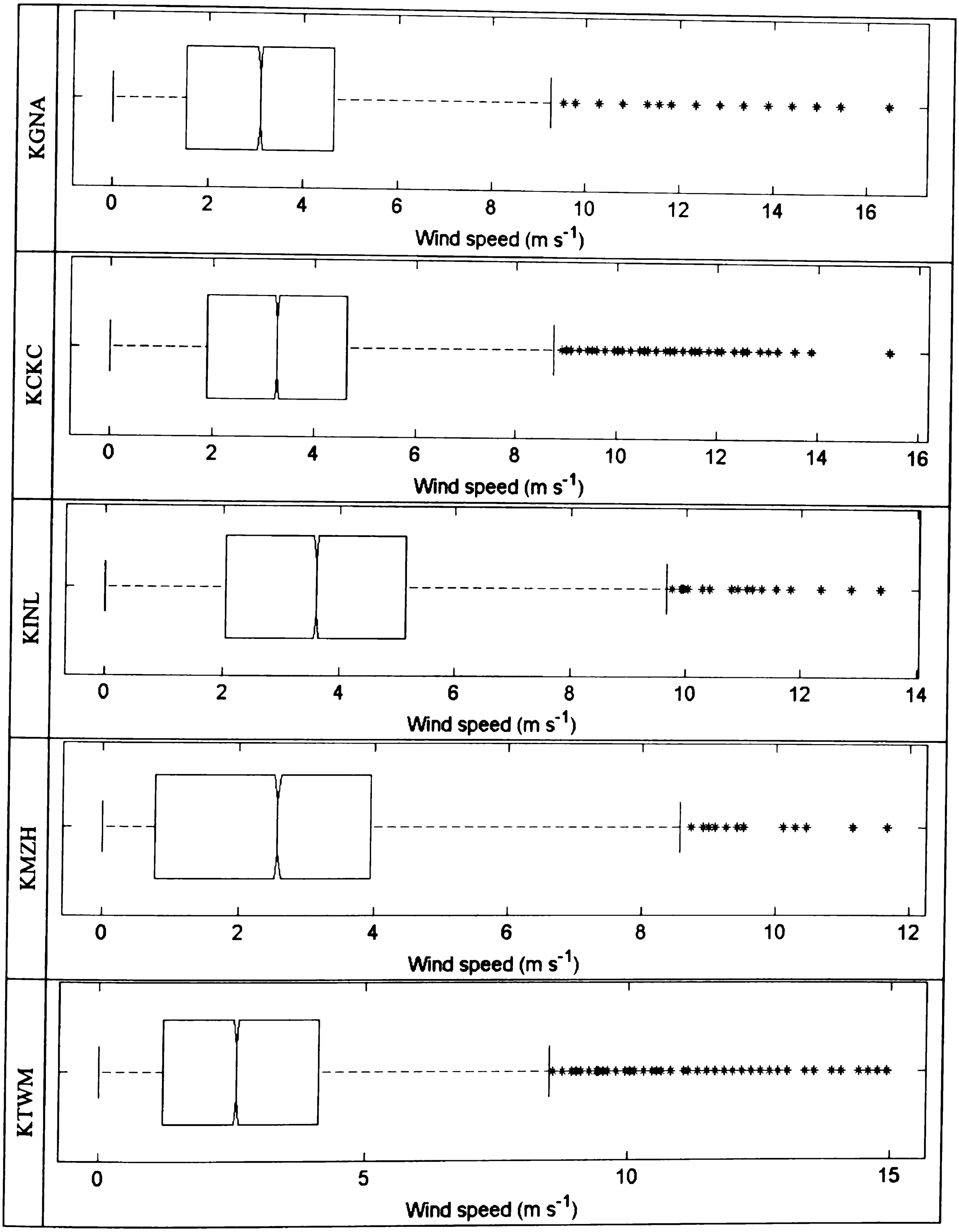
KGNA
0 2 4 6 8 10 12 14 16
Wind speed (m s-1)
KCKC
0 2 4 6 8 10 12 14 16
Wind speed (m s-1)
KINL
0 2 4 6 8 10 12 14
Wind speed (m s-1)
KMZH
0 2 4 6 8 10 12
Wind speed (m s-1)
KTWM
0 5 10 15
Wind speed (m s-1)

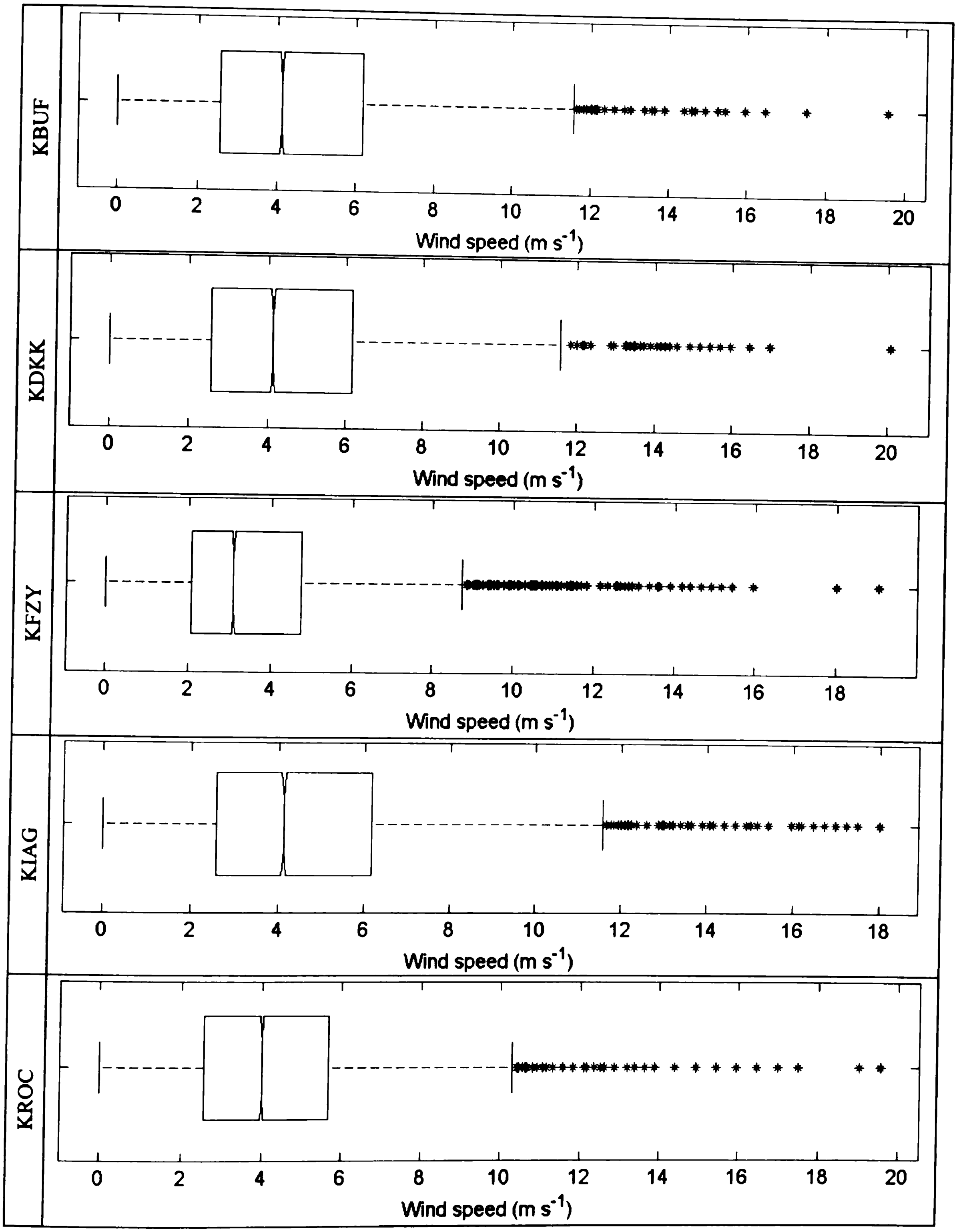
KBUF
0
2
4
6
8
10
12
14
16
18
20
Wind speed (m s-1)
KDKK
0
2
4
6
8
10
12
14
16
18
20
Wind speed (m s-1)
KFZY
0
2
4
6
8
10
12
14
16
18
Wind speed (m s-1)
KIAG
0
2
4
6
8
10
12
14
16
18
Wind speed (m s-1)
KROC
0
2
4
6
8
10
12
14
16
18
20
Wind speed (m s-1)

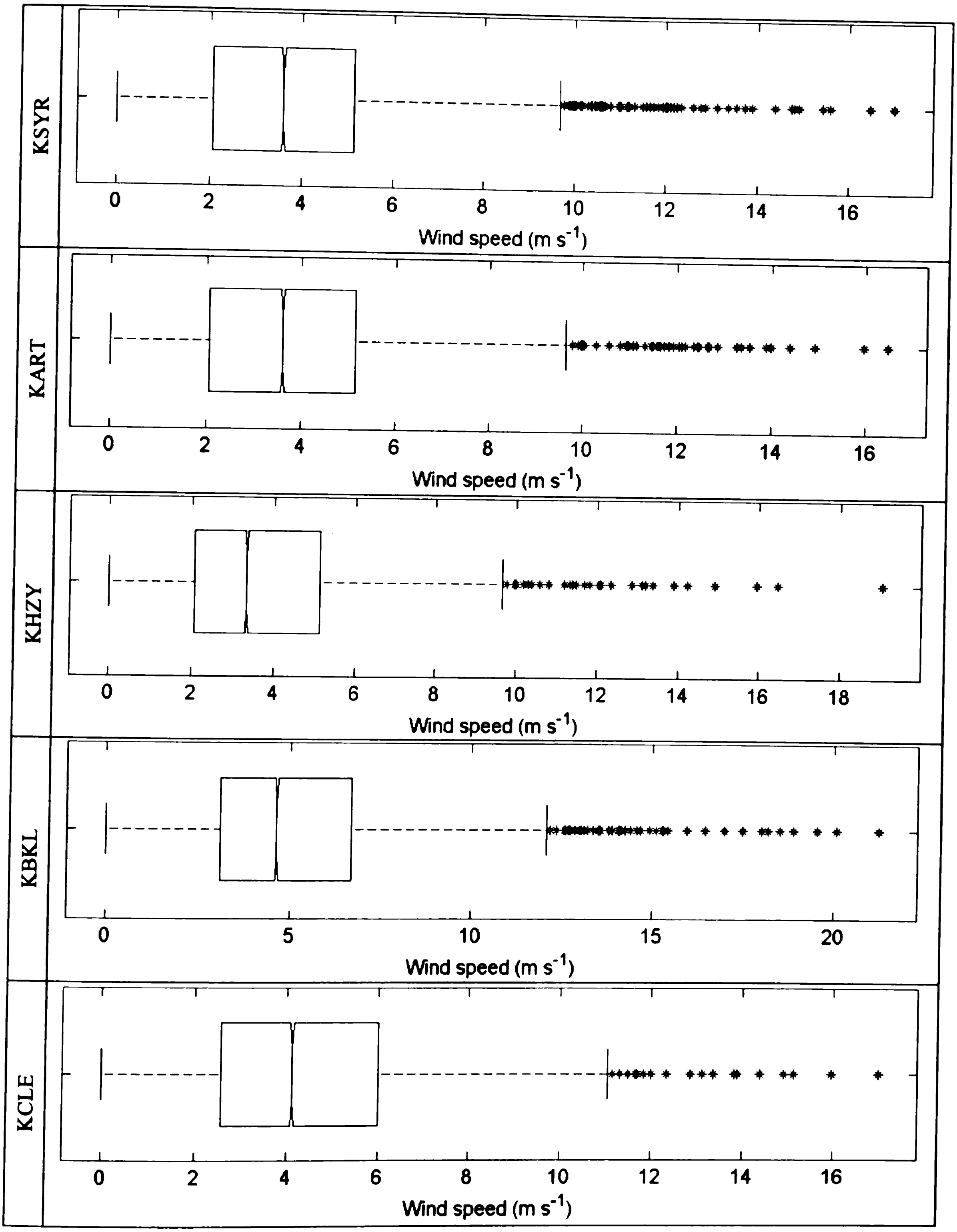
KSYR
0 2 4 6 8 10 12 14 16
Wind speed (m s-1)
KART
0 2 4 6 8 10 12 14 16
Wind speed (m s-1)
KHZY
0 2 4 6 8 10 12 14 16 18
Wind speed (m s-1)
KBKL
0 5 10 15 20
Wind speed (m s-1)
KCLE
0 2 4 6 8 10 12 14 16
Wind speed (m s-1)

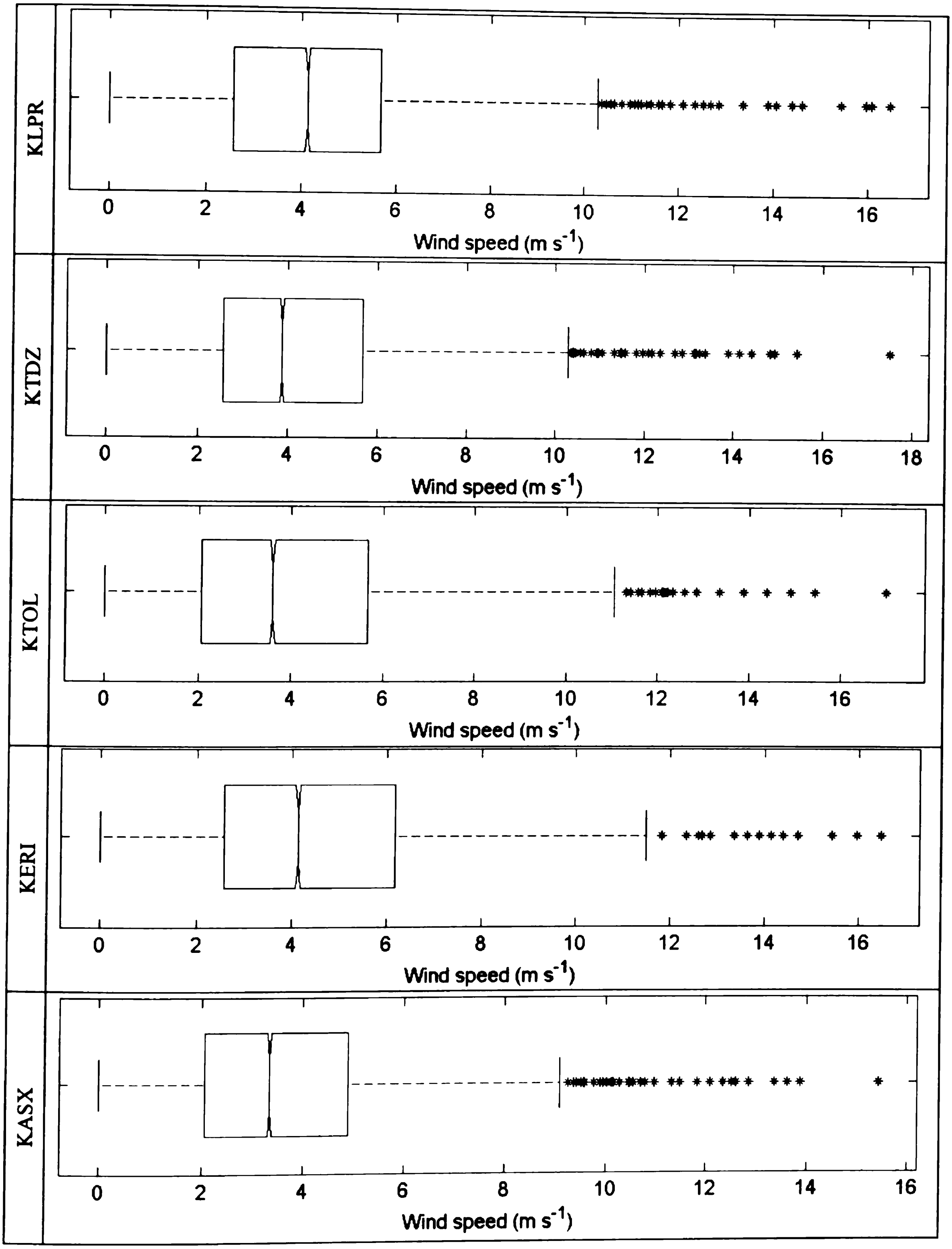
KLPR
0 2 4 6 8 10 12 14 16
Wind speed (m s-1)
KTDZ
0 2 4 6 8 10 12 14 16 18
Wind speed (m s-1)
KTOL
0 2 4 6 8 10 12 14 16
Wind speed (m s-1)
KERI
0 2 4 6 8 10 12 14 16
Wind speed (m s-1)
KASX
0 2 4 6 8 10 12 14 16
Wind speed (m s-1)

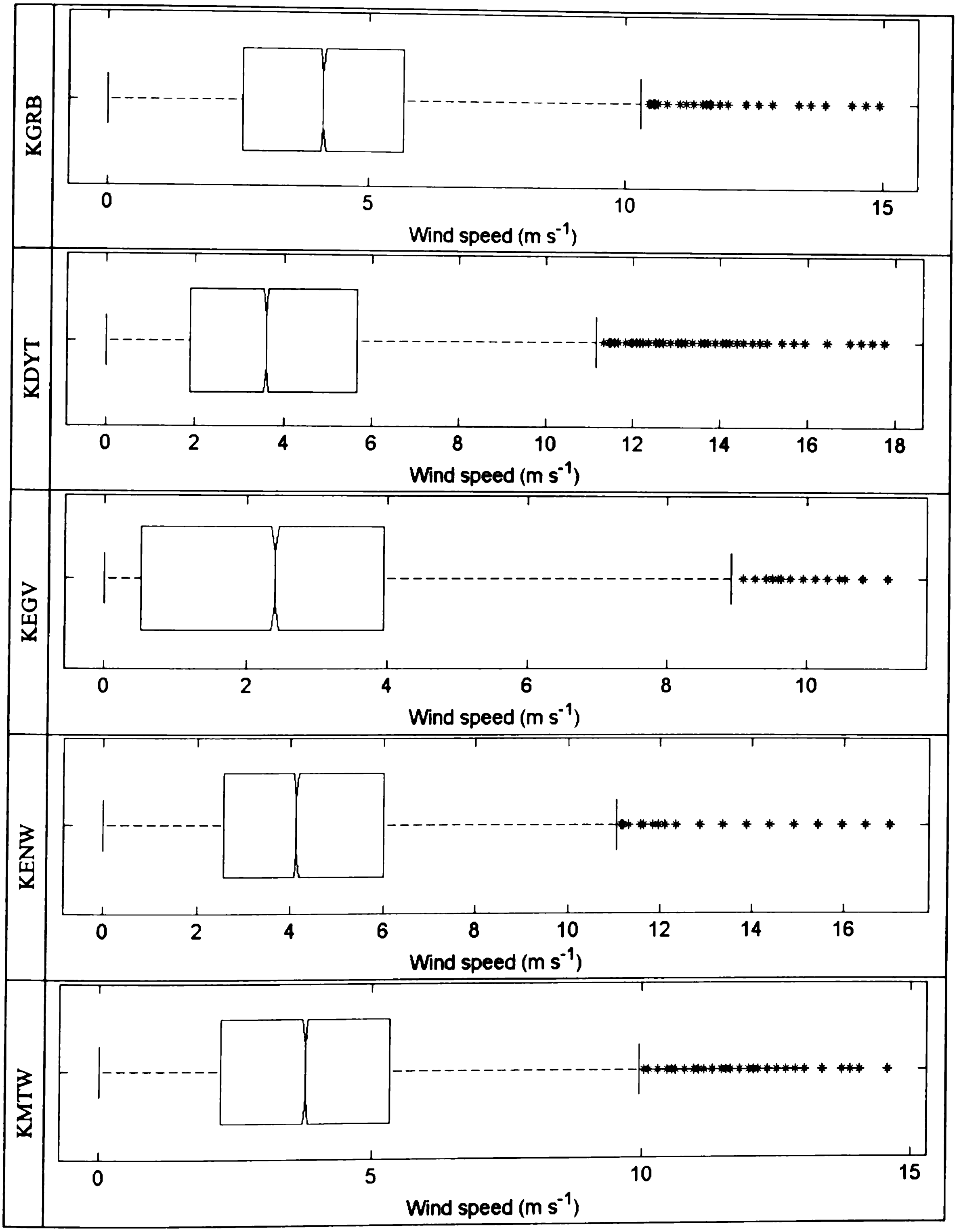
KGRB
0
5
10
15
Wind speed (m s-1)
KDYT
0
2
4
6
8
10
12
14
16
18
Wind speed (m s-1)
KEGV
0
2
4
6
8
10
Wind speed (m s-1)
KENW
0
2
4
6
8
10
12
14
16
Wind speed (m s-1)
KMTW
0
5
10
15
Wind speed (m s-1)

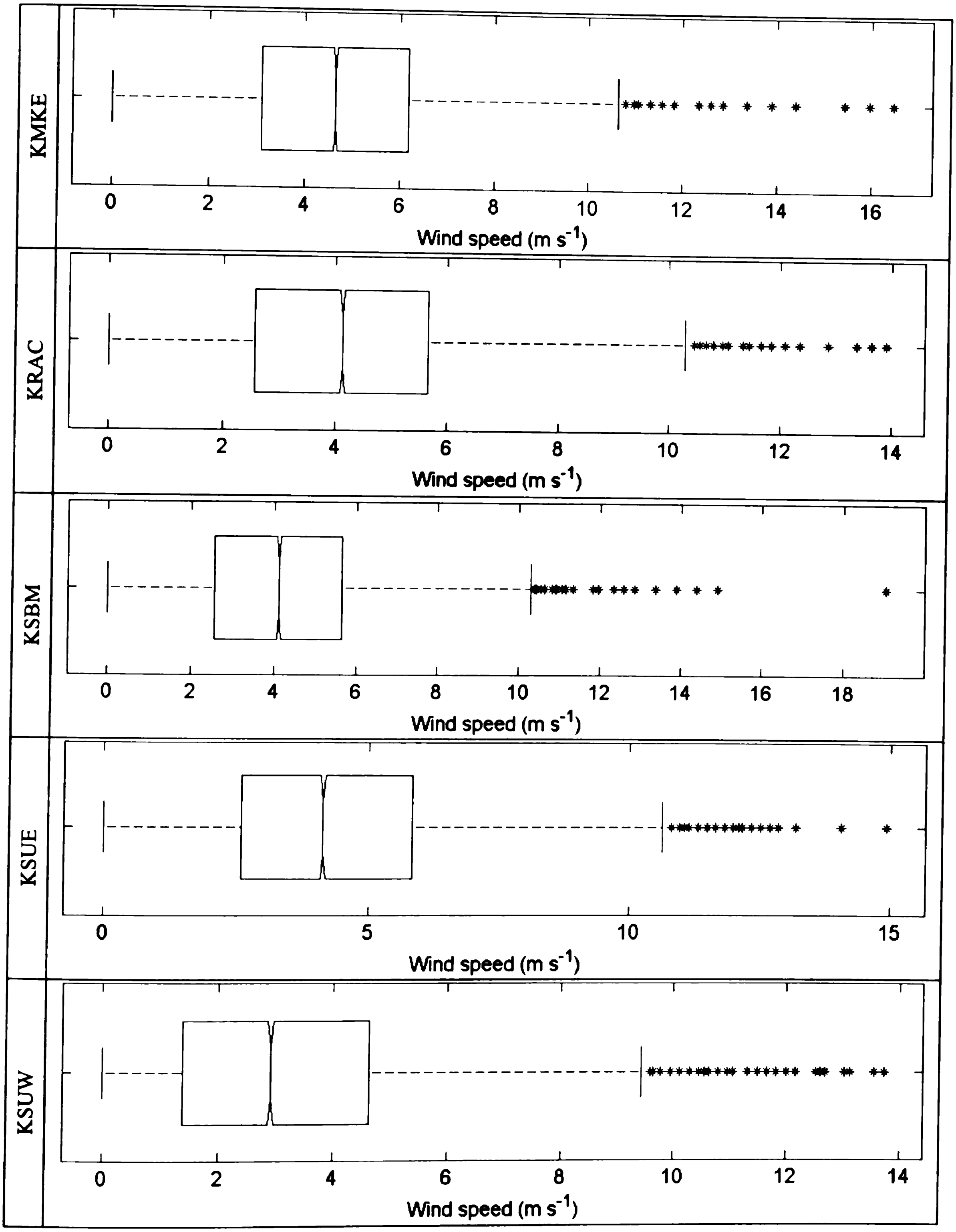
KMKE
0 2 4 6 8 10 12 14 16
Wind speed (m s-1)
KRAC
0 2 4 6 8 10 12 14
Wind speed (m s-1)
KSBM
0 2 4 6 8 10 12 14 16 18
Wind speed (m s-1)
KSUE
0 5 10 15
Wind speed (m s-1)
KSUW
0 2 4 6 8 10 12 14
Wind speed (m s-1)

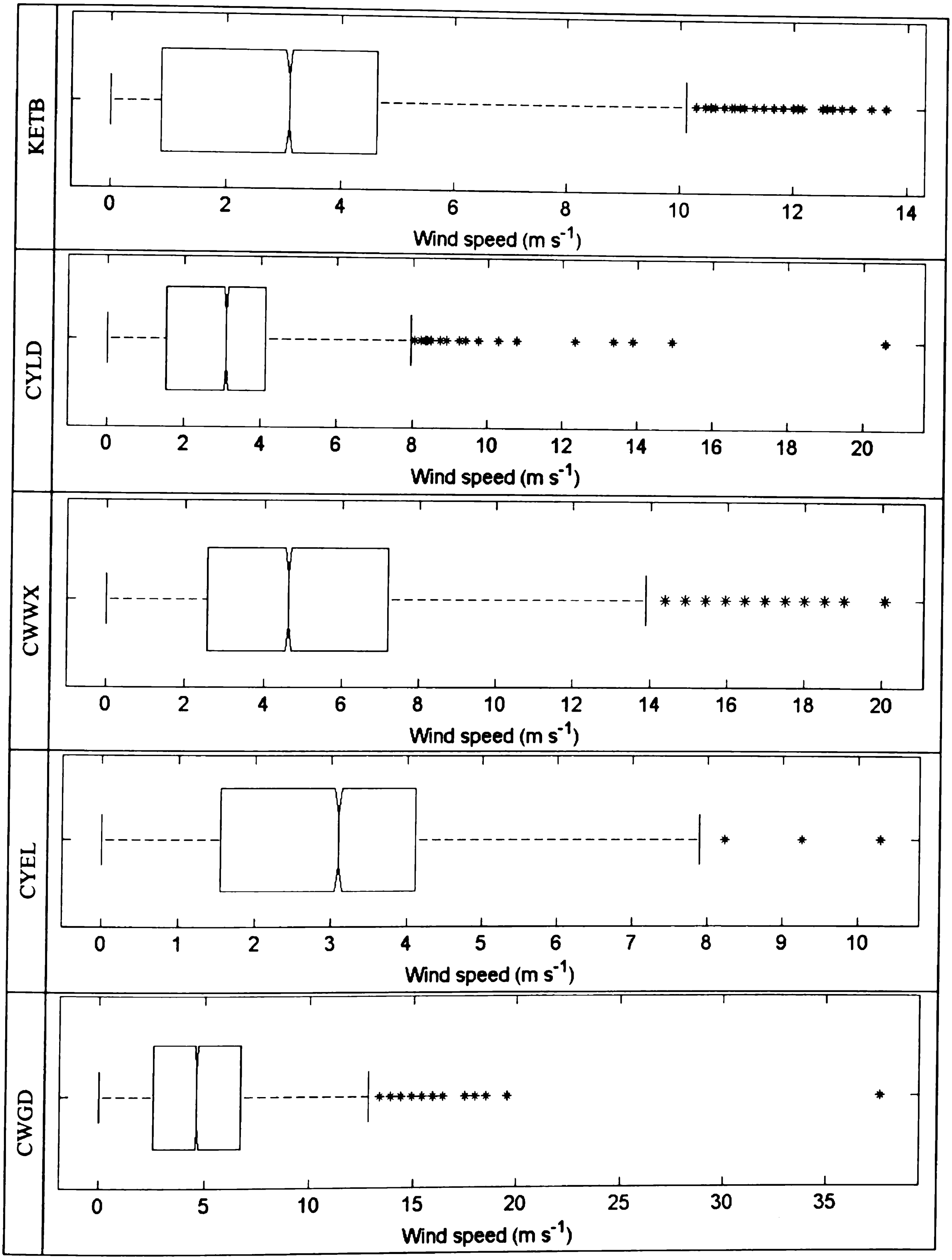
KETB
0 2 4 6 8 10 12 14
Wind speed (m s-1)
CYLD
0 2 4 6 8 10 12 14 16 18 20
Wind speed (m s-1)
CWWX
0 2 4 6 8 10 12 14 16 18 20
Wind speed (m s-1)
CYEL
0 1 2 3 4 5 6 7 8 9 10
Wind speed (m s-1)
CWGD
0 5 10 15 20 25 30 35
Wind speed (m s-1)

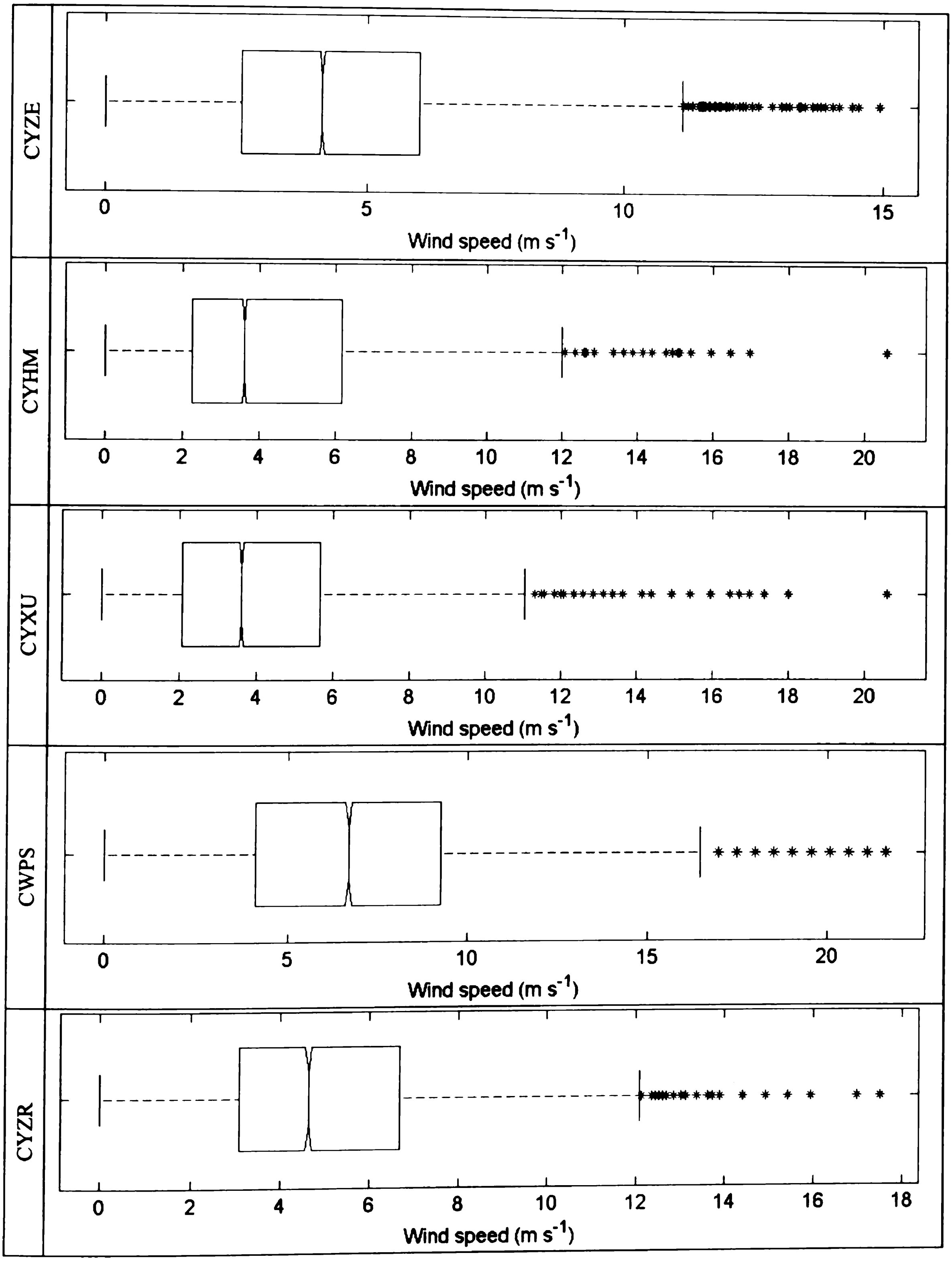

CYZE
0
5
10
15
Wind speed (m s-1)
CYHM
0
2
4
6
8
10
12
14
16
18
20
Wind speed (m s-1)
CYXU
0
2
4
6
8
10
12
14
16
18
20
Wind speed (m s-1)
CWPS
0
5
10
15
20
Wind speed (m s-1)
CYZR
0
2
4
6
8
10
12
14
16
18
Wind speed (m s-1)

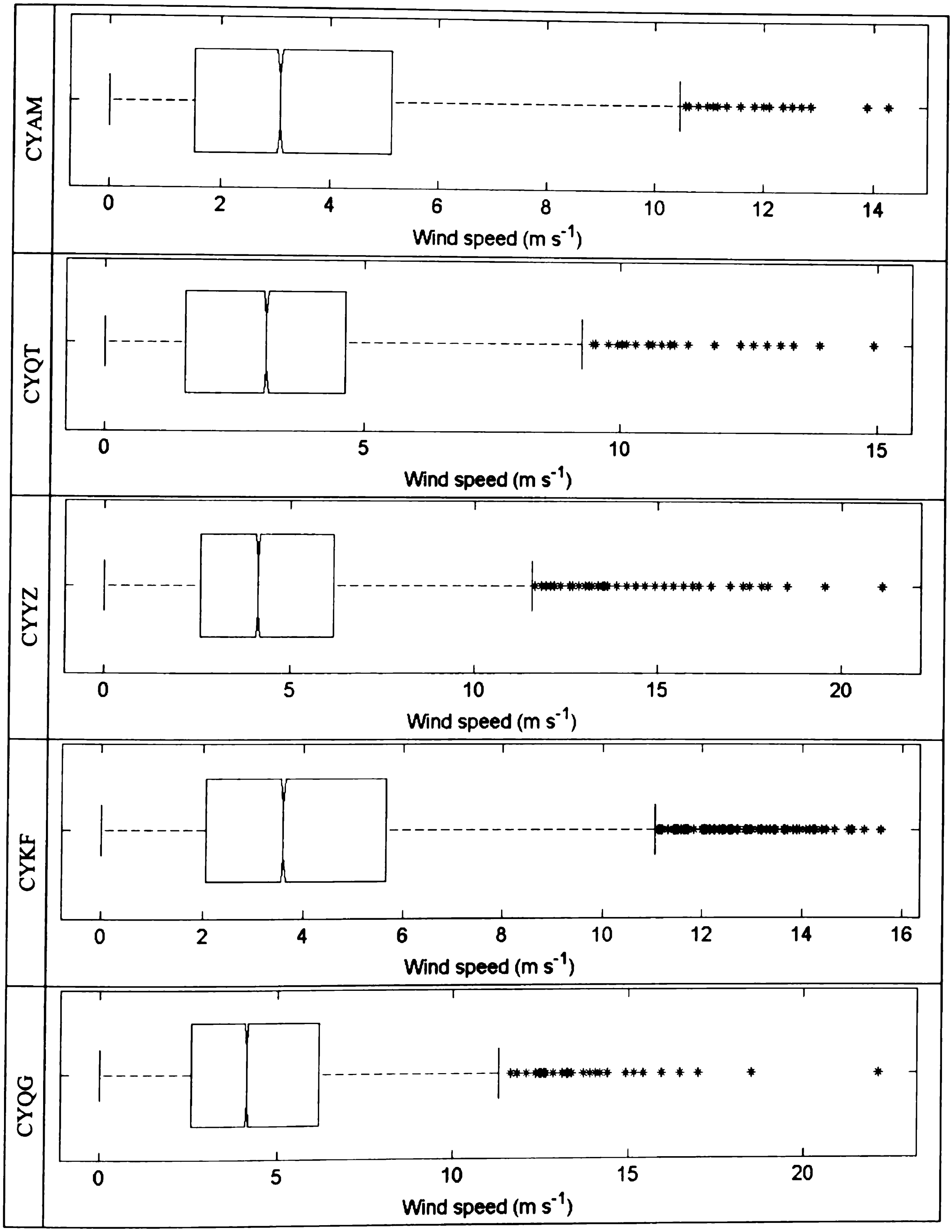
CYAM
0 2 4 6 8 10 12 14
Wind speed (m s-1)
CYQT
0 5 10 15
Wind speed (m s-1)
CYYZ
0 5 10 15 20
Wind speed (m s-1)
CYKF
0 2 4 6 8 10 12 14 16
Wind speed (m s-1)
CYQG
0 5 10 15 20
Wind speed (m s-1)

Wind Rose Diagrams for each ASOS Station

KADG

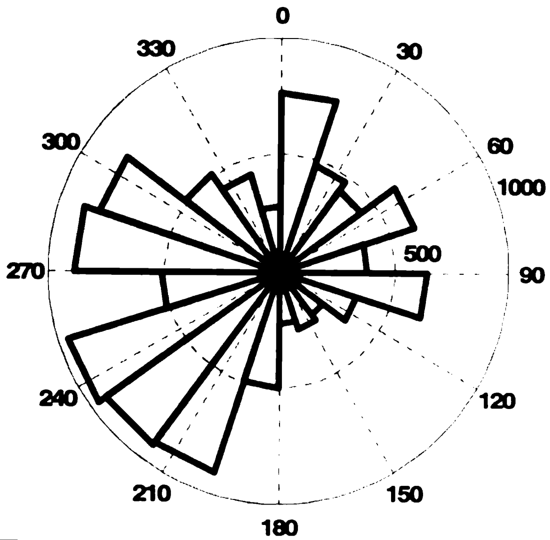

KAMN

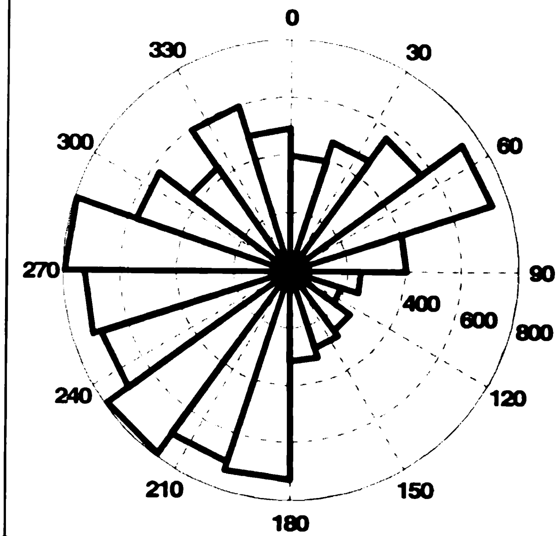

KAPN

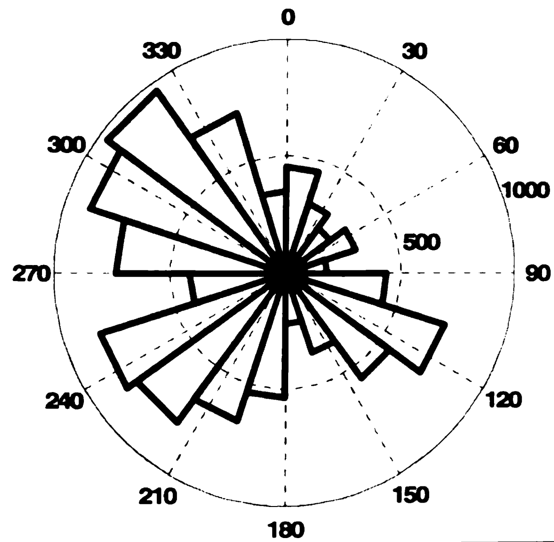

KARB

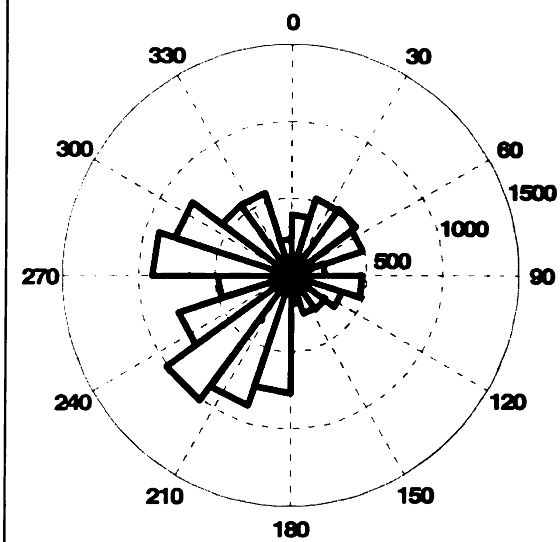

KBAX

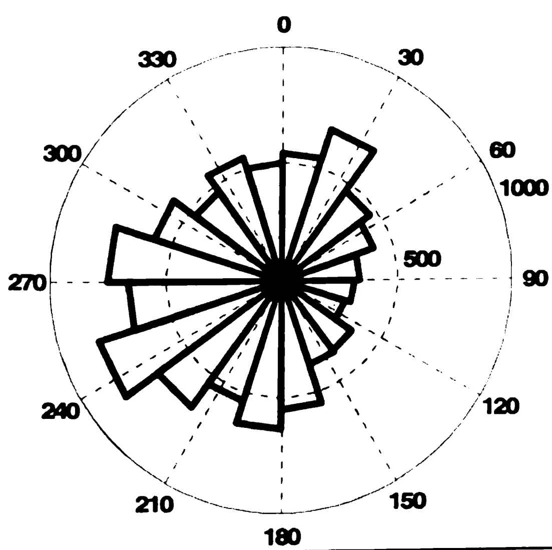

KBTL

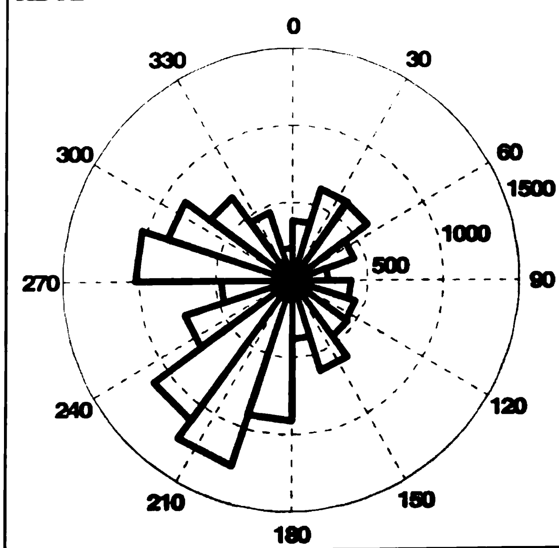

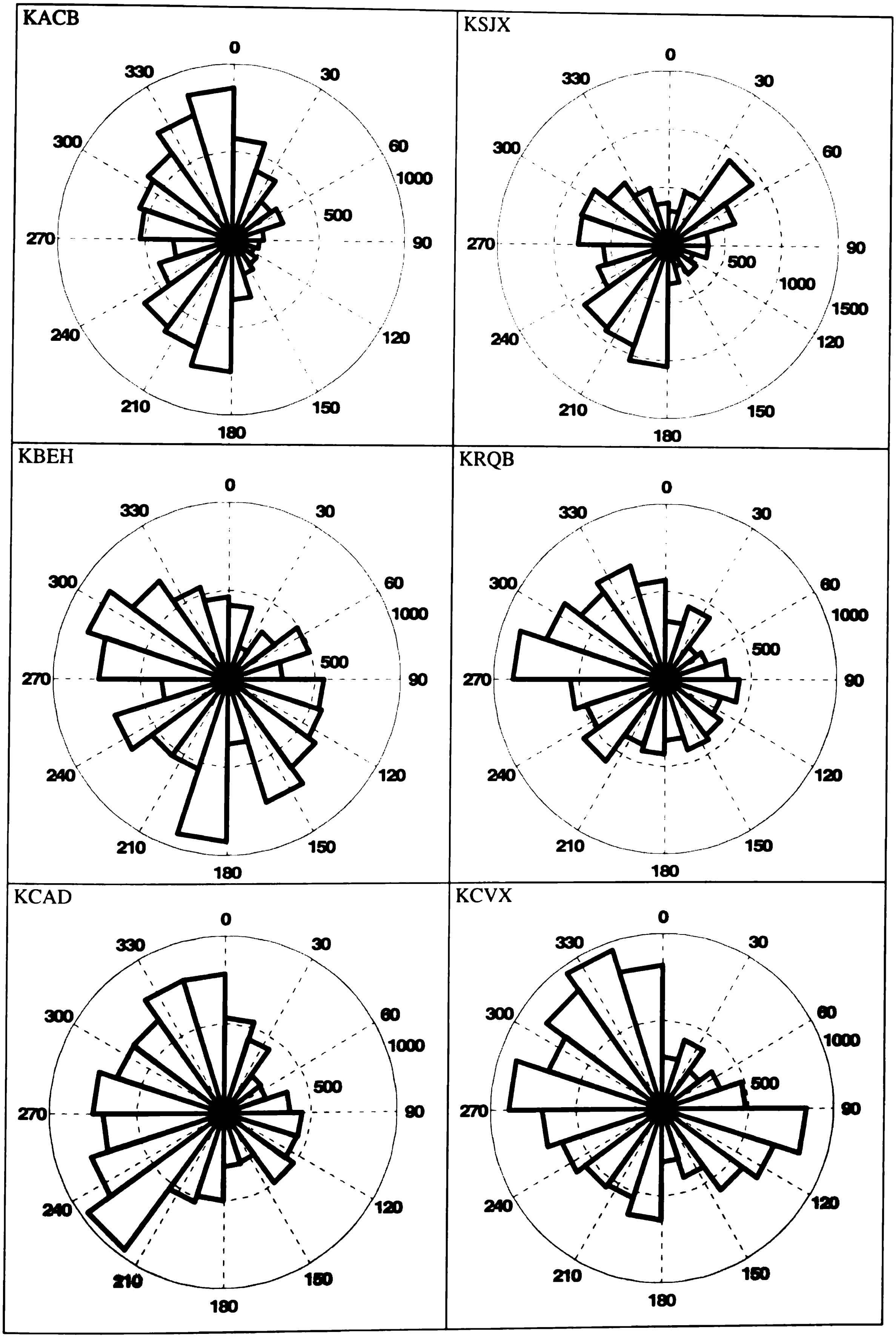
KACB
0
30
60
90
120
150
180
210
240
270
300
330
500
1000
KSJX
0
30
60
90
120
150
180
210
240
270
300
330
500
1000
1500
KBEH
0
30
60
90
120
150
180
210
240
270
300
330
500
1000
KRQB
0
30
60
90
120
150
180
210
240
270
300
330
500
1000
KCAD
0
30
60
90
120
150
180
210
240
270
300
330
500
1000
KCVX
0
30
60
90
120
150
180
210
240
270
300
330
500
1000

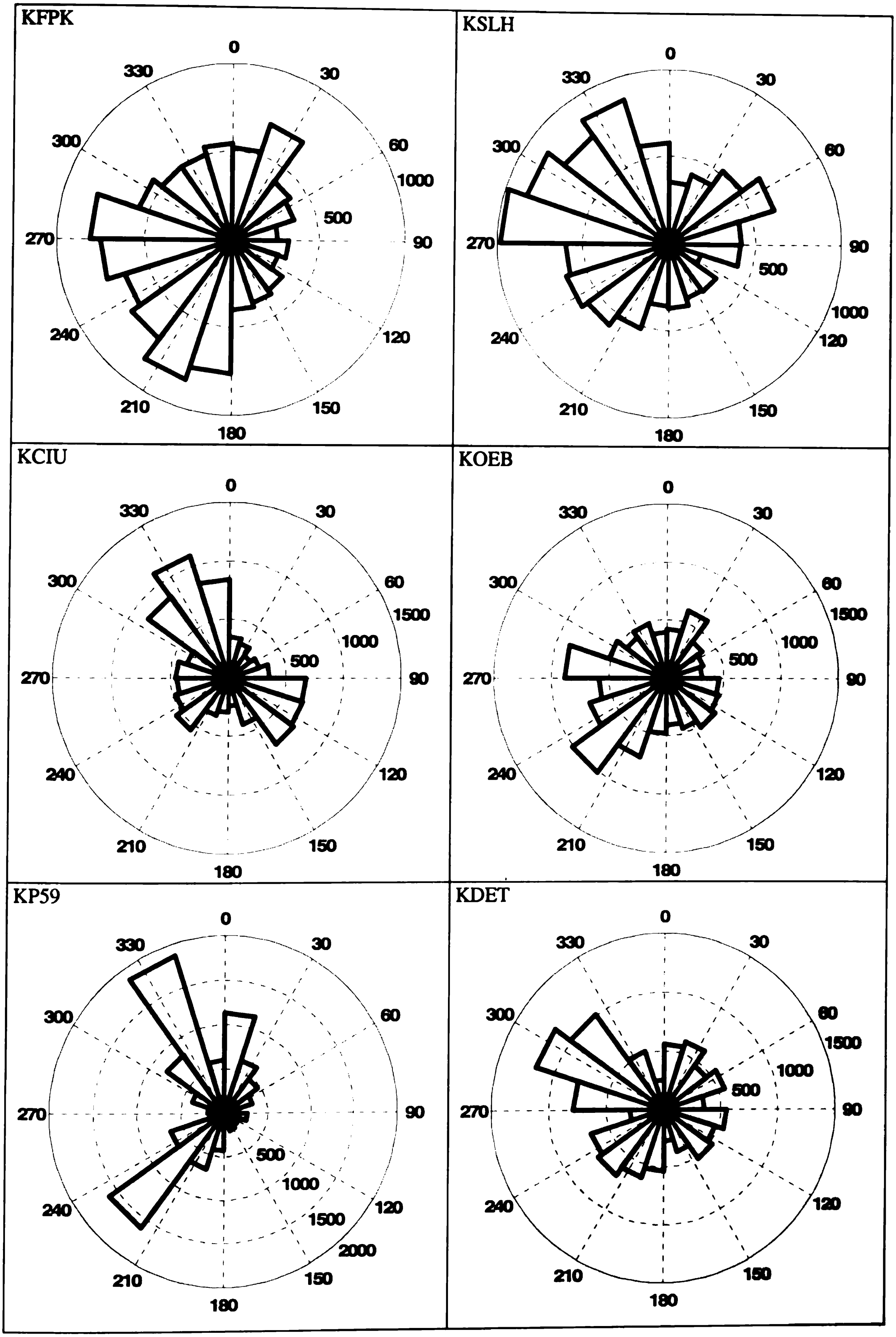
KFPK
0
30
60
90
120
150
180
210
240
270
300
330
500
1000
KSLH
0
30
60
90
120
150
180
210
240
270
300
330
500
1000
KCIU
0
30
60
90
120
150
180
210
240
270
300
330
500
1000
1500
KOEB
0
30
60
90
120
150
180
210
240
270
300
330
500
1000
1500
KP59
0
30
60
90
120
150
180
210
240
270
300
330
500
1000
1500
2000
KDET
0
30
60
90
120
150
180
210
240
270
300
330
500
1000
1500

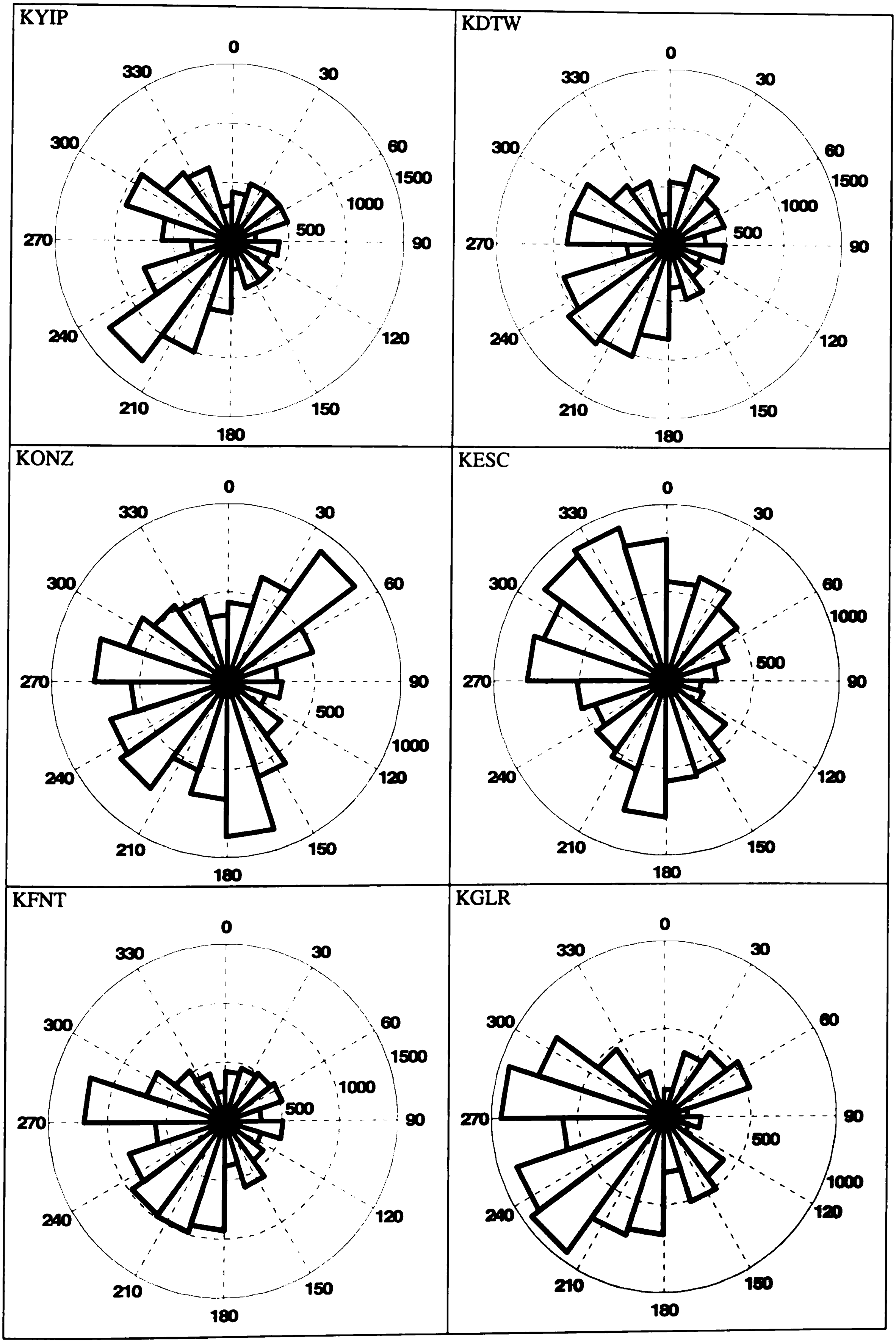
KYIP
0
30
60
90
120
150
180
210
240
270
300
330
500
1000
1500
KDTW
0
30
60
90
120
150
180
210
240
270
300
330
500
1000
1500
KONZ
0
30
60
90
120
150
180
210
240
270
300
330
500
1000
KESC
0
30
60
90
120
150
180
210
240
270
300
330
500
1000
KFNT
0
30
60
90
120
150
180
210
240
270
300
330
500
1000
1500
KGLR
0
30
60
90
120
150
180
210
240
270
300
330
500
1000

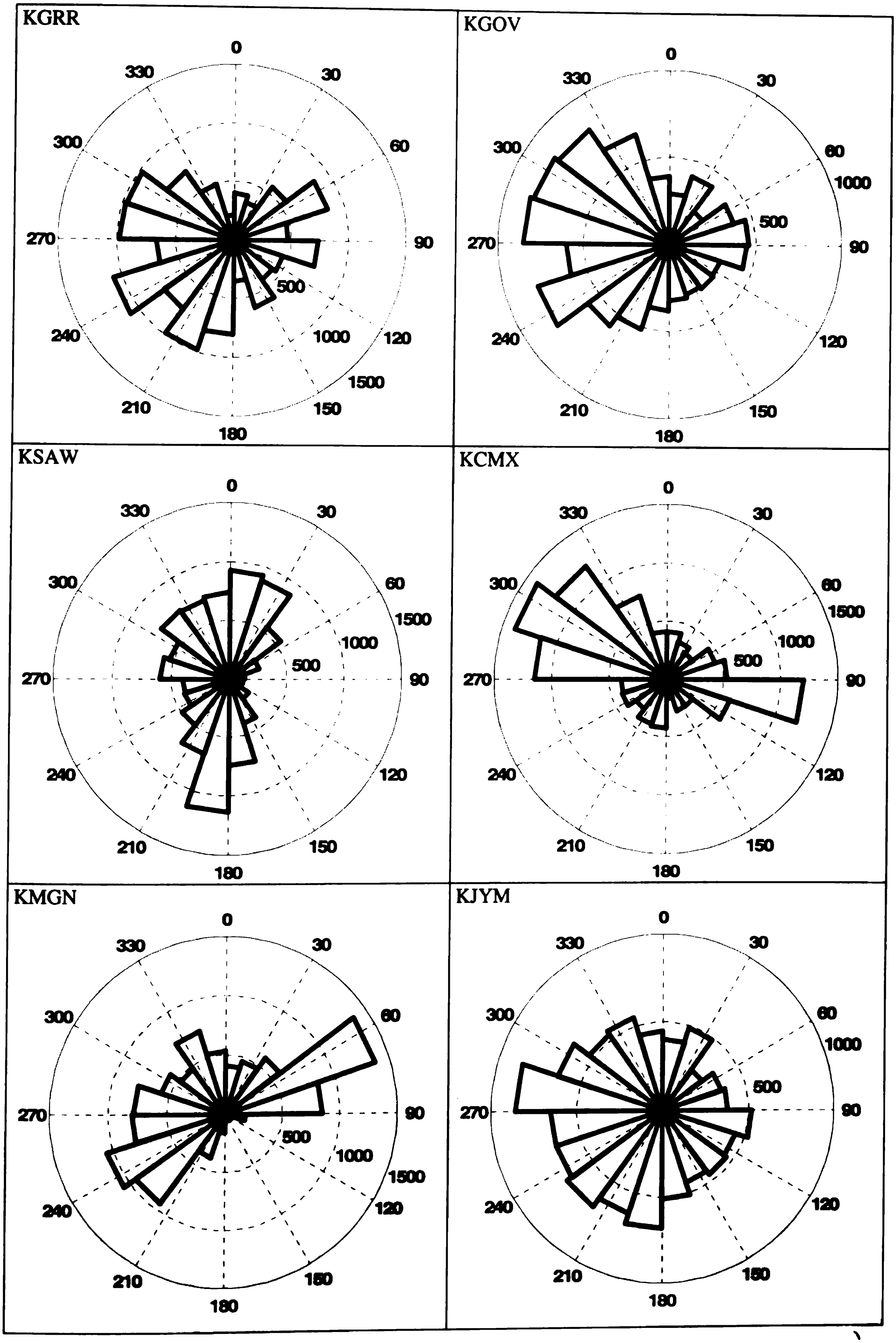
KGRR
0
30
60
90
120
150
180
210
240
270
300
330
500
1000
1500
KGOV
0
30
60
90
120
150
180
210
240
270
300
330
500
1000
KSAW
0
30
60
90
120
150
180
210
240
270
300
330
500
1000
1500
KCMX
0
30
60
90
120
150
180
210
240
270
300
330
500
1000
1500
KMGN
0
30
60
90
120
150
180
210
240
270
300
330
500
1000
1500
KJYM
0
30
60
90
120
150
180
210
240
270
300
330
500
1000

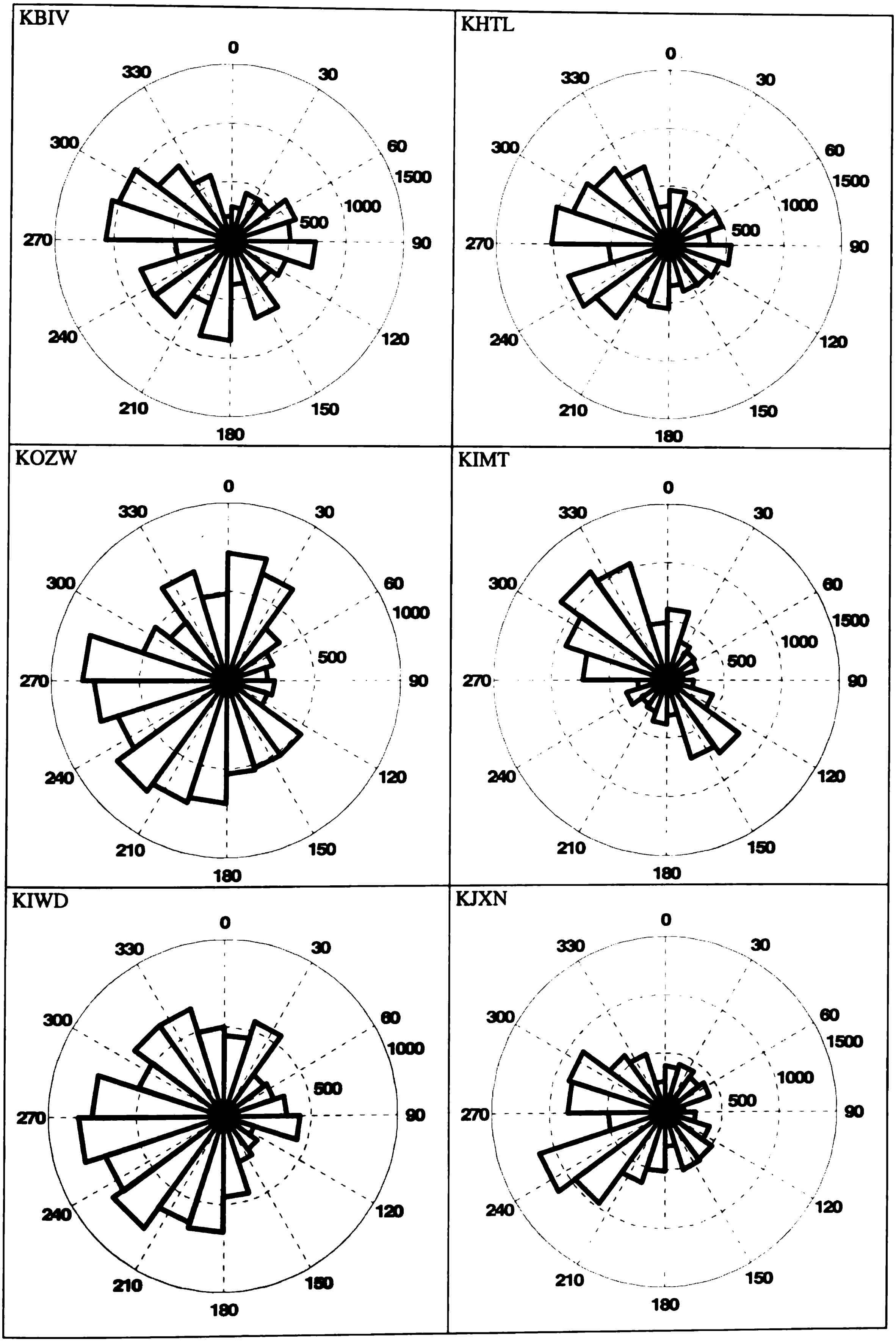
KBIV
KHTL
KOZW
KIMT
KIWD
KJXN
0
30
60
90
120
150
180
210
240
270
300
330
500
1000
1500

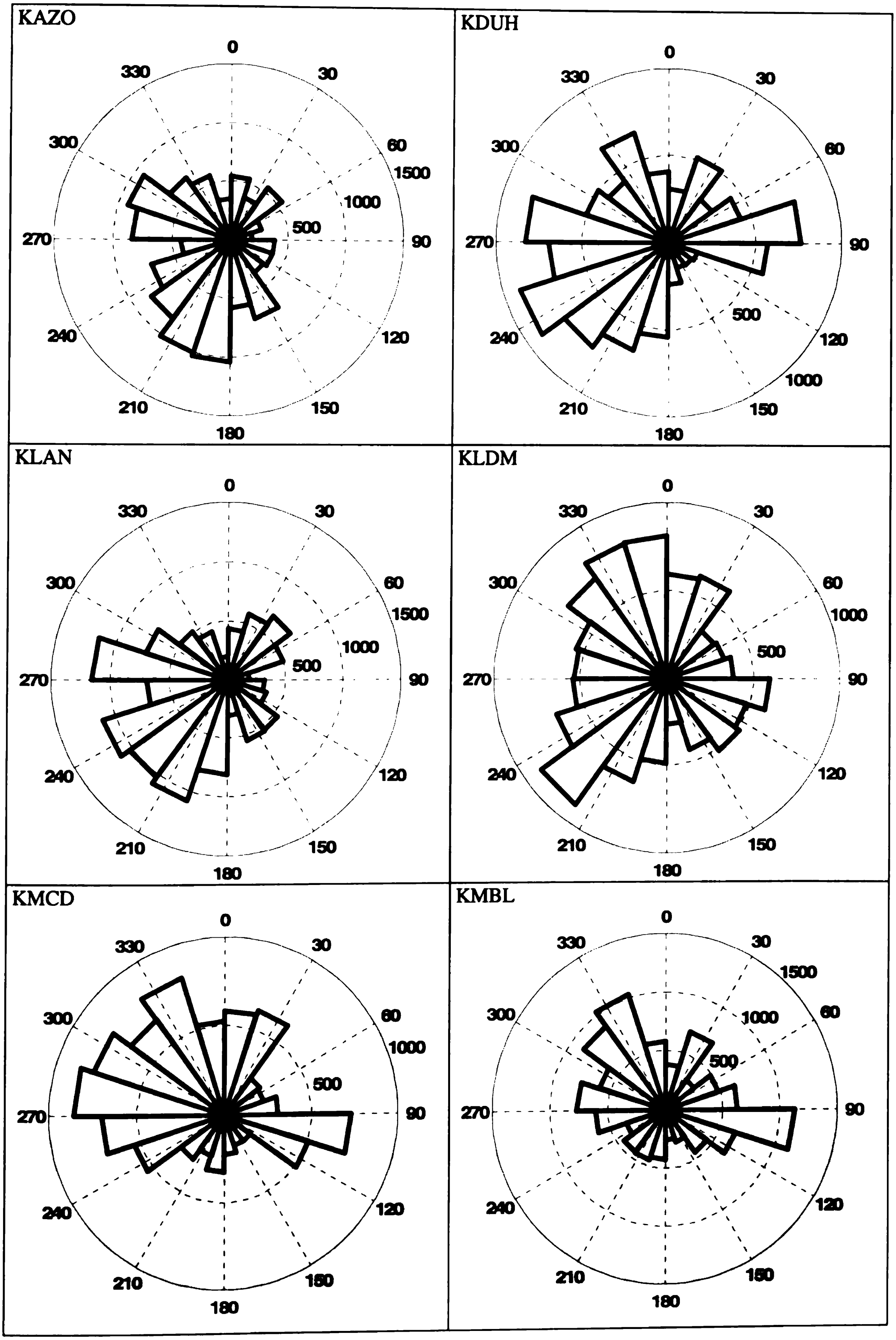
KAZO
0
30
60
90
120
150
180
210
240
270
300
330
500
1000
1500
KDUH
0
30
60
90
120
150
180
210
240
270
300
330
500
1000
KLAN
0
30
60
90
120
150
180
210
240
270
300
330
500
1000
1500
KLDM
0
30
60
90
120
150
180
210
240
270
300
330
500
1000
KMCD
0
30
60
90
120
150
180
210
240
270
300
330
500
1000
KMBL
0
30
60
90
120
150
180
210
240
270
300
330
500
1000
1500

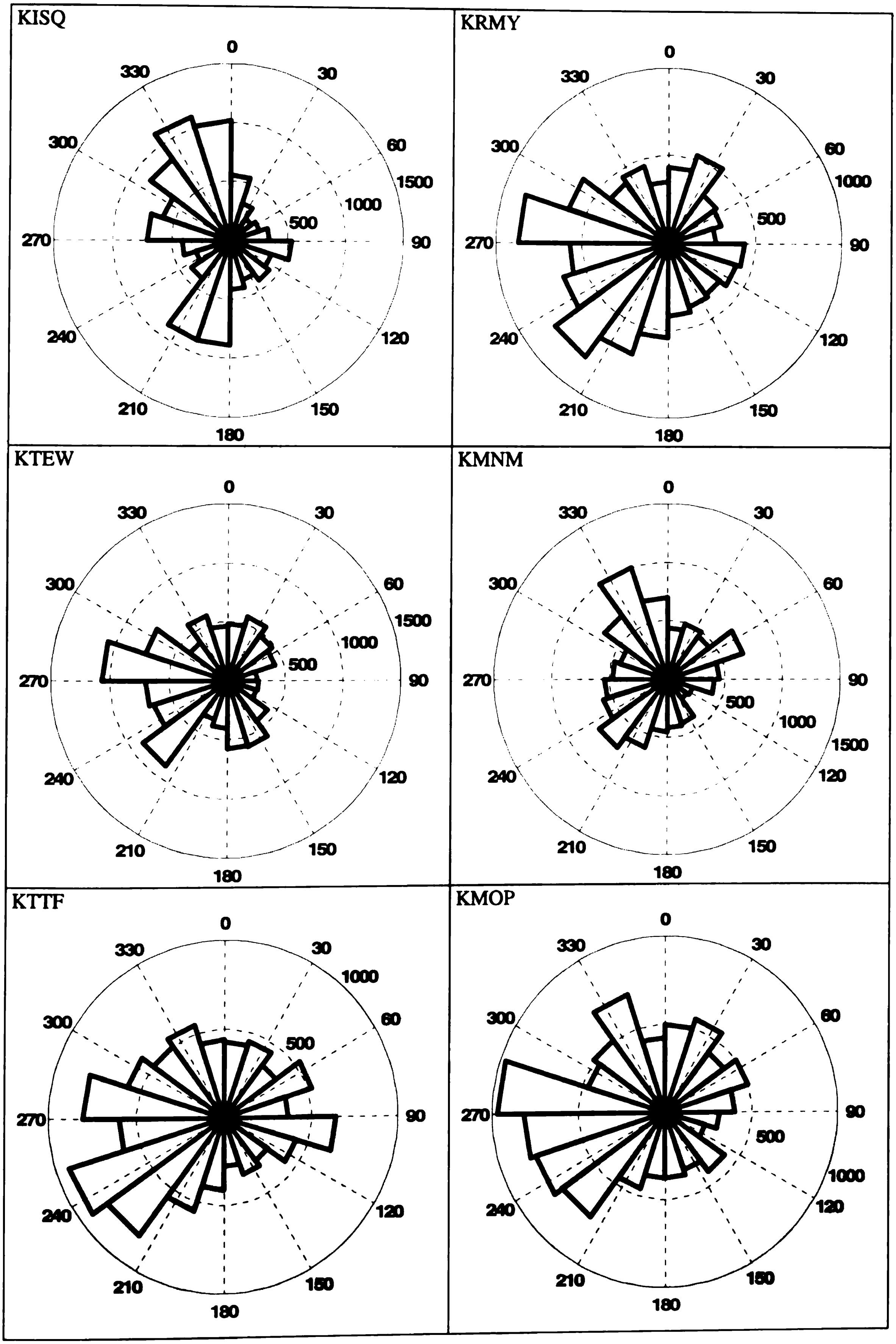
KISQ
0
30
60
90
120
150
180
210
240
270
300
330
500
1000
1500
KRMY
0
30
60
90
120
150
180
210
240
270
300
330
500
1000
KTEW
0
30
60
90
120
150
180
210
240
270
300
330
500
1000
1500
KMNM
0
30
60
90
120
150
180
210
240
270
300
330
500
1000
1500
KTTF
0
30
60
90
120
150
180
210
240
270
300
330
500
1000
KMOP
0
30
60
90
120
150
180
210
240
270
300
330
500
1000

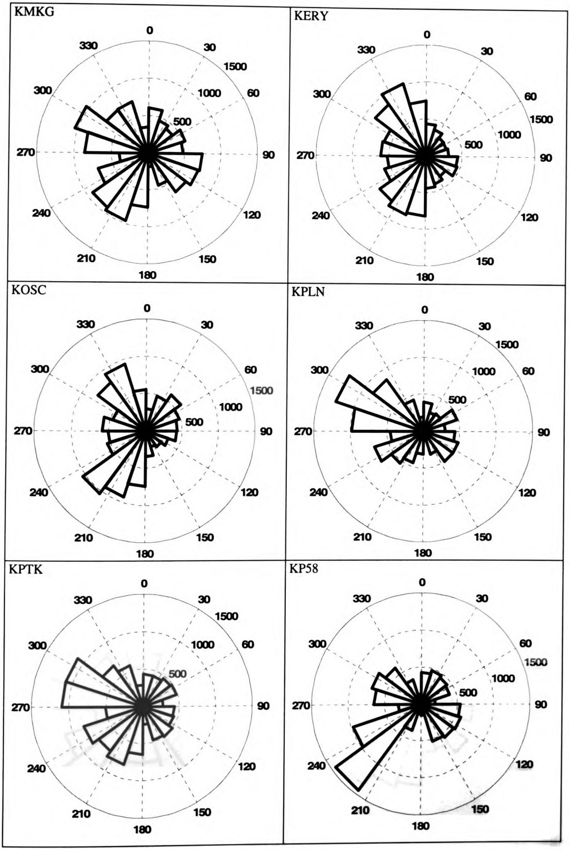
KMKG
KERY
KOSC
KPLN
KPTK
KP58
0
30
60
90
120
150
180
210
240
270
300
330
500
1000
1500

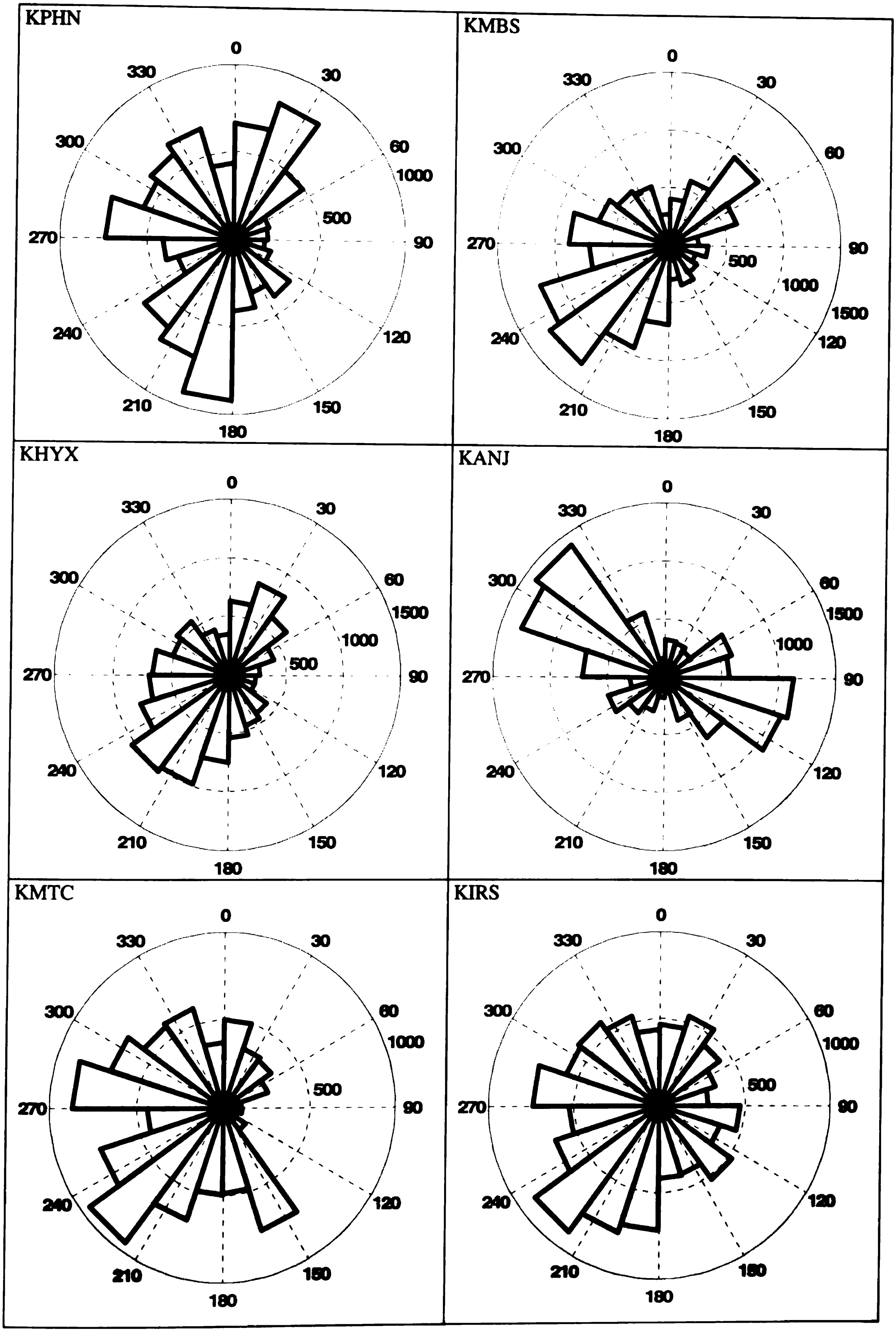
KPHN
0
30
60
1000
500
90
120
150
180
210
240
270
300
330
KMBS
0
30
60
90
500
1000
1500
120
150
180
210
240
270
300
330
KHYX
0
30
60
1500
1000
500
90
120
150
180
210
240
270
300
330
KANJ
0
30
60
1500
1000
90
120
150
180
210
240
270
300
330
KMTC
0
30
60
1000
500
90
120
150
180
210
240
270
300
330
KIRS
0
30
60
1000
500
90
120
150
180
210
240
270
300
330

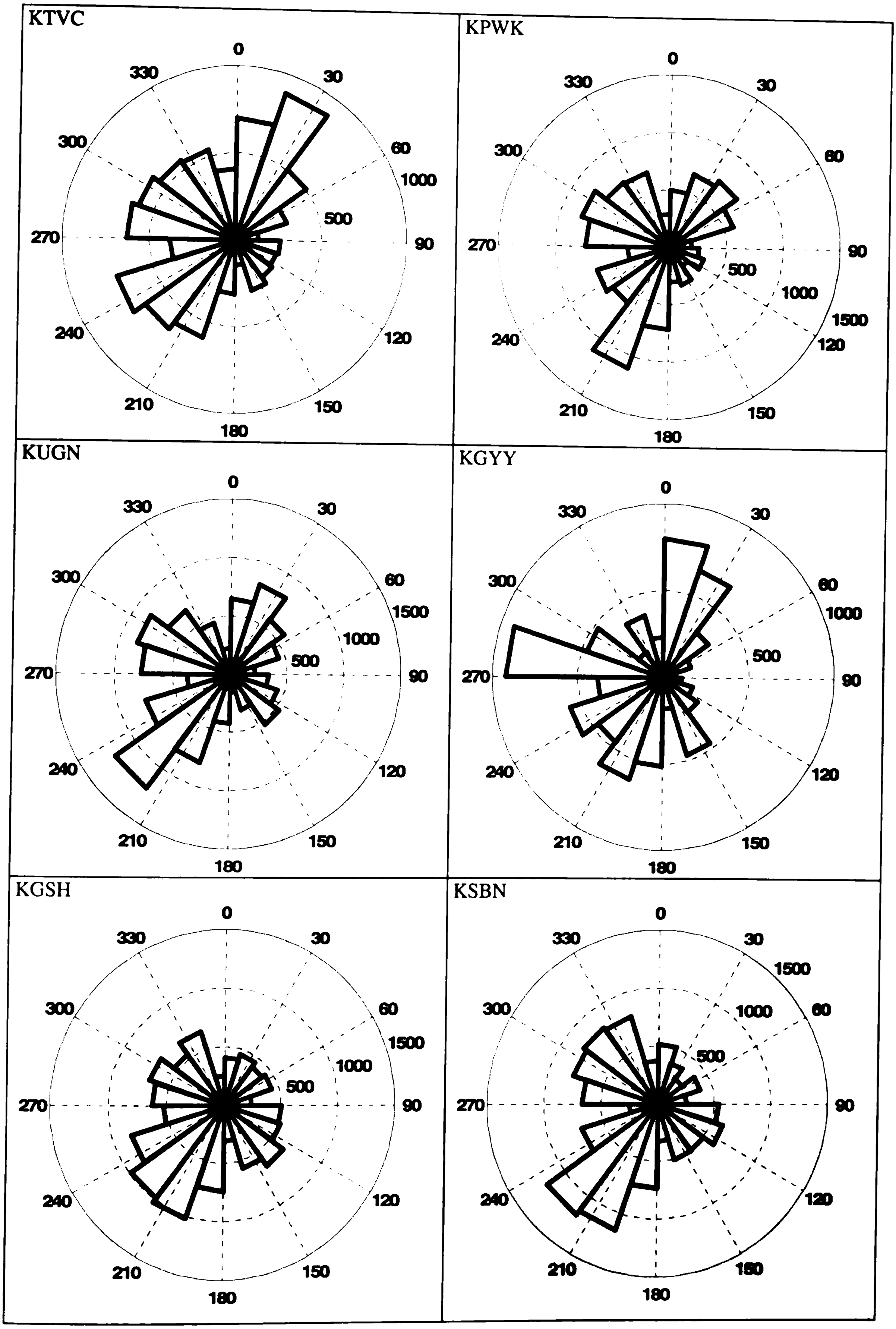
KTVC
0
30
60
90
120
150
180
210
240
270
300
330
500
1000
KPWK
500
1000
1500
KUGN
500
1000
1500
KGYY
500
1000
KGSH
500
1000
1500
KSBN
500
1000
1500

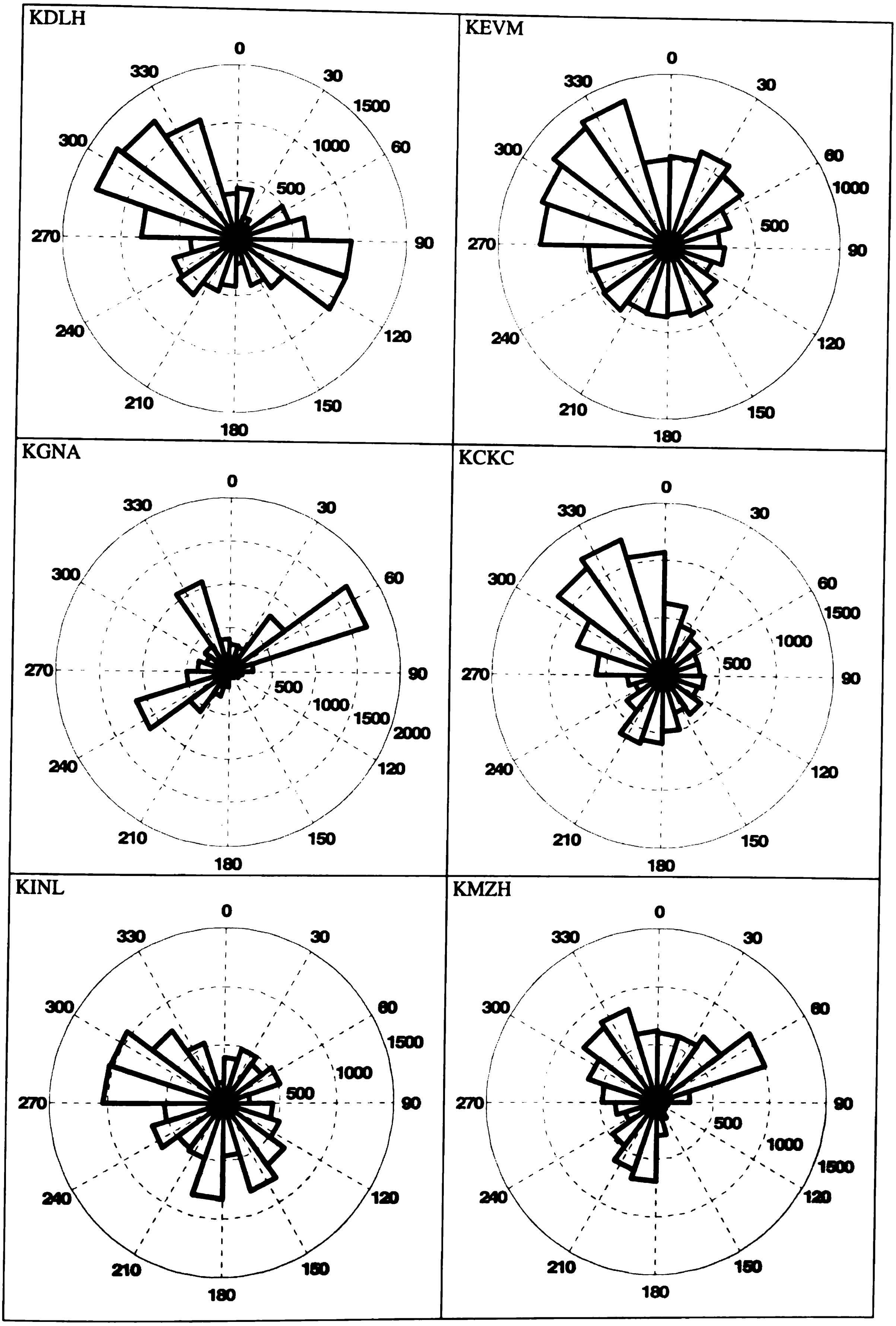
KDLH
0
30
60
90
120
150
180
210
240
270
300
330
500
1000
1500
KEVM
0
30
60
90
120
150
180
210
240
270
300
330
500
1000
KGNA
0
30
60
90
120
150
180
210
240
270
300
330
500
1000
1500
2000
KCKC
0
30
60
90
120
150
180
210
240
270
300
330
500
1000
1500
KINL
0
30
60
90
120
150
180
210
240
270
300
330
500
1000
1500
KMZH
0
30
60
90
120
150
180
210
240
270
300
330
500
1000
1500

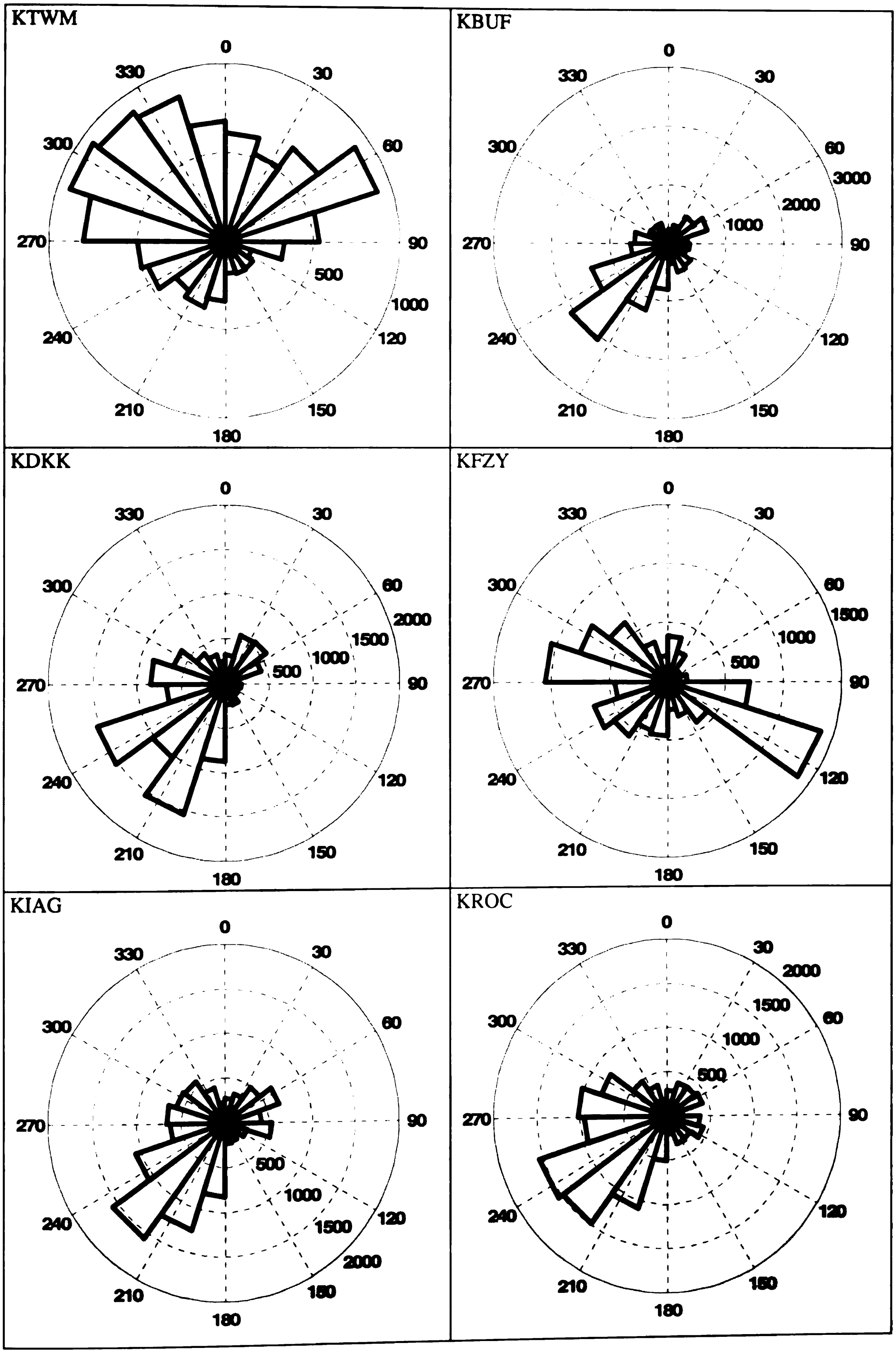
KTWM
0
330
30
300
60
270
90
500
1000
240
120
210
150
180
KBUF
0
330
30
300
60
3000
2000
1000
270
90
240
120
210
150
180
KDKK
0
330
30
300
60
2000
1500
1000
500
270
90
240
120
210
150
180
KFZY
0
330
30
300
60
1500
1000
500
270
90
240
120
210
150
180
KIAG
0
330
30
300
60
270
90
500
1000
1500
2000
240
120
210
150
180
KROC
0
330
30
2000
1500
300
60
1000
500
270
90
240
120
210
150
180

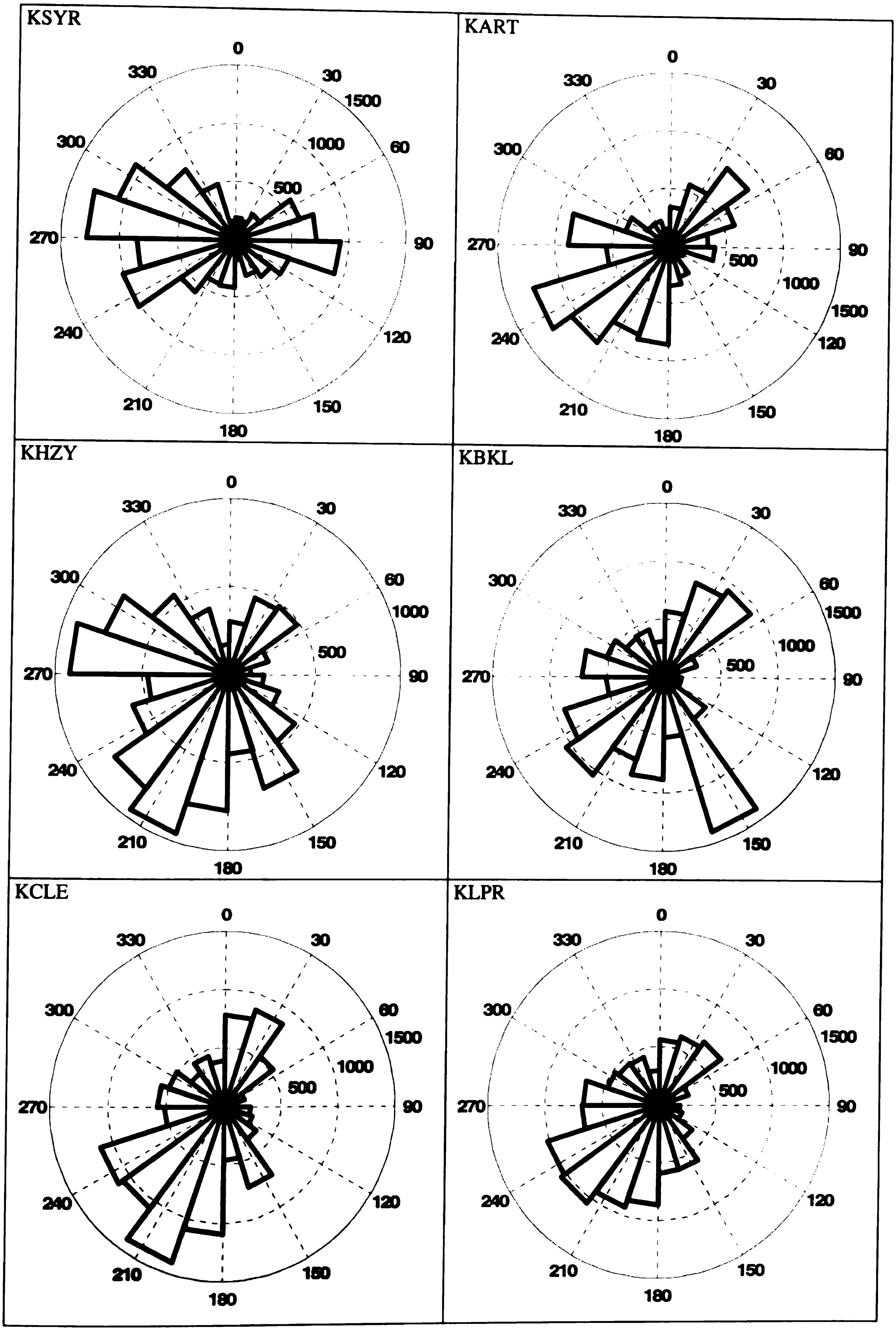
KSYR
0
30
60
90
120
150
180
210
240
270
300
330
500
1000
1500
KART
0
30
60
90
120
150
180
210
240
270
300
330
500
1000
1500
KHZY
0
30
60
90
120
150
180
210
240
270
300
330
500
1000
KBKL
0
30
60
90
120
150
180
210
240
270
300
330
500
1000
1500
KCLE
0
30
60
90
120
150
180
210
240
270
300
330
500
1000
1500
KLPR
0
30
60
90
120
150
180
210
240
270
300
330
500
1000
1500

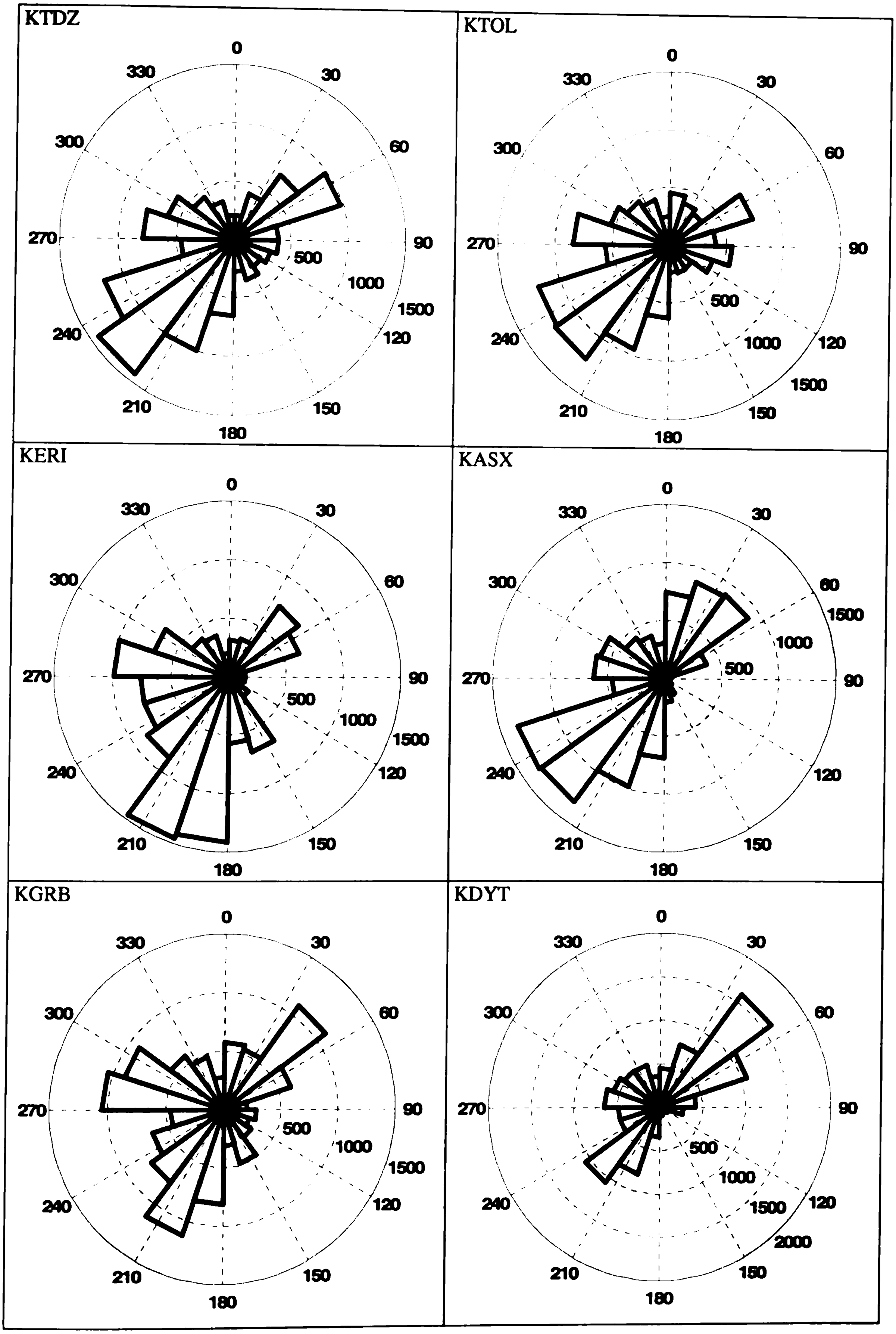
KTDZ
KTOL
KERI
KASX
KGRB
KDYT
0
30
60
90
120
150
180
210
240
270
300
330
500
1000
1500
2000

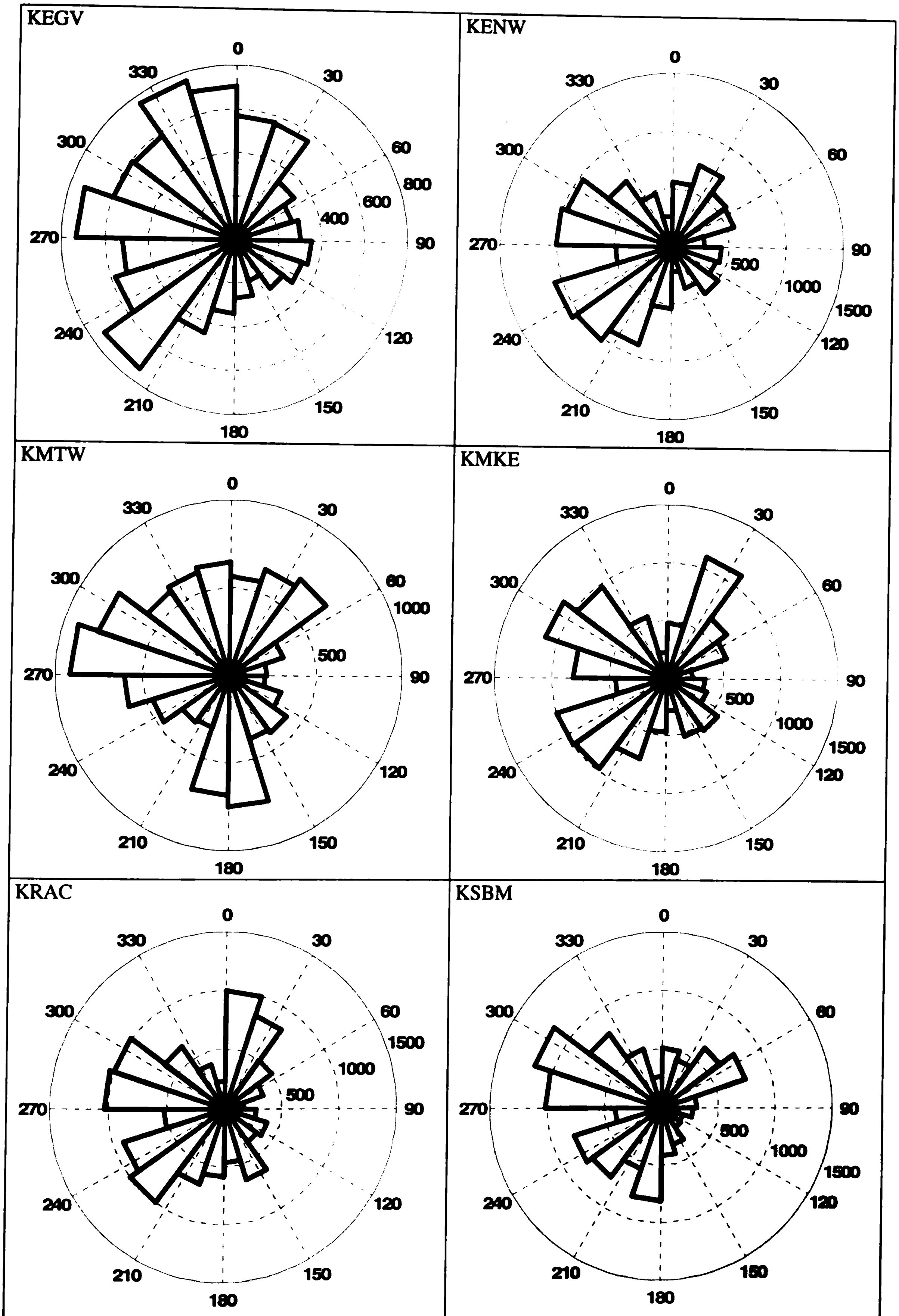
KEGV
0
30
60
90
120
150
180
210
240
270
300
330
400
600
800
KENW
0
30
60
90
120
150
180
210
240
270
300
330
500
1000
1500
KMTW
0
30
60
90
120
150
180
210
240
270
300
330
500
1000
KMKE
0
30
60
90
120
150
180
210
240
270
300
330
500
1000
1500
KRAC
0
30
60
90
120
150
180
210
240
270
300
330
500
1000
1500
KSBM
0
30
60
90
120
150
180
210
240
270
300
330
500
1000
1500

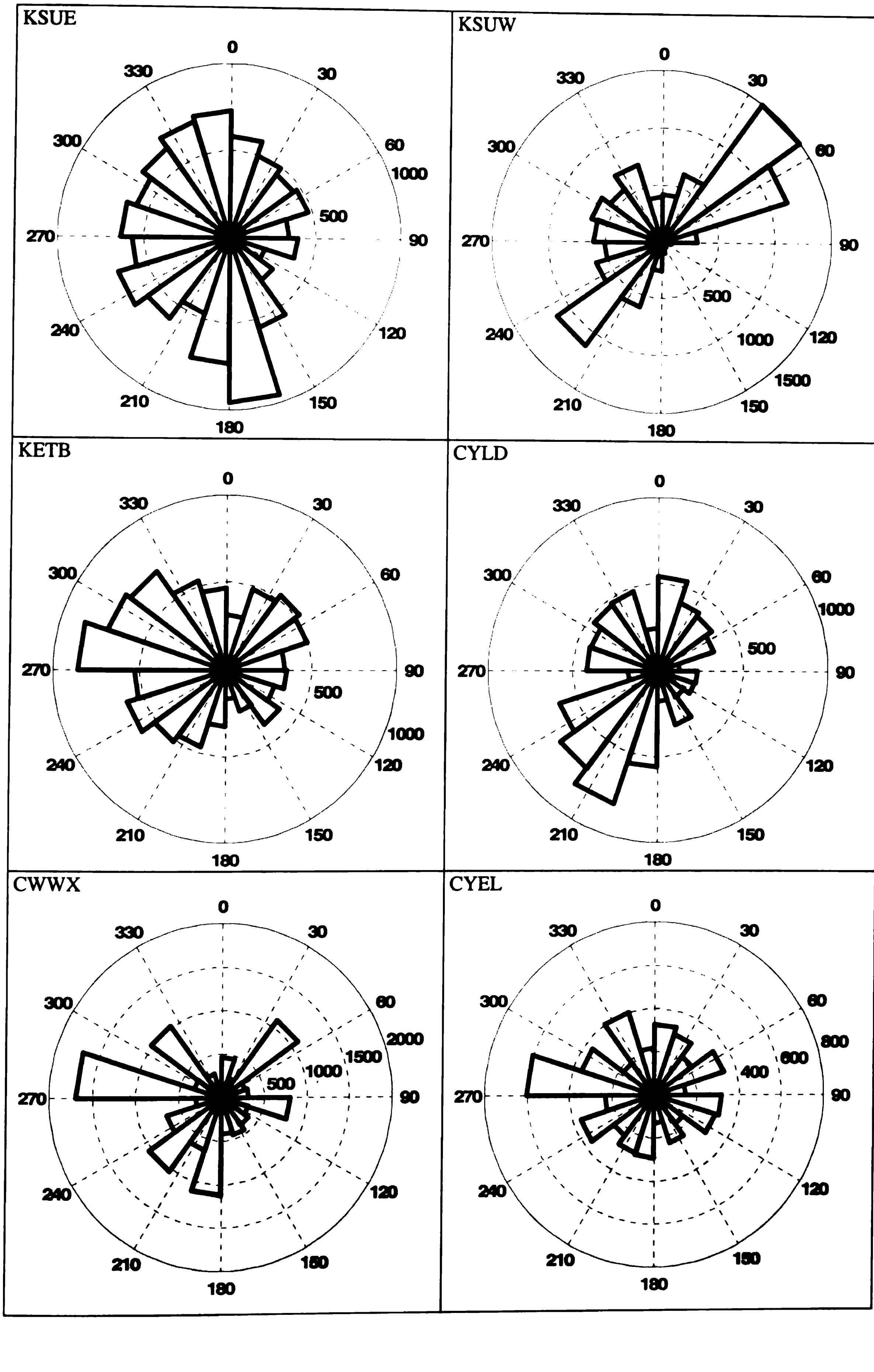
KSUE
KSUW
KETB
CYLD
CWWX
CYEL
0
30
60
90
120
150
180
210
240
270
300
330
500
1000
1500
2000
400
600
800

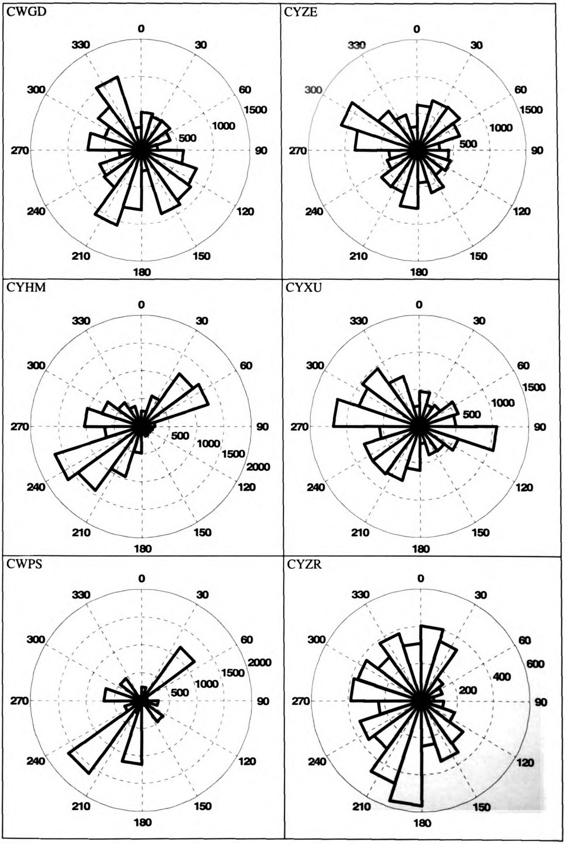
CWGD
0
30
60
90
120
150
180
210
240
270
300
330
500
1000
1500
CYZE
0
30
60
90
120
150
180
210
240
270
300
330
500
1000
1500
CYHM
0
30
60
90
120
150
180
210
240
270
300
330
500
1000
1500
2000
CYXU
0
30
60
90
120
150
180
210
240
270
300
330
500
1000
1500
CWPS
0
30
60
90
120
150
180
210
240
270
300
330
500
1000
1500
2000
CYZR
0
30
60
90
120
150
180
210
240
270
300
330
200
400
600

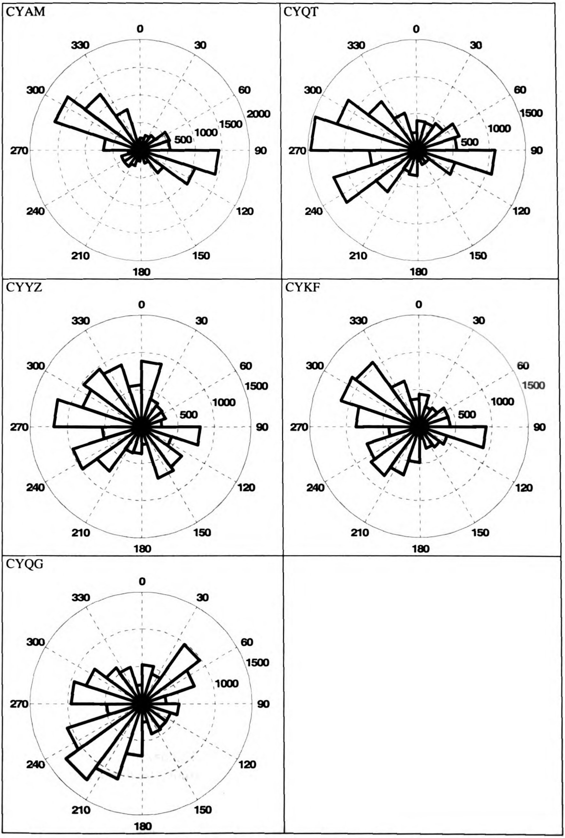
CYAM
0
30
60
90
120
150
180
210
240
270
300
330
500
1000
1500
2000
CYQT
0
30
60
90
120
150
180
210
240
270
300
330
500
1000
1500
CYYZ
0
30
60
90
120
150
180
210
240
270
300
330
500
1000
1500
CYKF
0
30
60
90
120
150
180
210
240
270
300
330
500
1000
1500
CYQG
0
30
60
90
120
150
180
210
240
270
300
330
1000
1500

REFERENCES

Adams, J. and D. Vos, 2002: Small college supercomputing: building a Beowulf cluster at a comprehensive college. *Sigcse Bulletin*, **34**, 411-415.

Al-Alawy, I.T. and A.Y. Mohammed, 1985: A mathematical model of wind energy for selected locations in Iraq. *Solar and Wind Technology*, **1**, 187 – 191.

Alexiadis, M.C., P.S. Dokopoulos, H.S. Sahsamanoglou and I.M. Manousaridis, 1998: Short-term forecasting of wind speed and related electrical power. *Solar Energy*, **63**, 61 – 68.

Alexiadis, M.C., P.S. Dokopoulos and H.S. Sahsamanoglou, 1999: Wind speed and power forecasting based on spatial correlation models. *IEEE Transactions on Energy Conversion*, **14**, 836 – 842.

All Weather, 2004: *International AWOS Technical Description.* All Weather, Inc., Sacramento, CA, 28 p.

Anderson, T.W. and D.A. Darling, 1954: A test of goodness of fit. *American Statistical Association Journal*, **49**, 765 - 769.

Arya, S.P., 2001: *Introduction to Micrometeorology.* Academic Press, San Diego, 450 p.

AWEA (American Wind Energy Association), 2002: The Economics of Wind Energy. American Wind Energy Association, On-line document: http://www.awea.org/pubs/factsheets/EconomicsofWind-March2002.pdf.

AWEA (American Wind Energy Association), 2004a: Global Outlook 2004. American Wind Energy Association, On-line document: http://www.awea.org/pubs/documents/globalmarket2004.pdf

AWEA (American Wind Energy Association), 2004b: Windpower Outlook 2004. American Wind Energy Association, On-line document: http://www.awea.org/pubs/documents/Outlook2004.pdf

Ayotte, K.W., R.J. Davy and P.A. Coppin, 2001: A simple temporal and spatial analysis of flow in complex terrain in the context of wind energy modelling. *Boundary-Layer Meteorology*, **98**, 275 – 295.

Baker, R.W., E.W. Hewson, N.G. Butler and E.J. Warchol, 1979: Wind power potential in the Pacific Northwest. *Journal of Applied Meteorology*, **17**, 1814 - 1826.

Bardsley, W.E., 1980: Note on the use of the inverse Gaussian distribution for wind energy applications. *Journal of Applied Meteorology*, **19**, 1126 – 1130.

Barros, V.R. and E.A. Estevan, 1983: On the evaluation of wind power from short wind records. *Journal of Climate and Applied Meteorology*, **22**, 1116 – 1123.

Barthelmie, R.J., B. Lange, and M. Nielsen, 1999: *Wind Resources at Rødsand and Omø Stålgrunde*. Report Risø-I-1456(EN). Risø National Laboratory, Roskilde, DK. 96 p.

Barthelmie, R.J. and S.C. Pryor, 2003: Can satellite sampling of offshore wind speeds realistically represent wind speed distributions? *Journal of Applied Meteorology*, **42**, 83 - 94.

Bayley, G.V. and J.M. Hammersley, 1946: The effective number of independent observations in an autocorrelated time series. *Journal of the Royal Statistical Society*, **8**, 184-197.

Beck, M.B., A.J. Jakeman, and M.J. McAleer, 1993: Construction and evaluation of models of environmental systems. In *Modelling Change in Environmental Systems.* Jakeman, A.J., M.B. Beck, and M.J. McAleer, eds. John Wiley and Sons, New York. pp. 3 - 35.

Beljaars, A.C.M., 1987: The influence of sampling and filtering on measured wind gusts. *Journal of Atmospheric and Oceanic Technology*, **4**, 613 - 626.

Betz, A, 1926: Wind-Energie und ihre Ausnutzung durch Windmühlen, Bandenhoeck & Ruprect, Göttingen 1926. Facsimile edition by Ökobuch Verlag, Staufen, 1994.

Beyer, H.G. and K. Nottebaum, 1995: Synthesis of long-term hourly wind speed time series on the basis of European Wind Atlas data. *Solar Energy*, **54**, 351 - 355.

Birnbaum, Z.W., 1953: Distribution-free tests of fit for continuous distribution functions. *Annals of Mathematical Statistics*, **24**, 1-8.

Box, G.E.P. and G. Jenkins, 1976: *Time Series Analysis: Forecasting and Control.* Holden-Day, San Francisco, 575 p.

Brett, A.C. and S.E. Tuller, 1991: The autocorrelation of hourly wind speed observations. *Journal of Applied Meteorology*, **30**, 823 – 833.

Brown, B.G., Katz, R.W. and A.H. Murphy, 1981: An evaluation of statistical distributions of wind power. *Preprints, 7th Conference on Probability and Statistics in the Atmospheric Sciences*, American Meteorological Society, 142-147.

Brown, B.G., R.W. Katz and A.H. Murphy, 1984: Time series models to simulate and forecast wind speed and wind power. *Journal of Climate and Applied Meteorology*, **23**, 1184 – 1195.

Buckley, B.W. and L.M. Leslie, 2000: The Australian Boxing Day storm of 1998 - Synoptic description and numerical simulations. *Weather and Forecasting*, **15**, 543 - 558.

Carlin, J. and J. Haslett, 1982: The probability distribution of wind power from a dispersed array of wind turbine generators. *Journal of Applied Meteorology*, **21**, 303 – 313.

Celik, A.N., 2003: Energy output estimation for small-scale wind power generators using Weibull-representative wind data. *Journal of Wind Engineering and Industrial Aerodynamics*, **91**, 693 – 707.

Charney, J.J., X. Bian, B.E. Potter, and W.E. Heilman, 2003: The role of a stratospheric intrusion in the evolution of the Double Trouble State Park wildfire. *Proceedings 5th Symposium on fire and forest meteorology*. American Meteorological Society, Orlando, FL. P5.3.

Chorley, R.J. and P. Haggett, 1965: Trend-surface mapping in geographical research. *Transactions Institute of British of British Geographers*, **37**, 47-67.

Chou, K.C. and R.B. Corotis, 1981: Simulation of hourly wind speed and array wind power. *Solar Energy*, **26**, 199 – 212.

Colle, B. A., K. J. Westrick, and C. F. Mass, 1999: Evaluation of MM5 and Eta-10 precipitation forecasts over the Pacific Northwest during the cool season, *Weather and Forecasting*, **14**, 137 - 154.

Conrad, V. and L.W. Pollack, 1962: *Methods in Climatology*. Harvard University Press, Cambridge, MA. 459 pp.

Conradsen, K.L.B., L.B. Nielsen and L.P. Prahm, 1984: Review of Weibull statistics for estimation of wind speed distributions. *Journal of Climate and Applied Meteorology*, **23**, 1173 - 1183.

Corotis, R.B., A.B. Sigl and M. Cohen, 1977: Variance analysis of wind characteristics for energy conversion. *Journal of Applied Meteorology*, **16**, 1149 - 1157.

Corotis, R.B., A.B. Sigl and J. Klein, 1978: Probability models of wind velocity and persistence. *Solar Energy*, **20**, 483 - 493.

Conradsen, K., L.B. Nielsen, and L.P. Prahm, 1984: Review of Weibull statistics for estimation of wind speed distributions. *Journal of Climate and Applied Meteorology*, **23**, 1173 - 1183.

Counihan, J., 1975: Adiabatic atmospheric boundary layers: A review and analysis of data from the period 1880-1972. *Atmospheric Environment*, **9**, 871 - 905.

Crutcher, H.L. and L. Baer, 1962: Computations from elliptical wind distribution statistics. *Journal of Applied Meteorology*, **14**, 1512 - 1520.

Cressie, N.A.C., 1993: *Statistics for Spatial Data.* John Wiley & Sons, New York, 900 p.

Davenport, A.G., 1963: The relationship of wind structure to wind loading. *Proceedings Conference on Wind Effects on Structures.* London, UK.

Davis, J.C., 1986: *Statistics and Data Analysis in Geology.* John Wiley and Sons, New York. 646 p.

De Rooy, W.C. and K. Kok, 2004: A combined physical – statistical approach for the downscaling of model wind speed. *Weather and Forecasting*, **19**, 485 – 495.

Derrick, A., 1992: Development of the measure-correlate-predict strategy for site assessment. In *Wind Energy Conversion 1992.* B.R. Clayton, ed. Mechanical Engineering Publications. London, pp. 259 - 265.

Diab, R.D. and M. Garstang, 1984: Assessment of wind power potential for two contrasting coastlines of South Africa using a numerical model. *Journal of Climate and Applied Meteorology*, **23**, 1645 - 1659.

Dinkelacker, O, 1949: Über spezielle Windverteilungsfunktionen. *Wetter und Klima*, **2**, 129 - 138.

Dodge, D.M., 2002: Illustrated History of Wind Power Development. On-line document: http://telosnet.com/wind/.

Draxler, R.R., 1990: The calculation of low-level winds from the archived data of a regional primitive equation forecast model. *Journal of Applied Meteorology*, **29**, 240 - 248.

Dudhia, J., 1989: Numerical study of convection observed during winter monsoon experiment using a Mesoscale two-dimensional model. *Journal of Atmospheric Science*, **46**, 3077 - 3107.

Dudhia, J. 2004: The weather research and forecast model version 2.0: Physics update. *Proc. 5th WRF / 14th MM5 Users' Workshop.* National Centers for Atmospheric Research, Boulder, CO. 1.1

Dukes, M.D.G. and J.P. Palutikof, 1995: Estimation of extreme wind speeds with very long return periods. *Journal of Applied Meteorology*, **34**, 1950 – 1961.

DWIA (Danish Wind Industry Association), 2003: History of Wind Turbines. Danish Wind Industry Association, On-line document: http://www.windpower.org/en/pictures/index.htm

Efron, B. and G. Gong, 1983: A leisurely look at the bootstrap, the jackknife, and cross-validation. *The American Statistician*, **37**, 36-48.

Eichenlaub, V., 1979: *Weather and Climate of the Great Lakes Region*. University of Notre Dame Press, South Bend. 335 p.

Eichenlaub, V.L., J.R. Harman, F.V. Nurnberger and H.J. Stolle, 1990: *The Climatic Atlas of Michigan*. University of Notre Dame Press, South Bend. 165 pp.

Eidsvik, K.J., 1981: Estimation of time series models for horizontal wind on the Norwegian west coast. *Wind Engineering*, **2**, 66 – 72.

Elliott, D.L., C.G. Holladay, W.R., Barchet, H.P. Foote and W.F. Sandusky, 1987: *Wind Energy Resource Atlas of the United States*. Solar Energy Research Institute, Golden, CO. 210 pp.

EWEA (European Wind Energy Association) and Greenpeace, 2002: Wind Force 12: A Blueprint to Achieve 12% of the World's Electricity from Wind Power by 2020. 50 p. Online document: http://www.ewea.org/doc/WindForce12.pdf

FAA (Federal Aviation Administration), 1999: *Aeronautical Information Manual / Federal Aviation Regulations*. C.F. Spence, Ed., McGraw-Hill, New York, 780 p.

Feller, W., 1966: *An Introduction to Probability Theory and Its Applications. Vol. 2.* John Wiley and Sons. 669 pp.

Fiedler, F. and H.A., Panofsky, 1970: Atmospheric scales and spectral gaps. *Bulletin of the American Meteorological Society*, **51**, 1114 – 1119.

Fillibin, J.J. and A. Heckert, 2003: Exploratory Data Analysis. In *NIST/SEMATECH e-Handbook of Statistical Methods*. C. Croarkin and P. Tobias, eds. National Institute of Standards and Technology, Washington, D.C., On-line: http://www.itl.nist.gov/div898/handbook/.

Filtenborg, M, 2004: New product programme matches the wishes and demands of the market. *VestasGlobal*, **2**, 8-10.

Finzi, G., P. Bonelli and G. Bacci, 1984: A stochastic model of surface wind speed for air quality control purposes. *Journal of Climate and Applied Meteorology*, **23**, 1354 – 1361.

Fox, D.G., 1981: Judging air quality model performance. *Bulletin American Meteorological Society*, **62**, 599-609.

Frank, H.P. and L. Landberg, 1997: Modelling the wind climate of Ireland. *Boundary-Layer Meteorology*, **85**, 359 - 378.

Frank, H.P., O. Rathmann, N.G. Mortensen and L. Landberg, 2001: *The Numerical Wind Atlas – the KAMM/WAsP method.* Risø-R-1252(EN), Roskilde, 60 p.
Online document: http://www.risoe.dk/rispubl/VEA/ris-r-1252.htm

Fritschen, L.J. and L.W. Gay, 1979: *Environmental Instrumentation.* Springer-Verlag, NY. 209 p.

Garcia-Rojo, R., 2004: Algorithm for the estimation of the long-term wind climate at a meteorological mast using a joint probabilistic approach. *Wind Engineering*, **28**, 213-224.

Geiger, R., P. Todhunter, R.H. Aron, 1995: *Climate Near the Ground.* Informatica International, 600 p.

Gerdes, G. and M. Strack, 1999: Long-term correlation of wind measurement data. *DEWI Magazin*, **15**, 18 – 24.

Gerrity, J.P., T.L. Black, and R.E. Treadon, 1994: The numerical solution of the Mellor-Yamada Level 2.5 turbulent kinetic energy equation in the Eta model. Monthly Weather Review, 122, 1640-1646.

Goh, T.N. and G.K. Nathan, 1979: A statistical methodology for study of wind characteristics from a close array of stations. *Wind Engineering*, **3**, 197 – 206.

Goh, T.N . and P.S. Eu, 1986: Some practical aspects of wind speed time component analysis. *Wind Engineering*, **10**, 190 – 195.

Golding, E.W., 1955: *The Generation of Electricity by Wind Power.* Philosophical Library, 332 p.

Goodin, W.R., G.J. McRae and J.H. Seinfeld, 1979: A comparison of interpolation methods for sparse data: Application to wind and concentration fields. *Journal of Applied Meteorology*, **18**, 761 - 771.

Gunn, D.M. and D.F. Furmage, 1976: The effect of topography on surface wind. *Meteorological Magazine*, **105**, 8 – 23.

Gunst, R.F., 1995: Estimating spatial correlations from spatial-temporal meteorological data. *Journal of Climate*, **8**, 2454 – 2470.

Haagenson, P.L., J. Dudhia, D.R. Stauffer and G.A. Grell, 1994: *The Penn State/NCAR Mesoscale Model (MM5) Source Code Documentation.* NCAR Technical Note NCAR/TN-392 + STR, March, 1994. On-line:
http://www.mmm.ucar.edu/mm5/documents/mm5-code-doc-pdf.html

Hannah, P., J.P. Palutikof and C.P. Quine, 1992: The use of statistical modelling techniques in the prediction of windspeed time-series. In *Wind Energy Conversion 1992.* B.R. Clayton, ed. Mechanical Engineering Publications. London. Pp. 267-273.

Hannah, P., P. Rainbird, J. Palutikof, and K. Shein, 1996: *Prediction of Extreme Wind Speeds at Wind Energy Sites.* Report ETSU W/11/00427/REP. UK Department of Trade and Industry, Energy Technology Support Unit., London. 250 p.

Hansen, M.O.L, 2000: *Aerodynamics of Wind Turbines, Rotors, Loads and Structure.* James & James Ltd., London. 152 p.

Harman, J.R., 1987: Mean monthly North American anticyclone frequencies, 1950 - 79. *Monthly Weather Review*, **115**, 2840 - 2848.

Haslett, J. and A.E. Raftery, 1989: Space-time modelling with long-memory dependence: Assessing Ireland's wind power resource. *Applied Statistics*, **38**, 1 – 50.

Heilman, W.E., B.E. Potter, J.J. Charney, and X. Bian, 2003: National fire plan – Eastern Area Modeling Consortium: Research, product development, and partnerships. *Proceedings 5th Symposium on fire and forest meteorology.* American Meteorological Society, Orlando, FL. J12.6.

Henderson-Sellers, A. and K. McGuffie, 1997: Climate Models. In *Applied Climatology: Principles and Practice.* Thompson, R.D. and A. Perry, Eds., Routledge, New York. pp. 36-50.

Hennessey, J.P., 1977: Some aspects of wind power statistics. *Journal of Applied Meteorology*, **16**, 119 - 128.

Hewson, E.W., 1975: Generation of power from the wind. *Bulletin American Meteorological Society*, **56**, 660 - 675.

Holton, J.R., 1979: *An Introduction to Dynamic Meteorology, 2nd ed.*. Academic Press, NY. 391 p.

IEA (International Energy Agency), 2001: *Long-term Research and Development Needs for Wind Energy for the Time Frame 2000 to 2020.* IEA R&D Wind Executive Committee. 12 p. On-line document: http://www.afm.dtu.dk/wind/iea/.

In, H.-J., S. Zhong, X. Bian, J. Charney, W. Heilman, and B. Potter, 2004: Evaluation of real-time high-resolution MM5 predictions over the Great Lakes region. *Proceedings 5th WRF / 14th MM5 Users' Workshop.* National Centers for Atmospheric Research, Boulder, CO. 3.2

Julian, P.R. and H.J. Thiebaux, 1975: On some properties of correlation functions used in optimum interpolation schemes. *Monthly Weather Review*, **103**, 605 – 616.

Justus, C.G., W.R. Hargraves, and A. Yalcin, 1976: Nationwide assessment of potential output from wind powered generators. *Journal of Applied Meteorology*, **15**, 673 - 678.

Justus, C.G., W.R. Hargraves, A. Mikhail and D. Graber, 1978: Methods for estimating wind speed frequency distributions. *Journal of Applied Meteorology*, **17**, 350 – 353.

Justus, C.G., K. Mani and A.S. Mikhail, 1979: Interannual and month-to-month variations of wind speed. *Journal of Applied Meteorology*, **18**, 913-920.

Kaganov, E.I. and A.M. Yaglom, 1976: Errors in wind speed measurements by rotation anemometers. *Boundary-Layer Meteorology*, **10**, 1-11.

Kain, J.S. and J.M. Fritch, 1990: A one-dimensional entraining/detraining plume model and its aoolication in convective parameterization. *Journal of Atmospheric Science*, **47**, 2784 - 2802.

Kaminsky, F.C., R.H. Kirchoff, C.Y. Syu and J.F. Manwell, 1991: A comparison of alternative approaches for the synthetic generation of a wind speed time series. *Journal of Solar Energy Engineering*, **113**, 280 – 289.

Kariniotakis, G.N., G.S. Stavrakakis and E.F. Nogaret, 1996: Wind power forecasting using advanced neural network models. *IEEE Transactions on Energy Conversion*, **11**, 762 – 767.

Katz, R.W. and R.H. Skaggs, 1981: On the use of autoregressive-moving average processes to model meteorological time series. *Monthly Weather Review*, **109**, 479 – 484.

Klink, K., 1999: Climatological mean and interannual variance of United States surface wind speed, direction and velocity. *International Journal of Climatology*, **19**, 471-488.

Kretzschmar, R., P. Eckert and D. Cattani, 2004: Neural network classifiers for local wind prediction. *Journal of Applied Meteorology*, **43**, 727 – 738.
Kristensen, L., 1999: The perennial cup anemometer. *Wind Energy*, **2**, 59-75.

Kristensen, L., 2002: Can a cup anemometer 'underspeed'? *Boundary-Layer Meteorology*, **103**, 163-172.

Landberg, L., 1998: Short-term prediction of power production from wind farms. *Journal of Wind Engineering and Industrial Aerodynamics*, **80**, 207-220.

Landberg, L., 2001: Short-term prediction of local wind conditions. *Journal of Wind Engineering and Industrial Aerodynamics*, **89**, 235-245.

Lewis, P.A.W., 1961: Distribution of the Anderson-Darling statistic. *Annals of Mathematical Statistics*, 32, 1118-1124.

Lun, I.Y.F. and J.C. Lam, 2000: A study of Weibull parameters using long-term wind observations. *Renewable Energy*, **20**, 145 – 153.

Luna, R.E. and H.W. Church, 1974: Estimation of long-term concentrations using a "Universal" wind speed distribution. *Journal of Applied Meteorology*, **13**, 910 - 916.

Mass, C.F., D. Ovens, K. Westrick, B.A. Colle, 2002: Does increasing horizontal resolution produce more skillful forecasts? *Bulletin American Meteorological Society*, **83**, 407 - 430.

MathWorks, Inc., 2005: *Matlab, Version 5.11.* The MathWorks, Inc. http://www.mathworks.com.

McQueen, J.T., R.R. Draxler and G.D. Rolph, 1995: Influence of grid size and terrain resolution on wind field predictions from an operational mesoscale model. *Journal of Applied Meteorology*, **34**, 2166 - 2181.

McWilliams, B. and D. Sprevak, 1982: Time series models for horizontal wind. *Wind Engineering*, **6**, 219 – 228.

Mellor, G.L. and T. Yamada, 1974: A hierarchy of turbulence closure models for planetary boundary layers. *Journal of Atmospheric Science*, **31**, 1791 - 1806.

Mellor, G.L. and T. Yamada, 1982: Development of a turbulence closure model for geophysical fluid problems. *Review of Geophysical and Space Physics*, **20**, 851 - 875.

Merzouk, N.K., 2000: Wind energy potential of Algeria. *Renewable Energy*, **21**, 553 – 562.

Michalakes, J., J. Dudhia, D. Gill, T. Henderson, J. Klemp, W. Skamarock and W. Wang, 2004: The Weather Research and Forecast model: Software architecture and performance. *Proceedings ECMWF Workshop on the Use of High Performance Computing in Meteorology*. G. Mozdzynski, ed., Reading, UK. 13 p.

Milligan, M., M. Schwartz and Y.Wan, 2003: Statistical wind power forecasting models: Results for U.S. wind farms. *Preprints WINDPOWER 2003*, American Wind Energy Association, Austin, TX, 17 p.

Mortensen, N.G., L. Landberg, I. Troen and E.L. Petersen, 1993: Wind Atlas Analysis and Application program (WAsP), Vol. 2: User's guide. *Technical Report Risø-I-666(EN)(v.2)*, Risø National Laboratory.

Murphy, A.H., 1988: Skill scores based on the mean square error and their relationships to the correlation coefficient. *Monthly Weather Review*, **116**, 2417 – 2424.

National Renewable Energy Laboratory, 1993: *Solar and Meteorological Surface Observation Network 1961-1990.* Version 1.0. NSRDB-Volume 1. Distributed by the National Climatic Data Center, Asheville, NC.

NCDC (National Climatic Data Center), 1994a: *Local Climatological Data: Annual Summaries for 1993 - Part I.* National Climatic Data Center, Asheville, NC.

NCDC (National Climatic Data Center), 1994b: *Local Climatological Data: Annual Summaries for 1993 - Part III.* National Climatic Data Center, Asheville, NC.

NCDC (National Climatic Data Center), 2002: *Data Documentation for Data Set 9767B (DSI-9767B): Master Station History Report.* National Climatic Data Center, Asheville, NC, 20 p.

Nelson, W.B., 1982: *Applied Life Data Analysis.* John Wiley and Sons, NY. 656 p.

Neumann, J. and S. Parpola, 1983: Wind vanes in ancient Mesopotamia, about 2000 to 1500 B.C.. *Bulletin American Meteorological Society*, **64**, 1141 - 1143.

Nfaoui, H., H. Essiarab and A.A.M. Sayigh, 2004: A stochastic Markov chain model for simulating wind speed time series at Tangiers, Morocco. *Renewable Energy*, **29**, 1407 - 1418.

Nielsen, M., 1999: A method for spatial interpolation of wind climatologies. *Wind Energy*, **2**, 151 – 166.

Nielsen, T.S., A. Joensen, H. Madsen, L. Landberg and G. Giebel, 1998: A new reference for wind power forecasting. *Wind Energy*, **1**, 29 - 34.

NOAA (National Oceanic and Atmospheric Administration), 1998: *Automated Surface Observing System (ASOS) User's Guide.* National Oceanic and Atmospheric Administration, Department of Defense, Federal Aviation Administration, United States Navy, Washington, D.C., 72 p.

NOAA (National Oceanic and Atmospheric Administration), 2000: *ASOS Site Technical Manual.* Chapter 4, Sec. 1: Wind Sensor Description and Leading Particulars. U.S. Department of Commerce, National Oceanic and Atmospheric Administration. Washington, D.C., 4 p.

NOAA (National Oceanic and Atmospheric Administration), 2001: *The United States Detailed National Report on Systematic Observations for Climate: United States Global Climate Observing System (U.S.-GCOS) Program.* U.S. Department of Commerce, National Oceanic and Atmospheric Administration, Washington, D.C., 158 p.

NOAA (National Oceanic and Atmospheric Administration), 2003: *Automated Surface Observing System (ASOS): Release Note: Software version – 2.7A: Replacement wind sensor (Vaisala 425 Ice-Free Wind Sensor).* U.S. Department of Commerce, National Oceanic and Atmospheric Administration, 21 p.

OFCM (Office of the Federal Coordinator for Meteorological Services and Supporting Research), 1994: *Federal Standards for Siting Meteorological Sensors at Airports.* Report FCM-S4-1994. U.S. Department of Commerce, National Oceanic and Atmospheric Administration, Office of the Federal Coordinator for Meteorological Services and Supporting Research, Washington, D.C., On-line document: http://www.ofcm.gov/siting/text/a-cover.htm.

OFCM (Office of the Federal Coordinator for Meteorological Services and Supporting Research), 1995: *Federal Meteorological Handbook No. 1: Surface Weather Observations and Reports.* Report FCM – H1 – 1995. U.S. Department of Commerce, National Oceanic and Atmospheric Administration, Office of the Federal Coordinator for Meteorological Services and Supporting Research, Washington, D.C., 94 p.

Oke, T.R., 1988: *Boundary Layer Climates.* Routledge, NY, 450 pp.

Palomino, I. and F. Martín, 1995: A simple method for spatial interpolation of the wind in complex terrain. *Journal of Applied Meteorology*, **34**, 1678 – 1693.

Palutikof, J.P, T.D. Davies and P.M. Kelly, 1984: A databank of wind speed records for the British Isles and offshore waters. *Wind Energy Conversion 1984*, P. Musgrove, ed., Cambridge University Press, pp. 414 – 425.

Palutikof, J.P., J.A. Halliday, X. Guo, R.J. Barthelmie and T.J. Hitch, 1993: The impact of climate variability on the UK wind resource. Report to the UK Department of Energy. Report #ETSU WN 6029-P1.

Palutikof, J.P., J.A. Halliday, G.M. Watson, T. Holt, R.J. Barthelmie, J.P. Coelingh, L. Folkerts and J.W. Cleijne 2002: Predicting the wind energy resource in the offshore seas of Europe. *Preprints 3rd Symposium on Environmental Applications*, American Meteorological Society, paper 5.4.

Palutikof, J.P., P.M. Kelly and T.D. Davies, 1986: Windspeed variations and climatic change. *Wind Engineering*, **10**, 182 – 189.

Palutikof, J.P., P.M. Kelly, T.D. Davies and J.A. Halliday, 1987: Impacts of spatial and temporal windspeed variability on wind energy output. *Journal of Climate and Applied Meteorology*, **26**, 1124 - 1133.

Panofsky, H.A., 1958: *Introduction to Dynamic Meteorology.* Penn State University Press, State College, PA. 243 p.

Pawlowicz, R., 2004: M_map Matlab Toolbox. Version 1.4b. http://www2.ocgy.ubc.ca/~rich/map.html.

Pérez, S., P.A. Jimenez, J. Navarro, J.P. Montavez, C.G. Barquero, A. Cuerva, J.F. Gonzalez-Rouco and F. Valero, 2003: Using the MM5 model for wind prediction in a complex terrain site. *Proceedings European Wind Energy Conference and Exhibition EWEC 2003*, Madrid, ES. 8 p.

Petersen, E.L., N.G. Mortensen, L. Landberg, J. Højstrup and H.P. Frank, 1998a: Wind power meteorology. Part I: Climate and turbulence. *Wind Energy*, **1**, 2 – 22.

Petersen, E.L., N.G. Mortensen, L. Landberg, J. Højstrup and H.P. Frank, 1998b: Wind Power Meteorology. Part II: Siting and Models. *Wind Energy*, **1**, 55 - 72.

Petersen, E.L., I. Troen and N.G. Mortensen, 1988: The European wind energy resources. *Proceedings European Community Wind Energy Conference*, Herning, Denmark, pp. 103 – 109.

Petersen, E.L., I. Troen and J. Wieringa, 1984: Development of a method for wind climate analysis for non-mountainous terrain in Europe. *Proceedings European Wind Energy Conference*, Hamburg, Germany, pp. 6 – 12.

Petersen, E.W. and J.P. Hennessey, 1978: On the use of power law estimates of wind power potential. *Journal of Applied Meteorology*, **17**, 390 – 394.

Pielke, R.A., 1974: A three-dimensional model of the sea breezes over South Florida. *Monthly Weather Review*, **102**, 115 - 139.

Pielke, R.A., 1985: The use of mesoscale numerical models to assess wind distribution and boundary-layer structure in complex terrain. *Boundary – Layer Meteorology*, **31**, 217 – 231.

Pielke, R. A., W. R. Cotton, R. L. Walko, C. J. Tremback, M. E. Nicholls, M. D. Moran, D. A. Wesely, T. J. Lee and J. H. Copeland, 1992: A comprehensive meteorological modeling system- RAMS. *Meteorological and Atmospheric Physics*, **49**, 69 - 91.

Pielke, R.A., R.T. McNider, M. Segal and Y. Mahrer, 1983: The use of a mesoscale numerical model for evaluations of pollutant transport and diffusion in coastal regions and over irregular terrain. *Bulletin American Meteorological Society*, **64**, 243 – 249.

Pinson, P., N. Siebert and G. Kariniotakis, 2003: Forecasting of regional wind generation by a dynamic fuzzy-neural networks based upscaling approach. *Proceedings European Wind Energy Conference and Exhibition EWEC 2003*, Madrid, ES. 5 p.

Poje, D. and B. Cividini, 1988: Assessment of wind energy potential in Croatia. *Solar Energy*, **41**, 543 - 554.

Pötz, C.H., 1988: *Wetterfahnen*. Callwey, München, 100 p.

Powell, M.D., 1993: Wind measurement and archival under the automated surface observing system (ASOS): User concerns and opportunity for improvement. *Bulletin American Meteorological Society*, **74**, 615 - 624.

Pryor, S.C. and R.J. Barthelmie, 2001: Comparison of potential power production at on- and offshore sites. *Wind Energy*, **4**, 173 - 181.

Pryor, S.C. and R.J. Barthelmie, 2004: Can satellite sampling of offshore wind speeds realistically represent wind speed distributions? Part II: Quantifying uncertainties associated with distribution fitting methods. *Journal of Applied Meteorology*, **43**, 739 - 750.

Putnam, P.C., 1948: *Power from the Wind*. Van Nostrand Reinhold. 224 pp.

Quine, C.P., 2000: Estimation of mean wind climate and probability of strong winds for wind risk assessment. *Forestry*, **73**, 247 – 258.

Rainbird, P., K.A. Shein, P. Hannah and J.P. Palutikof, 1996: Prediction of extreme wind speeds at wind energy sites. *Proceedings European Wind Energy Conference*, Goteburg, Sweden. 4 p.

Reed, J.W., 1974: Wind power climatology. *Weatherwise*, **27**, 236 - 242.

Reisner, J., R.J. Rasmussen, and R.T. Bruintjes, 1998: Explicit forecasting of supercooled liquid water in winter storms using the MM5 mesoscale model. *Quarterly Journal Royal Meteorological Society*, **124B**, 1071-1107.

Robeson, S.M.,1993: *Spatial Interpolation, Network Bias, and Terrestrial Air Temperature Variability*. Publications in Climatology, C.W. Thornthwaite Associates Laboratory of Climatology. 51 p.

Robeson, S.M. and K.A. Shein, 1997: Spatial coherence and decay of wind speed and power in the North-Central United States. *Physical Geography*, **18**, 479 - 495.

Rohatgi, J.S. and V. Nelson, 1994: *Wind Characteristic: An Analysis for the Generation of Wind Power*. Alternative Energy Institute, Canyon, TX. 239 p.

Rogerson, P.A., 2001: *Statistical Methods for Geography*, Sage Publications, London, 236 p.

Romeu, J.L., 2003a: Empirical assessment of Weibull distribution. *Selected Topics in Assurance Related Technologies*, **10**, *3*, 1-6.

Romeu, J.L., 2003b: Anderson-Darling: A goodness of fit test for small samples assumptions. *Selected Topics in Assurance Related Technologies*, **10**, *5*, 1-6.

Sahin, A.D. and Z. Sen, 2001: First-order Markov chain approach to wind speed modelling. *Journal of Wind Engineering and Industrial Aerodynamics*, **89**, 263 - 269.

Salmon, J.R. and J.L. Walmsley, 1999: A two-site correlation model for wind speed, direction and energy estimates. *Journal of Wind Engineering and Industrial Aerodynamics*, **79**, 233 – 268.

Sandwell, D.T., 1987: Biharmonic spline interpolation of GOES-3 and SEASAT altimeter data. *Geophysical Research Letters*, **2**, 139 - 142.

Sansom, J. and A. Tait, 2004: Estimation of long-term climate information at locations with short-term data records. *Journal of Applied Meteorology*, **43**, 915 – 923.

Schwartz, M. and D. Elliott, 2002: Re-mapping of the wind energy resource in the Midwestern United States. *Preprints* 3rd Symposium on Environmental Applications, American Meteorological Society, Paper 5.2.

Sfetsos, A., 2000: A comparison of various forecasting techniques applied to mean hourly wind speed time series. *Renewable Energy*, **21**, 23 – 35.

Sfetsos, A., 2002: A novel approach for the forecasting of mean hourly wind speed time series. *Renewable Energy*, **27**, 163 - 174.

Shein, K.A., 1995: *Wind Speed Variability in the Midwestern United States 1961-1990: Implications for Wind Power Assessment.* MA Thesis, Indiana University, 110 p.

Sherlock, R.H., 1951: Analyzing winds for frequency and duration. *Meteorological Monographs*, No. 4. American Meteorological Society, pp. 72-79.

Sherman, C.A., 1978: A mass-consistent model for wind fields over complex terrain. *Journal of Applied Meteorology*, **17**, 312 - 319.

Smith, O.E., 1971: An application of distributions derived from the bivariate normal density function. *Preprints International Symposium on Probability and Statistics in the Atmospheric Sciences*. American Meteorological Society, Honolulu, HI, 162 – 168.

Snedecor, G.W. and W.G. Cochran, 1989: *Statistical Methods, 8th Ed.* Iowa State University Press, Ames, IA. 503 p.

Steinitz, G.A., Huss, A., Manes, A., Sinai, R. and Z. Alperson, 1971: Optimum station networks in the tropics. *Journal of Applied Meteorology*, **10**, 364 - 369.

Stephens, M.A., 1974: EDF statistics for goodness of fit and some comparisons. *Journal of the American Statistical Association*, **69**, 730 - 737.

Stephens, M.A., 1976: Asymptotic results for goodness-of-fit statistics with unknown parameters. *Annals of Statistics*, **4**, 357 - 369.

Still, D., 2001: Offshore winds at Blyth. *Renewable Energy*, **24**, 545 - 551.

Stull, R.B., 1999: *An Introduction to Boundary Layer Meteorology*. Springer, NY. 680 p.

Taylor, P.A. and R.J. Lee, 1984: Simple guidelines for estimating wind speed variations due to small scale topographic features. *Climatological Bulletin*, **18**, 3 – 32.

Tennekes, H., 1973: The logarithmic wind profile. *Journal of the Atmospheric Sciences*, **30**, 234 – 238.

Tetzlaff, G., 1984: Problems assessing the wind power potential for large areas. *Proceedings European Wind Energy Conference*, Hamburg, Germany, pp. 14 - 17.

Thiebaux, H.J., 1975: Experiments with correlation representations in objective analysis. *Monthly Weather Review*, **103**, 617 – 627.

Thor, S. and P. Weis-Taylor, 2002: Long-term research and development needs for wind energy for the time frame 2000-2020. *Wind Energy*, **5**, 73 - 75.

Tobler, W.R., 1970: A computer movie simulating urban growth in the Detroit region. *Economic Geography*, **46**, 234 - 240.

Toriumi, R., H. Katsuchi and N. Furuya, 2000: A study on spatial correlation of natural wind. *Journal of Wind Engineering and Industrial Aerodynamics*, **87**, 203 – 216.

Torres, J.L., A. García, E. Prieto and A. De Francisco, 1999: Characterization of wind speed data according to wind direction. *Solar Energy*, **66**, 57 – 64.

Touma, J.S., 1977: Dependence of the wind profile power law on stability for various locations. *Journal of the Air Pollution Control Association*, **27**, 863 - 866.

Troen, I. and E.L. Petersen, 1989: *European Wind Atlas*. Risø National Laboratory, Roskilde, DK. 656 p.

Tukey, J.W., 1977: *Exploratory Data Analysis*. Addison-Wesley, Reading, MA. 688 p.

Tustison, B., D. Harris and E. Foufoula-Georgiou, 2001: Scale issues in verification of precipitation forecasts. *Journal of Geophysical Research*, **106(D11)**, 11775 - 11784.

USDA Forest Service, 2002: *National fire plan research and development – 2001 business summary.* USDA Forest Service, North Central Research Station, St. Paul, MN. 29 p.

Van der Hoven, I., 1957: Power spectrum of horizontal wind speed in the frequency range from 0.0007 to 900 cycles per hour. *Journal of Meteorology*, **14**, 160 – 164.

Van Lieshout, P., 2004: Time dependent energy calculations. *Proceedings Wind flow and Trees workshop*, British Wind Energy Association, Glasgow, UK. 4 p.

Wallace, J.M. and P.V. Hobbs, 1977: *Atmospheric Science: An Introductory Survey.* Academic Press, San Diego, CA. 467 p.

Walmsley, J.L. and D.L. Bagg, 1978: A method of correlating wind data between two stations with application to the Alberta Oil Sands. *Atmosphere-Ocean*, **16**, 333 – 347.

Walmsley, J.L., R.J. Barthelmie and W.R. Burrows, 2001: The statistical prediction of offshore winds from land-based data for wind-energy applications. *Boundary-Layer Meteorology*, **101**, 409 - 433.

Weber, R., 1990: Interpolation of the wind field in a terrain following coordinate system over complex topography. *Atmospheric Environment*, **24**, 1971 – 1972.

Wendland, W.M., 1982: Wind power as an electrical energy source in Illinois. *Journal of Applied Meteorology*, **21**, 423 – 428.

Weibull, W., 1951: A statistical distribution function of wide applicability. *Journal of Applied Mechanics*, **18**, 293 - 297.

Whiteman, C.D. and J.C. Doran, 1993: The relationship between overlying synoptic-scale flows and winds within a valley. *Journal of Applied Meteorology*, **32**, 1669 - 1682.

Whittaker, L.M. and L.H. Horn, 1981: Geographical and seasonal distribution of North American cyclogenesis. *Monthly Weather Review*, **109**, 2312 - 2322.

Widger, W.K, 1977: Estimations of wind speed frequency distributions using only the monthly average and fastest mile data. *Journal of Applied Meteorology*, **16**, 244 - 247.

Wieringa, J., 1980: Representativeness of wind observations at airports. *Bulletin American Meteorological Society*, **61**, 962 - 971.

Wieringa, J., 1989: Shapes of annual frequency distributions of wind speed observed on high meteorological masts. *Boundary-Layer Meteorology*, **47**, 85 - 110.

Wilks, D.S., 1995: *Statistical Methods in the Atmospheric Sciences.* Academic Press, San Diego, CA, 467 p.

Williamson, D. L., J. T. Kiehl and J. J. Hack, 1995: Climate sensitivity of the NCAR Community Climate Model (CCM2) to horizontal resolution. *Climate Dynamics*, **11**, 377 - 397.

Willmott, C.J., 1981: On the validation of models. *Physical Geography*, **2**, 184-194.

Willmott, C.J., 1982: Some comments on the evaluation of model performance. *Bulletin American Meteorological Society*, **63**, 1309 - 1313.

Willmott, C.J., 1984: On the evaluation of model performance in physical geography. In *Spatial Statistics and Models*, Gaile, G.L. and C.J. Willmott, eds., Kluwer, Boston, pp. 443 – 460.

Willmott, C.J., S.G. Ackleson, R.E. Davis, J.J. Feddema, K.M. Klink, D.R. Legates, J. O'Donnell, and C.M. Rowe, 1985: Statistics for the evaluation and comparison of models. *Journal of Geophysical Research*, **90**, 8995 - 9005.

Willmott, C.J., S.M. Robeson and J.J. Feddema, 1991: Influence of spatially variable instrument networks on climatic averages. *Geophysical Research Letters*, **18**, 2249 - 2251.

Willmott, C.J. and D.E. Wicks, 1980: An empirical method for the spatial interpolation of monthly precipitation within California. *Physical Geography*, **1**, 59 - 73.

Wylie, D.P., B.B. Hinton, M.R. Howland and R.J. Lord, 1985: Autocorrelation of wind observations. *Monthly Weather Review*, **113**, 849 – 857.

Wyngaard, J.C., 1981: Cup, propeller, vane, and sonic anemometers in turbulence research. *Annual Review of Fluid Mechanics*, **13**, 399 - 423.

Zhong, S., H.-J. In, X. Bian, J. Charney, W. Heilman and B. Potter, 2005: Evaluation of real-time high-resolution MM5 predictions over the Great Lakes region. *Weather and Forecasting*, **20**, 63 - 81.